The University of Leeds

Faculty of Medicine and Health

Leeds Institute of Cardiovascular and Metabolic Medicine

Functions and mechanisms of Rab46 in endothelial cells

Lucia Pedicini

October, 2019

Thesis submitted to The University of Leeds in accordance with the requirements for the Degree of Doctor of Philosophy

Intellectual Property and Publication Statements

The candidate confirms that the work submitted is his own and that appropriate credit has been given where reference has been made to the work of others.

Acknowledgments

My PhD journey has been a great personal and professional challenge since the very beginning. I will never forget the first days when I had to face the Northern accent and quickly realise that my English knowledge was not enough in the North of England, a land far away from the posh Queen's English that I learnt at school. Undertaking this PhD has been a truly life-changing experience for me and it would not have been possible without the people I met throughout this journey.

First and foremost, I would like to thank the continued guidance and support of my supervisor, Dr Lynn McKeown. Thanks for your patience every time I asked you to slow down and 'say it again' during our lab meetings – how we have put up with each other accents I still do not know! I will be eternally grateful for believing in me and for always having an open door especially when things did not work out. I could not have imagined having a better advisor for my PhD study. I look forward to continuing working together.

I gratefully acknowledge Professor David Beech for all his constant support and guidance throughout my PhD. All the invaluable advice helped me working at my full potential without being lost within my research. I feel privileged to have had the opportunity to carry out my PhD in his lab.

I also would like to thank Dr Izzy Jayasinghe for being always very welcoming in his lab and for all the extremely useful advice on imaging analysis.

My PhD has been a continuous learning curve and I am especially grateful to all the old and new members of the Beech lab for their help and support over the years. Hannah who has always been patient in teaching me all the techniques from scratch at the very beginning of my PhD. Beth, Nikki, Katy and Nele who have been part of these three years as good teammates. Beth with your posh accent, you have always made me laugh and smile with all the hilarious stories of your daily life. Thanks for always being a good friend and a good lab mate, especially with our fury friends. I'll miss you so much but moving it's part of the scientist's life and I know you'll be a brilliant and successful scientist. Nikki, I will always remember your bagels and your very precise western blots. We shared this last few months of writing and it was a good feeling not to being alone. Katy, thanks for your fluent Italian and for your mild Manchester accent, I am sorry for all the time you had to express yourself again. Also, you're an artist, keep drawing you're amazing!

Nele, thanks for always being very supportive and for helping me since the beginning when I was struggling to adjust myself to live in a foreign country. Thanks for listening, for understanding my struggle about living abroad and for always being a very good friend. So many things have changed in these last years but definitely the best one is your little girl.

Marj and Fiona thanks for being enormously helpful in this year. Fiona thanks for answering my very stupid PCR questions and Marj for sharing the pain of our western blot session together, we will never know which friends show up at our party! Thanks to both of you for sharing your Tuscany trip with me, you know how much I miss it. Anyway I'm very happy you'll be part of whatever is coming next in my LICAMM experience. And please keep filming our daily life!

Last but not least a huge thank you for someone who has been sharing this adventure for me since the very first day, Kat. It was hard at the beginning to find a balance between me and you as we were both experiencing hard time but now, I feel I couldn't do it without you on my side. You have always been very helpful, you have never left me alone and most and foremost you have been the most supportive person in these last few months. You know better than anyone how hard it was for me, how much I sacrificed trying to work hard and finish this PhD on time. I am indebted to you for being a patient listener, I have always felt better after all our complain sessions! Kat you are really a good friend and the best lab mate ever, I'll always be grateful for all the times you made me laugh during the experiments, to always keep a sense of humour when I had lost mine and for all the crimes that somehow always happen to us. Hope to return everything you did for me in the next year!

I also like to thank the rest of the McKeown's group. Ash and Sabina we couldn't ask for better new entries than you. Thanks a lot for your help and proofreading and I really think we should do more Aberdeen trips together. It was a very good time.

I also want to thank my new and old friends. My Italian friends who have always waited for my return maybe for just a dinner together and friends whose although the distance made hard to see each other, are still part of my life. Moving to Leeds was not easy and first and foremost I want to thank my friend Guada who is the first person I met here. We shared the house during my first year and since the beginning was like we knew each other from years. They say that Italians and Spanish have something in common, I have to say that maybe it's true. You have been the closest friend here in the UK, you were always there to help me when I was alone and definitely think we built a long-lasting friendship.

A very deep thank you must now go to my family, to my life-coaches: my granddad and my grandma and to the love of my life.

Un grazie di cuore a voi mamma e papà che siete e sarete per sempre la mia "casa", il mio rifugio sicuro. Grazie per avermi sempre sostenuto in tutte le mie scelte, so che è stato difficile lasciarmi andare. Ogni volta che parto lo vedo nei vostri occhi e lo sento in silenzio nel mio cuore…ma io vi porto sempre con me, porto con me i valori che mi avete insegnato e spero di potervi far sentire orgogliosi del futuro che sto cercando di costruire. Magari un giorno chissà a furia di venirmi a trovare vi verrà anche voglia di viaggiare! C'è un mondo da scoprire e anche se l'Italia sarà sempre il posto più bello del mondo ne vale la pena di scoprire il resto.

Francesco e Noemi, che dire non potevamo essere più diversi di così ma siete la parte diciamo frizzante della famiglia. Mi sono sempre sentita un po' mamma e un po' sorella per voi…chissà forse solo per tenere a bada i vostri animi ribelli…comunque vogliate io ci sarò sempre per voi anche perché cosa fareste senza di me? Chi sarà la parte saggia del trio? Grazie semplicemente di esserci.

E poi è difficile ringraziare le persone che hanno fatto di me quella che sono oggi, trovare le parole per descrivere cosa siete per me è davvero difficile. Siete la mia più grande fortuna, ci siete sempre stati, mi avete regalato tutti i ricordi più belli e la gioia nel cuore di tornare a casa. Grazie a te nonno che sei sempre stato il mio più grande sostenitore, sei la mia motivazione e vedere nei tuoi occhi la tua soddisfazione quando parlo di scienza è il mio regalo più grande. Grazie per avermi trasmesso l'amore per scoprire cose nuove e soprattutto l'amore per viaggiare….sarete con me in ogni mio viaggio!

Grazie a te a nonna per aspettare ogni volta le mie telefonate per sapere quando torno. Come dici tu non è semplice stare lontani (anche se non esattamente con queste parole). Ma non importa la distanza perché i momenti che passiamo insieme sono i più belli di sempre, abbiamo tante cose da fare e anche se ora forse ti sembra più difficile, niente è impossibile perché l'amore smuove le montagne e io ne ho abbastanza per smuoverti da quella poltrona.

L'ultimo grazie è sempre per Te che hai sempre creduto in me, mi hai spinto a guardare in alto, ad essere una persona migliore prima di tutto per me stessa. Mi hai spesso, a volte con forza, posto davanti i miei limiti e spinto a superarli. Non sarei qui oggi, alla fine di questa avventura se non fosse stato per te. Mi sei stato accanto quando ne avevo bisogno, sei stato il mio sole sotto questo cielo grigio, sei stato il mio migliore amico e il mio compagno di viaggio…continueremo a viaggiare e chissà che il meglio deve ancora venire.

Abstract

Endothelial cells maintain vascular integrity by regulating a number of physiological and pathophysiological processes, including haemostasis, thrombosis and inflammation. A pivotal contribution to these processes is the exocytosis of cargo from specialized endothelial storage organelles, namely Weibel-Palade bodies (WPBs). WPBs provide an intracellular storage pool of pro-thrombotic and pro-inflammatory mediators which can be differentially released in response to different stimuli. Ca^{2+} raising agonists such as thrombin and histamine, respectively released following vascular injury or an immunogenic insult, evoke WPB exocytosis. However, inappropriate and untimely exocytosis of WPBs can promote the pro-thrombotic and pro-inflammatory environment evident in cardiovascular diseases. The mechanisms underlying differential cargo release in order to produce physiologically distinct responses are poorly understood. Some Rab GTPase family members, have been reported to be implicated in regulating the exocytosis of WPBs.

Here, we describe a novel Rab GTPase (Rab46) in endothelial cells that is located on WPBs. Super-resolution microscopy confirmed that Rab46 is juxtaposed to von Willebrand Factor (vWF), on the cytosolic side of individual WPBs, whilst quantitative imaging analysis suggested that Rab46 may regulate a subpopulation of WPBs. Interestingly, Rab46 was necessary for acute histamine, but not thrombin, WPB trafficking towards the perinuclear area identified as the Microtubule Organizing Centre (MTOC). Biochemical analysis and mass spectrometry was used to investigate the molecular mechanisms underlying Rab46-dependent retrograde trafficking and the dynein heavy chain was identified as a candidate effector protein. Further biochemical experiments suggested a direct interaction between endogenous Rab46 and the dynein motor complex. Taken together, these results suggest that after acute histamine stimulation, dynein-bound Rab46 mediates retrograde transport of a subset of WPBs along microtubules to the MTOC.

These observations indicate Rab46 as a key regulator of differential WPB cargo secretion, allowing an appropriate acute pro-inflammatory response whilst avoiding release of excessive pro-thrombotic mediators. Characterization of *in vivo* model of Rab46 represents the beginning of understanding the physiological contribution of Rab46 as well as its response to pathological conditions. Understanding the Rab46/WPB signalling axis, both *in vitro* and *in vivo*, could be important for achieving better appreciation of how the endothelial cell fine-tunes it's secretory response and thereby providing novel therapeutic targets for the prevention of endothelial dysfunction, which is often the trigger for cardiovascular diseases.

Table of contents

List of Figures

List of Tables

Abbreviations

AMI	Acute Myocardial Infarction
APEX	Ascorbate peroxidase
ATP1α	Na^+/K^+ ATPase subunit α1
BSA	Bovine Serum Albumin
Ca^{2+}	Calcium
cAMP	Cyclic adenosine 3',5'-monophosphate
CCVs	Clathrin-Coated Vesicles
cDNA	Complementary DNA
CRAC	Calcium-Release-Activated Calcium
CRMP-2	Collapsin Response Mediator Protein-2
CVD	Cardiovascular Disease
DAPI	4',6-diamidino-2-phenylindole
DHC	Dynein Heavy Chain
DLC	Dynein Light Chain
DMEM	Dulbecco Modified Eagles Media
DPBS	Dulbecco's Phosphate Buffered Saline
dSTORM	direct Stochastic Optical Reconstruction Microscopy
EBM-2	Endothelial Cell Basal Medium
EEA1	Endosome antigen 1
EM	Electron Microscopy
EPCR	Endothelial cell Protein C Receptor
ER	Endoplasmic Reticulum
ET-1	Endothelin-1
FBS	Fetal Bovine Serum
FRET	Förster Resonance Energy Transfer
GAP	GTPase accelerating protein
GDF	GDI-displacement Factor

GDI	GDP dissociation inhibitor
GDP	Guanosine diphosphate
GEF	Guanine nucleotide exchange factor
GFP	Green Fluorescent Protein
GLUT4	Glucose transporter 4
GpIbα	Glycoprotein Ibα
GTP	Guanosine triphosphate
GTT	Glucose Tolerance test
H&E	Haematoxylin and eosin
HCMEC	Human Cardiac Microvascular Endothelial Cells
HOPS	Homotypic fusion and protein-sorting
HPR	Horseradish Peroxidase
HUVEC	Human Umbilical Vein Endothelial Cells
IL	Interleukin
IP	Immunoprecipitation
IP3	Inositol trisphosphate
IS	Immunological Synapse
ITT	Insulin Tolerance Test
KIF	Kinesin heavy chain
LDL	Low Density Lipoprotein
LIC	Light intermediate chain
LMW-vWF	Low-Molecular Weight vWF
M6PRs	Mannose-6- Phosphate Receptors
MLC	Myosin Light Chain
mLEC	Mouse Liver Endothelial Cells
MLPH	Melanophilin
MTOC	Microtubule Organising Centre
MyoV	Myosin Va
NAADP	Nicotinic Acid Adenine Dinucleotide Phosphate
NAFLD	Non-Alcoholic Fatty Liver Disease

NFAT	Nuclear factor of activated T cells
NMR	Nuclear Magnetic Resonance
NO	Nitric Oxide
NSF	N-ethylmaleimide-sensitive factor
PALM	Photo-activated Localization Microscopy
PAR-1	Protease-Activated Receptor 1
PCR	Polymerase Chain Reaction
PFA	Paraformaldehyde
PKA	Protein Kinase A
PtdIns(4,5)P2	Phosphatidylinositol 4,5-bisphosphate
PVDF	Polyvinylidene Fluoride
qPCR	quantitative Polymerase Chain Reaction
Rab	Ras-related proteins in brain
Rab GTT	Rab Geranylgeranyltransferase
REP	Rab Escort Protein
RILP	Rab-interacting lysosomal protein
RT	Reverse Transcriptase
SDS	Sodium Dodecyl Sulphate
siRNA	Short Interfering RNA
Slp1	Synaptotagmin-like protein-1
Slp4a	Synaptotagmin-like protein 4-a
SMLM	Single Molecule Localization Microscopy
SNARE	Soluble NSF receptor
SNP	Single-Nucleotide Polymorphism
SOCE	Store-operated Ca^{2+} Entry
STIM1	Stromal Interaction Molecule 1
TCR	T-cell antigen receptor
TF	Tissue Factor
TGN	Trans-Golgi Network
TNF	Tissue Necrotic Factor

tPA	Tissue plasminogen activator
TTP	Thrombotic Thrombocytopenic Purpura
UL-vWF	Ultra-Large vWF
VEGF	Vascular Endothelial Growth Factor
VPS	Vacuole Protein-Sorting
VSMC	Vascular Smooth Muscle Cells
VWD	Von Willebrand Disease
vWF	Von Willebrand Factor
WPBs	Weibel-Palade Bodies
WT	Wild-Type

Publications and communication

Katarina T. Miteva*, **Lucia Pedicini***, Lesley A. Wilson, Izzy Jayasinghe, Raphael G. Slip, Katarzyna Marszalek, Hannah J. Gaunt, Fiona Bartoli, Shruthi Deivasigamani, Diego Sobradillo, David J. Beech, Lynn McKeown. **Rab46 integrates Ca^{2+} and histamine signaling to regulate selective cargo release from Weibel-Palade bodies**. The Journal of Cell Biology Jul 2019, 218 (7) 2232-2246; DOI: 10.1083/jcb.201810118 (*) Equal contribution

Lucia Pedicini, Katarina T. Miteva, Verity Hawley, Hannah J. Gaunt, Hollie L. Appleby, Richard M. Cubbon, Katarzyna Marszalek, Mark T. Kearney, David J. Beech & Lynn McKeown. **Homotypic endothelial nanotubes induced by wheat germ agglutinin and thrombin** Scientific Reports volume 8, Article number: 7569 (2018)

Martina Giannaccini, **Lucia Pedicini**, Guglielma De Matienzo, Federica Chiellini, Luciana Dente & Vittoria Raffa. **Magnetic nanoparticles: a strategy to target the choroidal layer in the posterior segment of the eye**. Scientific Reports volume7, Article number: 43092 (2017)

Communications

Interaction between Rab46 and dynein complex regulates Weibel-Palade body trafficking in response to inflammatory stimuli. **L.Pedicini**, K.Miteva, LA.Wilson, I.Jayasinghe, DJ. Beech, and L.McKeown. Physiology 2019, Aberdeen

Coordination of GTPase and Ca2+ signalling by Rab46 regulates histamine specific Weibel Palade body trafficking and protects the vasculature from a pro-thrombotic response. **L. Pedicini**, K. Miteva, LA. Wilson, D. Cutler, DJ. Beech, and L. McKeown. Frontiers in CardioVascular Biology, Vienna (2018)

Homotypic endothelial nanotubes induced by C-type lectin and thrombin. **Lucia Pedicini,** Katarina T. Miteva, Verity Hawley, Hannah J. Gaunt, Hollie L. Appleby, Richard M. Cubbon, Katarzyna Marszalek, Mark T. Kearney, David J. Beech & Lynn McKeown. IUPS 38th World Congress, Rhythms of Life, Rio de Janeiro (2017)

Chapter 1 Introduction

The luminal surface of the entire vasculature is delimited by a continuous monolayer of endothelial cells. The endothelial layer provides a strategic structural barrier between blood and the surrounding tissue. In addition to serving as a physical semipermeable barrier, endothelial cells also control many important functions in vascular homeostasis depending on their location. This phenotypic heterogeneity is due to exposure to different environmental as well as genetic factors. Endothelial cells have both metabolic and synthetic functions that influence vascular haemodynamics in the physiological and pathological state. Adaptation to physiological and pathological cues is essential to maintain vascular integrity. The endothelium is indeed, equipped to rapidly respond to local changes caused by trauma or inflammation. Specialized storage organelles, namely Weibel-Palade bodies (WPBs), are the main emergency machinery, which enable the endothelium to actively maintain a dynamic equilibrium between an antithrombotic physiological and a prothrombotic or proinflammatory state. WPBs are unique secretory organelles equipped with a multifunctional pack of haemostatic, inflammatory and angiogenic mediators that can be released upon demand. Regulated exocytosis of WPBs is a pivotal mechanism via which endothelial cells ensure differential release of bioactive molecules under different physiological conditions. Due to the complexity of WPB biogenesis and exocytosis, many aspects underlying these processes are still poorly understood. Several GTPases of the Rab family of small GTPases have recently been identified as regulators of WPB exocytosis and biogenesis. Rab GTPases are master regulators of cellular membrane trafficking, acting from organelle biogenesis to vesicle trafficking and exocytosis. Thus, the identity and function of Rabs associated with WPBs has been a particularly active area of WPB research in the last few years.

This chapter will offer a short background on the physiological role of endothelial cells and the consequences of endothelium dysfunction. Attention is then turned to the role of WPBs and the machinery that drives exocytosis of WPB contents from endothelial cells, focusing on the role of Rab GTPases and their effectors in intracellular trafficking.

Understanding how endothelial cells finely tune their secretory response in order to achieve context-dependent release of bioactive molecules from WPBs will potentially expose novel therapeutic targets for the treatment of haematological and cardiovascular dysfunction.

1.1 Vascular endothelium

The vascular endothelium constitutes approximately 1% of body mass (1 kg) with about ten trillion (10^{13}) cells covering an area between 1-7 (x 10^3) m^2 [1]. Endothelial cells are strategically positioned within the vessel wall, located between blood flowing through the vessel, and the surrounding tissues such as the vascular smooth muscle cells (VSMC) forming the tunica media of arteries and veins (Figure 1.1). Endothelial cell structure and functional integrity are important in the maintenance of the vessel wall and circulatory function, but the endothelium is much more than an inert semipermeable barrier that determines the exchange of substances between blood vessels and tissue spaces. The endothelium is a specialised organ that plays different roles in different locales of the vascular tree and in different organs; manifesting distinctive responses to injury according to its structure and location[2]. The endothelial layer as a dynamic and active tissue has vital metabolic and synthetic functions in addition to the secretory function that controls vascular homeostasis[3]. The endothelium senses and assesses the haemodynamic, humoral, and inflammatory signals to which it is constantly exposed and responds by secreting factors that affect vessel tone and structure. Endothelial cells contribute to the regulation of blood pressure and blood flow by releasing vasodilators such as nitric oxide (NO) and prostacyclin, as well as vasoconstrictors, including endothelin-1 (ET-1) and platelet-activating factor[4]. Normally the endothelium balances the equilibrium between vasorelaxation and vasoconstriction on the side of promoting vasodilatation and inhibiting cellular proliferation[5]. To this end, for instance, the release of NO has several beneficial effects on the cardiovascular system including inhibition of platelet aggregation and smooth muscle cell proliferation, culminating in an anti-atherosclerotic environment.

In addition to haemodynamic function, endothelial cells also regulate haemostasis and thrombosis. Haemostasis is mediated by a balance of procoagulant and anticoagulant factors[4]. Under normal conditions, the endothelium facilitates blood flow, maintaining its fluid state, by providing an antithrombotic surface that inhibits platelet adhesion and blood clotting. For example, thrombomodulin, which is present on endothelial surfaces, binds to thrombin and prevents platelet activation and fibrin production[6]. However, when the endothelium is perturbed by physical forces or by specific mediators, the cells rapidly undergo strategic biochemical changes that culminate in their transformation to a prothrombotic surface. The pivotal step in transforming the endothelial cell membrane from an anticoagulant to a procoagulant surface is the induction of tissue factor (TF). Tissue factor expression leads to the activation of factor X, which then combines with factor Va to convert prothrombin to thrombin[7]. Thrombin is a multifunctional protein with various pro-coagulant effects. For example, thrombin evokes von Willebrand factor (vWF) expression on the surface of endothelial cells which then interacts with the platelet glycoprotein receptor complex, initiating platelet adhesion and aggregation[3]. A dynamic equilibrium exists between a pro-thrombotic and anti-thrombotic state, which modulates all the physiological processes

to prevent excessive bleeding at the site of injury as well as maintaining normal blood flow in an unperturbed blood vessel, providing proper haemostatic balance.

In addition to the contribution of the endothelium in regulating blood coagulation, endothelial cells also express cell surface molecules that orchestrate the trafficking of circulating white blood cells as part of the immune response. The cell adhesion molecules expressed on the endothelial cell surface, such as integrins and selectins, help direct the migration of leukocytes into specific tissues under physiologic conditions and accelerate migration towards sites of inflammation[4,8]. Movement of leukocytes between tightly adjacent endothelial cells into the tissue towards the site of infection or injury occurs via a complex and highly regulated multistep cascade, maintaining the integrity of the endothelium whilst at the same time allowing the migration of activated inflammatory cells out of the circulation[1]. An early "rolling" adhesion of leukocytes occurs within the first 1–2 h of an assault followed by leukocyte activation as a result of upregulation of cell surface selectins. The interaction between chemokine receptors on leukocytes and proteoglycans on endothelial cells mediate firm adhesion of leukocytes prior to transendothelial migration. Lastly, transendothelial migration (diapedesis) involves integrins, ICAM-1 and VCAM-1, and changes in vascular permeability to recruit leukocytes to the site of inflammation[9]. Each of these sequential steps ensures that the appropriate leukocytes accumulate for a restricted period in response to a specific challenge.

It is evident how the endothelium, first described in 1980 as a simple cellophane wrapper, is now considered a large complex endocrine organ with a prominent role in vessel remodelling, vasomotion, vascular structure, secretion and mediation of interaction between circulating blood and the vessel wall. All these functions, summarised in Figure 1.2, are paramount to maintain the homeostasis of the entire vascular tree in the physiological state.

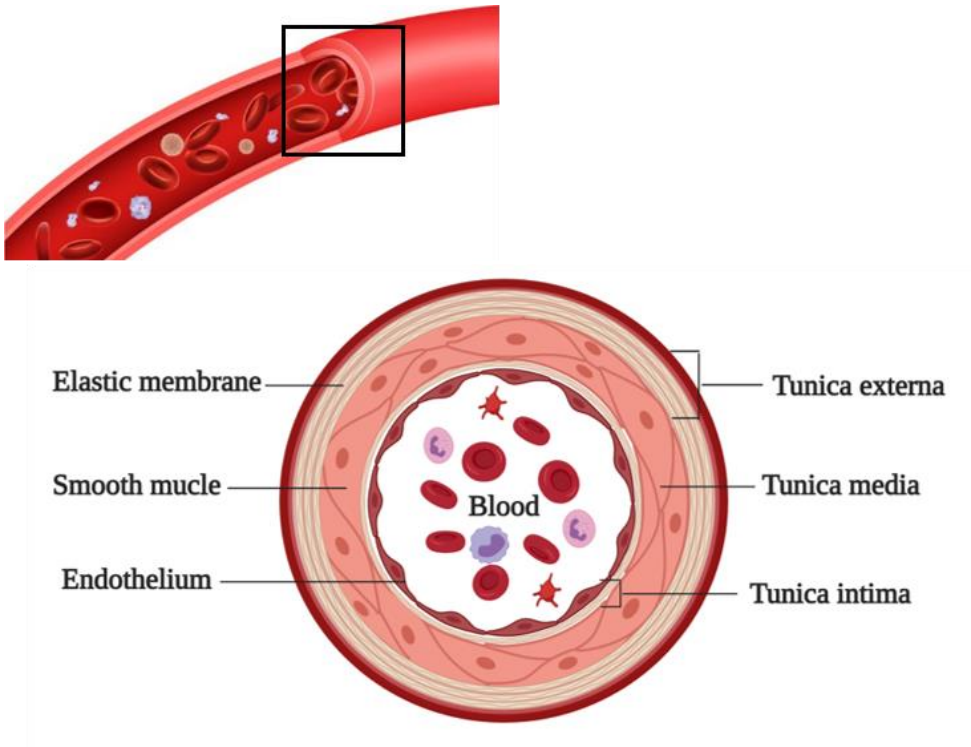

Figure 1.1 Schematic of an artery. The vascular endothelium consists of a monolayer of endothelial cells that line the blood vessel. They are strategically located next to vascular smooth muscle cells and the flowing blood. The endothelium supported by the sub-endothelium form a thin layer called tunica intima. The smooth muscle cells with elastin fibres compose the tunica media. The thick outside layer, called tunica externa is composed by an external elastic membrane and connective tissue.

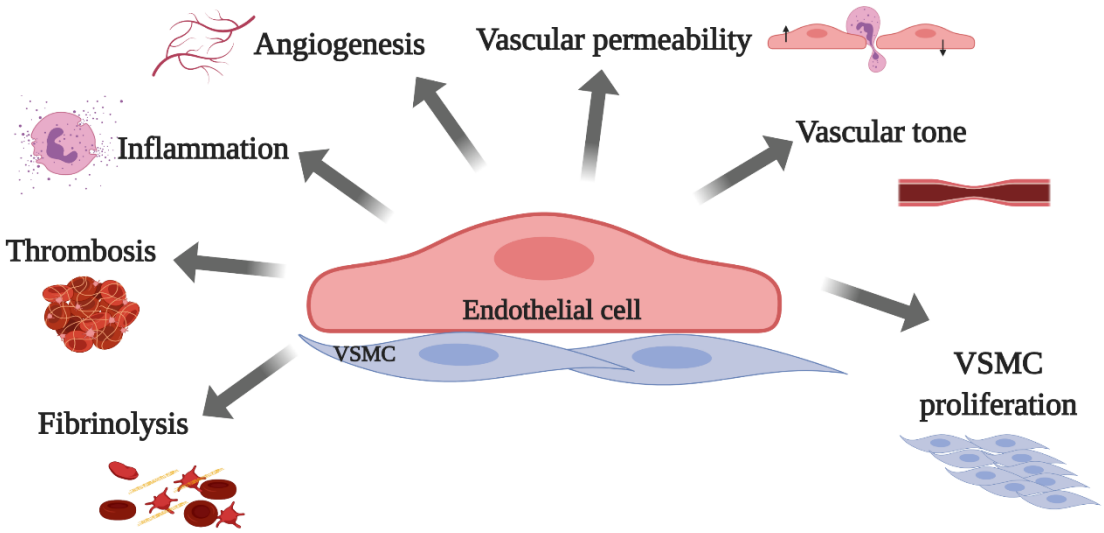

Figure 1.2 Schematic representation of the main endothelial cell functions. Endothelial cells maintain vascular homeostasis by maintain a fine equilibrium between the functions summarized in the above diagram.

1.1.1 Endothelial dysfunction

Given the number and range of processes in which the endothelium participates, endothelial dysfunction can be expected to have major pathological implications. It has been increasingly recognized that disruptions in normal endothelial function play a part in the progression of several diseases; for example, the development and progression of atherosclerosis, hypertension, diabetes, hypercholesterolaemia, and coronary artery disease[5].

Dysfunction of the endothelium can be defined as an imbalance between relaxing and contracting factors, between anti- and pro-coagulant mediators or growth-inhibiting and growth-stimulating factors. This imbalance can develop by impaired synthesis and release of protective factors or increased synthesis and release of pro-coagulant/growth promoting factors[10]. Phenotypic and functional alterations of endothelial cells lead to compensatory responses which alter the normal vascular homeostasis. Most forms of cardiovascular diseases are caused by functional and structural changes in the blood-vessel wall.

Endothelial dysfunction in atherosclerosis is demonstrated by impaired endothelium-dependent relaxation. Decreased production or activity of NO, manifested as impaired vasodilation, causes phenotypic changes to pro-thrombotic and pro-inflammatory state which may be one of the earliest signs of atherosclerosis. Several studies have reported an increased plasma vWF levels as a consequence of impaired endothelial NO production[11], suggesting the possibility that NO inhibits vWF endothelial secretion[12] (implying that impaired NO production increases vWF secretion). While elevated vWF levels may contribute to the pro-thrombotic state, the pro-inflammatory condition associated with atherosclerosis is mainly supported by increased expression of P-selectin on the cell surface, mediating leukocyte adhesion. It has been suggested that P-selectin may be involved in atherosclerosis because P-selectin deficiency also delays and reduces atherosclerotic lesion formation[13,14]. These changes increase monocytes adhesion and penetration through the vascular wall. Atherosclerosis is, indeed, a systemic disease triggered by chronic inflammatory processes. It is characterised by the thickening of the intimal and medial layers of the arteries due to the deposition of atheromatous plaques along the vessel together with loss of elasticity[15]. Low-density lipoproteins (LDL), monocytes and macrophages are able to accumulate in the vessel due to an increase in vessel permeability, another key characteristic of endothelial dysfunction. The monocytes in the intima differentiate into macrophages and engulf modified lipoproteins to become foam cells (the hallmark of early fatty streak lesions). Atherosclerotic lesion progression leads to the switch of medial smooth muscle cells to their migratory and proliferative phenotype and an increase synthesis of extracellular matrix molecules generating a fibromuscular plaque. Macrophages and smooth muscle cells that have accumulated in the intimal layer of the vessel begin to die and their lipid contents can accumulate in the central region of the plaque (the necrotic core) resulting in the formation of a fibrous cap[16]. Plaque development compromises the artery lumen leading to disturbed blood flow provoking tissue ischaemia. Rupture of the plaque exposes pro-coagulant material

and triggers thrombus formation which results in blockage of the vessel lumen causing clinical events such as myocardial infarction or stroke[16].

Accelerated atherosclerosis, associated with increased oxidative stress, is also a prominent characteristic of diabetic cardiovascular complications. Diabetes mellitus is a chronic condition that occurs when the body cannot produce enough or effectively use of insulin. Type 2 diabetes is characterized by a two-to fourfold increased risk of cardiovascular disease. In patients with diabetes, endothelial dysfunction appears to be a consistent finding, generally attributed to the adverse effects of hyperglycaemia and oxidative stress on vascular biology[17].

In healthy vessels, as already mentioned, the endothelium maintains a balance between opposite vasoactive factors to maintain vascular tone. An imbalance in this homeostasis with a predominance of vasoconstrictive elements, like ET-1, and vascular wall thickening leads to hypertension, a major risk factor for coronary events. Endothelial cell damage occurs in many vascular beds during hypertension. However, it is not clear whether hypertension is the cause or the result of this damage[18].

It is evident that endothelial cells are multifunctional cells, involved in the regulation not only of haemostasis but also of vascular tone, leukocyte adhesion and fibrinolysis among other functions which if impaired contribute to the onset and progression of different diseases.

Most of the molecules (like vWF, P-selectin, angiopoietin-2 and ET-1) that contribute to these processes are co-stored in endothelial specific secretory granules called Weibel-Palade Bodies (WPBs). How do endothelial cells control the release of granule content to allow differentiated responses? Understanding the mechanisms behind these responses will allow a better characterisation of the events causing the endothelial dysfunction which is often associated with cardiovascular diseases.

Therefore, the endothelium can act as a measure of cardiovascular health and investigation into targeting endothelial dysfunction and treatment of early endothelial dysfunction is paramount for future therapeutic strategies.

1.2 Weibel-Palade Bodies

Weibel-Palade bodies (WPBs) were first described in 1964 by Ewald Weibel and George Palade as "New cytoplasmic components of arterial endothelia"[19]. Using electron microscopy (EM), they observed rod-shaped constituents of the endothelial cytoplasm of 0.1 x 2-3 μm in size which consist of a bundle of fine tubules aligned parallel to the longitudinal axis, enveloped by a tightly fitted membrane (Figure 1.3). Although they suggested a connection between these bodies and vascular or blood physiology, the nature and significance of these cytoplasmic components remained unknown for the next twenty years.

In October 1982, evidence for the function of WPBs emerged from the Wagner lab. Using light and electron microscopy, Denisa Wagner and co-workers functionally rediscovered these organelles showing that the haemostatic protein vWF was stored in WPBs 'so as to allow rapid release of this protein upon appropriate stimulus or physiologic demand'[20]. The Wagner group went on to demonstrate that WPBs also stored other pre-made cargo, such as P-selectin with the potential to profoundly affect vascular function when released from cells.

Endothelial cells heterogeneity between different vascular beds[21] may explain the heterogeneous distribution of WPBs along the vascular tree[22]. The amount of WPBs in individual cells can vary between endothelial cells and differential distribution of vWF in the vascular endothelium has been shown[23]. vWF is not uniformly expressed on cells from all type of vessels as veins exhibit higher vWF content than arteries. However, WPBs can still be detected in ECs of all small arteries, the pulmonary arteries and arterioles, whereas these storage organelles are absent from pulmonary capillaries[24]. Therefore analysing spatial and temporal expression of vWF and others WPB components along the vasculature axis could give insight into their physiological role in anatomically restricted segments.

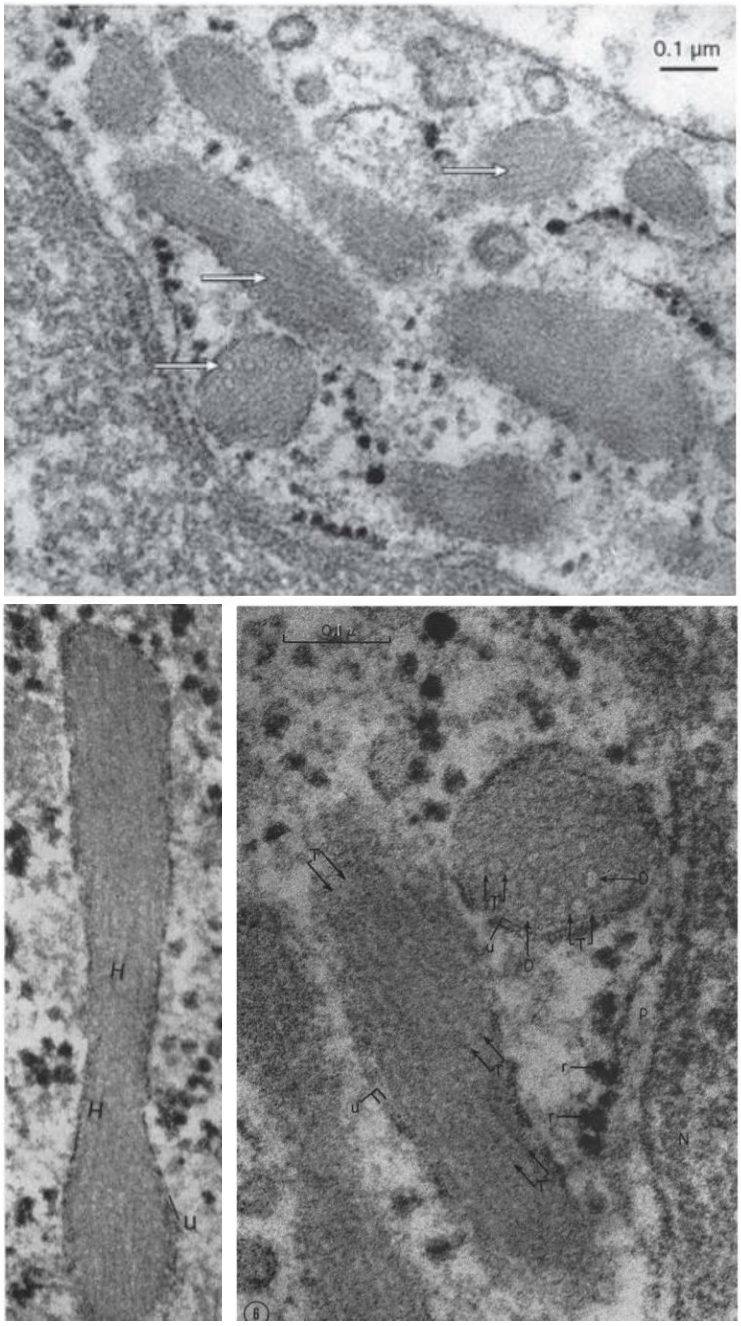

Figure 1.3 First micrograph of rod-shaped organelles in 1962. Endothelium of a small pulmonary artery of a rat, showing the cluster of rod-shaped particles, depicting the tubular structure of their content (arrows) in cross-section and in oblique sections. Higher-power micrograph of the same specimen (bottom panels), showing parallel arrangement of internal tubules (H) and arrow pairs on the right panel point to clearly visible outlines of internal tubules (T) in transverse or longitudinal sections. From Weibel ER, Palade GE, JCB (1964)[19]

1.2.1 Biogenesis of WPBs

vWF is the main cargo of WPBs and is a prerequisite for the existence of WPBs. It is synthesized only by endothelial cells[25] and megakaryocytes and is crucial for platelet adhesion at the site of vascular injury to form the first haemostatic plug[20]. Endothelial cells of vWF-deficient animals do not contain WPBs[26,27]. The expression of recombinant vWF in other cell types is enough to induce formation of cigar-shaped WPB-like granules[28], indicating that vWF has the intriguing property of inducing the elongated organelle in which it is stored. Therefore, the first step of WPB formation is vWF synthesis. Figure 1.4 summarises the main steps of WPB biogenesis and vWF processing. The vWF precursor is composed of a signal peptide followed by conserved structural domains (pre-pro-vWF). The signal peptide is responsible for ensuring the nascent polypeptide chain enters the endoplasmic reticulum (ER) where it is then cleaved and lost. Mature vWF is highly glycosylated and this process starts in the ER, where the pro-vWF also assembles into dimers in a "tail-to-tail" fashion by forming interchain disulphide bonds[29]. Both the N-linked glycosylation and C-terminal dimerization steps are required for vWF dimers to pass into the Golgi apparatus[30]. Within the trans-Golgi network (TGN), dimers of pro-vWF assemble into multimers by forming "head-to-head" interchain disulphide bonds and subsequently the pro-peptide is cleaved. Multimerization depends on the decrease in pH between the ER (pH 7.2) and TGN (pH 6.2)[30]. The vWF multimers and pro-peptide condense into tubules and become incorporated into nascent vesicles with clathrin/AP-1 coats that protrude from the TGN[29]. vWF pro-peptide is required for both multimerization of vWF and its storage into WPBs[31]. There also exists a relationship between the multimeric state of vWF and its' sorting to WPBs, i.e. less highly oligomerised vWF leaves the TGN and is constitutively secreted whilst high molecular weight vWF is sorted into WPBs, forming a pool of vesicles whose secretion is highly regulated[32]. Once a nascent WPB granule has left the TGN, there are still other steps through which it must pass before achieving maturation. One marker of maturation is acquiring the small GTPase Rab27a[33]. Rab27a is recruited after leaving the Golgi and forms part of a complex which anchors the WPBs to actin at the cell periphery. Moreover, with maturation, vWF tubules also become closer to each other and granule width decreases becoming more electron dense[34].

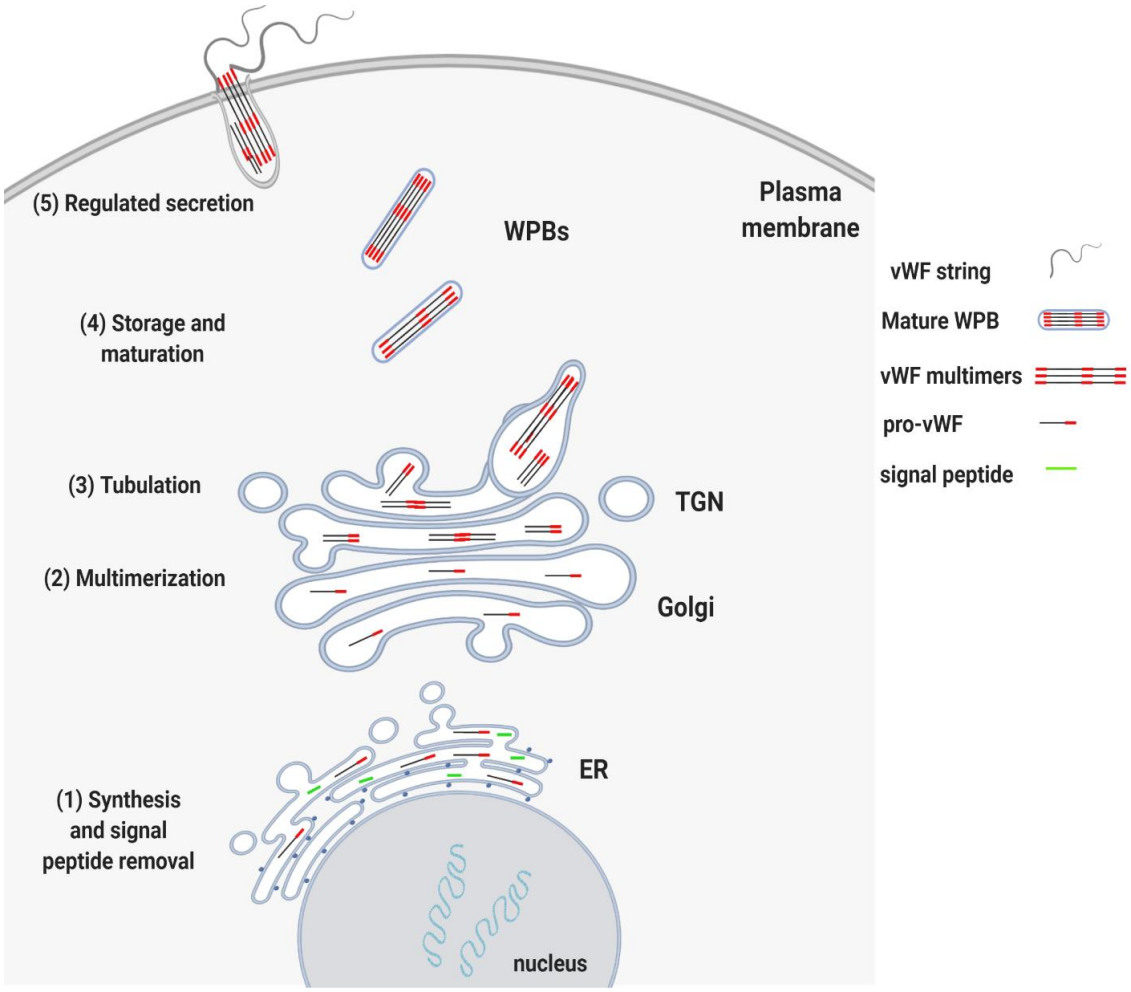

Figure 1.4 Biogenesis of WPBs and processing of vWF. Locations of vWF processing are indicated on the right and the nature of the main vWF modifications are on the left. Pre-pro-vWF is synthesized at the endoplasmic reticulum (ER) where the signal peptide (green) is cleaved to give a precursor, pro-vWF which is transported to the Golgi apparatus. At this time pro-vWF starts to multimerize through the formation of N-terminal disulphide bonds. The remodelling of the multimerizing protein into a protein tubule commences at the TGN where earliest-forming vWF tubules are incorporated into an immature carrier. The immature WPB then carries the vWF towards the cell periphery, and, during its subsequent maturation, the vWF continues multimerizing and forming high molecular weight multimers. At exocytosis, very high molecular weight vWF is released as long platelet-catching strings that are particularly effective in primary haemostasis.

1.2.2 Weibel-Palade Body cargo

Although vWF is the primary component of the WPBs, an increasing number of additional proteins (Table 1.1 and Table 1.2) are known to be recruited to these organelles[35], in line with the wide range of processes that involve WPB release such as inflammation, haemostasis, regulation of vascular tone and angiogenesis.

Table 1.1. List of known WPB components, role and recruitment point

WPB cargo	Role	Recruitment
vWF	Haemostasis	TGN
P-selectin	Inflammation	TGN
Osteoprotegerin	Vascular homeostasis	TGN
Angiopoietin-2	Angiogenesis	TGN
Endothelin-1	Vasoconstriction	TGN
Interleukin-8	Inflammation	TGN
Eotaxin-3	Inflammation	TGN
CD63	Membrane organisation	Post-Golgi
α 1,3-fucosyltransferase VI	Inflammation	TGN
Calcitonin gene-related peptide	Vasodilation	TGN
Insulin-like growth factor-binding protein 7	Angiogenesis	To be determined

Table 1.2 List of potentially novel components of WPBs[36]

Accession	Description
P11021	78 kDa glucose-regulated protein
P02765	Alpha-2-HS-glycoprotein
P21810	Biglycan
P27797	Calreticulin
P43121	MUC18
P10909	Clusterin
P02452	Collagen alpha-1(I) chain

P02461	Collagen alpha-1(III) chain
Q12805	FIBL-3
P14625	Endoplasmin
Q9UNN8	Endothelial protein C receptor
Q9Y2E5	MAN2B2
P02751	Fibronectin
P14616	Insulin receptor-related protein
P08648	Integrin alpha-5
Q86SG7	Lysozyme g-like protein 2
P08493	Matrix Gla protein
Q13201	Multimerin-1
Q02818	Nucleobindin-1
P26022	PTX3
Q9BTY2	Alpha-L-fucosidase
Q9Y646	Plasma glutamate carboxypeptidase
P05121	PAI-1
P16284	PECAM-1
Q9Y4D7	Plexin-D1
P30101	Protein disulphide-isomerase A3
P13667	Protein disulphide-isomerase A4
P07237	Protein disulphide-isomerase
A6NEC2	Puromycin-sensitive aminopeptidase-like protein
P50454	Serpin H1
P09486	SPARC
P07996	Thrombospondin-1
Q5TIE3	Von Willebrand factor A domain-containing protein 5B1
Q5VU13	V-set and immunoglobulin domain-containing protein 8

Some additional components of WPBs are recruited at the TGN whereas several others are delivered to mature WPBs. The secretory proteins angiopoietin-2, osteoprotegerin, and the leukocyte adhesion receptor P-selectin, are recruited during initial organelle formation at the TGN.

P-selectin is a transmembrane protein that is expressed on the endothelial cell surface upon activation and plays an essential role in leukocyte adhesion to the endothelium[37]. P-selectin promotes interaction of leukocytes with the endothelium and mediates the rolling of leukocytes over the endothelial surface leading to firm adhesion and transmigration to the site of inflammation. P-selectin incorporation into WPBs is directed by targeting motifs within the cytoplasmic tail as well as by its luminal domain which is recruited to nascent WPBs as it passes through the TGN and is able to interact with specific domains of vWF[38]. Deficiency of vWF disrupts the targeting of P-selectin to endothelial WPBs. Conversely, deficiency of P-selectin has no effect on the targeting of vWF[26]. Following its exposure at the cell surface, in response to appropriate stimulation, P-selectin is rapidly internalized and transported to the early and late endosomes, from where P-selectin can be recycled to the TGN and can be incorporated in newly forming WPBs by direct interaction with vWF[32]. Like P-selectin, osteoprotegerin appears to be incorporated into WPBs through direct interaction with vWF[39]. Thus, both P-selectin and osteoprotegerin are actively sorted into WPBs by virtue of their ability to interact with vWF.

Angiopoietin-2 is an autocrine regulator of Tie-2 signalling that is markedly induced in endothelial cells by vascular endothelial growth factor or hypoxia[40]. The Ang–Tie system functions as a key regulator of vascular quiescence. Angiopoietin-2 is the dynamic player of the system and its functions are context-dependent[41]. Therefore, further studies will be needed to unravel the molecular mechanisms by which angiopoietin-2 modulates rapid vascular homeostatic functions and responsiveness towards different cytokines and to elucidate the effects of angiopoietin-2 on chronic vascular disease, most notably, atherosclerosis, arthritis and tumour growth. Considering that many proangiogenic factors have been proposed to play a role in the setting of inflammatory angiogenesis, angiopoietins can be considered as proinflammatory mediators contributing to initial steps of pathologic angiogenesis[42]. Angiopoietin-2 incorporation into WPBs, probably occurring at the TGN, requires vWF and release of angiopoietin-2 from endothelial cells is increased in vWF-deficient cells. It has also been suggested a direct interaction between Angiopoietin-2 and vWF within the Golgi body where angiopoietin-2 bound predominantly to the vWF A1 domain[43]. However storage of angiopoietin-2 into WPBs occurs only into WPBs that lack P-selectin; thus the storage of angiopoietin-2 and P-selectin appears to be mutually exclusive[44]. Such findings suggest a further level of complexity in the control of WPB biogenesis; to generate subpopulations within a cell might require sequential formation of

the varied organelles through control of transcription of the non-vWF cargo or by differential recruitment.

Interestingly, another WPB cargo, is the potent vasoconstrictor endothelin-1 (ET-1)[45]. ET-1 is generated by processing of its precursor, big ET-1, by endothelin-converting enzymes. As endothelin-converting enzyme 1 is also localised to the WPBs, conversion of big ET-1 into vasoactive ET-1 most likely occurs in WPBs. This provides a mechanism for the rapid release of large amounts of the vasoconstrictive ET-1 in response to vascular injury[46].

Some WPB components are recruited post-Golgi in a time or maturity-dependent manner. A well-established membrane protein of mature WPBs is the tetraspanin CD63[47]. CD63 is delivered to maturing WPBs in an AP-3-dependent manner via late endosomes/multivesicular bodies. Sorting of endosomal proteins to post–Golgi secretory granules is a characteristic route of lysosome-related organelles suggesting that WPBs share some properties with lysosome-related organelles[38]. The function of CD63 is unclear, but it is a member of the tetraspanin family. These proteins have been shown to associate with integrins, which play important role in leukocyte recruitment. Moreover, it has been demonstrated that upon activation of endothelial cells and subsequent WPB exocytosis, CD63 is transported to the cellular surface where it forms co-clusters with P-selectin, suggesting that it may play a role in early stages of the endothelial inflammatory response[48].

Several additional components are only stored in the WPBs after prolonged activation of the cells with inflammatory mediators. This phenomenon has been observed for the cytokines interleukin-8 (IL-8) and interleukin-6 (IL-6) which are only expressed in the WPBs following their upregulation by interleukin-1β (IL-1β)[49,50]. Similarly, it was observed that eotaxin-3 was present in the WPBs after prolonged stimulation with interleukin-4[51]. Storage of pro-inflammatory mediators in WPBs following upregulation of their synthesis temporarily provide endothelial cells with a rapidly available source of inflammatory mediators.

Thus, endothelial cells appear to tailor WPB cargo in response to various stimuli; certain cargo are constitutively carried in WPBs whereas other constituents are only recruited to WPBs following an inflammatory stimulus. However, this is not sufficient to explain the coexistence of proinflammatory and prothrombotic proteins whose release could be evoked by functionally distinct stimuli. Interestingly, it has been suggested that subsets of granules can be subject to differential exocytosis and/or trafficking to tailor its response to the prevailing vascular condition, although the mechanism behind this differential release remains elusive. It is evident however that these cargos are powerful proteins that play a major role in vascular function.

1.2.3 WPB function

The extensive list of the different biologically active compounds contained into these distinctively cigar-shaped granules, reflect their role in the local and systemic regulation of processes as diverse as haemostasis, vasomotion, inflammation and fibrinolysis, as well as modulating vascular permeability and angiogenic sprouting. A myriad of stimulatory mediators that result from injury or inflammation, such as thrombin and histamine, cause WPB secretion, leading to surface expression of vWF and P-selectin (Figure 1.5). Thus, the Weibel-Palade body is a prominent link between inflammation and thrombosis[52].

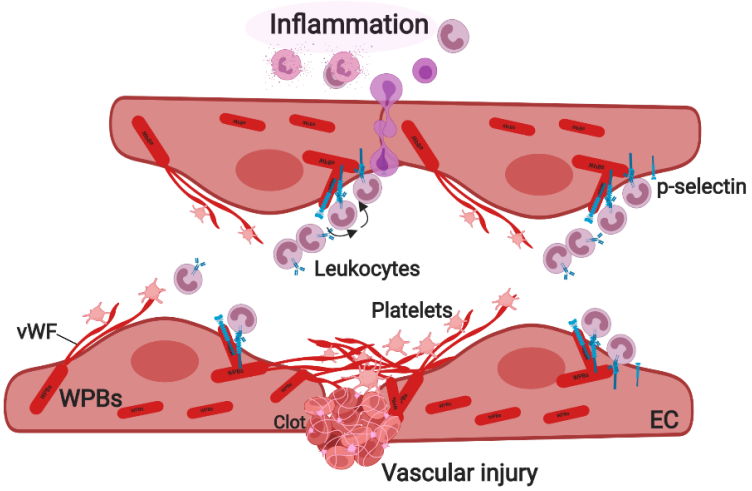

Figure 1.5 Schematic representation of WPB interplay in thrombosis and inflammation. On endothelial activation through vascular injury or inflammation, WPBs release their contents, leading to vWF and P-selectin expression. These adhesion molecules mediate platelets and leukocyte rolling on the vessel wall. The rolling step, mediated by P-selectin exposure on the cell surface, is crucial for leukocyte extravasation to the site of inflammation and it likely helps in the formation of the platelet plug. Vascular injury immediately induces vWF unfurling and formation of long haemostatic strings which play a crucial role in the adhesion of platelets to the damaged site. The platelet plug is stabilised by strands of fibrin.

1.2.3.1 vWF function

vWF is an adhesive plasma glycoprotein which performs its haemostatic functions through binding to FVIII, to platelets surface glycoproteins, and to constituents of connective tissue. vWF acts as a stabilizer of FVIII in the circulation. Formation of a non-covalently bound vWF-FVIII complex protects FVIII from degradation by activated protein C and localises FVIII to sites of platelet plug and subsequent clot formation[53]. When FVIII is activated during blood coagulation, thrombin destroys the vWF binding site and releases FVIIIa. Following a vascular injury, vWF binds specifically to fibrillar collagen type I and III. Once vWF is immobilised in subendothelial connective tissue, its main function is to mediate

adhesive interactions of platelets exposed to rapid blood flow. Hence, highly pro-thrombotic ultra-large vWF released from WPBs is able to form long strings under blood flow which spontaneously bind the GPIb–IX–V complex on platelets, resulting in spontaneous platelet aggregation to the damaged site. These platelet-binding strings are likely to play a significant role in forming a haemostatic plug. Platelet-bearing strings are prothrombotic, and can be cleaved into smaller, less prothrombotic vWF multimers by the metalloprotease ADAMTS-13. Haemostasis depends on the balanced participation of vWF multimers and their degradation by the ADAMTS-13 metalloprotease.

The clinical significance of vWF is also discussed in the section 1.2.5

1.2.3.2 P-selectin function

Alongside vWF, a considerable number of inflammatory and angiogenic mediators are co-packaged into WPBs. Their simultaneous release from this vascular emergency package will also direct leukocytes to sites of inflammation and promote vessel repair. The secretion of P-selectin from WPBs initiates the multistep process of leukocyte recruitment[54]. In the systemic microvasculature, P-selectin and E-selectin mediate the initial leukocyte capture and rolling along the wall of postcapillary and collecting venules. Circulating leukocytes may bind to the selectins expressed by activated endothelium, making the leukocyte quickly decelerate by rolling on endothelial cells. Leukocytes roll on stimulated endothelium and become activated before migrating to sites of inflammation or vascular injury. After activation, leukocytes firmly adhere to endothelial cells as a result of the interaction between their β2 integrins and members of the immunoglobulin superfamily on the endothelium. The same types of receptors also mediate the extravasation of leukocytes. A chemotactic signal present outside the venule induces leukocytes to squeeze between endothelial cells of the venule and migrate into the inflammatory centre[55].

P-selectin expression is crucial for leukocyte extravasation, but it also supports platelets rolling, helping the formation of the haemostatic plug. P-selectin can signal into leukocytes producing procoagulant microparticles containing TF that are recruited into the growing thrombus, where they facilitate generation of thrombin and fibrin[52].

The physiological processes of thrombosis and inflammation greatly influence each other. Therefore, it is not surprising that some of the first response mechanisms, such as secretion of WPBs, are shared in thrombosis and inflammation.

1.2.3.3 Additional WPB functions

WPBs are very versatile and provide the endothelium with a first emergency kit in order to rapidly respond to changes in its microenvironment. For instance, in case of vascular injury in addition to vWF and P-selectin, WPBs also release ET-1 which induces vasoconstriction to prevent unnecessary loss of blood components[56]. Angiopoietin-2 which is upregulated

following angiogenic activation is also readily released from WPBs destabilising endothelial cells by acting as a functional antagonist of Ang-1/Tie-2 system[41]. Following inflammation, some chemokine like IL-8 or eotaxin-3 can be also released from WPBs to support recruitment and migration of leukocytes.

Given WPB role in thrombosis and inflammation to maintain vascular haemostasis, learning how to control WPB trafficking and release will, inevitably, have important consequences for therapeutic interventions.

1.2.4 Mechanisms of WPB exocytosis

vWF is a large multifunctional glycoprotein, synthesised and secreted by endothelial cells, that is central to haemostasis, thrombosis and vascular inflammation. vWF provides a sticky platform that captures all the important components which contribute to these vascular processes. Following its journey through the biosynthesis and maturation process, vWF finds a critical crossroad at the trans-Golgi network: here, vWF is either packaged into nascent WPBs, distinctive regulated secretory organelles, or is secreted directly through the "constitutive" secretory pathway. WPBs store vWF for "regulated" secretion upon endothelial activation, but they can also fuse and release vWF in the absence of activation, a process termed "basal" secretion to distinguish it from "constitutive" secretion[57]. Therefore, vWF secretion from endothelial cells occurs via three main routes: constitutive secretion and basal secretion, both of which occur in the absence of stimulation, and regulated secretion of WPBs in response to stimuli (Figure 1.6). The degree of vWF multimerization is the first well recognised difference between the constitutive and basal/stimulated secretion pathways. While constitutively secreted vWF is composed of mainly low-molecular weight (LMW)-vWF multimers, basally secreted vWF, originating from WPB in the absence of stimuli, is composed of mostly ultra large (UL)-vWF multimers together with a prominent dimer band; and regulated vWF release is exclusively composed of UL-vWF multimers[58]. The multimeric form of secreted vWF largely dictates its haemostatic efficacy, as UL-vWF multimers have a much higher binding affinity for platelets. The secretion of such functionally distinct pools of vWF also differ in polarity of release[58]. Release from the constitutive pathway, is mainly directed to the basolateral side of endothelial cells and is mostly composed of LMW-vWF multimers. Basal vWF release from WPBs, occurs mostly toward the apical side of endothelial cells, with a small amount secreted basolaterally, and is composed of UL-vWF multimers which mediates platelet adhesion when the matrix is exposed following damage to the vessel wall. Regulated release, originating from WPBs after a secretagogue stimulant, occurs predominantly to the apical side of endothelial cells, with some release to the basolateral side, and is exclusively composed of UL-vWF multimers. Highly multimerized vWF, released into the vascular lumen, unfurl and assemble into large strings providing a

spiderweb-like network that function as adhesive platform for circulating platelets initiating a haemostatic event[59].

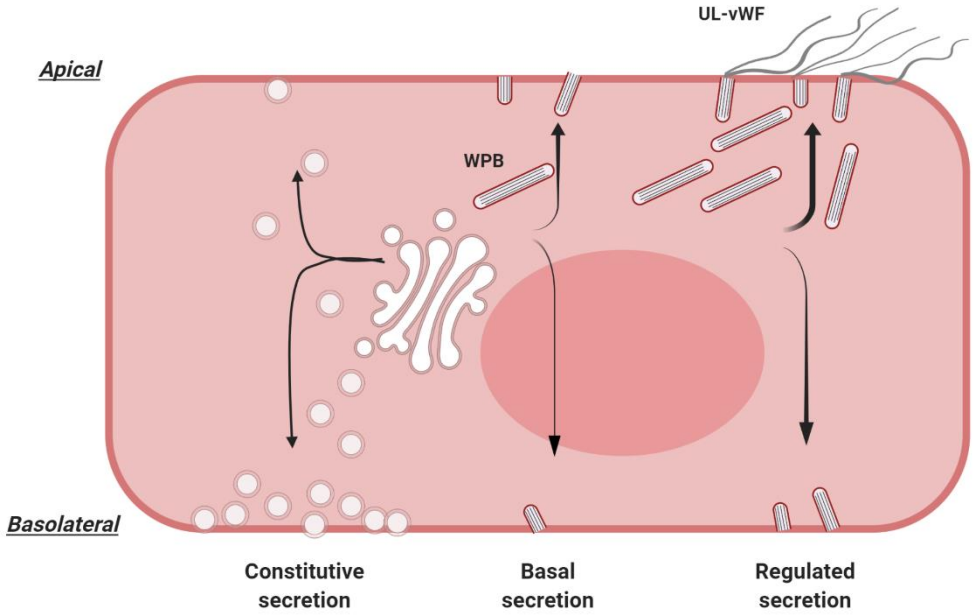

Figure 1.6 Various pathways of vWF secretion from endothelial cells. vWF secretion occurs via three pathways: (i) constitutive secretion of low molecular weight vWF, which is primarily released at the basolateral side of the endothelium; and (ii) basal and (iii) regulated secretion of high molecular weight vWF from WPBs, which is primarily directed towards the apical surface. From the large number of WPBs that undergo exocytosis upon stimulated release, UL-vWF multimers are released and assemble into vWF strings on the apical side of the endothelium.

1.2.4.1 Stimuli and signalling

The endothelium receives multiple stimuli: from surrounding cell types; from molecules and cells in the blood stream[60]; and from shear force[61]. Such signals may be pro-inflammatory, pro-angiogenic, pro-thrombotic and fibrinolytic. After maturation WPBs become responsive to a large number of these signals, termed secretagogues (Table 1.3). These agonists which trigger WPB secretion can be divided into two distinct groups, those that act by elevating intracellular Ca^{2+} levels and those that act by raising cAMP levels in the cell[56].

Table 1.3. Agonists of regulated WPB exocytosis

Secretagogue	Mediator
Thrombin	Ca^{2+}

Histamine	Ca^{2+}
VEGF	Ca^{2+}
Complement	Ca^{2+}
Sphingosine-1 phosphate	Ca^{2+}
Superoxide anion	Ca^{2+}
Ceramide	Ca^{2+}
Purine nucleotides	Ca^{2+} / cAMP
Epinephrine	cAMP
Vasopressin	cAMP
Serotonin	cAMP

Distinct sets of stimuli exist that induce WPB release through different pathways. As part of an integrated response to vascular injury, Ca^{2+}-mediated secretagogues such as histamine and thrombin locally promote a proinflammatory or prothrombotic state (respectively) by immediately causing release of vWF and other WPB constituents (P-selectin, etc.), while simultaneously increasing endothelial permeability and vascular tone. In contrast, cAMP-mediated stimuli such as epinephrine and vasopressin act systemically, increasing endothelial barrier function and inducing a slow but sustained release of WPBs[56].

The acute release of intracellularly stored factors in WPBs, achieved by secretagogues such as histamine and thrombin through intracellular Ca^{2+} release, is one of the main mechanisms controlling homeostasis in the vascular system. Histamine and thrombin use both distinct and common signalling circuits to converge at the same effector pathways which control differential WPB release in line with the appropriate physiological need. In case of vascular damage, thrombin binds a G-protein coupled protease-activated receptor (PAR1) and induces activation of phosphatidylinositol pathway, resulting in a rise of cytoplasmic Ca^{2+}. Ca^{2+} in complex with calmodulin[62] binds the small GTP-binding protein Ral which induces cytoskeleton rearrangements that precede the rapid and local exocytosis of most of the WPBs present in the cell[63].

Acute inflammatory processes can also challenge endothelial cells triggering rapid WPB exocytosis via activation of specific signalling pathways. Histamine is a potent pro-inflammatory mediators which induces WPB release that operates to elevate intracellular free calcium ion concentration ($[Ca^{2+}]_i$) through a G-protein–phospholipase C coupled H1 receptor and production of the second messenger inositol trisphosphate (IP3)[64,65]. Combination of transient increase of Ca^{2+} (with formation of Ca^{2+}-calmodulin complex) and activation of RHO pathway leads to increase myosin light chain (MLC) phosphorylation.

Phosphorylated MLC initiates contraction of actin filaments opening small gaps between adjacent endothelial cells to recruit plasma proteins. The activation of MLC in endothelial cells, in addition to causing plasma protein leakage, initiates the exocytosis of WPBs, bringing P-selectin to the luminal cell surface[66]. Interestingly, exocytosis of vWF induced by histamine is also dependent on nicotinic acid adenine dinucleotide phosphate (NAADP) signalling which evokes Ca^{2+} release from both acidic organelles and ER[67]. Therefore, the rise in intracellular Ca^{2+} in endothelial cells has a major role in leukocyte recruitment by the display of P-selectin on the endothelial luminal plasma membrane however this must be temporally and spatially controlled in order to achieve stimuli-specific responses.

The contents of WPBs are released into the circulation (e.g. angiopoietin-2) or exposed at the plasma membrane (e.g. P-selectin) in response to distinct physiological conditions. Different modes of exocytosis may enable the release of subsets of molecules from WPBs in response to diverse stimuli[29]. For example, WPBs can undergo transient fusion with the plasma membrane forming a small pore which acts as a molecular filter. During this "lingering kiss" small pro-inflammatory cargos such as IL-8 and eotaxin-3 are released whereas vWF is retained. In contrast, multigranular exocytosis has been proposed to be a significant mode of exocytosis in which WPBs coalesce into a "secretory pod" before fusing with the plasma membrane via a large pore. The formation of secretory pods may facilitate vWF string formation by accumulating the content of multiple WPBs before release of vWF long strings responsible for platelet recruitment. However, exocytosis of single WPBs may prevail when the release of other WPB constituents is required, such as the exposure of P-selectin to initiate leukocyte binding. Thus, different modes of regulating WPB secretion at the plasma membrane may provide a mechanism for selective release of WPB components in a stimulus-dependent manner (Figure 1.7).

The data suggests that release of cargo from WPBs is tightly controlled by either integration of distinct signalling pathways activated by different WPB-agonists or by the endothelial cells exocytotic machinery. To date, there has been no evidence of differential trafficking of subpopulations of WPBs, which could tailor the response in time and space.

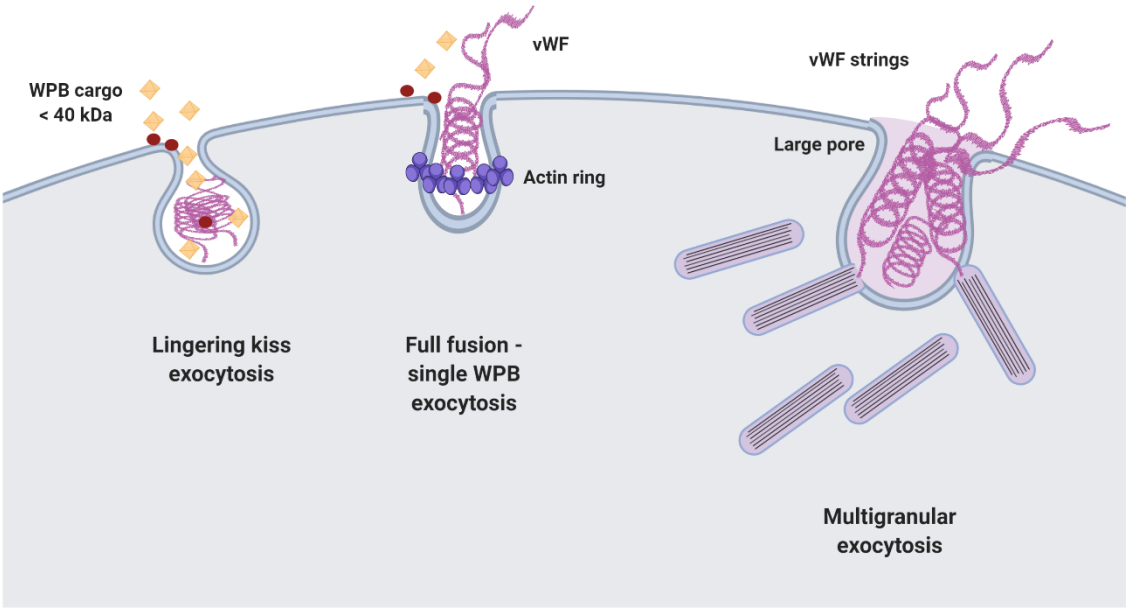

Figure 1.7 Schematic representation of different regulated WPB exocytosis. Lingering-kiss exocytosis is shown, where single WPBs fuse with the plasma membrane via a small fusion pore. Because of the small size of the fusion pore, larger cargo proteins such as P-selectin and vWF are retained, whereas the smaller cargo are released. "Conventional" full-fusion exocytosis in which single WPBs fuse with the plasma membrane, thereby releasing their cargo. The actin ring boost the release of vWF. Multigranular exocytosis where WPBs coalesce into large intracellular membrane vesicles, termed secretory pods, prior to exocytosis. The secretory pods then fuse with the plasma membrane and release vWF strings via a large pore.

1.2.4.2 Exocytotic machinery

Exocytosis of WPBs involves a series of discrete stages: loading of cargo into the nascent granule, granule budding, targeting of the granule to the endothelial membrane, priming of the granule, fusion of the granule and plasma membranes, and, finally, granule recycling. Several super families of proteins control these stages: N-ethylmaleimide-sensitive factor (NSF), soluble NSF receptor (SNARE) proteins, Sec1/Munc18 proteins, and Rab proteins[68].

After emerging from the TGN, in a maturation-dependent manner, WPBs recruit several GTPases of the Rab family (discussed later), including Rab27a, several Rab3 isoforms and Rab15. These Rabs are responsible for the subsequent recruitment of effector proteins to WPBs that correlate with the acquisition of secretion competence and enable redistribution of WPBs population to the cell periphery via interaction with the cytoskeleton and/or plasma membrane.

Rab27a was the first WPB-associated Rab identified in endothelial cells. Rab27a is recruited to WPBs in a content-driven, maturation-dependent mechanism[33]. Acquisition of Rab27a allows mature WPBs to interact with MyRIP (Rab27a specific effector) and myosin Va

(MyoVa); together these proteins anchor WPBs to cortical actin at the cell periphery[69,70]. The actin cytoskeleton plays opposing roles in the release of WPBs. On the one hand, it is necessary for peripheral distribution of WPBs, which is important for a ready releasable pool and depends on myosin IIa. On the other hand, anchoring WPBs to cortical actin at the TGN inhibits release of immature WPBs, allowing full multimerization to be completed before vWF exocytosis. The role of this tripartite complex (Rab27a-MyoVa-MyRIP) in WPB anchoring to actin filaments has been investigated in several studies[70,71]; inhibition of any member of this complex results in increased vWF secretion and a redistribution of WPBs from a peripheral to a more perinuclear localization.

It is noteworthy that Rab27a is involved in more than one stage of secretion, acting in different ways on each occasion. Munc13-4 and synaptotagmin-like protein 4-a (Slp4a) are other two important effectors of Rab27a which promote exocytosis by tethering and docking WPBs to release sites on the plasma membrane, which contain the annexin A2–S100A10 complex[72,73]. The Rab27A–Slp4-a complex docks WPBs and also forms the link between the WPB and the SNARE complex by recruitment of syntaxin-binding protein 1 (STXBP1)[74]. Balance between the negative and positive effectors recruited by Rab27a and cooperation with other Rab proteins like Rab15 and Rab3d, will determine the probability of WPB release allowing endothelial cells to fine-tune its secretory response.

It has also been suggested that Rab3d has a role in biogenesis of WPBs[75]. Overexpression of an active variant of Rab3d resulted in bigger and more spherical WPBs. However, overexpression of an inactive variant of Rab3d resulted in the absence of WPBs suggesting its role in biogenesis and regulation of granule size.

In the final phase of exocytosis, the WPB fuses with the plasma membrane; this process is catalysed by a complex of SNARE proteins that are positioned on the two opposing membranes: the target membrane (plasma membrane) and the vesicle membrane (WPB)[59]. VAMP3 on WPBs has been shown to form a complex with the plasma membrane t-SNARE proteins syntaxin 4 and SNAP23 in endothelial cells which is responsible for membrane fusion during WPB exocytosis. Other regulatory molecules such as synaptotagmin isoforms, Sec/Munc proteins, or syntaxin-binding proteins could interact with these SNARE members, further modulating exocytosis. Once the membrane has fused, there may be a further role for actin in expelling the vWF contents. An actomyosin ring has been proposed to form and localise to WPBs during exocytosis and help 'push' the vWF out into the extracellular environment[76].

A novel addition to the list of Rab proteins participating in the maturation and/or evoked exocytosis of WPBs is Rab35[77]. Rab35 activity is known in the endosomal system, however Bieseman et al., identified Rab35 and some potential downstream effectors as novel regulators of WPBs exocytosis and proposed a model where histamine-evoked WPB release is supported by Rab35 at the level of the plasma membrane. Rab35 depletion significantly

interfered with histamine evoked vWF secretion. Thus, Rab35 is another positive regulator of WPB exocytosis. Future experiments will be required to reveal whether Rab35 shares some effectors and cooperates with any of the other Rabs in the course of WPB exocytosis. Based on the Rab35 activity in the endosomal recycling system, it also remains possible that it acts indirectly by enhancing the recycling of components of the WPB fusion machinery (e.g. plasma membrane-resident SNAREs) back to the plasma membrane. Table 1.4 summarises all the components participating to WPB exocytosis.

Although many of these proteins operating on the fusion machinery represent the core of WPB exocytosis, these are only the skeleton of the complex process of regulated WPB secretion; how they interact with each other, what other components are involved and how they interact with the signalling pathways arising on endothelial activation are questions that are still to be addressed.

Table 1.4. List of WPB exocytotic machinery

WPB exocytotic machinery		
GTPases	Rab27a	RalA
	Rab3b-d	Rap1
	Rab15	RhoA
	Rab35	Rac1
GTPases-binding proteins	MyRIP	RalGDS
	Slp4-a	Epac
	MyoVa	P115RhoGEF
SNAREs	VAMP3	Syntaxin-4
	VAMP8	SNAP23
SNAREs-interacting proteins	Munc18-c	Syntaxin-binding protein 1
	Munc13-4	Syntaxin-binding protein 5
Others	Annexin A2 S100A10	Zyxin
	Phospholipase D	Alpha-actinin

1.2.5 Clinical importance of vWF

In 1926, Dr Erik von Willebrand, a Finnish physician, described an inherited bleeding disorder in the families in Aland Islands with features that suggested that this was distinct

from haemophilia. In contrast to haemophilia, both sexes were affected and a prolonged bleeding time with a normal platelet count was the most important abnormality[78]. It was not until 1971 that it was understood that the deficiency of a new factor, called von Willebrand factor (vWF) and different from FVIII, was actually responsible for the initially called "hereditary pseudo-haemophilia" disorder which was then renamed Von Willebrand's disease (VWD)[79].

Von Willebrand's disease is the most common inherited bleeding disorder and has an autosomal inheritance pattern[80]. The disease is characterized by defective platelet adhesion and aggregation with mainly mucosa-associated bleeding and bleeding after surgery and trauma. The diagnosis is based on a personal or family history of bleeding and laboratory evidence of abnormalities in vWF, factor VIII, or both. Affected patients have reduced levels of functional vWF, and various types of VWD can be distinguished on the basis of phenotypic characteristics. VWD is subdivided into types 1, 2, and 3.

- Type 1, which accounts for 70 to 80% of cases, is characterised by a quantitative deficiency of vWF.
- Type 2, accounting for approximately 20% of cases, is caused by dysfunctional vWF. This qualitative deficiency in vWF levels can be further subdivided into 4 sub-types:
  - Type 2A; decreased platelets adhesion due to selective absence of the largest, most biologically active multimers.
  - Type 2B; increased affinity for GpIbα leads to increased platelet binding and subsequent clearance of vWF.
  - Type 2M; decreased affinity for GpIbα leading to present but ineffective vWF.
  - Type 2N; decreased affinity for Factor VIII leading to present but ineffective vWF.
- Type 3 is rare (accounting for <5% of cases), is the most severe form, and is caused by the total loss of circulating vWF. In 80% of the patients the genetic defects in the vWF gene are null alleles, explaining the complete absence of vWF.

Even though many mutations causing type 1 VWD have been identified, no mutations are found in approximately 30% of patients. Genetic modifiers outside the vWF gene and physiological factors, such as age or pregnancy, probably play a role in reducing vWF levels. Genome wide association studies have identified several other genetic loci that are associated with vWF levels, including the ABO locus and loci involved in clearance or exocytosis of vWF (STX2 and STXBP5-components of the SNARE machinery)[81]. These newly recognised genetic loci may explain the variability in the VWD phenotypes.

A complication in VWD patients (5-20%), which arise from perturbated WPB release is angiodysplasia that causes recurrent gastrointestinal bleeding through small vascular malformations in the gut. The absence of storage compartment, such as in type 3 VWD,

leads to a dysregulated release of a number of angiogenic mediators, such as angiopoietin-2. Absence of WPBs induces constitutively release of angiopoietin-2 promoting pathological angiogenesis[82].

An interesting finding in two recent studies is that the risks of cardiovascular disease and ischaemic stroke are reduced among patients with VWD[83]. vWF deficiency is associated with decreased prevalence of arterial thrombosis among VWD patients and may provide protection against cardiovascular events.

In contrast, several studies have associated elevated levels of vWF with prevalence of cardiovascular disease (CVD), including coronary artery disease, myocardial infarction (MI), and ischemic stroke[83]. Almost all acute coronary syndromes result from thrombus formation in pre-existing atherosclerosis. As a result of plaque rupture and exposure of prothrombotic subendothelial matrix, local thrombus formation occurs, which subsequently leads to coronary artery occlusion and acute myocardial infarction (AMI). Several studies have shown the colocalisation of vWF with platelet thrombi, tissue factor, and platelets with fibrin in fresh coronary thrombi of patients with MI. Furthermore, the presence of vWF at sites of high shear, e.g, at the sites of lesions in the coronary arteries has been shown to play a pivotal role in enhanced platelet aggregation in patients with AMI compared with control plasma[84]. Interestingly, certain rare diseases, such as thrombotic–thrombocytopenic purpura (TTP), provide significant indirect evidence of a pathogenic role of vWF in AMI[85]. TTP is a rare disease caused by a decreased activity of metalloprotease ADAMTS13 and an accumulation of unusually large multimers of vWF. Pronounced rise in circulating UL-vWF which spontaneously binds to platelets to form large aggregates, is associated with tissue ischaemia and myocardial infarction. These various lines of evidence support the hypothesis that vWF is not merely a prognostic marker for presence of CVD and for outcome in AMI but rather directly involved pathogenically as a causative agent[84].

The relationship between altered biogenesis and secretion of WPBs and disease is quite direct in the case of VWD. However, changes in the quantity and quality of WPB exocytosis influence the plasma level of vWF and other prothrombotic and proinflammatory mediators, which in turn contribute to the pathophysiology of cardiovascular disorders. Therefore, advances in understanding the biogenesis and secretion of WPBs will help to identify additional targets for therapeutic intervention in a variety of haematologic and cardiovascular disorders.

1.3 Rab GTPases

Rab proteins are small GTP-binding proteins that form the largest family within the Ras superfamily. Ras superfamily contains five major kinds of small GTPases including Ras, Rho, Ran, Rab and Arf[86]. The GTPase proteins of each subfamily have similar structures, sequences and functions. However, different family proteins play multiple and divergent roles. The Ras family members mainly regulate signalling transduction, gene expression, cell proliferation and differentiation. The Rho family members mainly regulate cytoskeletal organisation but also have an effect on gene expression. The Sar/Arf family control vesicle budding whereas the Ran family regulate nuclear transport as well as microtubule organisation during mitosis. The Rab (Ras-related in brain) GTPase family consist of essential regulators of vesicular trafficking.

It has been 30 years since the yeast Ypt1 and Sec4 and the mammalian Rab GTPase were first identified as evolutionarily conserved, essential regulators of membrane trafficking[87,88]. Rab GTPase in mammalian cells were first identified by Touchot and colleagues in 1987[89]. By screening a rat cDNA library, they identified four genes encoding proteins homologous to the yeast YPT proteins; these genes were named Rab (Ras-like GTPase from rat brain)-1,-2,-3,-4. To date, more than 60 members of the Rab family have been identified in humans that are involved in regulating various stages of intracellular trafficking and exquisitely localised to specific intracellular membranes where they recruit a cohort of effectors to carry out their function[90].

1.3.1 Rab GTPase structure

A common structural design and shared molecular mechanism distinguish proteins in the GTPase superfamily[91]. Each protein in the family is a precise molecular switch that can be turned ON by binding guanosine triphosphate (GTP) and back OFF by hydrolysing GTP to guanosine diphosphate (GDP). This versatile switch enables the transduction of different signals. All Ras GTPases have a GTPase domain consisting of 5 regions (G1-G5) critical in GDP/GTP exchange, conserved throughout all GTP-binding proteins and comprised of 6 β-sheet strands flanked by five α-helices. The C-terminal of the GTPase fold consist of the hypervariable region (35-40 amino acids) followed by the prenylation motif that normally contains two cysteine residues available for geranylgeranylation; a crucial lipid modification that allows membrane association of Rab GTPases. Additionally, Pereira-Leal and Seabra performed bioinformatic analysis and identified additional features that distinguishes Rabs from other members of the Ras superfamily[92]. They identified five conserved motifs, the Rab Family (RabF) motifs 1-5. RabF1 is in the Switch I domain and RabF2, RabF3, RabF4 and RabF5 motifs are in the Switch II domain. The analysis also led to the identification of Rab subfamily-conserved sequences, named SF1– 4, that allowed for grouping of Rabs into

various subfamilies and were predicted to define the sites of interactions with their respective effectors (Figure 1.8).

Because of the overall structural conservation, the differences between the active and inactive states must define the regions that determine the specific functions of each Rab. The switch I and II regions of Rabs are the primary determinants of nucleotide-dependent Rab function as both switch regions interact with the γ phosphate of GTP. When GDP-bound, the switch regions tend to be disordered and undergo major changes to adopt a structurally well-ordered conformation upon binding GTP, allowing effectors binding[93].

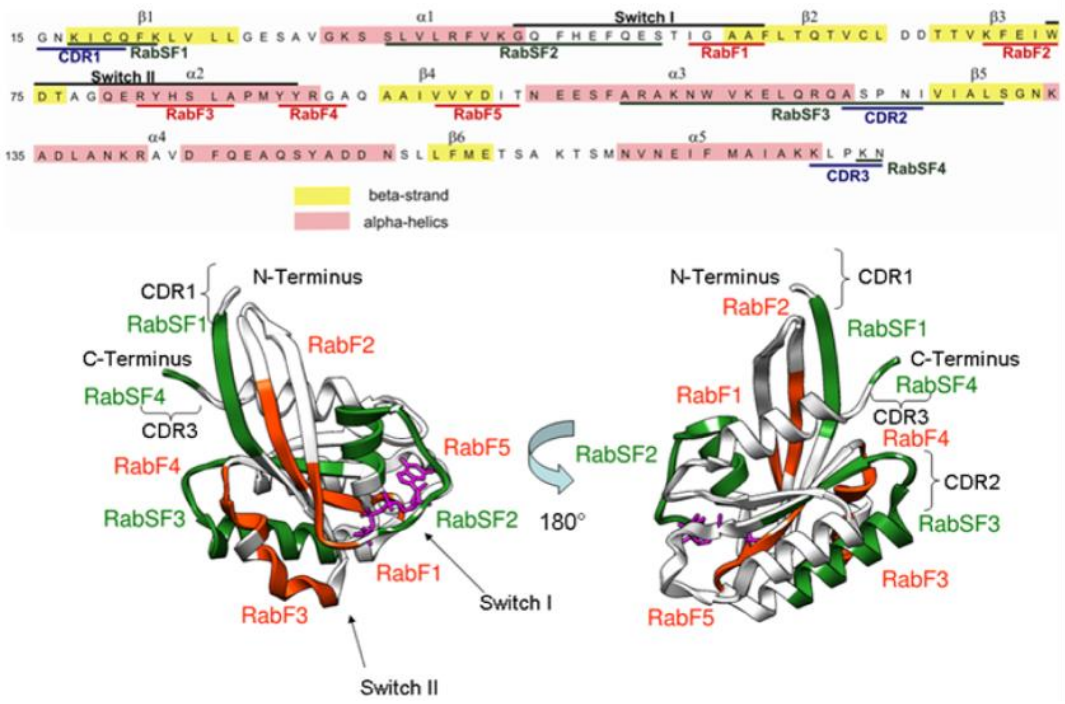

Figure 1.8 Sequence and structural mapping of characteristic segments of Rab proteins. All Rab proteins share a common structural fold, which is composed of five α-helices and six β-strands connected by ten loops. Rab family-specific (RabF1-RabF5) sequence segments that are distinct for Rab GTPases and distinguish them from other small GTPases of the Ras superfamily (Pereira-Leal and Seabra, 2001) are mapped onto the crystal structure of the Rab5A GTPase from H. sapiens in an active conformation (Terzyan et al., 2004) (displayed in orange-red). The nucleotide is shown in purple. The Switch I and II regions, which undergo large nucleotide dependent conformational transitions, are labelled. Adapted from Stein et al., Plos One (2012)[94]

1.3.2 Rab GTPase cycle

Rab proteins cycle between the cytosol and the respective target membrane, acting as molecular switches that alternate between two conformational states: the GTP-bound "ON" form and the GDP-bound "OFF" form[95]. Figure 1.9 shows a schematic representation of Rab GTPase cycle. The newly synthesised Rab protein is recognised by a Rab escort protein (REP) that directs the Rab to a geranylgeranyl transferase (RabGTT) that catalyses the addition of one or, in most cases, two geranylgeranyl lipid groups to the COOH terminus of the Rab in order to be able to bind to its target membrane. Next, REP delivers the Rab, in the GDP-bound form, to its target membrane. The nucleotide-bound state of the Rab influences its localisation and activity. Conversion of GDP-bound Rab into its GTP-bound form occurs through the exchange of GDP to GTP which is catalysed by a guanine nucleotide exchange factor (GEF). The high cytosolic concentration of GTP (~1 mM) ensures that GTP binds as soon as GDP has been released. The active Rab now interacts with effector proteins that specifically facilitate traffic in its respective pathway. The Rab is then converted back to its inactive state by a GTPase accelerating protein (GAP) binding to the Rab to catalyse hydrolysis of the bound GTP to GDP. The inactive Rab is then a substrate for a GDP dissociation inhibitor (GDI), which is able to extract the Rab in its GDP-bound conformation from the membrane and sequestered it in the cytosol. The Rab, bound to GDI, is now ready to be reinserted into a membrane and begin the cycle again. Re-delivery of Rab GTPase to a membrane requires displacement of Rab-GDI and this is proposed to be mediated by a GDI-displacement factor (GDF)[93].

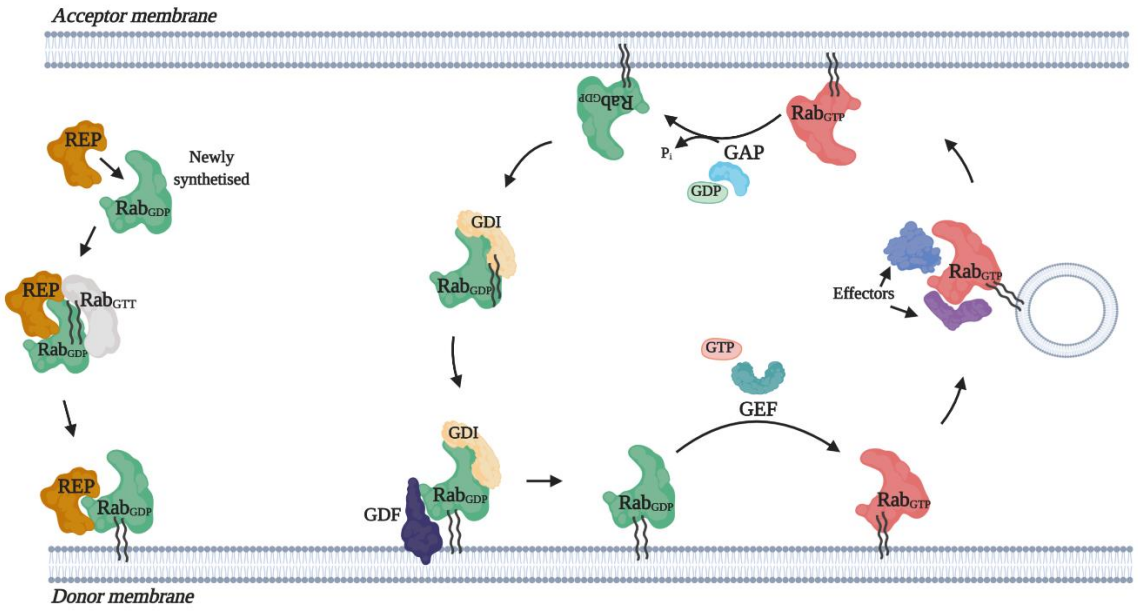

Figure 1.9 The Rab GTPase cycle. Newly synthesized Rab protein associates with Rab escort protein (REP) that present the Rab to the enzyme (RabGTT) that catalyses the addition of lipid tails. REP then delivers the Rab, in its GDP-bound state, to its target membrane where it can anchor to membranes via this geranyl-geranyl-group at the C-terminus. The membrane-bound GDI displacement factors (GDF) regulate the targeting of Rab-GDI complex to specific membranes. A guanine nucleotide exchange factor (GEF) catalyses exchange of GDP for GTP. The GTP-bound Rab (with its cargo) interacts with different effector proteins. Hydrolysis of GTP to GDP is then mediated by GTPase activating protein (GAP). The Rab then is removed from the membrane by guanine nucleotide dissociation inhibitor (GDI) in preparation for the next cycle. In the cytosol, GDIs bind already geranylgeranylated, GDP-bound Rab proteins and thereby control the membrane cycle of Rabs.

1.3.3 Rab GTPase regulation

Despite the very similar overall structure characterising the members of the small Rab GTPase family, the proteins that interact with them, to either regulate their activity or carry out their downstream functions, are very distinct.

1.3.3.1 GDI and REP

GDI and REP proteins are crucial for the molecular function of Rabs. Although both REP and GDI are members of the GDI superfamily, they play different roles in the life cycle of a Rab protein[93]. REP associates with RabGGT to facilitate the addition of geranylgeranyl lipid moieties to the COOH termini of Rabs while GDI extracts inactive, prenylated Rabs from membranes. The structures of Rab-GDI and Rab-REP show that both Rab-REP and Rab-

GDI contain a two-site interface with Rab GTPases where one domain recognises the GDP-bound Rab and the other domain interacts with Rabs geranylgeranylated C-terminus. Thus, they are structurally similar and related in function by their affinity for the GDP-bound form of Rabs. However, REP binds with high affinity to the GDP-bound Rab protein either prenylated or unprenylated, while GDI binds tightly to the Rab with its prenyl groups and binds poorly to the unprenylated Rab protein. The interaction of REP with unprenylated Rabs is consistent with its role in facilitating Rab prenylation by RabGGT, while the main function of GDI is to extract prenylated Rabs from membranes as part of the Rab cycle. The exact mechanism of Rab GTPase extraction from membranes by RabGDI has not been elucidated. However, the very high affinity of RabGDI for prenylated Rab GTPases indicates that another factor must facilitate RabGDI displacement and return of Rab GTPases to the membrane. This has led to the proposal that GDFs assist the correct membrane targeting of RabGDI complexed Rab GTPases.

1.3.3.2 GAP proteins

Small GTPases have a low intrinsic GTPase activity with the half-life of the active state being of the order of 30 min to several hours[96]. Therefore, to be turned off in a significant physiologically timeframe, additional proteins termed GTPase activating proteins (GAP) need to bind to the small GTPases and stimulate the hydrolysis. All characterised Rab GAP proteins to date contain a conserved TBC (Tre2/Bub2/Cdc16) domain that confers GAP activity[97]. The crystal structure of the catalytic TBC domain of a GAP in complex with a Rab GTPase shows that two conserved Arg and Gln 'finger' residues accelerate the catalytic activity of the Rab GTPase by stabilising the β-phosphate of GTP so that γ-phosphate of GTP easily hydrolyse and dissociate from Rab[98].

1.3.3.3 GEF proteins

The rate-limiting step in GTPases activation is the exchange of bound GDP for GTP. Although GDP-dissociation can occur intrinsically, this process is relatively slow and in cells is accelerated by Rab GEFs. GEFs catalyse the dissociation of the nucleotide from the G protein by modifying the nucleotide-binding site, in order to weaken the nucleotide affinity, thus, the nucleotide is released and subsequently replaced. In general, the affinity of the G protein for GTP and GDP is similar, however the resulting increase in GTP-bound over GDP-bound is due to the approximately ten times higher cellular concentration of GTP compared to GDP[99]. Unlike Rab GAP proteins, there are no clear motifs that define Rab GEF proteins. However, the structures of several GEF proteins indicate that they directly interact with the switch I domain, inducing a large conformational change which alters the Rab nucleotide or magnesium-binding site to cause displacement of the bound nucleotide. Rab GEFs can be subdivided into at least four types for their various functional domains[100]. The first large family of Rab GEFs identified were Vps9-domain containing proteins (at least 9 members in humans) that are specific toward Rab5 family members and act in early

endocytic trafficking. The second large family of Rab GEFs, with 18 members in humans, are DENN domain GEFs, acting on several different Rab proteins. Besides these two major families of related Rab GEFs, several other proteins have been shown to possess GEF activity, including multi-subunit complexes such as the TRAPP I and II complexes (GEFs for Rab1 and Ypt31/32, respectively), the Mon1/Ccz1 complex (GEF for Rab7/Ypt7). Furthermore, several GEFs may act on a particular Rab protein with each GEF responding to distinct upstream stimuli, providing multiple avenues for signal regulation.

Additionally, it has been shown that GEFs (together with other factors) play a major role in recruitment of Rabs to certain sites within cells. A Rab GEF cascade has been proposed for the class C vacuole protein-sorting/homotypic fusion and protein-sorting (VPS/HOPS) complex, an established GEF for Rab7, required for Rab5-to-Rab7 conversion within the transition from early to late endosomes[101]. The significance of Rab GEFs for correct Rab membrane targeting has also been demonstrated with Rab27A and its GEF Rab3 GEP involved in recruitment to melanocytes as well as with membrane recruitment of Rab5 by Rabex-5 GEF activity[102]. Therefore, Rab GEFs are also essential components for specific spatial and temporal recruitment of cognate Rab proteins.

1.3.4 Function of Rab GTPase in membrane trafficking

Different Rab GTPases regulate distinct stages in intracellular trafficking from vesicle formation at the donor membrane, trafficking along the cytoskeleton to vesicle fusion at the acceptor membrane (Figure 1.10). Rab proteins regulate their respective pathways by interacting with various effector proteins. Effectors are generally defined as proteins that preferentially interact with the GTP-bound form of their respective Rab. The role of Rab proteins is to recruit effectors such as motor proteins and tethering factors to facilitate downstream membrane traffic events.

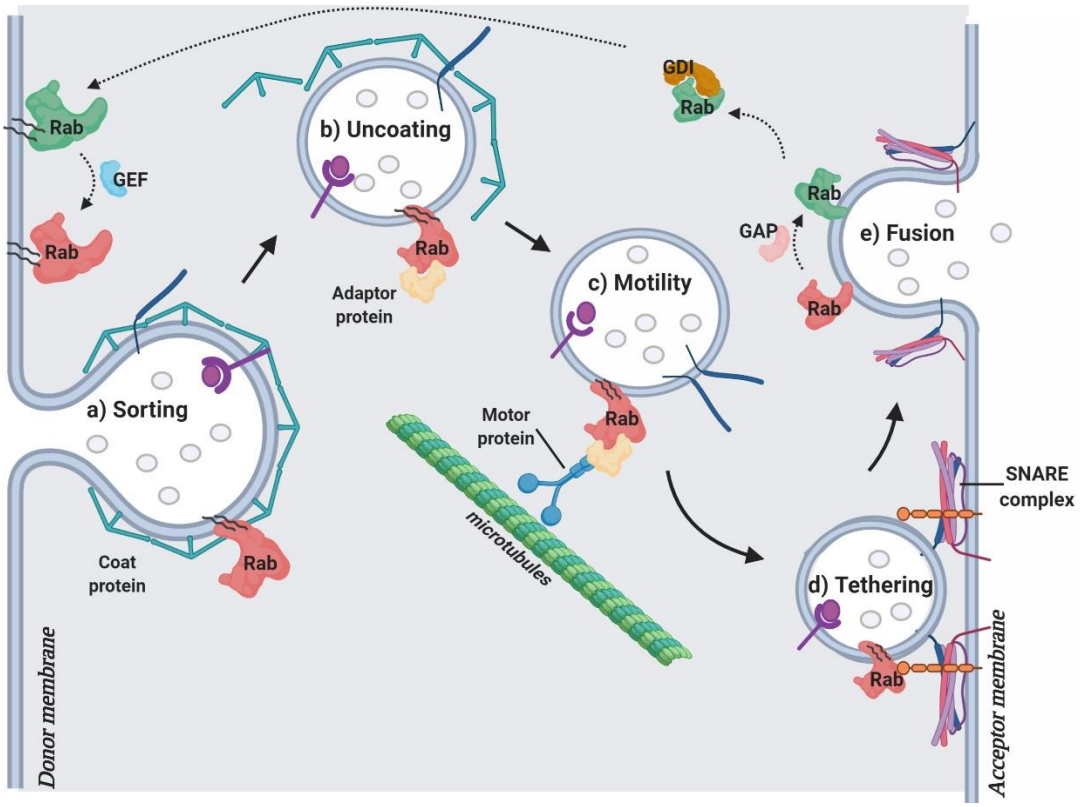

Figure 1.10 Rab GTPase function in vesicles trafficking. Rab GTPases and its effectors can regulate distinct membrane trafficking steps. a) Rab GTPase can recruit sorting adaptors to sort receptors into budding vesicles. b) Following budding of vesicles from donor membranes, the coat is shed to allow the vesicles to fuse with their target membrane. c) Rab GTPases can mediate transport along microtubules, using motor proteins, and actin filaments. d) Rab GTPases can mediate membrane tethering by recruitment of tethering factors which can also interact with and regulate SNARE complex formation and subsequent fusion. e) Following membrane fusion the Rab GTPase is inactivated by Rab GAP, removed from the membrane by Rab GDI and recycled. Subsequent re-insertion into the membrane is mediated by GDI-displacement factor (GDF) and Rab GTPase is GTP-loaded by Rab GEF.

1.3.4.1 Cargo sorting

Cargo selection into specific transport vesicles is a fundamental mechanism in intracellular trafficking. Central to the appropriate sorting of cargo is the recruitment of cytosolic coat complexes which specifically associate with distinct cargos[95]. In addition to the cargo itself, several other determinants, including membrane curvature, lipid composition and Rab GTPases, contribute to ensuring specific coat recruitment to distinct intracellular membranes. An example of a Rab GTPase involved in cargo-specific coat assembly is the late endosomal Rab9, which regulates membrane recycling of mannose-6-phosphate receptors (M6PRs) from late endosomes to the TGN. The cytosolic tail of M6PRs is recognised by the sorting adaptor TIP47, an effector of Rab9. The interaction of Rab9 with TIP47 enhances the interaction between the mannose-6-phosphate receptor and TIP47 during the formation of the transport vesicle and maintains the recycling of M6PRs from the

late endosome to the TGN[103]. Similarly, the cargo-selective subcomplex of retromer, which transports protein back to the TGN, has been shown to be recruited to late endosomes by Rab7[104]. Another Rab GTPase that is important for cargo sequestration is Rab5 which mediates assembly of clathrin-coated pits at the plasma membrane and clathrin-mediated endocytosis of transferrin receptors[105]. The emerging picture is that some Rab GTPases control several key events in vesicle budding from donor membranes, including coat assembly, cargo selection and physical budding.

1.3.4.2 Vesicle uncoating

Following budding of vesicles from donor membranes, the coat is shed to allow the vesicles to fuse with their target membrane. In addition to playing a role in coat formation, Rabs may also play a role in uncoating. A well-studied example is the clathrin coat and its cargo adaptor protein complex AP2 on endocytic vesicles, whose removal has proved crucial for proper membrane trafficking. Clathrin-coated vesicles contain Rab5, and a recent study has shown that this GTPase and its GEF coordinate AP2 uncoating by promoting dephosphorylation of μ2 subunit and increasing PtdIns(4,5)P_2 turnover[106].

1.3.4.3 Vesicle motility

Both the microtubule network and the actin filaments make essential contributions to local and long-range intracellular vesicle and organelle motility. Microtubules serve as tracks for transport via the motor protein dynein, which is implicated in retrograde motility, and kinesin which mediates movement towards the cell surface. Actin contributes to vesicle motility in distinct ways, for example functioning as a track for the myosin family of motor proteins. Attachment of motor protein to vesicles requires high specificity and there are several examples in which Rab GTPases and their effectors proofread these types of interactions[107].

A well-studied example involves Rab27a, which forms a complex with the motor Myosin-Va (MyoVa) and the adaptor protein, melanophilin, which is important for the peripheral actin association of melanosomes, lysosome related organelles[108]. MyoVa then shuttles these Rab27a positive vesicles towards the cell periphery, which is crucial for the proper functioning of melanocytes. A second Rab27a effector, MyRIP also recruits MyoVa forming a ternary complex in endothelial cells which is involved in linking WPB to the peripheral actin cytoskeleton[70]. Other examples include Rab8, Rab10 and Rab11, which can associate with MyoVa isoforms and transport cargo to the plasma membrane[109–111].

While actin is mostly involved in short-range movements of different vesicles, microtubules are mainly responsible for long-range anterograde and retrograde trafficking. Both types of microtubule-dependent motors are regulated by Rab GTPases. Kinesins can be direct effectors of Rab GTPases as first demonstrated by Echard et al., who described direct interaction between Rab6a and KIF20a (kinesin-6 subunit) required for correct cytokinesis[112]. However, published data from the literature indicate that Rab proteins more frequently

associate with their kinesin motors via adaptor/linker proteins that simultaneously bind the Rab and the kinesin motor[107]. For example, Rab27a and Rab27b regulate axonal transport of neurotrophin receptor-containing vesicles by association with KIF5/KLC1 (kinesin-1 subunit) via two linker proteins, Slp1 (synaptotagmin-like protein-1) and CRMP-2 (collapsin response mediator protein-2)[113]. Molecular links with cytoplasmic dynein-1 complexes and members of the Rab6 subfamily are the most understood. Rab6a and Rab6b all directly bind the cytoplasmic dynein-1 Roadblock LC1 subunit and Rab6A also can associate with cytoplasmic dynein-1 via binding the dynactin p50/dynamitin and $p150^{glued}$ subunits[114]. Alternatively, indirect associations with dynein motors has been shown for the late endosomal Rab7[115]. The Rab7 effector Rab-interacting lysosomal protein (RILP) mediates minus-end-directed trafficking of late endosomes by recruiting a subunit of the dynactin complex, which is associated with dynein. Likewise, the Rab6 effector bicaudal D1 mediates attachment of Golgi vesicles to the dynein–dynactin complex in Golgi-to-ER transport. Another recent example is Rab11a which controls trafficking of recycling endosomes processes by linking to the cytoplasmic dynein-1 LIC1 and LIC2 subunits via the Rab11 effector protein FIP3[116]. The multiple ways by which Rab GTPases associate with motor proteins probably reflect the important role these proteins have in attaching the right transport vesicle to the right motor.

1.3.4.4 Vesicle tethering

To ensure fidelity of transport, most membrane transport pathways require factors that "tether" the vesicles to the target membrane before they fuse[117]. These tethering factors fall into two categories: long coiled-coil tethers or multiprotein complexes. Members of both categories of tethers are Rab effectors. Thus, Rab GTPases mediate vesicle tethering by recruiting rod-shaped tethering factors that interact with molecules in the acceptor membrane. Such factors might interact with SNAREs and their regulators to regulate SNARE-mediated fusion of their respective vesicles to the target membrane.

An example of coiled-coil tether protein is the early endosome antigen 1 (EEA1), an effector of Rab5 involved in tethering and homotypic fusion of early endosomes. In particular, formation of EEA1 homodimers tethers two Rab5 vesicles together, promoting homo-fusion[118]. Additionally, a number of Rab27a effectors have been implicated in vesicle docking of exocytic dense-core vesicles to the plasma membrane in a variety of cell types. Specifically, granuphilin tethers Rab27a-positive vesicles at the plasma membrane before fusion through its interaction with the SNARE component syntaxin-1 in a Munc18-1 dependent or independent manner[119,120]. Similarly, rabphilin3a, a Rab27a and Rab3a effector, binds SNAP25, another SNARE component, docking vesicle to the plasma membrane before fusion[121]. Furthermore, additional Rab27a effectors, as already mentioned, are responsible to tether WPBs to the actin cytoskeleton or to the SNARE protein before fusion with the plasma membrane (section 1.2.4.2).

1.3.4.5 Vesicle fusion

The final step of vesicular transport is fusion with the acceptor membrane. Vesicle fusion occurs following the formation of a SNARE complex. Interactions between SNAREs on the target membrane (t-SNARE) and vesicle (v-SNARE) promote fusion by pulling the membranes together. Rab proteins also regulate the SNARE-dependent fusion of transport and target membranes. Rabs can either interact directly with SNARE proteins or with proteins that regulate SNARE function to perform this regulatory function[122]. On Rab5 vesicles, EEA1 and rabenosyn-5 are Rab5 effectors that interact with the SNARE protein syntaxin-6 and the SNARE regulator protein VPS45, respectively[123,124]. Importantly, the reconstitution of Rab5-mediated fusion of proteoliposomes, supplemented with specific SNAREs and Rab5 effectors, has recently been achieved and directly demonstrates the coordination of SNARE-mediated fusion by a Rab and its effectors. As mentioned in previous section, Rab27a effector also bind to SNARE proteins (syntaxin-1 and SNAP25) but how these interactions regulate fusion is still unclear[125]. Specificity of membrane fusion is determined by selection among the many SNARE and proteins which assist assembly of the SNARE-complex. For example, fusion of WPBs with the plasma membrane upon stimulation is highly regulated by the activation of the effector RalA. RalA mediates assembly of the exocyst complex and activation of phospholipase D1 inducing accumulation of fusogenic lipids that facilitate fusion of WPBs after the Munc18c-assisted assembly of the SNARE-complex[29].

1.3.5 Localisation of Rab GTPases in the cells

The ability of Rab GTPases to tightly regulate membrane traffic is in part achieved by the specificity of their association with distinct intracellular membranes. Within cells, they are localised to the cytosolic face of distinct intracellular membranes. Zerial and coworkers were the first to provide evidence that each membrane compartment in the cytoplasm is likely to be decorated with distinct Rab proteins[126]. This was an incredibly important finding because Rabs became the first true molecular markers for different membrane compartments of the endocytic and secretory pathways.

Rab GTPases are reversibly associated with membranes through the post-translation addition of two hydrophobic geranylgeranyl groups to two carboxy-terminal cysteine residues, and this is intrinsic to their role in regulating membrane traffic. The C-terminal hypervariable region has long been proposed to contain the targeting information required to direct Rab GTPases to their correct membrane; however, this domain is required but not sufficient for correct targeting of Rab proteins to their specific locations in the cell[127,128]. In most cases this membrane association is tightly linked with GTP loading and activation of Rab GTPase to stabilise Rab GTPase on the membrane. This ensures strict temporal and

spatial regulation of effector recruitment. The mechanism by which precise Rab GTPase targeting is achieved is yet to be elucidated.

Each Rab protein is localized to the cytoplasmic surface of a distinct membrane bound organelle and appears to control a specific membrane transport pathway[90]. Some Rabs are expressed ubiquitously in human tissues, whereas others are more tissue-specific[129]. For example, Rab3A is a member of Rab protein family that is exclusively associated with the synaptic vesicle of neurons[130], Rab17 is expressed in epithelial cells with Rab13 which regulates assembly of tight junctions,[131] while Rab27a has been found to be predominantly expressed in hemopoietic cell lineages[132]. Rab18 is associated with lipid droplets with a role in releasing lipids in adipocytes[133] whereas, active Rab32 is involved for the fission of mitochondria[134]. Rab12 is involved to transport from peripheral region of cell to perinuclear centrosomes to associate with centrosomes and maintains its integrity[135]. Rab proteins are present on all compartments of the endomembrane system (ER, Golgi, endosomes, lysosomes), the nucleus, the plasma membrane (including cell junctions and focal adhesions), mitochondria and centrioles. The sub-cellular localisation of Rab proteins defines the pathway that they regulate[95,126]. Several reviews summarise the relationship between Rab localisation and function. Stenmark (2009) described Rab GTPases as coordinators of a wide range of vesicles transport reactions (summarised in the Figure 1.11). For example, Rab1 and Rab2 are localized at the ER regulating ER-Golgi trafficking while the Golgi-localized Rab6, Rab33 and Rab40 mediate intra-Golgi trafficking. Rab8 mediates constitutive biosynthetic trafficking from the TGN to the plasma membrane and also participates in GLUT4 vesicle translocation (with Rab10 and Rab14) and ciliogenesis (with Rab17 and Rab23). Rab5, which is localised to early endosomes, phagosomes, caveosomes and the plasma membrane, mediates endocytosis and endosome fusion of clathrin-coated vesicles (CCVs), micropinocytosis (with Rab34 which also mediate lysosomes positioning) and maturation of early phagosomes (with Rab14 and Rab22). Rab21 mediates integrin endocytosis. Rab11 and Rab35 mediate slow endocytic recycling through recycling endosomes, whereas Rab4 mediates fast endocytic recycling directly from early endosomes. Rab15 is involved in the trafficking from early endosomes to recycling endosomes and in the trafficking from apical recycling endosomes to the basolateral plasma membrane. Transport from early endosomes and late endosomes is mediated by Rab7 which mediates maturation of late endosomes and phagosomes, and their fusion with lysosomes. Another late endosomal GTPase, Rab9, mediates trafficking from late endosomes to the TGN. Secretory granules and vesicles are transported from TGN to apico-lateral membranes by Rab3, Rab26, Rab27, Rab37, and Rab38. Rab27 also mediates the translocation of melanosomes and WPBs to the cell periphery. Rab32 and Rab38 are involved in the biogenesis of melanosomes. In this way, Rab GTPases regulate plasma membrane delivery, organelle biogenesis and degradative pathways (lysosomal and autophagic).

Characterisation of around half of the known Rab GTPases, highlighting the diversity of Rab proteins and their effectors, has revealed the extraordinary complexity of membrane trafficking circuits that are controlled by multiple Rab GTPases. Therefore, they truly deserve the name of "master regulator of membrane trafficking"[136].

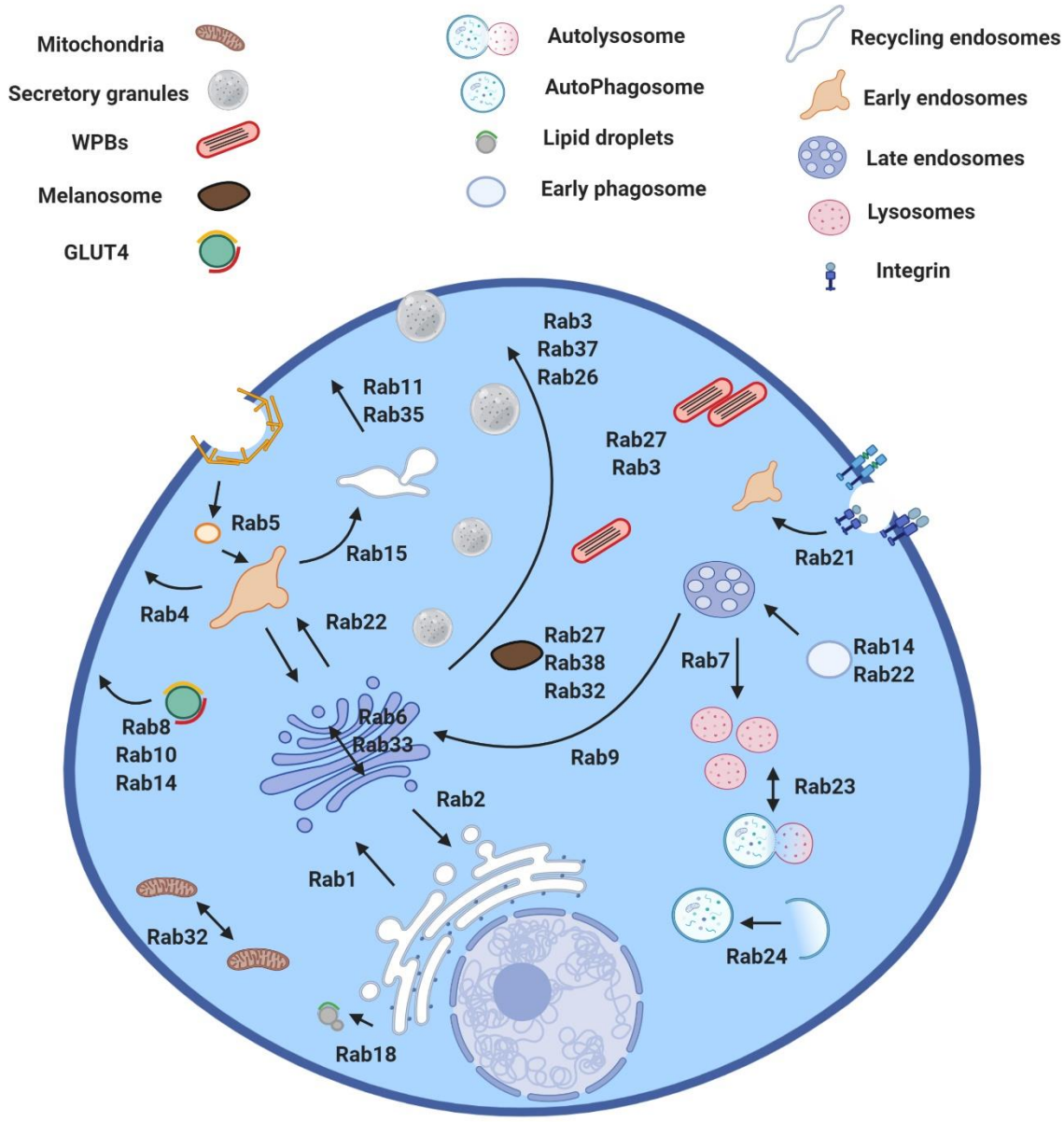

Figure 1.11 Localisation and function of Rab GTPases. Schematic representation of a generic cell with its vesicle transport pathways. The localisation of selected mammalian Rab proteins in the membrane compartments participating in these transport processes is indicated. All of the organelles involved in biosynthetic/secretory and endocytic pathways carry at least one Rab protein on their cytoplasmic face.

1.3.6 Rab GTPases in endothelial cells

A number of small GTP-binding proteins of the Rab subfamily which mediate vesicular transport along the secretory pathway have been found in endothelial cells. An early report in 1992 described for the first time the molecular cloning of an isoform of Rab5 from endothelial cells[137]. Subsequent studies about Rab proteins established the localisation of Rab1, Rab2, Rab3b, Rab4, Rab6, Rab7, Rab8, Rab9, Rab11, Rab13, Rab15, Rab22b, Rab30 in endothelial cells[138,139] (Table 1.5). Most of these Rabs are ubiquitously expressed and localise to specific endosomal structures which have been shown to have a conserved role in the endocytic and exocytic pathways in different cell types. For example, the small GTPase Rab5 has been well defined to control the vesicle-mediated plasma membrane protein transport to the endosomal compartment. Rab5, in endothelial cells, is involved in integrin endocytosis controlling cell adhesion as well as in the internalisation of vascular endothelial (VE)-cadherin, an important component of adherens junctions regulating the endothelial cell polarity and barrier function[140]. Furthermore, the small GTPases Rab4, Rab5, and Rab11 regulate the internalisation and intracellular trafficking of the endothelial cell protein C receptor (EPCR) and internalised FVIIa at different stages in endothelial cells[141]. A Rab-dependent mechanism, involving Rab5a and Rab7a for regulating VEGFR2 trafficking and signalling toward early and late endosomes has also been proposed as specific regulator of endothelial cells migration[142].

The Rab27 and Rab3 subfamilies are specialised Rab GTPases for regulated secretion in a variety of cells. In endothelial cells, as mentioned previously (section 1.2.4.2), Rab27a has a central role in maturation and secretion of WPBs. Rab27a was the first WPB-associated Rab protein to be identified and Hannah et al., showed that this Rab is recruited to and regulates the peripheral distribution and secretion of WPB, ensuring it only occurs once the cargo VWF is fully multimerised. As all Rabs act through their effectors, Nightingale et al., described several of the Rab27 effectors expressed in Human Umbilical Vein Endothelial Cells (HUVECs), including myosin and Rab27a-interacting protein (MyRIP), granuphilin (Slp4a), Slp3, Noc2, Munc13-4, and Slp2a. They are all part of the exocytotic machinery which support appropriate WPBs exocytosis upon stimulation (section 1.2.4.2).

The other Rabs associated with WPBs described by Bierings et al are Rab3D and Rab3B (representing 5% and 95% of expressed Rab3 isoforms, respectively), which indirectly regulate WPB exocytosis. A set of data from Zografou et al[143] significantly complicates this picture as they reported three more Rab GTPases, Rab15, Rab33a and Rab37 targeted to WPBs. However, among these, only Rab15 has a functional role in WPB secretion. More recently, a new study identified Rab35 and some potential downstream effectors as novel regulators WPBs exocytosis.

This very large collection of Rabs is consistent with the notion that they play more than one role in endothelial cell secretion. However, the individual contribution of different Rab

GTPase as well as their cooperation and competition in regulation of endocytic and secretory pathways in endothelial cells is still an open and challenging area of research.

Table 1.5. Rab GTPases identified in endothelial cells.

Rab protein	Localization/Function
Rab1	Ubiquitously expressed, Golgi-ER trafficking
Rab2	Ubiquitously expressed, Golgi-ER trafficking
Rab3b-d	WPBs, biogenesis and exocytosis
Rab4	EPCR trafficking
Rab5	Early endosomes, integrin endocytosis, VE-cadherin internalization, EPCR and VEGFR2 trafficking
Rab6	Golgi, post-Golgi vesicle trafficking
Rab7	Late endosomes, VEGFR2 trafficking
Rab8	Golgi, cell motility
Rab9	VE-cadherin internalization
Rab11	Recycling endosomes, EPCR trafficking
Rab13	Autophagy
Rab15	WPBs, exocytosis
Rab22b	Ubiquitously expressed
Rab27	WPBs, maturation and exocytosis
Rab30	Golgi, unknown function
Rab33a	WPBs, unknown function
Rab35	WPBs, exocytosis
Rab37	WPBs, unknown function

1.3.7 Rab related diseases

Considering the physiological importance of Rab GTPases in many cellular functions, it is not surprising that a number of human diseases can be associated with Rab GTPases and their regulators or effectors. Rab proteins work together with their effectors, coordinate the

dynamics of trafficking pathway and determine the cargo proteins' destination in cells. Aberrant Rab GTPase functions caused by mutations or post-translational modifications will disrupt the regulatory network of vesicle trafficking, which have implications in many human diseases ranging from neurological disorders to cancer.

There are a number of inherited Rab-related disorders which have contributed to the understanding of the physiological function of Rab GTPases and their effectors. A summary of the various monogenic diseases caused by Rab proteins or Rab-associated proteins are listed in Table 1.6.

Table 1.6. Inherited diseases caused by Rab proteins or Rab-associated proteins.

Disease	Rab protein/Rab associated protein	Description
Griscelli syndrome type I	Myo5a[144]	Autosomal recessive, albinism, neurological impairment
Griscelli syndrome type II	Rab27a[145]	Autosomal recessive, albinism, hemophagocytic syndrome
Griscelli syndrome type III	MLPH[146]	Autosomal recessive, albinism
Choroideremia	REP1[147]	X-linked, progressive loss of vision
Non-specific mental retardation	GDI1[148]	X-linked, affected males show moderate to severe mental retardation
Charcot-Marie-Tooth disease type IIb	Rab7a[149]	Autosomal dominant, peripheral sensory neuropathy
Warburg Micro syndrome	Rab3GAP1[150]	Autosomal recessive, neurodevelopment defects

In addition to mutations in Rabs and Rab-interacting proteins, increased or decreased Rab expression or activity is associated with diseases like cancer and neurological diseases such as Alzheimer's[151], Huntington's disease[152] and Parkinson[153].

Membrane traffic plays a significant role in cancer biology, primarily in the loss of cell polarity and in the metastatic transformation of tumour cells[154]. Unlike Ras, no activating mutations in Rab GTPases have been found in any cancers thus far. However, most Rabs show altered expression levels in various types of cancers[155]. Many Rab GTPases have been proposed to

be involved in the progression of multiple cancer types[156,157]. Furthermore, Rab protein overexpression also increases the resistance of carcinogenic cells to chemotherapy[158].

There is also evidence that alterations in Rab function play an important role in the progression of multifactorial human diseases, such as infectious diseases (with role in counteracting bacterial[159] and viral infections[160]) and type 2 diabetes. Abnormal trafficking of the insulin-sensitive glucose transporter 4 (GLUT4) has been described in patients with type 2 diabetes. GLUT4 accumulates in the dense membrane compartments, suggesting that defects in membrane trafficking may be involved in insulin resistance[161]. Rab4 has been found to be implicated in GLUT4 biogenesis, sorting and movement but more studies are needed to define the exact role of this and other Rabs and Rab-associated proteins in GLUT4 trafficking[162].

Recently, upregulation of several Rab family members has been shown in a model of cardiac failure with specific increased myocardial Rab1a expression that can be profoundly deleterious to the heart[163].

In summary, Rab GTPases and associated regulatory factors are frequent targets of mutations which may cause altered expression and/or regulation in a variety of human diseases. In most cases, however, the cause-effect relationship in the pathogenesis is unclear, which opens new avenues for further research in the field.

Although, it is of significant interest to consider the therapeutic potential of modulating Rab protein function, two main points have to be first considered[164]. The first issue is the requirement for cell- or tissue-specific targeting. This is an important consideration for ubiquitous Rab proteins, which may exhibit altered function only in distinct tissues as well as for Rab proteins expressed in a tissue-specific manner. The second issue pertains to transient versus a more permanent modulation of expression. For example, in the treatment of some cancers it may be sufficient to transiently downregulate Rab protein expression, while in the case of genetic loss of function diseases, it will be crucial to have sustained and permanent reconstitution of protein function. Finally, it is important to consider therapeutic interventions that can restore Rab protein function, as well as those that can block function, when the trafficking of specific cargo may need to be modulated. Rab proteins may be regulated at the level of expression or activation. Changes in expression or activation to restore normal function may be achieved either by gene therapy or by modulating specific signalling pathways via small molecule intervention. Due to the lack of clear binding pockets in the active conformation of small GTPases, the use of small molecules has been recently developed to modulate the activity of the small GTPase. To improve the therapeutic efficacy of inhibitors of small GTPases, new approaches have been developed by using different strategies (Figure 1.12), for example by targeting GEF and/or GAP proteins which can specifically modulate "oncogenic" GTPase proteins[99]. However, the generation of these

inhibitors is a challenging goal due to the fine regulatory roles assigned to each of the members of the small GTPases protein family. Most of the new drugs that hamper these strategies have only been proven successful in *in vitro* studies, while demonstrating some limitations at the *in vivo* model and clinical trial stages due to compensatory mechanisms that mask the effect of the inhibitor. Therefore, more studies are required to further validate GEFs and GAPs as therapeutic targets and to further evaluate the capability of these small molecules to specific achieved the desired GTPase modulation.

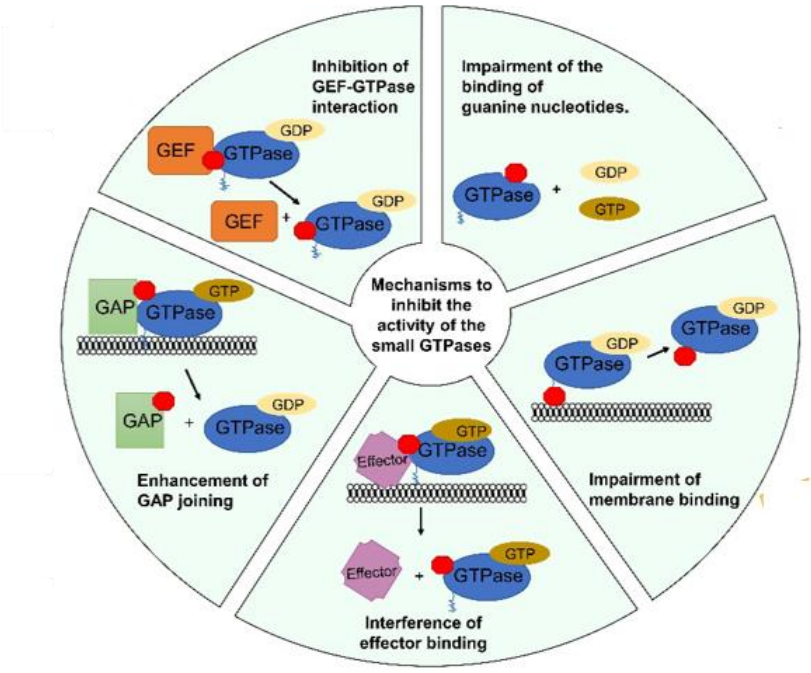

Figure 1.12 New strategies to target small GTPases. Those include generation of new molecules that function as inhibitor of GEF-GTPase interaction or impair nucleotide attachment and small molecules that can enhance GAP activity. Given that most of small GTPases need to be attached to the organelle membrane to exert their actions, the development of novel molecules with the ability to abolish this binding has arisen recently as an innovative strategy to inhibit these molecules. Finally, the development of some drugs that interfere with effector binding could also be great to inhibit small GTPases. Adapted from Prieto-Dominguez et al., Cells Review (2019)[165].

Therefore, in-depth understanding of the molecular mechanisms of Rab proteins function and characterisation of Rab-interacting proteins will undoubtedly provide crucial insights into disease processes and it will ultimately lead to greater success in directing endocytosed drugs to their desired cellular and intracellular targets, geared toward restoring normal function or modulating pathways central to normal physiology.

1.4 CRACR2A-L: a new large Rab GTPase

Most Rab proteins are 20–25 kDa, comprising primarily of a GTPase domain[86]. Recently a new putative Rab protein (CRACR2A-L: calcium-release-activated calcium (CRAC) regulator 2A) has been discovered in endothelial cells[166] and in both human and murine T-cells[167]. It is considered to be a non-canonical Rab protein as it has a molecular mass of 95 kDa, larger than most of the other Rabs, due to the presence of additional Ca^{2+} sensing and coiled-coil domains. Structurally this new Rab is similar in size to Rab44 and Rab45, which have predicted masses of 108 and 83 kDa respectively. They all contain two EF hands at their N-termini, a mid-region containing a coil-coiled domain and a Rab domain at their C-termini.

Currently, Rab44 has only been investigated in one study which shows Rab44 localisation in the Golgi complex and lysosomes and suggests its role in regulation of osteoclast differentiation by modulating Ca^{2+} influx[168].

Shintani et al[169] provide an initial characterisation of Rab45 as a self-interacting protein localized in the perinuclear area of Hela cells and a following linkage study identifies Rab45 as a potential tumour-suppressor gene in uveal and cutaneous melanoma[170]. Moreover, investigating the signalling pathway of chronic myelogenous leukaemia, Nakamura and colleagues[171] identified a role of Rab45 in mediating p-38 activation in apoptosis of chronic myeloid leukaemia progenitor cells.

Human CRACR2A (alternatively EFCAB4B) gene encodes two transcriptional isoforms, CRACR2A-a (herein CRACR2A-L, NM_001144958.1) a long isoform with a predicted molecular weight of 95 kDa and CRACR2A-c (CRACR2A-S, NM_032680.3) a short isoform with a predicted mass of 46 kDa (Figure 1.13).

The short isoform CRACR2A-S, which commonly exists in both human and mouse genome was previously identified to facilitate calcium-release-activated calcium (CRAC) channel function by stabilising Orai1-STIM1 interaction[172]. In particular, the Ca^{2+} release activated channel regulator 2A (CRACR2A), is Ca^{2+}- binding protein that is reported to play a key role in store-operated Ca^{2+} entry (SOCE). In T-cells CRACR2A acts as a cytoplasmic Ca^{2+}-sensor by regulating CRAC channel activation. It facilitates the clustering of Orai1 and STIM1 at the junctional regions between the plasma membrane and the ER at low intracellular Ca^{2+} concentration. This clustering facilitates the activity of CRAC channels, allowing entry of Ca^{2+} into the cells and thus increasing intracellular Ca^{2+} levels. Subsequent dissociation of Orai1 and STIM1 is then mediated by Ca^{2+} binding to CRACR2A and destabilising the ORAI1-STIM1 complex, preventing Ca^{2+} overload. Structurally, the short isoform contains two EF-hands and a coil-coiled domain and share 52% of similarity with the longer isoform which was first identified in endothelial cells by Wilson et al[166] and next by Srikanth et al[167] in T-cells.

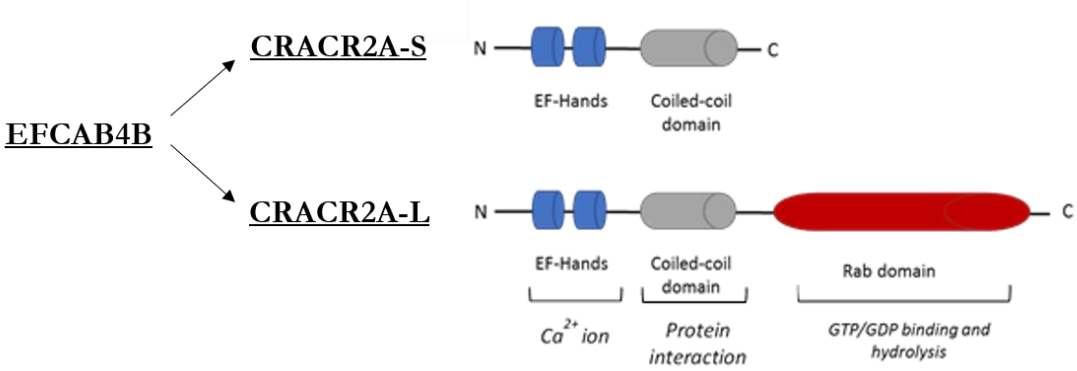

Figure 1.13 Schematic representation of CRACR2A-S (short isoform) and CRACR2A-L (long isoform). Alternative splicing of EFCAB4B gene generates: i) a short isoform (45 kDa) characterised by two EF-hands Ca^{2+}-sensing domain and a coiled-coil domain; ii) a long isoform (95 kDa) characterised by an addition Rab domain at C-terminal.

1.4.1 CRACR2A-L in endothelial cells

CRACR2A protein, as mentioned previously, was initially described in T-cells as an EF-hand-containing modulator of CRAC channels. Investigating CRACR2A in endothelial cells, Wilson et al., found no function of CRACR2A in endothelial cells. Unexpectedly, anti-CRACR2A antibody failed to detect protein of 45 kDa, which is the expected mass of CRACR2A. However, a band around 95 kDa was labelled by the antibody. Moreover, short interfering RNA designed to deplete CRACR2A had no effect on SOCE in endothelial cells but reduced the abundance of a protein with about twice the mass of CRACR2A (Figure 1.14). To obtain an explanation for the larger mass, reference to genome sequence databases indicated that the gene encoding CRACR2A, EFCAB4B, is predicted to be alternatively spliced to give two variants: the short (CRACR2A) and long (CRACR2A-L) variants with a C-terminal Rab GTPase extension. Full-length cloning demonstrated for the first time the expression of the long variant, designated as CRACR2A-L, in endothelial cells. Sequence analysis and construction of a dendrogram suggested CRACR2A-L to be a previously unrecognised member of the Rab GTPase family which is an EF-hand-containing Rab protein that lacks impact on CRAC channels. Therefore, CRACR2A-L was proposed as a novel protein with potential to couple changes in cytosolic Ca^{2+} to cellular trafficking events, thereby impacting endothelial cells responses.

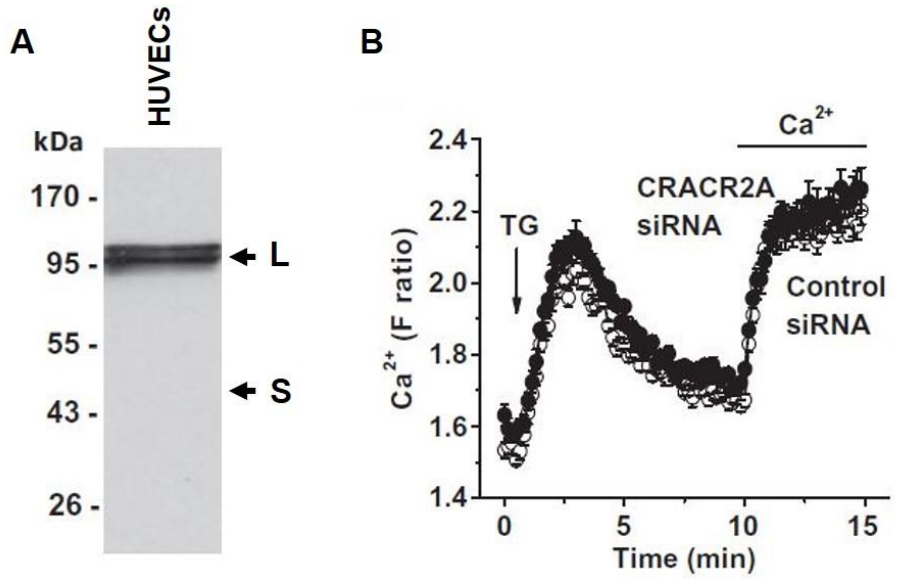

Figure 1.14 CRACR2A expression in endothelial cells. (a) Western blot showing detection of long (L) but not short (S) CRACR2A in endothelial cells. (b) No effect of CRACR2A siRNA on CRAC channels in endothelial cells. TG: thapsigargin. From Wilson et al., BBRC (2015)[166]

1.4.2 CRACR2A-L in T-cells

Srikanth et al., validated the presence of CRACR2A-L in both human and murine immune cells and examined its functions compared to the short isoform[167]. Based on the amino acid sequence, CRACR2A-L contains a Rab domain with a predicted prenylation site at the C-terminal in addition to the N-terminal domains shared with the short isoform (Figure 1.13).

The Rab domain contains a characteristic P-loop, switch I and II regions of small G proteins. The P-loop and switch I region make contact with the γ-phosphate of GTP via Mg^{2+} ions while the switch II region plays a major role in hydrolysis of GTP by interaction with phosphates and water molecules. In this study they also proved the functional activity of the GTPase domain by showing the ability of WT CRACR2A-L to hydrolyse GTP. In contrast the nucleotide binding mutants (T559, Q604, and N658) showed a pronounced reduction in GTPase activity possibly due to defects in GTP binding (T559N and N658I) and hydrolysis (Q604L). Moreover, the amino acid sequence of the GTPase domain showed high similarity to that of Rab GTPases and three-dimensional homology modelling of the high-resolution crystal structure of Rab3a mapped to CRACR2A-L showed almost complete overlap (Figure 1.15).

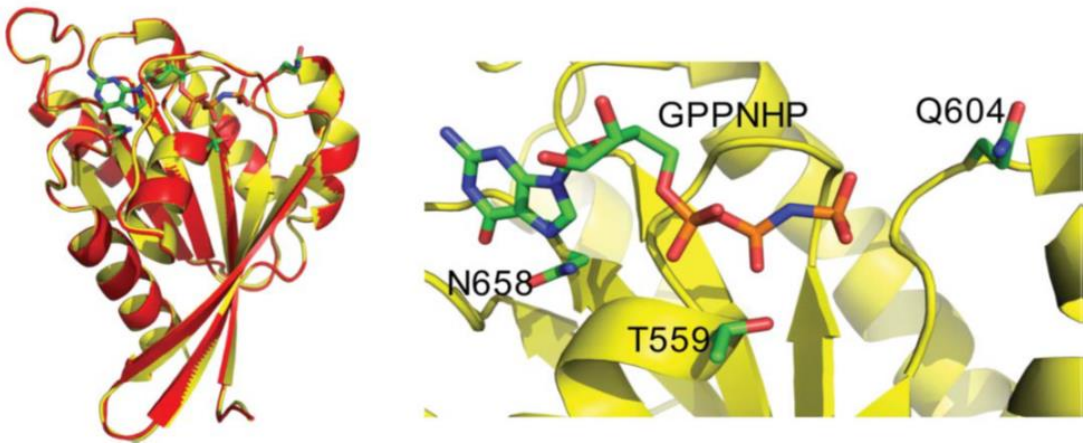

Figure 1.15 Homology modelling of CRACR2A-a GTPase domain (yellow) with Rab3a (red). A zoomed-in view of the GPPNHP binding site (right). GPPNHP and side-chains of residues important for GTP binding and hydrolysis, Thr559, Gln604 and Asn658 are shown in stick representation. From Srikanth et al., Sci Signal. (2016)[167]

In resting T-cells, CRACR2A-L is localised to the TGN and both C-terminal prenylation and GTP binding determine its localisation. Upon TCR stimulation, CRACR2A-L translocates via distinct subsynaptic vesicles from the Golgi to the immunological synapse (IS) where signalling molecules clustered to activate the Jnk pathway. Functionally, CRACR2A-L is necessary for both SOCE and Jnk signalling, whilst the role of the short isoform is limited to SOCE. Furthermore, to elucidate the mechanism of CRACR2A-L recruitment to the immunological synapse, Srikanth and co-worker showed that the interaction with Vav1, via the proline-rich domain of CRACR2A-L, is crucial for its recruitment to the IS after TCR stimulation. These data suggest that additional domains of CRACR2A-L are important to support its unique function to modulate T cell activation by bridging two important TCR signalling pathways: Ca^{2+}-NFAT and Jnk.

Recently, the role of CRACR2A-L in T-cell has been further characterised by Ron Vale's group[173]. Based on the structural similarity between this large Rab GTPase and some well-known dynein adaptors, they provided evidence indicating CRACR2A-L (and Rab45) as new adaptor proteins that activate dynein-dynactin motility. They also demonstrated that the dynein adaptor function of CRACR2A-L is regulated by Ca^{2+} *in vitro*, and that Ca^{2+} release after T cell activation results in up-regulation of CRACR2a–dynein–mediated trafficking. Consistent with Srikanth et al., they found that CRACR2a vesicles move toward the IS during Jurkat cell activation, likely due to the repositioning of the MTOC and the associated endomembrane system. However, Vale and co-workers also observed actin dependent formation of numerous CRACR2A-L cortical puncta at the cell membrane. During T-cell activation, CRACR2A-L activate the dynein-dynactin complex inducing the detachment of these cortical puncta (matured into endocytic vesicles) from the actin cortex and initiate

microtubule retrograde transport towards the MTOC. Thus, the study provides the first evidence about the novel Rab GTPase CRACR2A-L acting as dynein adaptor and mediating Ca^{2+}-regulated endocytic trafficking in T-cells.

1.4.3 CRACR2A-L associated diseases

Various small G proteins of the Ras superfamily are known to play an important role in proximal TCR signalling with some Rab proteins involved in secretion of cytokines and chemokines[174] and transport regulation of immune receptors[175]. The evidence of CRACR2A-L function in activation of the vav1/Jnk signalling pathway necessary for secretion upon T-cell activation suggested a potential contribution of CRACR2A-L to physiological and pathological mechanisms of immune cell related inflammatory diseases.

A genome-wide association study (GWAS) study using histological data, revealed associations between a SNP in CRACR2A gene (EFCAB4B) and lobular inflammation evident in non-alcoholic fatty liver disease (NAFLD)[176]. As a previous GWAS study also showed EFCAB4B association with hypertension[177], it may explain the genetic bases of co-occurrence of hypertension among individuals with NAFLD. Interestingly, a recent study[178] identified EFCAB4B gene as a novel candidate gene involved in pulmonary arterial hypertension, a rare and severe disease affecting small pulmonary arteries and caused by abnormal proliferation of their smooth muscle cells and endothelial cells leading to an increase in pulmonary vascular resistance and heart failure. Consistent with Srikanth et al., EFCAB4B (CRACR2A) is highly expressed in the lung and the study from Barozzi et al[178], suggested that disruptive variants at EFCAB4B gene could interfere with Ca^{2+} homeostasis of smooth muscle cells and/or endothelial cells in which intracellular levels are finely regulated to control vascular tone.

Moreover, five single CRACR2A (EFCAB4B) nucleotide variations have been associated with rheumatoid arthritis, a complex autoimmune disease mediated by interactions between genetic and environmental exposures[179]. Recently, another GWAS study identified associations between variants in CRACR2A (EFCAB4B) gene and the chronic periodontitis suggesting a possible role of this gene in the inflammatory response underlying pathogenesis of periodontal disease[180].

Taken together these data suggest that genetic variations in CRACR2A gene may lead to the pro-inflammatory environment necessary for development of many human diseases which have a prevailing theme of chronic inflammation. Further investigations are required to understand the molecular mechanisms of the inflammatory response underlying these conditions and the role of CRACR2A-L in the onset and/or progression of these diseases.

1.5 Summary

In summary, Rab proteins are implied in a variety of regulatory functions of membrane trafficking, protein secretion, endocytosis and vesicle trafficking. The ability of Rabs to perform these different tasks in a co-ordinated and regulated manner depend on their interaction with different Rab-associated proteins regulating Rab activation, post-translational modification and intracellular localisation.

The central role of these proteins has become clear during the past decade, as part of the progress that has been made in understanding in detail the mechanistic principles of intracellular transport, vesicle formation, movement, and fusion. Acting from organelle formation to exocytosis, Rab proteins have been reported as essential components of the endothelial exocytotic machinery which regulates WPB secretion. Multiple layers of this cellular machinery act together at different stages, leading to differential release of cargo from WPBs. Therefore, a highly regulated secretory system controls the on-demand release of WPB content allowing differentiated endothelial cell responses. However, a fully and detailed picture of how such a complex process acts in an integrated and physiologically responsive way still need to be drawn.

Recently, the identification of a novel large G protein, CRACR2A-L in both endothelial cells and T-cells reveals novel functions of Rab GTPases. Unlike the canonical role of small Rab GTPases, CRACR2A-L contains multiple functional domains and plays an unexpected role in regulating intracellular signalling pathways important for T-cell activation.

The expression of this large GTPase in endothelial cells suggests it could couple Ca^{2+} signalling events to cellular trafficking of specific endothelial secretory granules which respond to changes in intracellular Ca^{2+}; thus, contributing to the molecular mechanisms which control the broad range of endothelial cell functions.

Identification of CRACR2A-L as an EF-hand-containing Rab protein led to the addition of a new Rab family member. Therefore, hereafter, I will refer to the long CRACR2A-L isoform as Rab46 to distinguish from the short non-Rab isoform: CRACR2A.

1.6 Aims and Objectives

Aim

Rab46 may play a role in coupling cytosolic Ca^{2+} elevation to protein trafficking in endothelial cells. The presence of an EF-hand domain raises the possibility that this Rab may be involved in vesicle trafficking in response to alterations in intracellular [Ca^{2+}], thus making it a potential candidate in regulation of WPB trafficking and vWF secretion.

Understanding the function and mechanisms of this novel putative Ca^{2+}-regulated Rab GTPase in physiologically relevant endothelial cells will lead to define new events in vascular physiology and pathologies, contributing for example to the discovery of new targets to manipulate WPB secretion in athero-thrombotic disease.

Hypothesis

Rab46 is a Ca^{2+}-regulated Rab GTPase with important roles in endothelial cells that include regulation of WPB trafficking and secretion of vWF.

Objectives

1. Establish the cellular localisation of Rab46 in endothelial cells;
2. Determine the role of Rab46 in stimuli-dependent WPB trafficking ;
3. Explore the contribution of Rab46 nucleotide-binding domains to regulation of trafficking and localisation;
4. Investigate the molecular machinery necessary for Rab46-dependent WPB trafficking;
5. Identify Rab46 protein partners;
6. Develop a method to investigate direct interactions;
7. Characterise Rab46 global knock-out mice for future studies.

Chapter 2 Material and Methods

2.1 Chemicals and Reagents

All general salts and solutions were purchased from Sigma unless otherwise stated. Other chemicals are summarised in Table 2.1.

Table 2.1. List of reagents

Product	Solvent	Stock	Working concentration	Supplier
Thrombin	H_2O	1000 U/ml	2.5 U/ml	Sigma
Histamine	H_2O	100 mM	30 μM	Sigma
Nocodazole	DMSO	50 mM	1 μM	Merck Millipore
Ciliobrevin D	DMSO	50 mM	40 μM	Merck Millipore

2.2 Cell culture

2.2.1 Human Umbilical Vein Endothelial Cells

Pooled HUVECS (Human Umbilical Vein Endothelial Cells) purchased from Lonza or PromoCell were maintained in Endothelial Cell Basal Medium (EBM-2) supplemented with a bullet kit (Cell Media CC-3156 and Bullet Kit, Lonza, CC-4176). Cells were maintained at 37°C and 5% CO_2 in a humidified incubator. Cells were grown to 95% confluency before passage and used from passage 2 to passage 5.

2.2.2 Human Microvascular Cardiac Endothelial cells

Human Cardiac Microvascular Endothelial Cells (HCMEC) purchased from PromoCell were grown in Endothelial Cell Growth Medium MV2 (EGM MV2). HCMEC were maintained at 37°C and 5% CO2 in a humidified incubator and used between passage 2 and 7.

2.2.3 COS-7

Cos-7 cells were purchased from the American Type Culture Collection (ATCC) and maintained in Dulbecco Modified Eagles Media (DMEM) supplemented with 10% Fetal Bovine Serum (FBS) and 100 U/ml penicillin + 100 μg/ml streptomycin. Cells were maintained at 37°C and 5% CO_2 in a humidified incubator and used between passage 2 and 20.

2.2.4 Mouse Liver Endothelial Cells

Animals were sacrificed at 12 weeks, then dissection and removal of the whole liver was performed. Samples placed into EBM-2 were transferred on ice to the tissue culture laboratory, with all subsequent steps being performed in a laminar flow hood. Mouse liver sinusoidal endothelial cells were isolated using an immunomagnetic separation technique. A whole mouse liver was added to a Petri dish containing dissociation solution consisting of 9 ml 0.1% collagenase II, 1 ml 2.5 U ml^{-1} dispase, 1 μM $CaCl_2$ and 1 μM $MgCl_2$ in PBS solution and then minced with 2 scalpel blades. The tissue-dissociation mix was then transferred into 15 ml centrifuge and incubated at 37°C for 50 mins on a MACSmix rotator. At the end of enzymatic digestion, the sample was passed through 100 and 40 μm cell strainers to remove any undigested tissue. Cells were washed twice in PEB buffer consisting of PBS, 2 mM EDTA and 0.5% BSA, pH 7.2. The washed pellets were resuspended in 1 ml PEB buffer and 30 μl CD146 microbeads (Miltenyi Biotec) and incubated at 4 °C for 15 mins with continuous agitation. CD146 is a specific membrane protein marker for endothelial cells and is highly expressed in mouse endothelial cells.

After incubation, cell suspension was passed through an MS column, set on a magnetic stand and primed with 1 ml of PEB buffer. CD146 positive cells were retained in the column and CD146 negative cells (non-endothelial cell fraction) passed through as eluate. Columns were rinsed twice with PEB buffer, then removed from the magnetic stand and placed into 15 ml centrifuge tubes. 500 μL PEB buffer (x3) were added then the plunger from the kit was applied forcibly through the column to extract the endothelial cells. Samples were centrifuged for 5 mins at 1000 g then resuspended in 500 μL PEB buffer and applied to MiniMACS columns as previously described. The final endothelial samples were centrifuged at 1000 g for 5 mins then resuspended in EGM-2 before being plated onto 6 well plate coated with 0.1% poly-D-Lysine. Cells were incubated in a 5 % CO_2 incubator at 37°C and a full media change was performed 2 hours following isolation to remove cell debris, with half media changes every day thereafter. Purity of mLECs was assessed by phase contrast microscopy and CD31 immunostaining has been shown in previous papers form our lab using the same protocol (Rode B et al., 2017).

2.3 Transfection

2.3.1 cDNA

HUVECs were plated either into Ibidi µ-slide 8-well ($7*10^4$ cells/ml) or into a 10 cm Petri dish ($10*10^5$ cells/ml) and after 24 hours they were transfected using Lipofectamine™ 2000. A 3:1 ratio between Lipofectamine and cDNA (100 ng and 6 µg respectively) was used. 1 hour after transfection the medium was removed and fresh cell culture medium added. Experiments were performed 24 hours post-transfection.

COS-7 cells were plated into a 10 cm Petri dish ($2*10^6$ cells/petri dish) and transfected after 24 hours as described above.

2.3.2 Short-interfering RNA (siRNA)

HUVECs were plated in a 6-well plate ($2*10^5$ cell/well) and after 24 hours they were transfected using Lipofectamine 2000 with 1 ul of EFCAB4B (Rab46) siRNAs or control non-targeting siRNA 50 µM (final concentration of 50 nM) (Table 2.2). Per well of a 6-well plate: 1 µl siRNA was added to 100 µl Opti-MEM in tube 1 and 3 µl Lipofectamine™2000 was added to 100 µl Opti-MEM in tube 2. The tubes were incubated at room temperature for 5 mins. After this time, 100 µl of tube 1 was added to 100 µl of tube 2 and the mixture was incubated at room temperature for 20 mins. The 200 µl transfection mixture was added to 90% confluent HUVECs/well plus 1 ml of cell culture medium. After 5 hours, the medium was removed and replaced with fresh cell culture medium. Experiments were performed 48-72 hours post transfection. Knockdown efficiency was assessed by western blot as described in section 2.6.

Table 2.2. siRNA sequence

siRNA target	Sequence (5'-3')	Supplier
siRNA-1 EFCAB4B	GUGUGAAGGUCAAAAGAGAtt	Ambion
siRNA-2 EFCAB4B	GGAGUUCACUACUGGAUUUtt	Ambion
Control siRNA	UGGUUUACAUGUCGACUAA	Dharmacon
Control siRNA	Unknown	Ambion

2.4 Mutagenesis

A site-directed mutation encoding single amino acid change (T559N) was introduced into the CRACR2A-L gene. Substitution of a threonine (T) residue for an asparagine (N) residue was generated. Mutagenic primers are shown in Table 2.3. Phusion DNA polymerase was used for the reaction. PCR reaction was run for 18 cycles. PCR products were treated with the enzyme Dpn1 (2 μl) to digest any (parental) methylated DNA strands. The mutated plasmid DNA was transformed in E.coli competent cells as per manufacturer's protocol and isolated using the Mini-prep kit (Qiagen). The presence of each desired mutation was confirmed by sequencing (GENEWIZ) and results analysed with ApE software. After sequence analysis, Maxiprep (Qiagen) was performed as per the manufacturer's protocol.

Table 2.3. List of primer for Rab46 mutagenesis

Mutation	Primer (5'-3')
Rab46_T559N	**F**: 5' GGTGGGGAAGAATTCCTTCCTGAGG 3' **R**: 5' CCTCAGGAAGGAATTCTTCCCCACC 3'

Figure 2.1 Sequence alignment of WT-Rab46 and T559N mutant. Highlighted ACA codon (blue) codes for a Threonine in WT sequence of Rab46. Site directed mutagenesis, highlighted in red, changed the codon to AAT coding for an Asparagine.

2.5 Quantitative Polymerase Chain Reaction of RNA samples

2.5.1 RNA isolation

2.5.1.1 RNA isolation from cells

HUVECs were grown to confluence in 6-well tissue culture plates and total RNA was extracted from fresh cells using high pure isolation kit (Roche) as per manufacturer's

instruction. Briefly, medium was removed, the cells were washed with PBS and harvested. Cells pellet was resuspended in 200 µl PBS and 400 µl of lysis buffer was added. After vortexing, the sample was transferred to a filter tube and centrifuged. For each sample 90 µl of DNase incubation I and 10 µl of DNase was added to the tube and centrifuged again. Following three washing steps the RNA was eluted, quantified using the Nanodrop and stored at -80°C for later analysis.

2.5.1.2 RNA isolation from tissues

Samples were harvested by myself and Mrs Katarina Miteva with RNA extraction, Reverse Transcriptase PCR and qPCR on liver and spleen tissues performed by myself and heart and lung by Mrs Katarina Miteva.

Samples were harvested from 12 weeks old mice following sacrifice by appropriate Schedule 1 procedure. The tissues were immediately snap-frozen in liquid nitrogen. In order to process the samples, tissues were placed in a tube with a metal lysis bead and 1 ml Trizol Reagent was added to each sample. Tubes were then placed in a tissue lyser and agitated at 26 Hz for 3 x 1 min sessions. The resultant liquid was transferred to 1.5 ml centrifuge tubes, 200 µl of phenol-chloroform were added and left to settle for 3 mins at room temperature, then spun at 12000g (4°C) for 15 mins. The supernatant (top aqueous phase) was transferred to new tubes and 500 µl of isopropanol were added to each tube and gently mixed before being left to stand for 10 mins. The samples were then spun for 15 mins at 12000g (4°C), and the supernatant discarded. The pellets were resuspended in 1 ml of 75% ethanol (in dH_2O) before a further spin at 8000g (4°C) for 5min. The supernatant was removed carefully, the pellet dried and then 20-50 µl of RNA-free dH_2O was added to each sample which were then stored at -80°C. RNA was quantified using a NanoDrop®.

2.5.2 Reverse Transcriptase PCR

Complimentary DNA (cDNA) was synthesised using a High Capacity RNA-to-cDNA RT kit (Applied Biosystems). 1 µg of RNA was mixed with 5 µl 2x RT buffer, 0.5 µl 20x enzyme mix and nuclease-free water to make a 10 µl total reaction volume. Non-reverse transcribed (-RT) control solutions were prepared and tested in parallel. The solutions were mixed, centrifuged and incubated for 1 hour at 37°C followed by 5 mins at 95°C. This produces cDNA that is ready for use in real-time qPCR application or short-term storage at 4°C.

2.5.3 qPCR

RT-qPCR was carried out using SYBR Green I (Bio-Rad) on a LightCycler (Roche). SYBR Green I intercalates with double stranded DNA and fluoresces when excited at 470 nm. Each reaction had a 10 µl total volume and contained the following components: 5 µl of 2x iTaq™ Universal SYBR® Green Supermix (containing antibody-mediated hot-start iTaq DNA polymerase, dNTPs, $MgCl_2$, SYBR® Green I dye, enhancers and stabilizers), 0.75 µl of

forward primer (0.375 µM), 0.75 µl of reverse primer (0.375 µM), 1 µl cDNA and 2.5 µl nuclease-free water. Real-time PCR primers were designed using the Primer3-BLAST tool (https://www.ncbi.nlm.nih.gov/tools/primer-blast/) and the primer sequences and information are displayed in Table 2.4. All the primers were obtained from Invitrogen. DNA amplification started with 10 mins at 95°C, followed by 40 cycles with 10 seconds at 95°C and 60 seconds at 60°C. The relative abundance of target genes amplified by RT-qPCR were calculated relative to the housekeeping genes, β-actin and GAPDH.

Table 2.4. RT-qPCR primers

Target	Primer sequence (5'-3')
h-vWF	**F**: 5' TTCCCGACAAGGTGTGTGTC 3' **R**: 5' GCCTTCATGCAGAACGTAAGTG 3'
h-Rab46	**F**: 5' GGTCATCCTTGCCTACG 3' **R**: 5' GCTCGCATGAGATCAAGT 3'
h-Rab44	**F**: 5' TCTGAGAGGAGGCCAGGTTC 3' **R**: 5'ATTCTTCCAGCGACAGGTGG 3'
h-Rab45	**F**: 5' CAGCTGGTCAGGAAGTTCA 3' **R**: 5' GCAGTGTCACGAATGTCAGC 3'
h-Rab27a	**F**: 5' AGTTGATGGAGCGAACTGCT 3' **R**: 5' ACATGTCCTCTTCAGGAAGGTT 3'
h-Rab7a	**F**: 5' TTAAGCAGGAAACGGAGGTGG 3' **R**: 5' GGCCTACGTGTGTTCTTGGT 3'
m-Cracr2a	**F**: 5' CTGGAGCGACTCAATCAGAAGC 3' **R**: 5' GAGGCAAGCTGAGTTGGAAGAG 3'
m-Rab46	**F**: 5' GGGCAGCCTGTTGGAAAAGA 3' **R**: ACTCGGTAGTCGATGCCCAC
m-Cracr2a + mRab46	**F**: 5' GATGGACAGACTTGGAGCCC 3' **R**: 5' CAGCAATTTTCTTTCTGAGGGCA 3'
m-Rab44	**F**: 5' GCTGAGCAGACAGTGACCTC 3' **R**: 5' CTGAACCTGGCCTCCTCTC 3'
m-Rab45	**F**: 5' GGAGATCTGGAGTTACGGTGA 3'

	R: 5' AACACGACTAAGCAGCCACA 3'

2.6 Western Blot

Cells grown in 6-well plates or 10 cm petri dishes were washed in PBS and harvested in respectively 70 and 300 µl of lysis buffer (NP-40 supplemented with protease and phosphatase inhibitor cocktail (Sigma). Lysates were centrifuged at 12000g for 10 mins at 4°C. The supernatant containing the soluble fraction was collected and pellet containing nuclei and cell debris was discarded. For quantitative experiments, the protein concentration in each sample was measured using a Bio-Rad Assay (Bio-Rad Laboratories) as per the manufacturer's protocol. Protein concentrations in each sample were estimated by comparison against a BSA protein standard curve.

Equal amounts (10-20 µg) of samples were mixed with a 4x sample loading buffer and boiled for 5 mins at 95°C to fully denature the proteins. The protein samples were loaded alongside with a molecular weight ladder (Bio-Rad or HiMark™ - ThermoFisher) either on a 4-20% gradient gel for protein up to 200 kDa or 7.5% SDS polyacrylamide gel (Bio-Rad) for proteins bigger than 200 kDa. Samples were resolved by SDS-PAGE: low voltage (70V) was applied until proteins migrate into the resolving gel and then higher voltage (120V) for about 1hour was applied to carry on the electrophoresis.

The separated proteins in the gel were then transferred onto PVDF membranes (Millipore) by using wet transfer system for 50 mins at 100 V, except for high molecular weight proteins (such as dynein heavy chain) which were transferred for 90 mins at 90 V with ice pack to reduce the heating. The membrane was then incubated in 5% non-fat milk in TBS-T for 1 hour at room temperature to block non-specific binding sites. Subsequently, membranes were incubated overnight at 4°C with primary antibodies (Table 2.6 primary antibodies with respective dilution). After three washes, 10 mins each, in TBST-T membranes were incubated with horse radish-peroxidase (HRP) donkey anti-mouse or rabbit secondary antibodies (1:5000) (Jackson ImmunoResearch) for 1 hour at room temperature in 5% milk. Membranes were washed 4 times with TBS-T before visualization with SuperSignal Femto Detection Reagents (ThermoScientific) using GeneSys software. If membranes were re-probed, stripping buffer (Restore™- Stripping Buffer) was applied for 20 mins at room temperature and the protocol was repeated from the blocking stage.

Data were analysed using ImageJ Fiji. Bands intensity was compared by drawing a rectangle around each band to generate profile plots which represent the relative intensity of the content of the rectangle per each lane (ex. higher peaks represent darker bands). As western blots will always have some background signal, so the peaks do not reach down to the baseline of the profile plot. Therefore, it is necessary to close off the peak, using a straight

line, so that the size can be measured. When each peak has been closed off at the base with the straight line selection tool, select the wand tool to highlight each peak and get the mean intensity values of each band. These values are then expressed as relative values normalized to a corresponding housekeeping gene (GAPDH or vinculin).

Table 2.5. Western blotting solutions

Solutions	Composition
Sample (loading) buffer (4x)	200 mM Tris pH 6.8, 8% SDS, 40% glycerol, 8% mercaptoethanol, 0.1% bromophenol blue
Running buffer	25 mM Tris, 192 mM glycine and 0.1% SDS, pH 8.3
Transfer buffer	48 mM Tris, 39 mM glycine, 0.5% SDS and 20% methanol
TBS-T	145 mM NaCl, 20 mM Tris-base, 0.5% Tween 20, pH 7.5.

Table 2.6. Primary antibodies used for Western Blot

Primary antibody	Species	Dilution	Supplier	Cat. #
Anti-human vWF	Mouse	1:500	DAKO	MO6016
Anti-human EFCAB4B	Rabbit	1:800	Proteintech	15206-I-AP
Anti-mouse EFCAB4B	Rabbit	1:200	ThermoFisher	PA5-21060
Anti-DYNC1H1	Rabbit	1:1000	Proteintech	12345-I-AP
Anti-vinculin	Mouse	1:1000	Bio-Rad	MCA465GA
Anti-p150	Mouse	1:2000	BD Biosciences	610473
Anti-Na^+/K^+-ATPase α1	Mouse	1:500	Santa Cruz	sc-21712
Anti-GFP	Mouse	1:1000	ThermoFisher	PA5-15256
Anti-Histidine	Mouse	1:1000	Bio-Rab	MCA13964GA

2.7 Pull-down

2.7.1 GFP-trap

HUVECs plated in 10 cm Petri-dishes were transfected with the appropriate GFP plasmids for 24 hours. Cells were washed with PBS and lysed with 250 µl NP-40 lysis buffer. Lysates were left on ice for 20 mins and then centrifuged at 12000g for 10 mins at 4°C. The supernatant was then collected and the protein content was quantified using a Bio-Rad assay. GFP trap is a matrix coupled to agarose beads. These beads are advantageous as they avoid contaminations by heavy and light chain on the western blot, they have a very high affinity binding even to low abundant proteins and they only need a short incubation time with lysate. 25 µl GFP-Trap bead 50% slurry (Chromotek) was used and all wash steps were performed with washing buffer containing 10 mM Tris/Cl pH 7.5, 150 mM NaCl and 0.5 mM EDTA.

GFP-Trap beads were washed 3x with dilution buffer prior to addition to cell lysate. Beads were incubated with cell lysate at 4°C for 2 hours following another wash step (x3). To elute the proteins off the beads 40 µl sample buffer (Table 2.5) was added and samples were boiled at 95°C for 5 mins. Western blotting was used for analysis (section 2.6).

2.7.2 His-tagged protein interaction pull-down

Cos-7 cells were plated in a 10 cm Petri dish and transfected with WT-Rab46 cDNA. 24 hours after transfection cells were washed with ice cold PBS and lysed with 400 µl EDTA-free lysis buffer (BOSTER) plus protease/phosphates inhibitor cocktail EDTA-free 100x (ThermoFisher). Cell lysate was left on ice for 20 mins and then centrifuged at 4°C 12000 g for 10 mins. Supernatant was collected and protein quantified as described. 20 µg of total lysate was used to incubate with pre-equilibrated beads. 100 µl of His Mag Sepharose® Ni beads (GE Healthcare) were equilibrated with equilibration buffer containing 20 mM sodium phosphate, 500 mM NaCl, 20 mM imidazole. Immediately after equilibration, total lysate was added and incubated for 1 hour at 4°C, rotating. The pre-cleared lysate was collected and the beads discarded. At this point, 10 µg of recombinant his-tagged dynein heavy chain (DYNC1H1-CloudClone) were mixed with the cleared lysate and incubated for 1 hour. After incubation, the mixture containing the complex (WT-Rab46 + His_6DYNC1H1), was added to 100 µl of pre-equilibrated His Mag Sepharose® Ni beads and incubated for 1 hour at 4°C, rotating. At this point, the his-tagged protein should be bound the Ni^{2+} beads, thus, the supernatant could be discarded and a linear gradient of imidazole (up to 90 mM) was applied to the beads to reduce unspecific binding. Following these washing steps, elution was performed with elution buffer containing 20 mM sodium phosphate, 500 mM NaCl, 500 mM imidazole. The eluted samples were collected and analysed by western blot (2.6)

2.8 Immunoprecipitation

2.8.1 Immunoprecipitation of exogenous proteins

HUVECs were plated and transfected with cDNA in 10 cm Petri-dishes (3 per condition). 24 hours after transfection cells were washed with ice cold PBS and lysed with 300 µl of NP-40 lysis buffer supplemented with protease and phosphates inhibitors (Sigma). Lysate were left on ice for 20 mins and then centrifuged at 12000 g for 10 mins at 4°C. 20 ug of lysates were saved in order to be used as total input during western blot analysis and the rest incubated with 1 µg of anti-GFP antibody for 4 hours at 4°C, rotating. The mixture was then added to pre-equilibrated Protein G-Sepharose beads (GE Healthcare) and incubated overnight. The next day the beads were pelleted and following removal of the supernatant, washed 3 times with ice-cold lysis buffer and then eluted with 20 µl of sample buffer (4x). The samples were boiled at 95°C for 3 mins and the immunoprecipitated fraction analysed by western blot.

2.8.2 Immunoprecipitation of endogenous proteins

HUVECs plated in 10 cm Petri-dishes were grown for 72 hours. Before harvesting, cells were washes with PBS and cross-linked using 1% PFA for 1 min. Thus, washed with ice cold PBS once and harvested with NP-40 lysis buffer. Lysates were left on ice for 20 mins and then centrifuged at 12000 g for 10 mins at 4°C. Supernatant was quantified (as per section 2.6) and 0.5 mg of total lysate was used to incubate with 2 µg of respective antibody or control IgG from the same species of the primary antibody for 4 hours at 4°C, rotating. 40 µl of washed Protein G-Sepharose beads were added to the lysate/antibody mix and incubated overnight rotating at 4°C. The following day the beads were pelleted, washed 3 times with ice-cold lysis buffer and then eluted with 4x sample buffer. The samples were boiled at 95°C for 3 mins and the immunoprecipitated fraction was analysed by western blot.

2.9 Immunocytochemistry

Cells were seeded ($8*10^4$cells/ml) into Ibidi µ-slide 8 well (IbiTreat). HUVECs were grown for 72 hours before the experiments and the medium was changed every day. Cells, after treatments, were fixed with 4% paraformaldehyde (PFA) for 10 mins at room temperature, washed 3 times with PBS and then permeabilised with 0.1% Triton-X solution for 10 mins at room temperature. Cells were incubated in primary antibody (in PBS) for 1 hour followed by three washes in PBS and incubated with the relevant species-specific fluorescent dye-conjugated secondary antibodies for 30 mins (see Table 2.7 and Table 2.8). Cells were washed three times in PBS and briefly incubated in HOECHST (nuclear stain) before being mounted with Ibidi mounting medium. Cells were imaged on either the DeltaVision microscope

(Applied Precision) or confocal microscope (Zeiss) with Airyscan system as described below. Images were processed using ImageJ software.

Table 2.7. Primary antibodies used for immunofluorescence

Primary antibody	Species	Working dilution	Supplier	Cat.#
Anti-vWF	Mouse	1:200	DAKO	MO6016
Anti-vWF	Rabbit	1:400	DAKO	A0082
Anti-vWF	Sheep	1:200	GeneTex	GTX74137
Anti-EFCA4B	Rabbit	1:100	Proteintech	15206-I-AP
Anti-pericentrin	Rabbit	1:1000	Abcam	ab4448
Anti-pericentrin	Mouse	1:100	Abcam	ab28144
Anti-calnexin	Mouse	1:100	Santa Cruz	sc-46669
Anti-58K Golgi protein	Mouse	1:100	GeneTex	GTX26284
Anti-Lamp1	Mouse	1:200	DSHB	H4A3-C
Anti-tPA	Mouse	1:100	Santa Cruz	sc-515562
Anti-GM130	Mouse	1:100	BD Biosciences	51-9001978
Anti-Rab11	Mouse	1:100	Santa Cruz	sc-166912
Anti-α-tubulin	Mouse	1:200	Santa Cruz	sc-32293

Table 2.8. Secondary antibodies used for immunofluorescence

Secondary antibody	Species	Working dilution	Supplier
Alexa Fluor 488 anti-rabbit IgG	Rabbit	1:300	Jackson ImmunoResearch Labs
Alexa Fluor 594 anti-mouse IgG	Mouse	1:300	Jackson ImmunoResearch Labs
Alexa Fluor 594 anti-goat IgG	Goat	1:300	Jackson ImmunoResearch Labs
Alexa Fluor 647 anti-mouse IgG	Mouse	1:300	Jackson ImmunoResearch Labs

2.10 Microscopy

2.10.1 DeltaVision

DeltaVision is a wide field microscope that uses an iterative algorithm to restore out of focus light (deconvolution) from one plane of a Z stack to another. For each of the imaging experiments 10 focal planes at 0.2 μm per z stack were taken using a Roper CoolSNAP HQ CCD camera. The filter sets used were DAPI (excitation 360/40 and emission 457/50); FITC/GFP/Cy2 (excitation 490/20 and emission 528/38); TRITC/Rhodamine/Cy3/DsRed (excitation 555/28 and emission 617/73) and Cy5 (excitation 632/22 and emission 685/40). The objectives used were 40x/1.35 oil, 60x/1.4 oil or 100x/1.4 oil, as stated in the figures. Image acquisition and processing was performed using SoftWoRx software.

2.10.2 High-resolution

Images were taken on an inverted confocal laser scanning microscope Zeiss LS880 with AiryScan system delivering a resolution of imaging beyond that of a classic confocal point scanning microscope as it can resolve 140 nm laterally and 400 nm axially. This improvement in resolution is achieved by the use of a multichannel area detector with 32 elements –each detector element functions as a single pinhole and allows more light to be collected (Figure 2.2). This differs from a classical confocal microscope, which illuminates one spot on the sample and employs a single pinhole to reject out of focus light. Images were captured using a 63x/1.4 oil objective and 405 nm Diode; Argon/2 (458, 477, 488, 514 nm); HeNe 543 nm and HeNe 633 nm lasers. Images were taken with 2x zoom and Z-series were taken setting the upper and lower limit along with the optimal sectioning suggested. All the images were acquired and processed with Zen software.

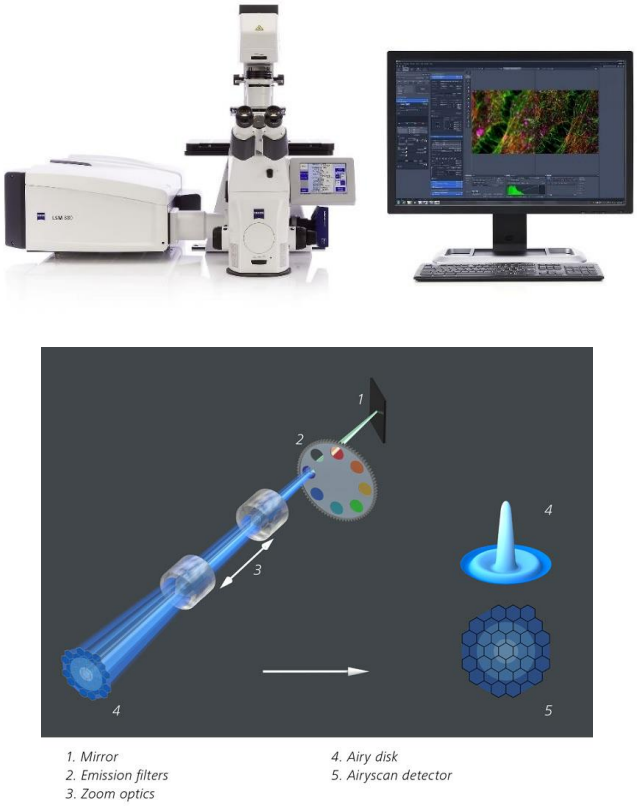

Figure 2.2. Zeiss LSM880 + Airyscan Inverted Confocal Microscope. Microscope and Zen software used for image acquisition with beam path Airyscan diagram. Light from samples is projected onto 32 channel GaAsP detector and the hexagonal design (5) allows to detect the Airy orders in one snap without losing any signal. A better signal-to-noise, resolution and speed is achieved.

2.11 Image analysis

Maximum intensity projections and 3D surface rendering images performed using DeltaVision Softworx or Zeiss Zen accordingly and analysed in ImageJ Fiji. In ImageJ the channels were split, then vWF and Rab46 channels subjected to background subtraction depending of the noise level. The noise estimated using a region of interest in the background for measurement and the mean subtracted to the entire image. Pixels whose intensity values are similar to the background were replaced with the mean background intensity value.

2.11.1 WPBs counting

For WPBs counting, segmentation of WPBs was applied. A local threshold algorithm (Bernsen method) with 15 radius applied and a binary image was created. The numbers of particles (WPBs) were calculated according to their size in every image and normalized to

the numbers of nuclei per image. Number of vWF positive cells and the number of nuclei was determined using cell counter plugin.

2.11.2 Colocalization analysis

WPBs marked with vWF antibody and endogenous Rab46 fluorescent structures quantified using ICY software (Spot detector plugin). WPBs and Rab46 vesicles were delineated by ~ 14 px and 4-7 px spot size respectively. Detection of Rab46 (green spot) only over WPBs structures (red spot) was performed selecting the red channel as driver channel and the ROI module to detect the green spots.

2.11.3 Analysis of the cellular distribution of Rab46 Mutants

Pixels intensity of Rab46 mutants in the perinuclear area was measured using Oval profile plugin in ImageJ (https://imagej.nih.gov/ij/plugins/oval-profile.html). At first step, an oval was drawn around the nucleus, enlarged by 20% and then the plugin, with the option radial sum, was executed to create a pixel intensities profile plot per each cell.

2.11.4 WPBs and Rab46 cellular distribution

The first analysis of vWF and Rab46 distribution in the perinuclear area was obtained using the RGB profiler plugin in ImageJ (https://imagej.nih.gov/ij/plugins/rgb-profiler.html). Pixels intensity was measured along a straight line across different nuclei and the obtained plot profile shows the pixel intensity on the y-axis and the distance along the line is on x-axis.

Cellular distribution and particle intensity were determined using Fiji (Figure 2.3). I designed a customised macro (see Appendix) to automate the analysis. Briefly, a 16-bit image was loaded in Fiji. The channels were split and a binary mask was created using a Default threshold on the DAPI channel. Noise was reduced using a median filter and if required adjacent sites split using the watershed algorithm. A distance map was generated. Green and red channels were duplicated to sample the original pixel intensities of WPBs and Rab46 structures. Each channel was segmented using a threshold algorithm (Max Entropy) and the distance and intensity of each particles from the nucleus was measured. The macro automatically exports results tables with distance and intensity values per each particle, binary images of the distance map and .tiff images of each channel per analysed image. 5 to 10 widefield images (40x) were analysed per experimental group. Distance (Min) and integrated intensity (IntDen) values imported in OriginPro as X and Y values respectively. Distance values range from 0 px (nucleus) to 255 px (Periphery). This list of numerical values was binned into three areas: Perinuclear ($x < 2\ \mu m$) – Intermediate ($2\ \mu m < x > 5\ \mu m$) – Periphery ($x > 5\ \mu m$) where x is the distance from the nucleus to cells periphery. The integrated intensity normalized by the total fluorescence intensity of the image. The mean values were calculated for each area and averaged among all analysed images. The mean values averaged

among all the biological repeats were presented as bar-plots with mean ± SEM where Y-axis denoting "Normalized (integrated) intensity" and the X-axis denoting the distance from the nucleus indicated the average distribution of the analysed signal based into the three areas in the analysed cell population.

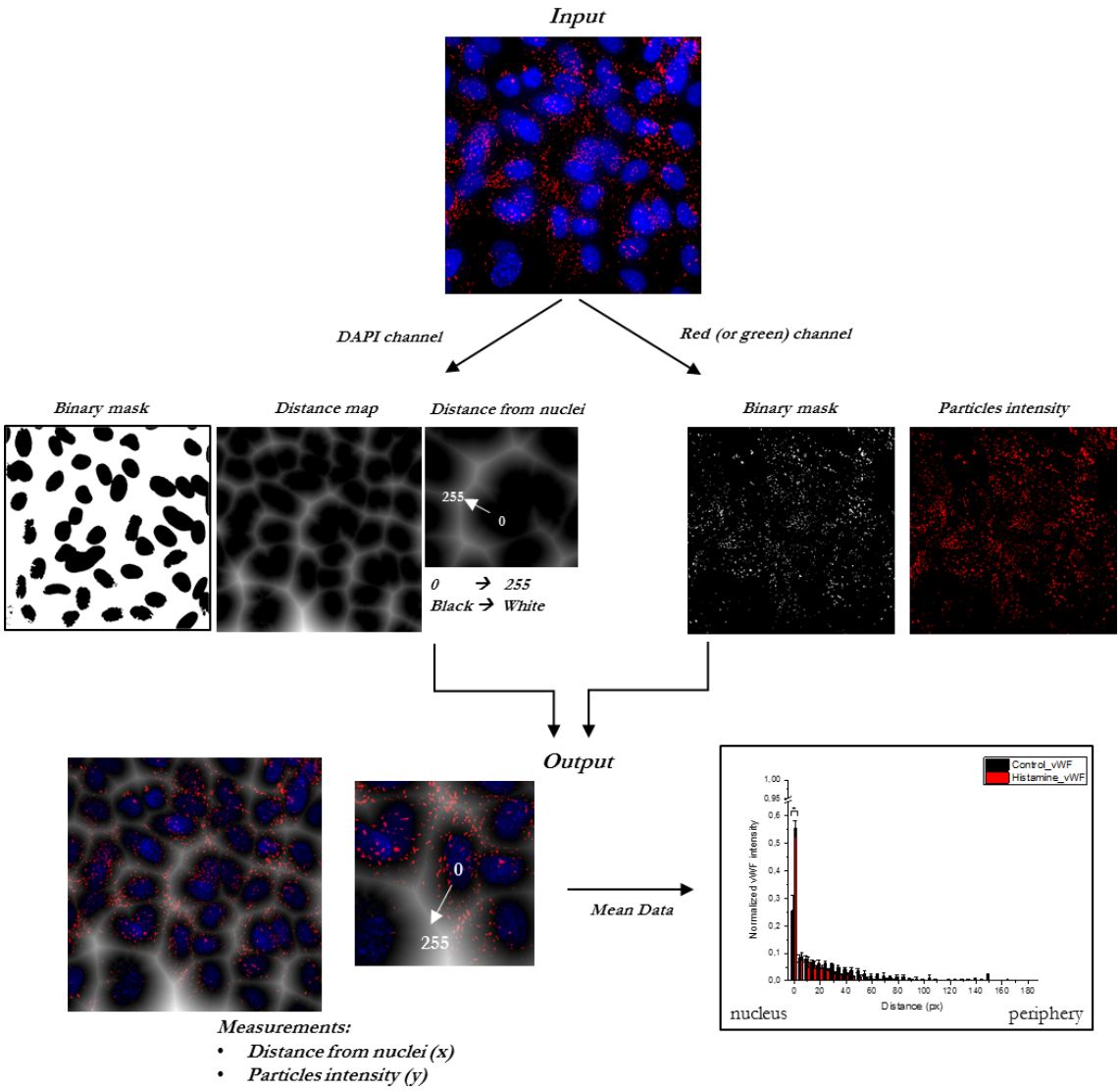

Figure 2.3 Image analysis workflow to quantify Rab46 and vWF cellular distribution. Raw images were uploaded on Fiji as input. The channels were separated and thresholded individually to get an accurate binary mask. A distance map was generated on the DAPI channel were each pixel is replaced with a grey value equal to that pixel distance from the nearest background pixel (nucleus: black = 0). Distance from the nucleus of each segmented particle on the red or green channel, with their respective intensities was measured. Therefore, the outputs (distance and intensity measurements) of the summarised workflow were analysed and plotted in OriginPro. The distance is on the x-axis and the mean normalized intensity is on the y-axis.

2.12 Data analysis

All average data is represented by mean ± S.E.M. Paired t-test performed as appropriate when comparison among two data groups was sought. For comparison among three or more mean values, one- or two-way ANOVA performed to determine whether significant differences exist amongst groups, coupled with Bonferroni post hoc test. Statistical significance was considered to exist at probability (p) ≤ 0.05 (* ≤ 0.05, ** ≤ 0.01, *** ≤ 0.001). Where comparisons lack an asterisk, they were not significantly different and/or marked as not significant, n.s. OriginPro 2017 software (USA) used for data analysis and presentation. n/N represents number of independent biological repeats/number of technical repeats.

2.13 Mice studies

2.13.1 General

Murine work was carried out in accordance with The Animals (Scientific Procedures) Act 1986 (Amended 2012). Mice were kept in the University of Leeds animal facility under standard conditions, including a 12-hour sleep/wake cycle, with access to water and chow diet ad libitum. Experiments were conducted under Home Office Project License P606230FB. All studies were approved by the University of Leeds Ethics Committee. Male and female animals were ear notched at weaning, with these samples being used for genotyping (see section 2.13.3).

2.13.2 Cracr2a $^{-/-}$ mice

The Cracr2a mouse strain used for this research project was created from ES cell clone 15424A-C4, generated by Regeneron Pharmaceuticals, Inc. and obtained from the KOMP Repository (www.komp.org). The colony C57BL/6N-Cracr2a$^{tm1.1(KOMP)Vlcg}$ is generated following the strategy illustrated in Figure 2.

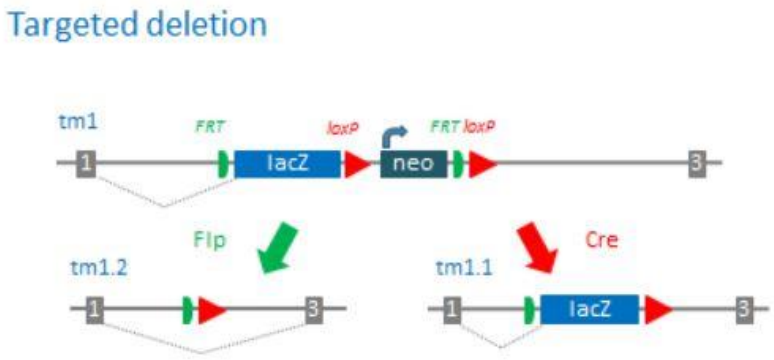

Figure 2.4. Velocigene CREed Deletion allele strategy. Mice that contained the reporter-tagged null allele, (tm1) were bred to Cre-expressing mice. This resulted in removal of the B-actin promoter and the Neomycin gene it activated. The tm1.1 allele remains a lacZ reporter and is a NON-conditional knock-out of the gene.

The litter we received from the KOMP repository was a mix of a few heterozygous mice with C57BL/6N wildtype mice. Therefore, for the first round of breeding, we first increased the numbers of heterozygous mice to ensure a stronger breeding colony prior to setting up het x het matings. The latter strategy illustrated in Figure 6.1 led to generation of some homozygous mice as well as control wild-type. Genotyping was performed and homozygous and wild-type mice were selected for breeding (hom x hom and WT x WT) to generate a strong homozygous and wild-type colony. At this point genotyping was not needed anymore. As for a preliminary study littermate controls were not used at the moment. Littermate controls will be used for future studies.

2.13.3 Genotyping

Mouse genotyping was performed by taking ear notches at weaning age. The samples were sent for automated genotype PCR service (Transnetyx – Cordova, TN) using specific primers designed by the company.

2.13.4 Phenotyping

Both female and male mice between 8 and 12 weeks were used for the initial phenotyping studies. Physical appearance, fertility and mortality rate was observed at the beginning. Next metabolic phenotyping was performed.

2.13.4.1 Body weight

Both Cracr2a $^{-/-}$ knockout and control WT mice were weighed at 8 weeks and 12 weeks until they were sacrificed for further experiments.

2.13.4.2 Organ weight

Animals at 12 weeks were sacrificed following schedule 1 procedure. Body weight was measured prior to organ collection. The heart, pancreas, kidneys, spleen and subcutaneous and visceral fat were dissected and weighed prior to being snap frozen in liquid nitrogen and stored at -80°C for mRNA/protein analysis for subsequent analysis. Liver and lungs were weighed as well and either snap frozen for PCR analysis or fixed in 4% PFA for histological analysis. Organ-to-body weight ratios were calculated normalising the weight of each organ with its respective body weight.

2.13.4.3 Histological analysis

Liver samples were fixed overnight and then kept in 70% ethanol until further analysis. Liver tissues from female Cracr2a $^{-/-}$ and control mice were processed at the St. James's hospital histology facility (Leeds). H&E staining was performed by the histology department at St. James's hospital and imaged slices were sent and opened with Aperio ImageScope for analysis.

2.13.5 Metabolic phenotyping

2.13.5.1 GTT

Animals were fasted overnight with access to water ad libitum. The following morning, the mice were weighed before being placed under conscious restraint. A small incision was made in the distal part of the tail of each animal in order to obtain a tail vein blood sample of 1-2 µl that was analysed with a glucometer and testing strips. Fasting glucose was measured first and then mice were treated with 200 mg/mL glucose solution (1 mg per gram of body weight) administered via intraperitoneal injection. Repeat tail vein blood samples were taken at 30 min intervals until 120 mins after the initial injection. Between measurements animals had free access to water and were not restrained.

2.13.5.2 ITT

This experiment was conducted in similar fashion to the GTT (section 2.13.5.1) except that animals were fasted for two hours, rather than overnight. Fasting glucose was measured and mice then underwent intraperitoneal injection of insulin at a dose of 0.75 IU/Kg of body weight with tail vein blood glucose measurements taken at the same time intervals as for GTT. Animals were monitored closely for any signs of hypoglycaemia throughout the experiment. No mice required injection of glucose to correct hypoglycaemia.

Chapter 3 Rab46 is a novel Rab GTPase that localises to Weibel-Palade bodies

3.1 Introduction

CRACR2A isoform-a (Rab46) is a unique Rab GTPase with multiple functional domains. The existence of CRACR2A-a was discovered and validated in endothelial cells by Wilson et al[166]. CRACR2A protein (CRACR2A-c) was initially described as a 45 kDa protein involved in Ca^{2+} channel dynamics in immune cells[172] . However, in endothelial cells, Wilson et al using a validated anti-CRACR2A antibody in western blot only detected a band at 95 kDa. Molecular cloning and sequence analysis revealed this 95 kDa protein to be the proposed CRACR2A isoform-a, a longer isoform than CRACR2A-c, that contains an additional highly conserved Rab domain. In endothelial cells, CRACR2A-a has no effect on Ca^{2+} channels so we hypothesize that the additional C-terminal Rab GTPase sequence affects the location and function of this protein. We have since named CRACR2A-a Rab46, which is how I will reference it going forward.

Srikanth et al. validated the presence and function of Rab46 in murine and human immune cells[167]. Rab46 localises to TGN in resting T-cells and its localisation is strictly dependent on the intrinsic GTPase activity of the Rab domain. The sequence of the GTPase domain shows several conserved residues with other small Rab GTPases. Moreover, mutations which impair the nucleotide binding activity show a reduction in the GTPase activity indicating high similarity with already characterized functionally active G-proteins. Besides its intracellular localisation being influenced by the nucleotide binding activity of the Rab domain, other domains contributed to activation-dependent Rab46 translocation to the immunological synapse and its subsequent activation of Ca^{2+} dependent-NFAT and JNK signalling.

The main aim of this chapter is to gain insight into the endogenous localisation of Rab46 in endothelial cell in resting conditions. Identifying its intracellular distribution will help us determine its role in endothelial cell trafficking. Super-resolution imaging was used for more precise Rab46 localisation and single point mutations were introduced into the Rab domain to study the effect of the GTPase activity on Rab46 localisation. Moreover, siRNA specifically targeting Rab46 was used to investigate the effect of protein silencing on endothelial cell function. This chapter reveals that endogenous Rab46 is primarily targeted to a subpopulation of Weibel-Palade bodies (WPBs) suggesting a potential role of Rab46 in regulating WPB trafficking and vWF secretion.

3.2 Rab46 localisation in endothelial cells

First, in order to study Rab46 localisation in endothelial cells, I validated a commercially available antibody raised against Rab46 using western blot analysis. A first indication of the antibody specificity was given by Wilson et al., showing the presence of a single band at 95 kDa in HUVEC lysate. For further validation, Rab46 was depleted in endothelial cells using two siRNAs targeting different regions of Rab46 mRNA and the antibody specificity analysed with western blot (Figure 3.1a). A single band at the known molecular weight (95 kDa) was observed in the mock and control siRNA transfected cells whereas a reduced band intensity was observed in Rab46 siRNA transfected cells. As a single band of the correct molecular weight was only identified in the endothelial cells expressing Rab46, this encouraged the use of this antibody for immunofluorescence imaging studies. Here, overexpression of Rab46 was used as positive control to further test antibody specificity (Figure 3.1b). Wild-type Rab46 (WT-Rab46) was overexpressed in endothelial cells and immunostained after 24 hours for Rab46. Immunostaining depicts cells with small rod-shaped vesicles which resemble endothelial specific WPBs, therefore vWF was used as a marker of WPBs to co-stain endothelial cells transfected with Rab46. Merged images show specific localisation of exogenous expressed Rab46 (green) to WPBs (red). However, some cells displayed a strong cluster in the perinuclear area, most likely due to a slow intrinsic GTP hydrolysis typical of many Rab proteins (data not shown). In order to observe the suitability of the antibody in detecting endogenous Rab46, endothelial cells transfected with Rab46 siRNA or control siRNA were fixed and immunostained. Control cells immunostained for Rab46 using anti-Rab46 antibody (green) revealed an evenly distributed vesicle-like pattern similar to the overexpressed protein. Despite the presence of some non-specific fluorescence, green intensity was greatly reduced in Rab46 depleted cells confirming suitability of the antibody to detect endogenous Rab46 in endothelial cells (Figure 3.1c). Validation of commercially available anti-Rab46 antibody for both western blot analysis and immuno-fluorescence assays in endothelial cells lays the foundation for all the next investigations.

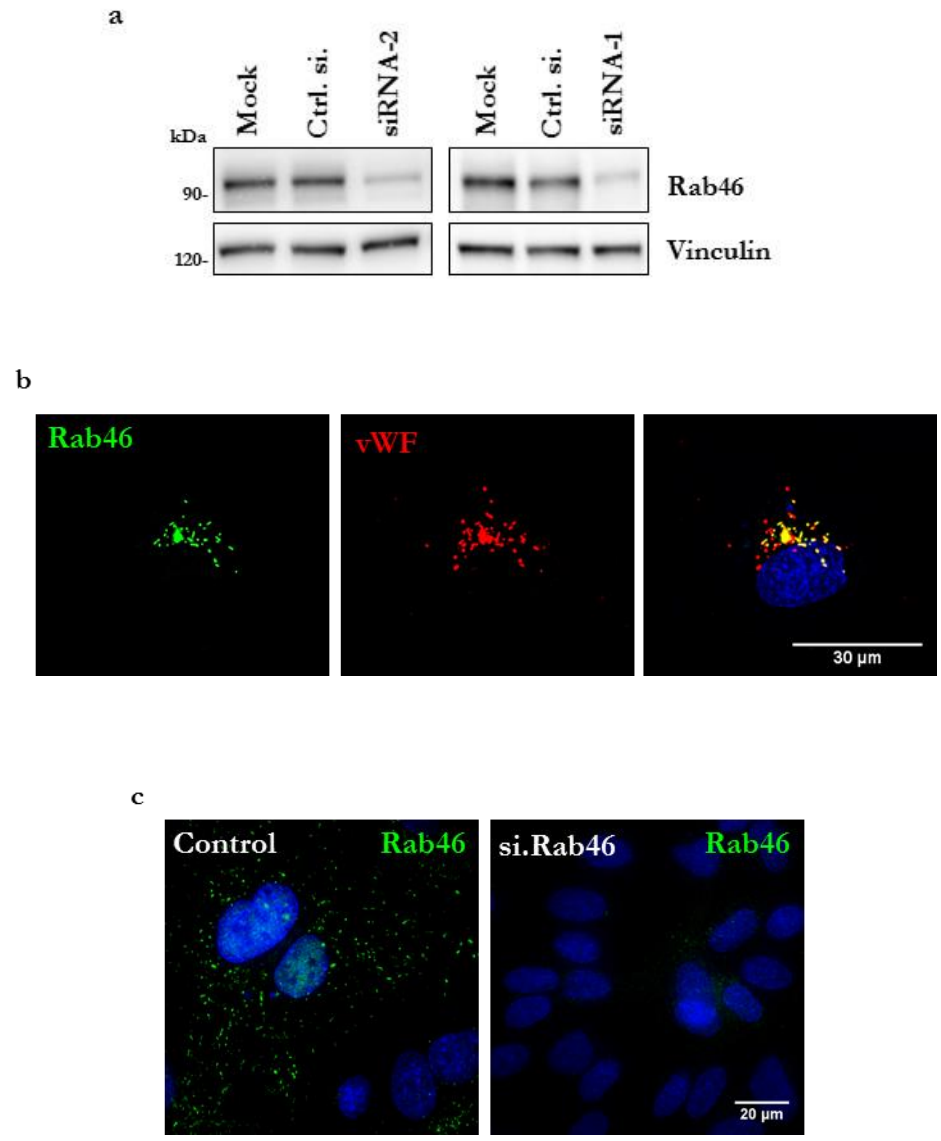

Figure 3.1 Validation of Rab46 antibody. (a) Representative western blots depicting specificity of Rab46 antibody. Rab46 depleted cells, transfected with two different siRNAs, show reduced intensity bands compared to control siRNA. (b) Immunofluorescent DeltaVision imaging of HUVECs transfected with wild-type Rab46 (green: anti Rab46) show Rab46 is localised to WPBs (red: anti vWF). DAPI (blue) shows nuclei. Scale bar = 30 µm. (c) Immunofluorescence showing endogenous Rab46 (green) in control and Rab46 depleted endothelial cells. Scale bar = 20 µm

3.3 Endogenous Rab46 localises to Weibel-Palade bodies

In order to establish the role of Rab46 in endothelial cells, subcellular localisation of endogenous Rab46 was investigated. HUVECs were grown for 72 hours into Ibidi µ-slides and immunostained for Rab46. As overexpressed Rab46 localised to endothelial WPB rod-shaped vesicles, cells were co-stained for vWF, a marker for WPBs, in addition to Rab46. Endothelial cells were first imaged using a DeltaVision deconvolution microscope (Figure 3.2a) and then an inverted confocal laser scanning microscope Zeiss LS880 with AiryScan system to increase the resolution (Figure 3.3). Immunofluorescent staining of Rab46 (green) shows a cytoplasmic vesicular-like pattern characteristic of WPBs which was similar to the vWF staining (red). Indeed, merged images of cells stained for both vWF and Rab46 revealed co-localisation of Rab46 to WPBs in HUVECs (Figure 3.2a). HUVECs are a model system for studying WPB regulation. However, to confirm Rab46 specific localisation in endothelial cells from different vascular beds, human cardiac microvascular endothelial cells (HCMECs) were also stained for Rab46 and vWF (Figure 3.2b). Immunofluorescent imaging confirms that Rab46 (green) localises to WPBs (red) in cardiac microvascular endothelial cells, indicating this is not specific to HUVECs.

To further investigate Rab46 association with WPBs, high resolution microscopy was used to achieve a better understanding of the association. Endothelial cells stained for vWF (red) and Rab46 (green) were imaged using a confocal microscope with AiryScan system, z-stacks were acquired and maximum intensity projections were shown as representative images (Figure 3.3a). The cigar-shaped morphology of WPBs represented by vWF staining (red) was closely associated with the green Rab46 intensity as showed in the merged image. Moreover, the increased resolution allowed visualisation of single WPBs. Figure 3.3b shows representative single WPBs (red) associated with Rab46 (green) with their respective 3D reconstructions (bottom). High-resolution imaging revealed Rab46 was juxtaposed to vWF on the outside of WPBs, suggesting a role in WPB regulation.

High-resolution imaging permitted quantitative measurement to evaluate the extent of Rab46 localisation to WPBs. Multichannel images were processed to detect and count WPBs (red particles), Rab46 (green particles) and particles that were both green and red. Quantification of high-resolution images using Spot Detector algorithm revealed that not all WPBs are associated with Rab46, only 49% (± 13%) of particles were positive for both vWF and Rab46 (Figure 3.4). Therefore, Rab46 does not colocalise to a full population of WPBs. This data suggests that Rab46 regulates a subpopulation of WPBs which may contain specific cargo.

WPBs are endothelial-specific organelles and the main storage granules; nevertheless, other granules are present in the endothelial cells' cytoplasm. In order to confirm that Rab46 localised specifically to WPBs, co-staining with markers for secretory granules (Tissue Plasminogen-activator), lysosomes (Lamp1) and recycling endosomes (Rab11) was

performed (Figure 3.5). Immunofluorescent images revealed distinct localisation of Rab46 vesicles from all the other granules, suggesting that WPBs are the primary localisation of Rab46 in endothelial cells.

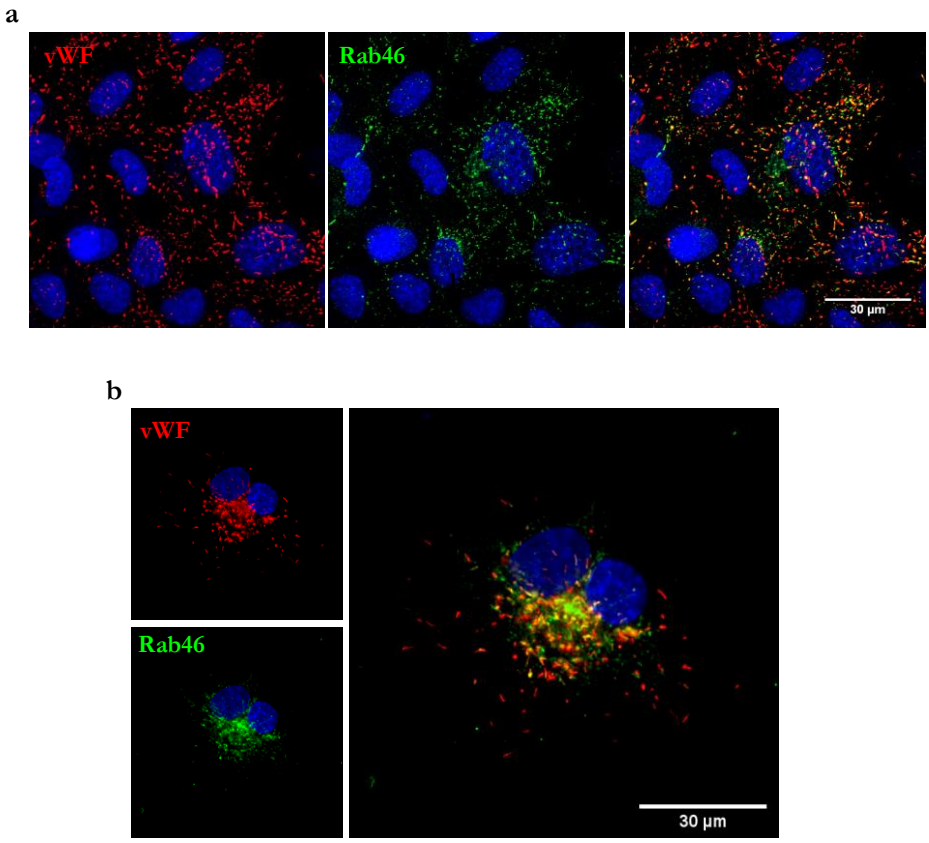

Figure 3.2 Endogenous Rab46 localises to Weibel-Palade bodies. Immunofluorescent images showing subcellular localisation of endogenous Rab46 (green) and vWF (red) in HUVECs (a) and HMCEC (b). DAPI (blue) shows nuclei. Merged images on the right to show colocalisation of Rab46 with vWF. Maximum intensity projections from DeltaVision z-stack are shown. Scale bar = 30 µm.

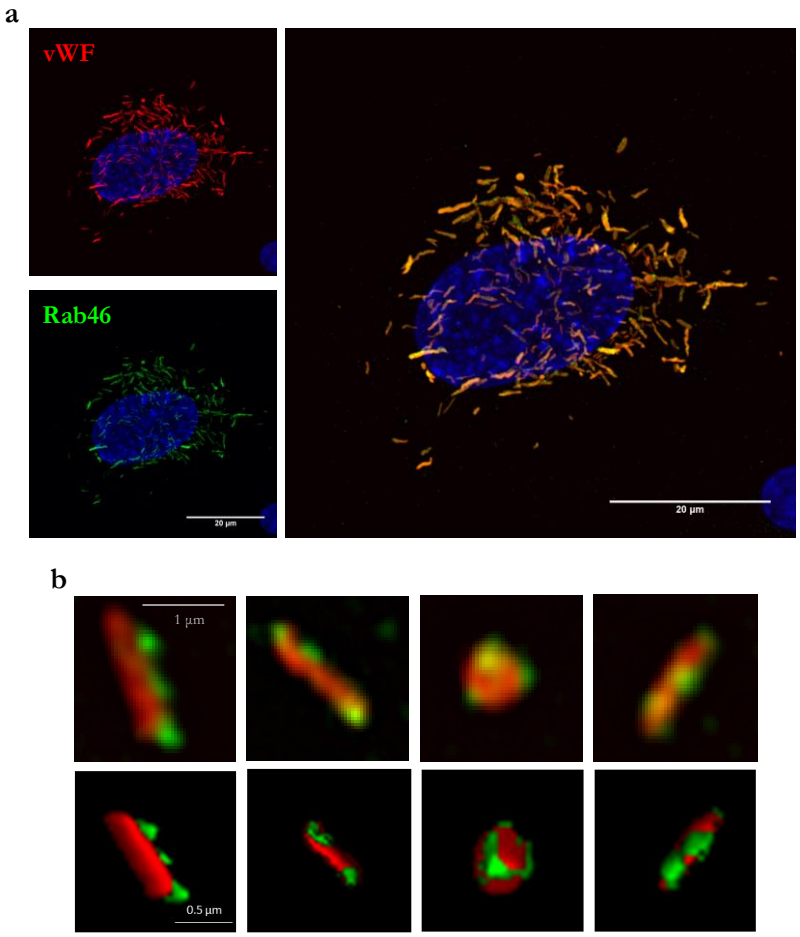

Figure 3.3 Specific Rab46 localisation to Weibel-Palade bodies in endothelial cells. (a) High-resolution Airyscan imaging showing detailed localisation of cigar-shaped WPBs (red) and Rab46 (green) in HUVECs, merged image showing colocalisation of Rab46 with vWF. Scale bar = 20 µm. (b). Zoomed-in and cropped high-resolution image (top) and 3D reconstruction (bottom) showing single WPBs (vWF: red) where Rab46 (green) is juxtaposed to vWF.

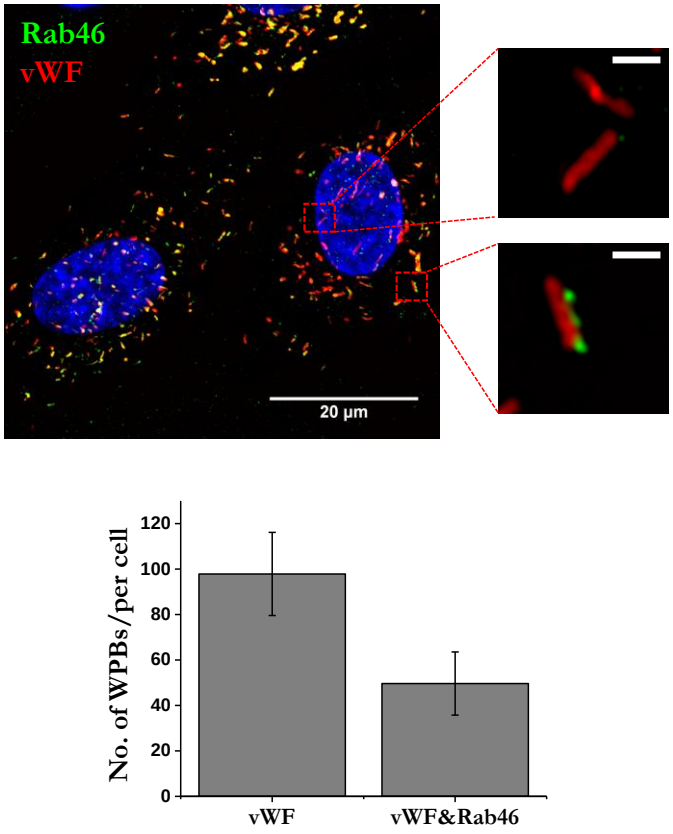

Figure 3.4 Rab46 localised with a subpopulation of WPBs. Representative high-resolution image stained for vWF and Rab46 and quantified using Spot detector plugin in ICY. The insets represent cropped single WPB either with no Rab46 (top) or with Rab46 localisation (bottom). Scale bar = 1 µm. The graph below shows the number of WPBs (counted as red spots as per methods) which colocalise with Rab46 vesicles (green spots). 49% (± 13%) of WPBs per cell localise with Rab46. n/N = 3/15

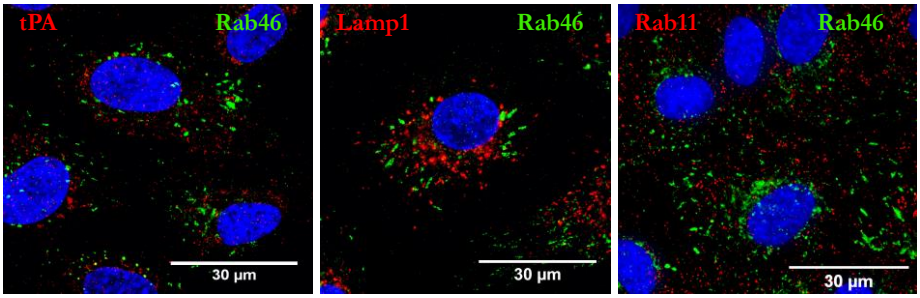

Figure 3.5 Rab46 does not localise to other endothelial granules. HUVECs co-stained with Rab46 (green) and tissue plasminogen activator (tPA: red) (left), lysosomal marker (Lamp1: red) (middle), recycling endosomes (Rab11: red) (right), show distinct localisations in endothelial cells. Scale bar = 30 µm.

3.3.1 Nucleotide binding to Rab46 influence its intracellular localisation

Srikanth et al., demonstrated that the GTPase domain of Rab46 is functionally active and the GTP/GDP switching regulates its association with the Golgi in T-cells[167]. Therefore, the importance of a functional GTPase domain was equally assessed in endothelial cells. The amino acid sequence of Rab46 GTPase domain contains conserved residues which are important for the GTPase function[167]. To confirm the role of these conserved residues, mutants with predicted impaired GTPase activity were generated. Single point mutation, involving the substitution of a threonine (T) to an asparagine (N) residue in the P-loop of the GTPase domain was introduced to generate a mutant (T559N) which is preferentially GDP-bound. Moreover, a GTP-bound (constitutively active) mutant (Q604L) and a nucleotide-free inactive mutant (N658I) were previously generated to assess whether GTPase activity influences the subcellular localisation of Rab46. The T559N, Q604L and N658I mutants were over-expressed in endothelial cells and localisation observed by immunofluorescence after 24 hours. Localisation of GTP/GDP binding defective mutants showed that mutants impaired in GTP binding have a predominant cytosolic localisation whereas defects in the hydrolysis of GTP cause a strong perinuclear localisation, at times similar to the exogenous expressed WT-Rab46. Quantitative measurement of Rab46 intensity around the perinuclear area was obtained from analysis of immunofluorescent images of Rab46 nucleotide-binding mutant. Both N658I and T559N show an even cytosolic distribution with impaired co-localisation to vWF. In contrast, constitutively active mutant Q604L shows a green intensity peak next to the nucleus driving localisation of vWF in the same area (Figure 3.6). These findings confirm that the GTPase domain of Rab46 is functionally active and that the conserved GTP-binding motif is important for Rab46 localisation to WPBs in endothelial cells.

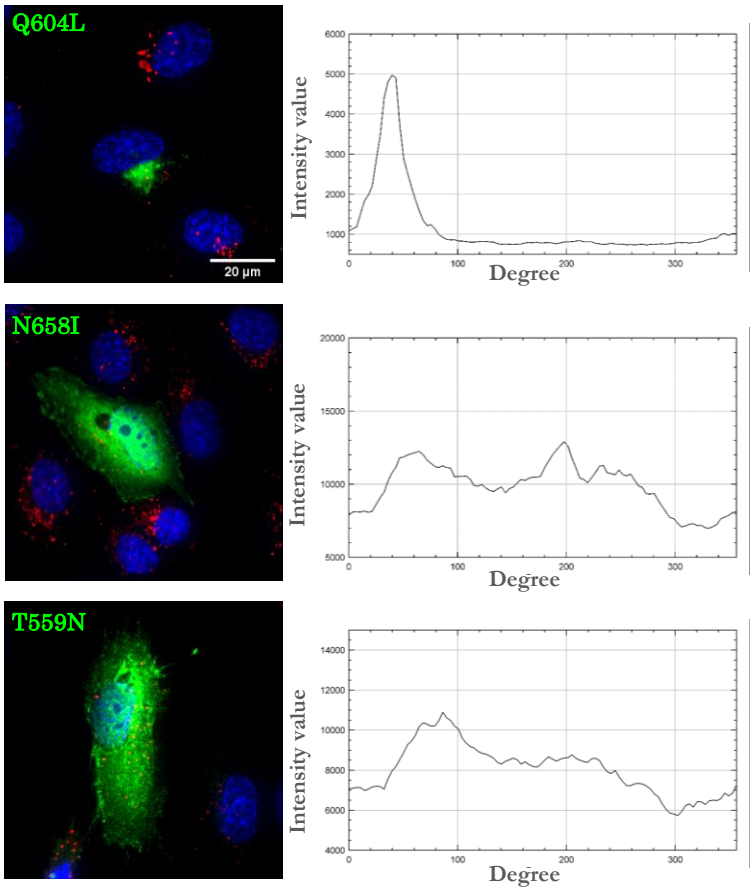

Figure 3.6 Subcellular localisation of Rab46 nucleotide binding mutants. Representative images of HUVECs expressing constitutively active form of Rab46 (Q604L: top) stained for vWF (red) with its respective Rab46 (green) intensity plot on the right side where the peak indicates a cluster in the perinuclear area. Representative images of the nucleotide-free mutant (N658I) and the inactive GDP-bound form of Rab46 (T559N) expressed in HUVECs and their representative intensity plots showing homogenous green distribution indicated a cytosolic localisation (middle and bottom respectively). All the plots were generated using the Oval profile method in ImageJ. n/N=3/28

3.4 Rab46 depletion increases vWF protein content

Rab proteins are known to orchestrate the dynamics of various intracellular and secretory vesicles by controlling vesicle biogenesis, motility and fusion events[95]. The identity and function of some Rab GTPases associated with WPBs in regulating their biogenesis and modulation of vWF exocytosis has been recently investigated[181].

To determine the role of Rab46 in WPB function, its expression was reduced using two siRNAs targeted against Rab46 or control siRNA (see methods). Downregulation of Rab46 in endothelial cells after 48 –72 hours was confirmed by western blot and quantified by densitometry analysis (Figure 3.7a). 70% and 64% of Rab46 protein knockdown was achieved using Rab46 siRNA-1 and siRNA-2 (respectively) compared to control siRNA (Figure 3.7b). Rab46 siRNA-1 was used throughout unless otherwise specified.

Next, the role of Rab46 in WPB biogenesis was questioned. WPB formation is driven by vWF content and tubulation[182]. Therefore, in order to look at the effect of Rab46 siRNA on WPB formation, mRNA and protein level of vWF was measured by qPCR and western blot. Firstly, mRNA expression of vWF was analysed after siRNA transfection. Figure 3.7c shows that siRNA-mediated knockdown of Rab46 does not affect vWF mRNA level, suggesting Rab46 does not have a role in vWF expression. However, western blot analysis shows that the amount of intracellular vWF protein increases by 2.3 fold (+/- 0.6) in Rab46 depleted endothelial cells compared to control siRNA (Figure 3.7d), suggesting a role for Rab46 in WPB trafficking.

To further investigate the increased abundance of vWF protein in response to Rab46 depletion, vWF expression and the number of WPBs per cell was analysed by immunostaining for vWF. Randomised images of endothelial cells transfected with Rab46 siRNA or control siRNA were taken with DeltaVision system. The images were then analysed and the number of vWF positive WPBs were counted using ImageJ. Representative images of WPBs population in transfected endothelial cells are showed in Figure 3.8a. Mean data (Figure 3.8b) showed an average of 95 ± 6 WPBs per cell in controls samples, versus a significant higher count (128 ± 8 WPBs/cell) in cells where Rab46 is depleted. Moreover, the number of vWF positive cells did not change after downregulation of Rab46, so siRNA transfection had no significant effect on the number of cells that contain WPBs (Figure 3.8c).

These results together suggest that Rab46 does not play a positive role in biogenesis. However, aforementioned downregulation of Rab46 results in a potential detention of vWF in the cell, probably leading to a reduction of vWF secretion. Thus, we propose Rab46 as a new Rab protein involved in vWF exocytosis and trafficking of WPBs.

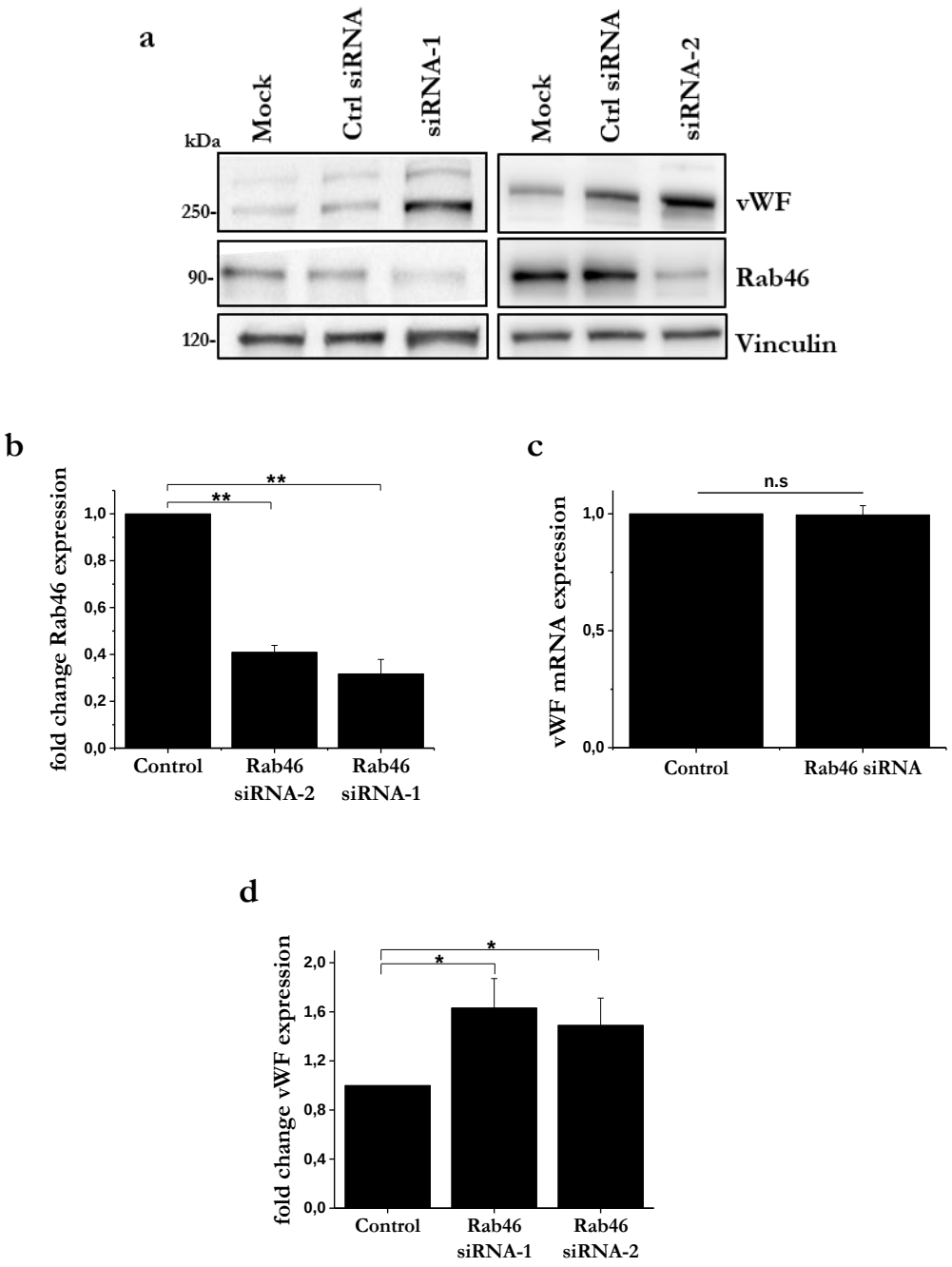

Figure 3.7 Rab46 depletion increases vWF protein content. (a) Representative western blots for Rab46 and vWF expressed in HUVECs transfected with two Rab46 siRNAs (si.1 and si.2) or control siRNA. (b) Quantification of Rab46 band intensity is shown as fold change relative to vinculin (n = 6). (c) qPCR ΔCT analysis of HUVECs transfected with Rab46 siRNA-1 demonstrate no difference in the expression of vWF mRNA as compared to cells transfected with control siRNA (n = 3). (d) Densitometry analysis from a western blot of vWF band intensity in HUVECs transfected with 2 different siRNAs specific for Rab46 is shown as fold change relative to housekeeping genes (siRNA Rab46-1, 1.63 ± 0.23 and siRNA Rab46-2, 1.49 ± 0.22) (n = 6)

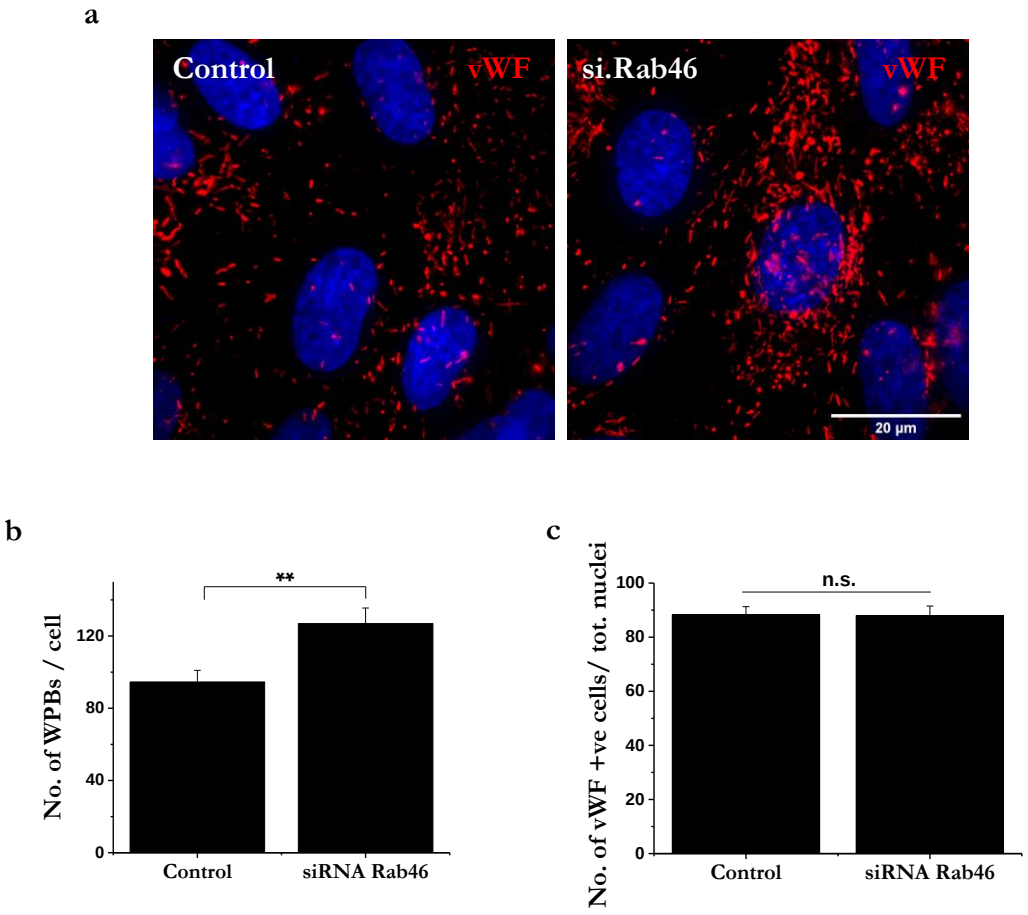

Figure 3.8 Rab46 depletion increases the number of WPBs per cell. (a) Example images used to quantify cells stained for vWF as a marker for WPBs in the presence or absence of Rab46 (siRNA-1). (b) The number of WPBs per cell as quantified as WPB counting (described in materials and methods) where cells were depleted of Rab46 versus siRNA control (control 95 ± 6, siRNA Rab46-1 128 ± 8). n/N = 3/18. (c) Quantification of cells that contain WPBs was performed counting the number of cells positive for vWF in HUVECs when cells were depleted of Rab46 by targeted siRNA (siRNA Rab46-1) or a control siRNA (n/N = 3/18). Graphs show mean ± SEM. n.s. not significant. *p-value < 0.05 **p-value < 0.01 from Student's t-test.

3.5 Rab46 depletion does not affect the expression of structurally and functionally related Rab GTPases

Rab46 is a non-conventional Rab protein as its GTPase domain is associated with a coil-coiled domain and two EF-hand domains which results in a large Rab GTPase. High similarity in the overall structure with Rab46 is presented by two other large GTPases: Rab44 and Rab45[7]. Both Rab44 and Rab45 have not been described in endothelial cells therefore, their relative mRNA expression was examined. In contrast several studies have already shown the role of other Rab proteins in endothelial cells trafficking events, such as Rab27a in trafficking of mature WPBs[69] or Rab7a in retrograde lysosomal trafficking[184]. In order to ascertain that Rab46 depletion does not result in an overall cellular imbalance, relative expression of Rab44, Rab45, Rab27a and Rab7a was first quantified in endothelial cells. Next, their mRNA abundance was measured in Rab46 depleted cells and control endothelial cells (Figure 3.9). Figure 3.9a shows mRNA relative expression of the indicated Rab proteins in endothelial cells demonstrating that the two structural related Rab44 and Rab45 are expressed at very low levels. In contrast, mRNA abundance of Rab27a is similar to Rab46 whereas, as expected, Rab7a mRNA has an increased expression as compared to other Rab proteins in endothelial cells. No change in the expression of the selected genes was observed (Figure 3.9b) when comparing mRNA abundance between non transfected endothelial cells and Rab46 siRNA transfected cells.

These data exclude the possibility of some off-target effects, such as genetic compensation by other related Rabs in response to Rab46 knockdown in endothelial cells, suggesting a specific role of Rab46 in regulating trafficking of a subpopulation of WPBs.

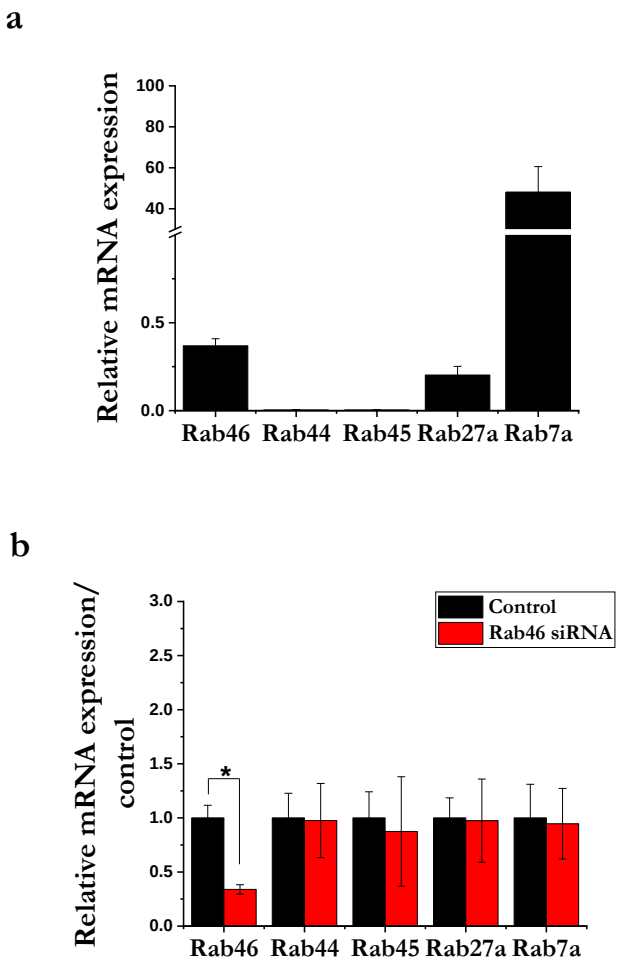

Figure 3.9 Rab46 depletion does not affect the expression of other related Rab proteins. (a) qPCR ΔCT analysis of total HUVECs lysate showing mRNA expression of Rab46, Rab44, Rab45, Rab27a and Rab7a normalized to housekeeping genes in endothelial cells. (b) qPCR ΔCT analysis of HUVECs transfected with Rab46 siRNA-1 showing mRNA expression normalized to housekeeping genes and compared to control siRNA. No difference in the mRNA expression of the indicated Rab proteins was measured as compared to HUVECs transfected with control siRNA (n = 3).

Chapter 4 Rab46 regulates Weibel-Palade body trafficking in response to histamine

4.1 Introduction

WPBs provide a dynamic storage pool in endothelial cells whose contents can be regulated and released by inflammatory or thrombotic mediators present in the vascular micro-environment[59]. Upon vascular perturbation, a rapid and immediate release of bioactive components from an intracellular storage pool is necessary to maintain vascular haemostasis. WPB contents can be released from endothelial cells in response to several different secretagogues, such as histamine and thrombin which act by raising intracellular Ca^{2+} or epinephrine and vasopressin which increase cAMP level in the cell[56]. Ca^{2+} raising agonists like histamine and thrombin are expected to induce a more rapid and vigorous response where release of pro-inflammatory and pro-thrombotic mediators from WPBs provide the vasculature with an emergency kit for wound repair. However, thrombin and histamine have distinct physiological roles. Thrombin, as part of the response to vascular injury, necessitates release of both pro-thrombotic and pro-inflammatory mediators whereas histamine stimulates release of mainly pro-inflammatory factors. In order to achieve an appropriate response to these physiologically distinct stimuli there must exist discrete cargo-restricted WPB populations whose trafficking and exocytosis is highly controlled. Regulated exocytosis of WPBs is a multistep process requiring translocation of mature WPBs from the cytoplasm toward the cell surface, docking and fusion with the plasma membrane[181]. Recent studies have unravelled the role of some Rab GTPase and their effectors in regulation of WPB trafficking and exocytosis[181]. However, it is unclear if subpopulations of WPBs are differentially trafficked in response to stimuli and how this is regulated.

In this chapter the function of Rab46, a novel Rab protein associated with a subset of WPBs is investigated. The presence of the Ca^{2+} binding sites together with a GTPase domain in the Rab46 sequence suggested a possible coordination by Rab46 of G-protein and Ca^{2+} signals in regulating WPB trafficking. Histamine and thrombin were used to induce mobilization and secretion of WPBs as both agonists induce intracellular Ca^{2+} mobilization but have distinct outcomes. Understanding how WPBs are able to recognise different stimuli, inducing differential release, will provide new insight into endothelial cells fine-regulation of different physiological responses. To study the role of Rab46 in WPB trafficking upon acute histamine and thrombin stimulation, siRNAs targeting Rab46 were used. In addition, chemical inhibitors of cellular proteins were used to unravel the mechanisms underlying Rab46-dependent WPB trafficking and a customised automated imaging analysis was designed for image quantification.

This chapter reveals that Rab46, a new Rab GTPase associated with a subset of WPBs, regulates histamine, but not thrombin, WPB trafficking. Acute histamine stimulation induces Rab46-dependent WPB clustering to the microtubule organizing centre (MTOC), moving along the microtubular network with the dynein motor protein.

4.2 Differential Weibel-Palade body trafficking

In basal conditions, WPBs are evenly distributed in the cytoplasm of endothelial cells. In order to establish WPB response and the role of Rab46 in WPB trafficking, cellular localisation of vWF and Rab46 was investigated in response to different stimuli. The two major agonists of WPB trafficking and vWF exocytosis are histamine and thrombin. They both act via increasing intracellular Ca^{2+} inducing a rapid depletion of WPBs.

HUVECs were grown for 72 hours in order to have a confluent monolayer and a full population of WPBs, representing a physiological condition. To mimic an on-demand response, cells were stimulated for 10 mins with histamine (30 μM) or thrombin (2.5 U/ml). WPB cellular distribution to these two different stimuli was examined by immunostaining. Endothelial cells fixed and immunostained for vWF show a clear difference in WPB cellular redistribution upon acute stimulation. Imaging of histamine stimulated endothelial cells reveals a striking perinuclear clustering of vWF, in contrast to thrombin treated cells which exhibited a more typical vWF patches on the cell surface, indicating vWF exocytosis (Figure 4.1).

Next, Rab46 under stimulated conditions was also examined together with vWF. Stimulated endothelial cells were co-stained for vWF and Rab46 to observe the distribution of WPBs and Rab46 elicited by the two agonists (Figure 4.2). Interestingly, whilst vehicle and thrombin-treated cells displayed an even distribution of Rab46 and WPBs throughout the cytoplasm, acute histamine stimulation induces a redistribution of Rab46 (green) as well as vWF (red) towards a perinuclear area. To better understand the difference in the distribution of WPBs and Rab46 under different conditions, pixels intensity across nuclei was measured (Figure 4.3a). Linear plot profiles on RGB images showed the presence of red (vWF) and green (Rab46) peaks only on one side of the nuclei (blue line) for histamine treated cells whereas more uniform or irregular profiles belong to non-treated or thrombin treated cells. To analyse the overall change in WPBs and Rab46 cellular distribution upon acute stimulation, I designed a customised macro using ImageJ that analysed the intensity of green and red particles and their distance from the nucleus (see methods 2.11.4). Briefly, each image was separated in 3 different channels and each channel processed separately. A binary mask was created using a default threshold on the DAPI (nuclear stain) channel and a distance map was generated. Green and red channels were duplicated to sample the original pixel intensities of WPBs and Rab46 structures. Each channel was segmented using a threshold

algorithm (Max Entropy) and the distance and intensity of each particles from the nucleus measured. Distance and normalized integrated intensity values were plotted as X and Y values respectively. Distance values (x), which range from 0 px (nucleus) to 255 px (periphery) were binned into three areas: Perinuclear (x< 2µm) – Intermediate (2µm < x > 5µm) – Periphery (x > 5µm). Figure 4.3b and c show the average distribution of vWF (red signal) and Rab46 (green signal) into the three indicated cellular areas in control and stimulated cells. This method confirmed that the accumulation of vWF and Rab46 in the perinuclear area upon histamine stimulation is highly significant (p-value ≤ 0.01).

These data show differential WPB trafficking in response to different physiological stimuli suggesting a role for Rab46 in regulating acute histamine stimulation.

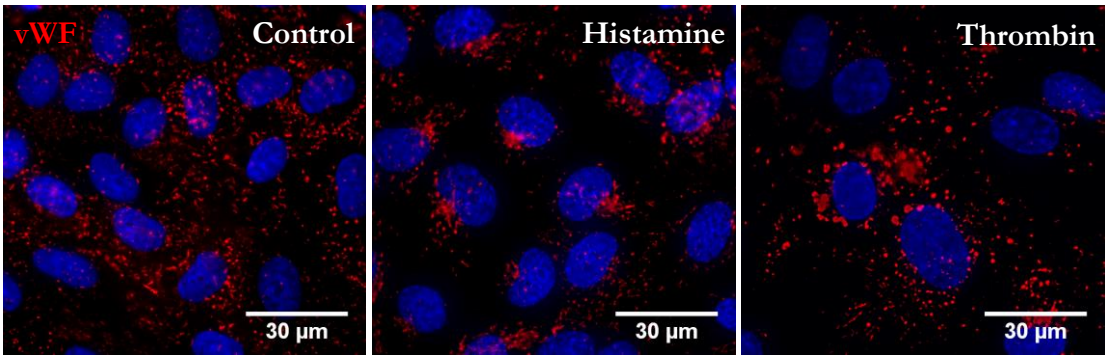

Figure 4.1 Histamine but not thrombin induces perinuclear trafficking of Weibel-Palade bodies. Immunofluorescent images showing endothelial cells fixed and stained for vWF (red) in resting condition (left) and upon acute stimulation (10 mins) with histamine 30 µM (middle) or thrombin 2,5 U/ml (right). DAPI (blue) shows nuclei. Scale bar = 30 µm. n/N=3/36

a

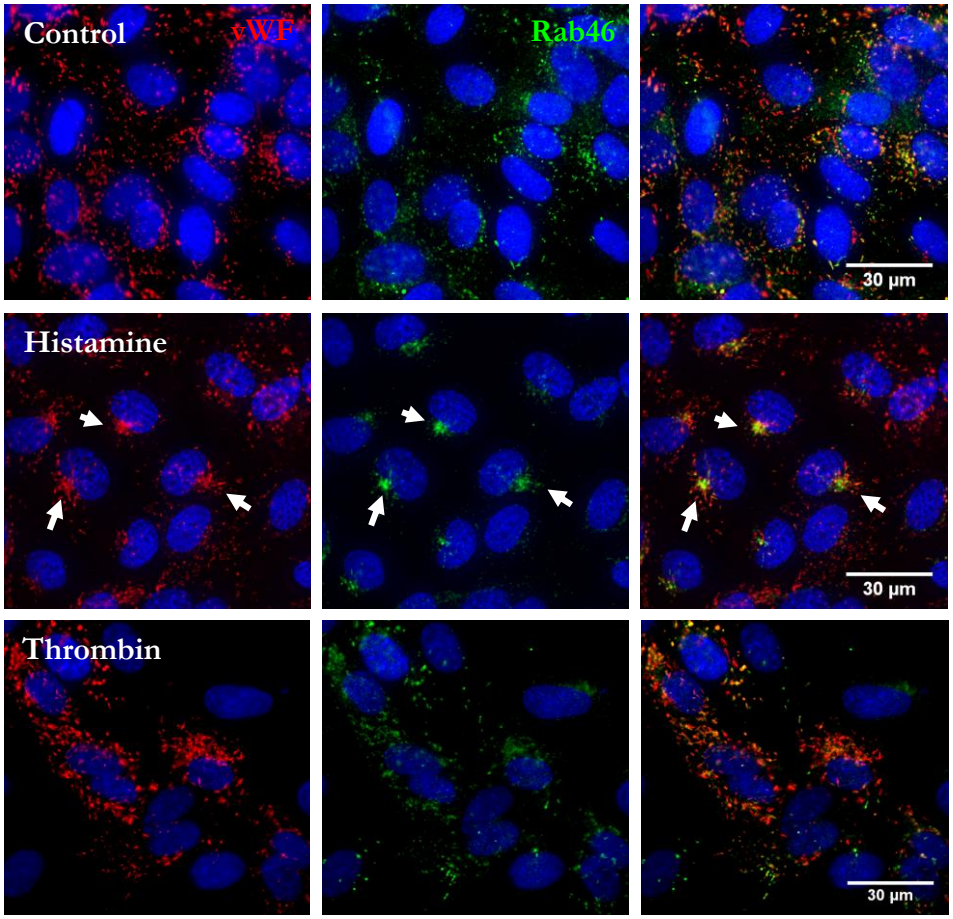

Figure 4.2 Weibel-Palade bodies and Rab46 traffic to a perinuclear area upon acute histamine stimulation. (a) Immunofluorescent images showing endothelial cells fixed and stained for vWF (red) and Rab46 (green) in resting condition (top) and upon 10 mins stimulation with histamine 30 µM (middle) or thrombin 2,5 U/ml (bottom). White arrows indicate perinuclear clusters of vWF and Rab46. DAPI (blue) shows nuclei. Scale bar = 30 µm

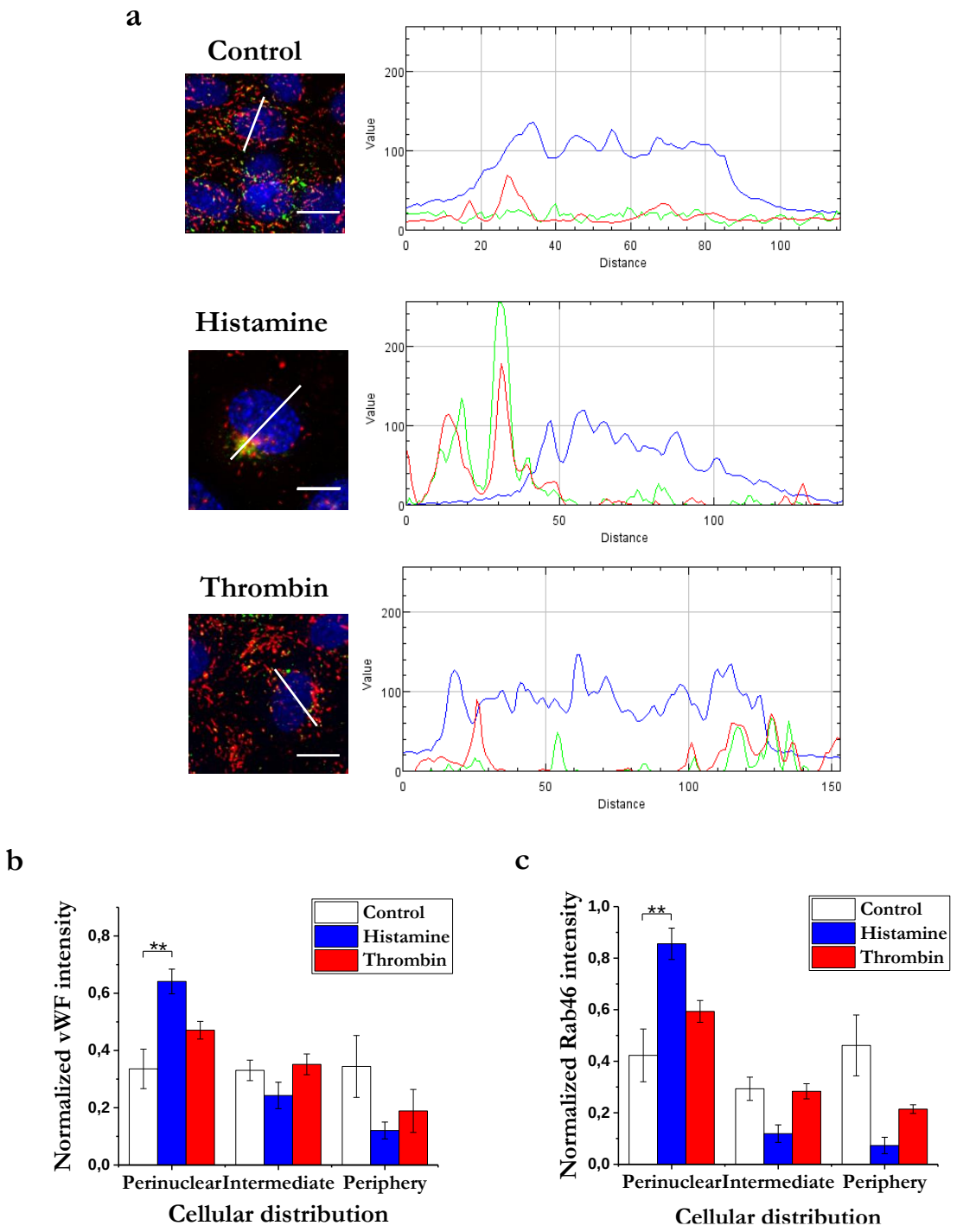

Figure 4.3 Quantification of the cellular distribution of WPBs and Rab46 upon histamine or thrombin stimulation. (a) HUVECs immunostained for vWF and Rab46 in resting condition (top) or after stimulation with histamine (middle) or thrombin (bottom) and their representative RGB profiles showing pixels intensities traces from different images measured according to a straight white line randomly drawn throughout different nuclei per images. Scale bar = 10 µm. Quantification of cellular distribution of vWF (b) and Rab46 (c) intensity in basal and histamine (30 µM) or thrombin (2,5 U/ml) acute 10 mins stimulation. Results were grouped into three areas: perinuclear, intermediate and periphery. The plot shows vWF or Rab46 signal intensity of each particles in the respective area where the mean (± SEM) was noted as percentage of the total signal intensity. n/N=3/36. **p-value < 0.01 from one-way ANOVA.

4.3 Histamine-induced WPB perinuclear trafficking is Rab46-dependent

Seeking the function of Rab46 in WPB trafficking, HUVECs were transfected with either Rab46 targeted siRNA or control siRNA and after 72 hours stimulated as above. Interestingly, imaging analysis showed that the depletion of Rab46 with specifically targeted siRNAs (Figure 4.4b siRNA-1 and Figure 4.4c siRNA-2) had no effect on the distribution of WPBs in basal conditions (Figure 4.4a image top right and mean data Figure 4.4b-c). However, histamine failed to induce perinuclear clustering of vWF in cells depleted of Rab46 (Figure 4.4a bottom right and mean data Figure 4.4b-c) suggesting that histamine-evoked clustering of a subpopulation of WPBs to the perinucleus is dependent on Rab46.

In contrast, depletion of Rab46 had no effect on WBP trafficking upon thrombin stimulation (Figure 4.5a). Quantification of cellular distribution in Figure 4.5b shows a slight non-significant increase in vWF accumulation in the perinuclear area, however uniform cellular distribution of vWF signal confirm no significant difference in thrombin-stimulated cells upon Rab46 depletion.

These results show that in resting cells WPBs are distributed in an apparently random manner throughout the cytosol, but differential trafficking was observed upon stimulation with the two agonists. Although exocytosis of WPBs is induced by two Ca^{2+}-raising agents such as histamine and thrombin, these data indicate that WPBs are able to distinguish two physiologically distinct stimuli and elicit a differential response. Whilst thrombin stimulation is Rab46-independent, acute histamine stimulation induces a directed movement of WPBs towards a perinuclear area in a Rab46-dependent manner.

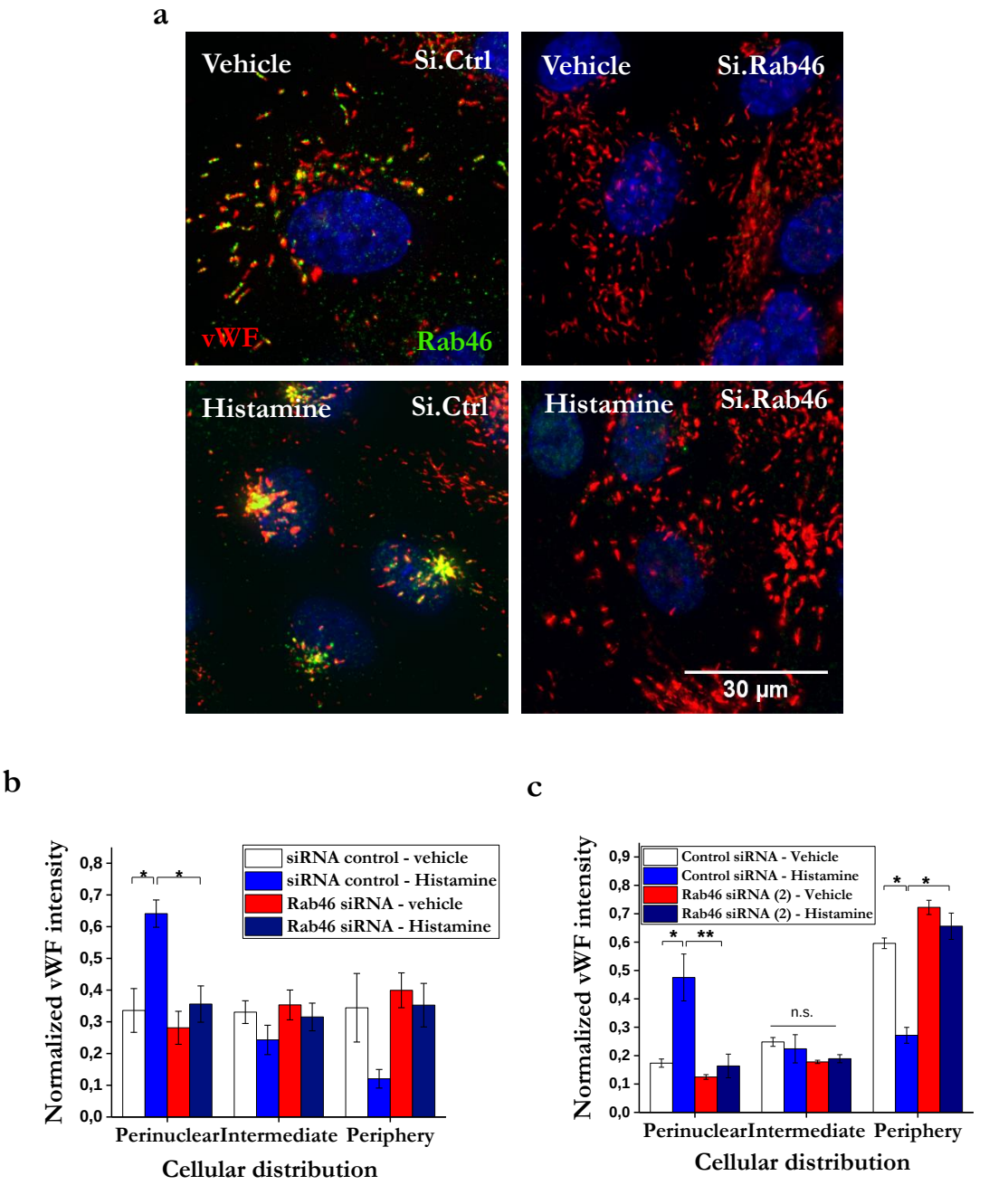

Figure 4.4 Histamine induced Rab46-dependent perinuclear clustering of WPBs. (a) Representative images of HUVECs transfected with Rab46 siRNA-1 or control siRNA in control conditions (vehicle) or after 10 mins histamine treatment (30 µM). Immunostaining of Rab46 (green) and vWF (red) shows perinuclear cluster of Rab46 and vWF in siRNA control cells upon histamine stimulation (bottom left). Perinuclear trafficking of WPBs is completely abolished in Rab46 depleted cells (bottom right). Scale bar = 30 µm and applies to all images. Quantitative analysis of vWF cellular distribution in siRNA control cells and Rab46 depleted cells with two different siRNAs, siRNA-1 (b) and siRNA-2 (c) upon histamine stimulation. Results were grouped into three areas: perinuclear, intermediate and periphery. The plot shows vWF signal intensity of each particles in the respective area where the mean (± SEM) was noted as percentage of the total signal intensity. n/N=3/36. *p-value < 0.05 from 2-way ANOVA.

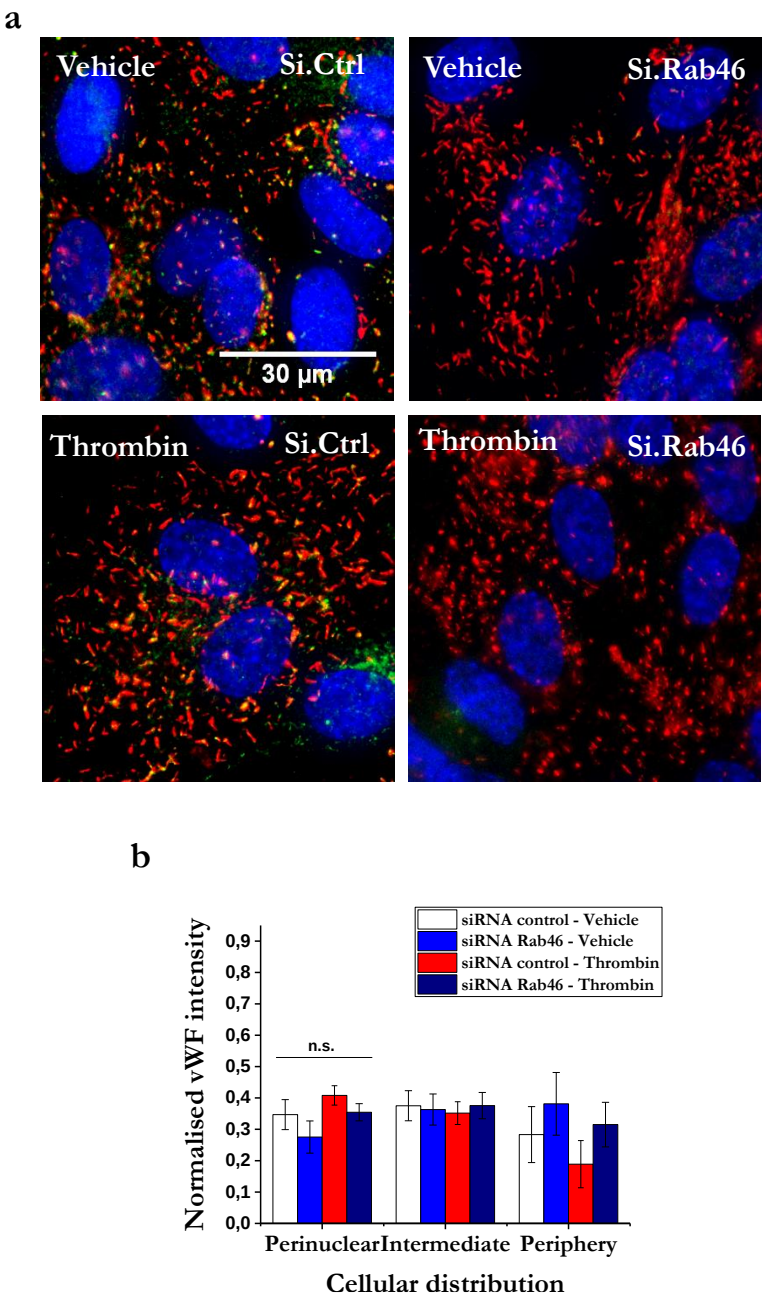

Figure 4.5 Thrombin-evoked trafficking of WPBs is independent of Rab46. (a) Representative images of HUVECs transfected with Rab46 siRNA-1 or control siRNA in control conditions (vehicle) or after 10 mins thrombin (2,5 U/ml) stimulation. Immunostaining of Rab46 (green) and vWF (red) shows that Rab46 depletion does not have affect WPB trafficking upon thrombin stimulation. Scale bar = 30 µm and applies to all images. (b) Quantitative analysis of vWF cellular distribution in siRNA control cells and Rab46 depleted cells upon thrombin stimulation. Results were grouped into three areas: perinuclear, intermediate and periphery. The plot shows vWF signal intensity of each particles in the respective area where the mean (± SEM) was noted as percentage of the total signal intensity. n/N=3/36. n.s. not significant

4.4 Histamine evokes WPBs and Rab46 redistribution to the Microtubule-Organising Centre

WPBs undergo retrograde transport to the perinuclear area by a Rab46-dependent mechanism when triggered by acute histamine stimulation. The region around the nucleus contains different compartments, such as the Golgi apparatus, endoplasmic reticulum (ER) and the MTOC.

Therefore, in order to exactly identify WPBs and Rab46 localisation upon acute histamine stimulation, immunofluorescence and super-resolution imaging was performed. Firstly, histamine-treated endothelial cells were co-stained for vWF (or Rab46) and pericentrin, a marker for the MTOC (Figure 4.6a-b). High-resolution imaging revealed a clear re-orientation of WPBs (red) towards the MTOC (green), and Rab46 (green) clusters were co-localised with pericentrin (red). In contrast, WPBs (vWF) and Rab46 failed to co-localise with the Golgi apparatus or the ER before and after histamine stimulation (Figure 4.7). Separate intracellular localisation of both Rab46 and vWF with those cellular compartments was revealed by super-resolution imaging.

These data identify the MTOC, an intracellular structure from which microtubules of the cytoskeleton radiate, as the perinuclear compartment where Rab46 clustering occurs upon histamine stimulation.

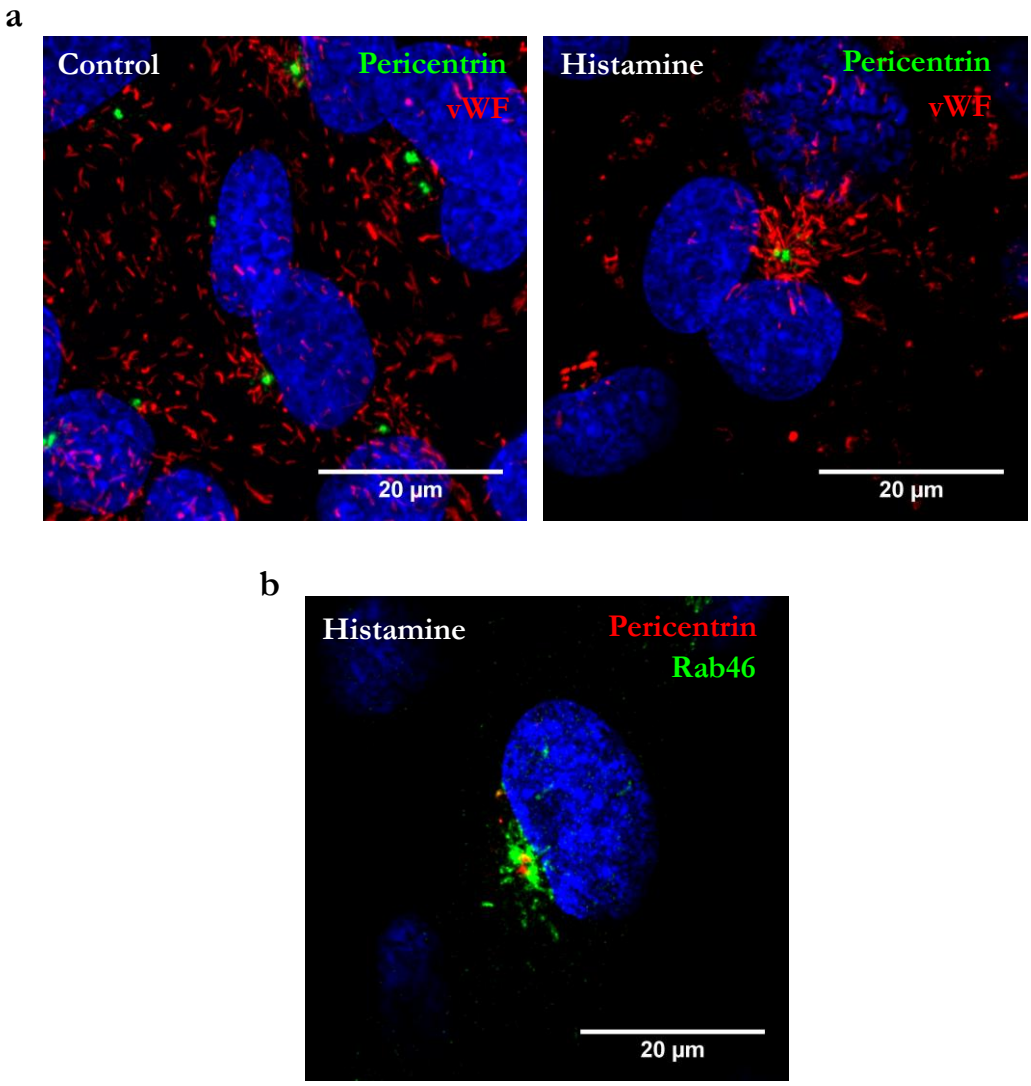

Figure 4.6 Histamine evokes redistribution of WPBs and Rab46 to the Microtubule Organising Centre (MTOC). (a) Airyscan images of HUVECs stained with vWF (red) and pericentrin (green). Control cells on the left and 30 µM histamine treated cells on the right showing reorientation of WPBs towards the MTOC. (b) High-resolution AiryScan image of cells treated with 30 µM histamine (10 mins) then immunostained with Rab46 (green) and pericentrin (red) showing Rab46 clustering at the MTOC. Maximum intensity projection from confocal microscopy z-stack are shown. DAPI (blue) shows nuclei. Scale bar = 20 µm

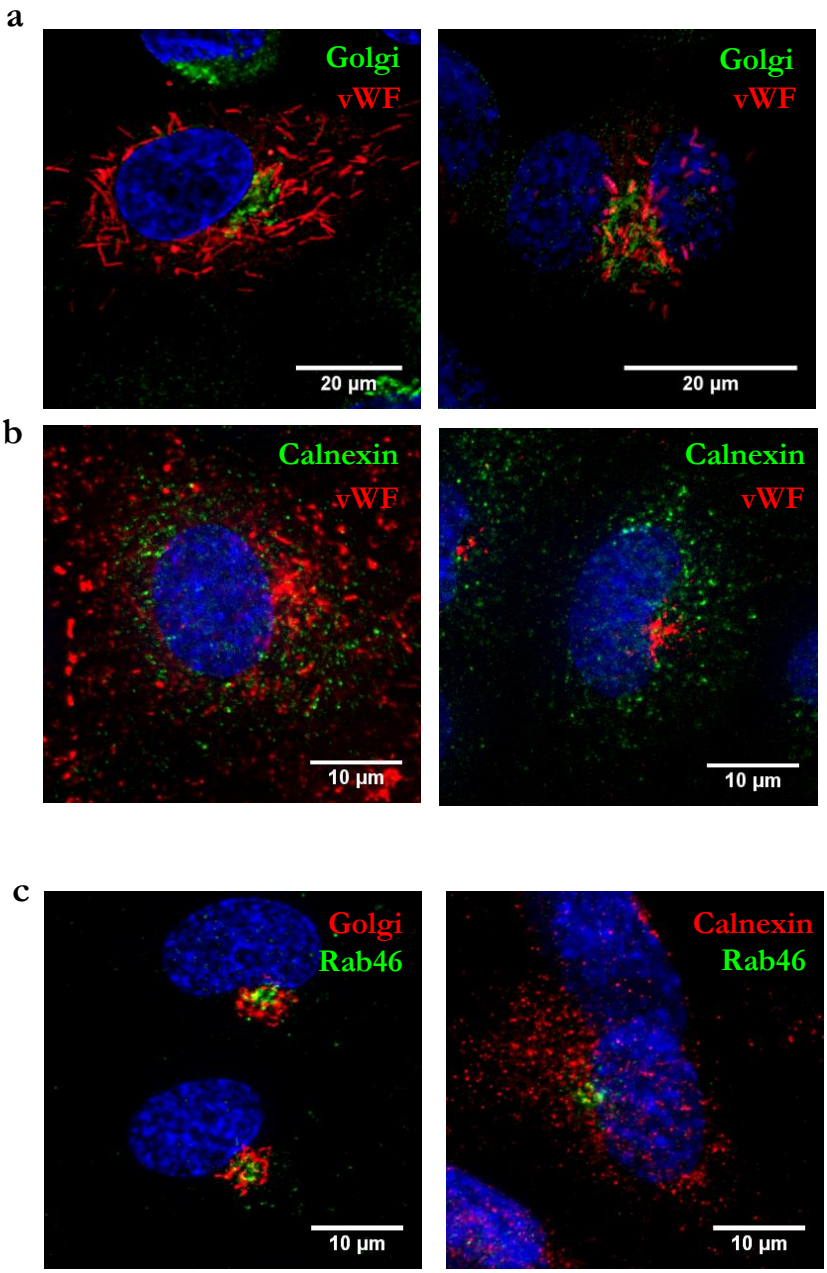

Figure 4.7 Subcellular distribution of WPBs and Rab46 following histamine stimulation. (a) High-resolution images of endothelial cells stained for vWF (red) and 58-k Golgi protein, a Golgi marker (green) before and after histamine treatment (left and right respectively). Maximum intensity projection from confocal microscopy z-stack are shown. Scale bar = 20 µm (b) HUVECs stained for vWF (red) and Calnexin (green) as marker for the ER, control cells on the left and histamine treated on the right. (c) Endothelial cells treated with histamine and stained for Rab46 (green) and GM130 (red) as a Golgi marker (left) and calnexin (red) as marker for the ER (right). Representative images to show no Rab46 colocalisation with these subcellular compartments. Maximum intensity projections from DeltaVision microscope z-stack are shown. DAPI (blue) shows nuclei. Scale bar = 10 µm

4.5 Nucleotide-binding is necessary for Rab46-dependent trafficking

As shown previously (3.3.1) Rab proteins contain highly conserved nucleotide binding sites that dictate GTPase membrane localisation and function[185]. Srikanth et al. have previously demonstrated that WT-Rab46 has the intrinsic ability to hydrolyse GTP whilst nucleotide binding mutants have no GTPase activity, suggesting that the GTPase domain is functionally active[167]. Therefore, whether the nucleotide binding to the GTPase domains of Rab46 would be necessary for histamine induced retrograde transport of WPBs was considered. Consistent with endogenous Rab46 localisation, exogenous expressed WT-Rab46 localised to WPBs. However, some of these Rab46-positive WPBs localise to a perinuclear region probably due to an effect of overexpression which could drive a GTP-bound state as many Rab proteins have slow intrinsic GTP hydrolysis rate. I have previously shown (3.3.1) that the constitutively active Rab46 mutant (Q604L) localised to the perinuclear region supporting the Rab46 motility to the perinucleus being dependent on GTP-binding. Here, the data suggest that GTP-bound Rab46 is necessary for WPB motility, as vWF (red) co-localised with Q604L Rab46 (green) at the MTOC, labelled with pericentrin (white), even in the absence of stimulation (Figure 4.8). In contrast, histamine failed to induce redistribution of Rab46 or perinuclear clustering of WPBs in cells overexpressing the N658I inactive Rab46 mutant (Figure 4.9).

The data suggest that GTP binding status governs the perinuclear localisation of WPBs, therefore GTPase activity regulates Rab46 localisation to WPBs as well as its function.

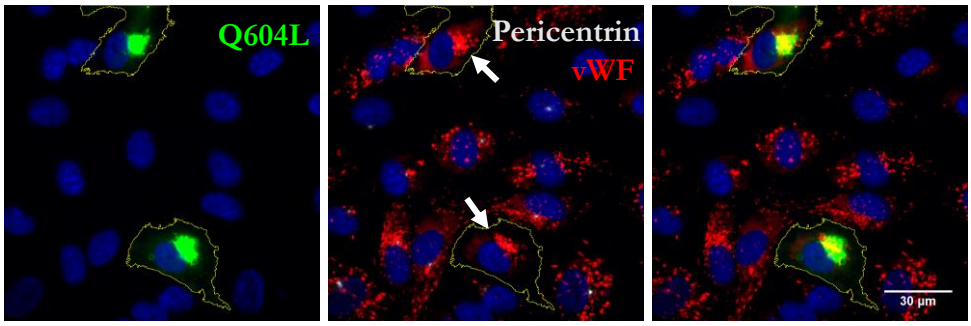

Figure 4.8 Constitutively active (Q604L) Rab46 localises vWF to the MTOC in the absence of stimulation. DeltaVision images of HUVECs immunostained for Rab46 Q604L (green), vWF (red) and pericentrin (white) as a marker of the MTOC in control conditions. vWF localises to the perinucleus (arrows) in cells expressing Q604L in the absence of stimulation. Scale bar 30 µm.

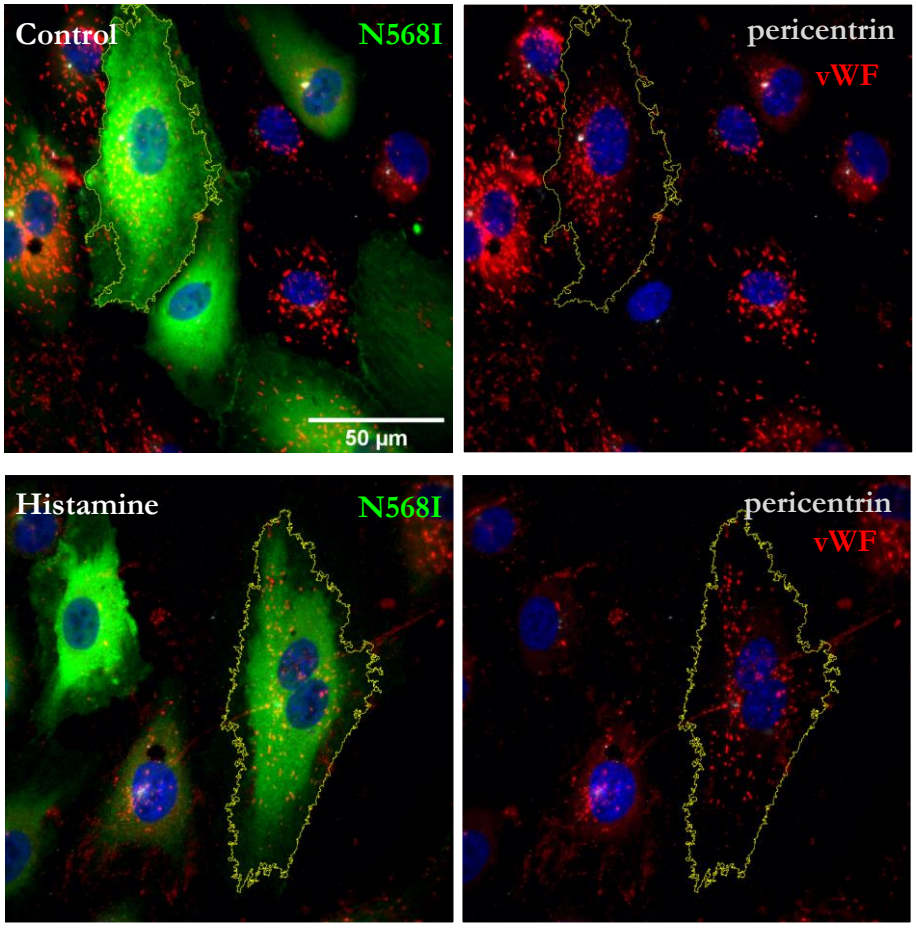

Figure 4.9 Rab46 GTPase activity is needed for WPB retrograde trafficking. Endothelial cells transfected with the inactive N658I Rab46 mutant treated with vehicle control (top) or 30 µM histamine (bottom) and immunostained for Rab46 (green), vWF (red) and pericentrin (white) as a marker of the MTOC. Histamine does not induce vWF perinuclear clustering of cells overexpressing the inactive N658I Rab46 mutant. Example cells outlined in yellow. n/N = 3/15. Scale bar = 50 µm.

4.6 Intact microtubule network is necessary for Rab46-dependent WPB trafficking to the MTOC

Intracellular transport of organelles along microtubules is a fundamental process essential to many cellular functions. The role of cytoskeleton in WPB motility has previously been studied. Microtubules are required for long-range movement of WPBs to the cell periphery[186]. Questioning how WPBs move back to the MTOC, the role of the microtubule network in Rab46-dependent WPB trafficking, following histamine stimulation, was evaluated. Endothelial cells were pre-treated with 1 μM nocodazole, a microtubule-disruptive agent, for 30 mins and then stimulated with histamine (30 μM) for 10 mins (Figure 4.10a). α-tubulin staining (small insets bottom right) reveals complete disassembly of microtubules in nocodazole-treated cells compared to non-treated cells. Moreover, to assess cell viability a washout experiment was performed where nocodazole was removed and cells were re-incubated with normal medium. Microtubules re-polymerization was monitored and after 2 hours microtubules were able to regenerate a complete network (data not shown). Immunofluorescent staining and imaging analysis show that disruption of microtubules inhibited histamine induced WPB and Rab46 perinuclear clustering. Rab46 intensity in the perinuclear area following histamine stimulation is indeed significantly reduced in nocodazole treated cells (Figure 4.10b).

The data show that microtubule integrity is required for Rab46-dependent WPB retrograde transport to the MTOC in response to histamine.

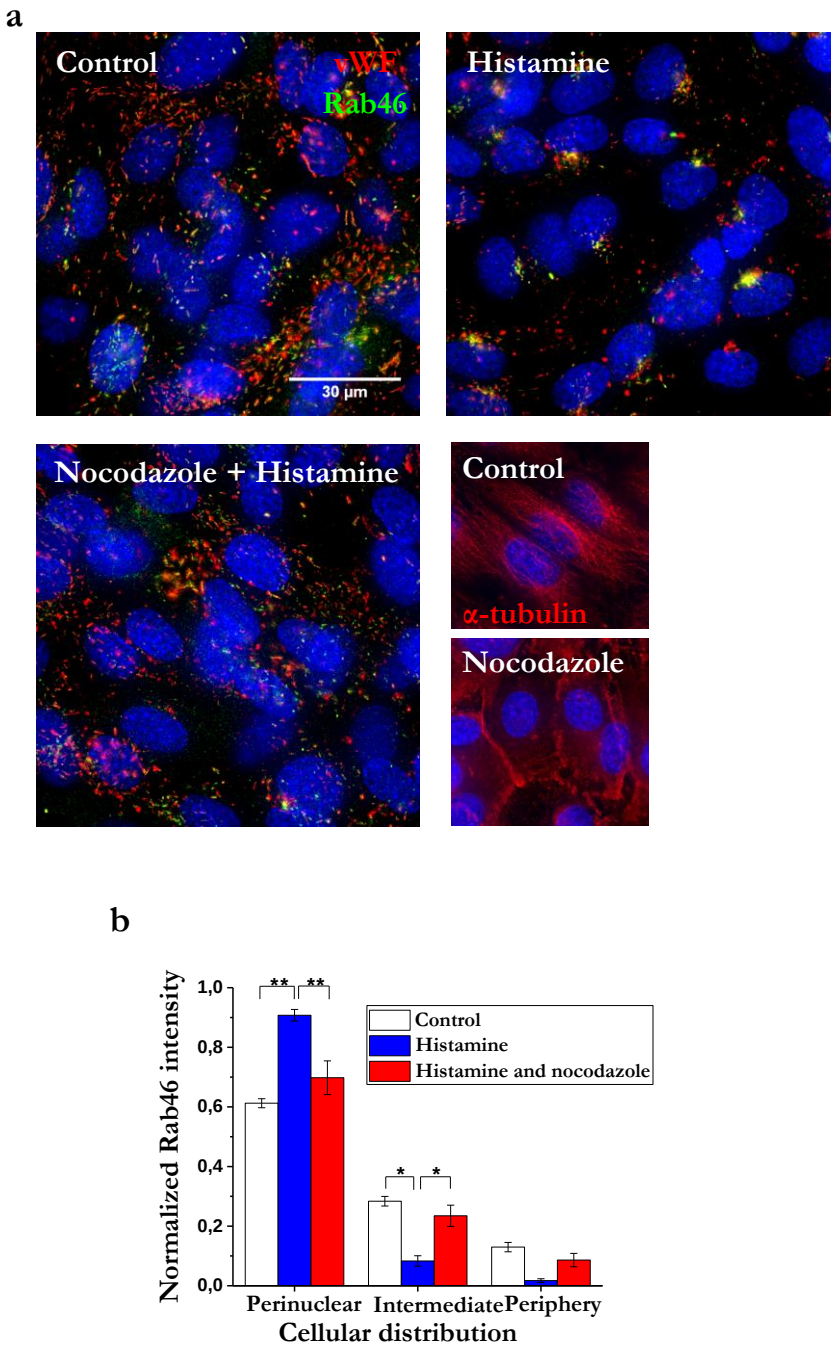

Figure 4.10 The integrity of microtubules is necessary for Rab46-dependent trafficking of WPBs to the MTOC. (a) Non-treated and histamine treated endothelial cells (top) compared with (bottom) endothelial cells pre-treated with nocodazole (1 µM) stimulated with 30 µM histamine for 10 mins and then fixed and stained for vWF (red) and Rab46 (green). Panels (bottom right) showing tubulin staining of endothelial cells before and after nocodazole treatment. (b) Mean data showing the cellular distribution of Rab46 upon histamine stimulation in cells pre-treated with nocodazole (b) and respective control cells. The plots quantify Rab46 signal intensity in the respective area where the mean (± SEM) was noted as percentage of the total signal intensity. n/N=3/18, *p-value < 0.05 **p-value < 0.01 from 1-way ANOVA.

4.7 Retrograde WPB trafficking is dynein-dependent

Microtubule-based transport of cargo is mainly directed by cytoskeletal-associated motor proteins which regulate spatio-temporal trafficking of different organelles. Bidirectional movements along the radially organized microtubules is driven by two main intracellular motor proteins: kinesin and dynein, which move in two opposite directions. Kinesin is a plus-end motor protein moving cargos to the cell periphery, whereas cytoplasmic dynein is a minus-end motor protein responsible for retrograde trafficking. Considering WPB retrograde trafficking upon histamine stimulation, the role of cytoplasmic dynein was investigated. Ciliobrevin D is an inhibitor of dynein ATPase activity, preventing the cycling activity of the motor protein necessary for dynein movement. Therefore, endothelial cells were pre-treated with ciliobrevin D (45 μM) for 45 mins to inhibit dynein activity and then treated with histamine for 10 mins. Rab46 and WPB localisation was observed by co-staining for Rab46 and vWF (Figure 4.11a). Representative images show typical Rab46 and WPBs clusters at the MTOC in histamine-treated cells in contrast with ciliobrevin pre-treated cells where histamine failed to induce Rab46-dependent WPB retrograde trafficking. Moreover, quantification of Rab46 cellular distribution in ciliobrevin-treated cells reveals significant reduction in Rab46 signal at the perinuclear area when compared to histamine-treated cells (Figure 4.11b).

These results show that dynein activity is necessary for Rab46-dependent trafficking of WPBs along the microtubules to the MTOC.

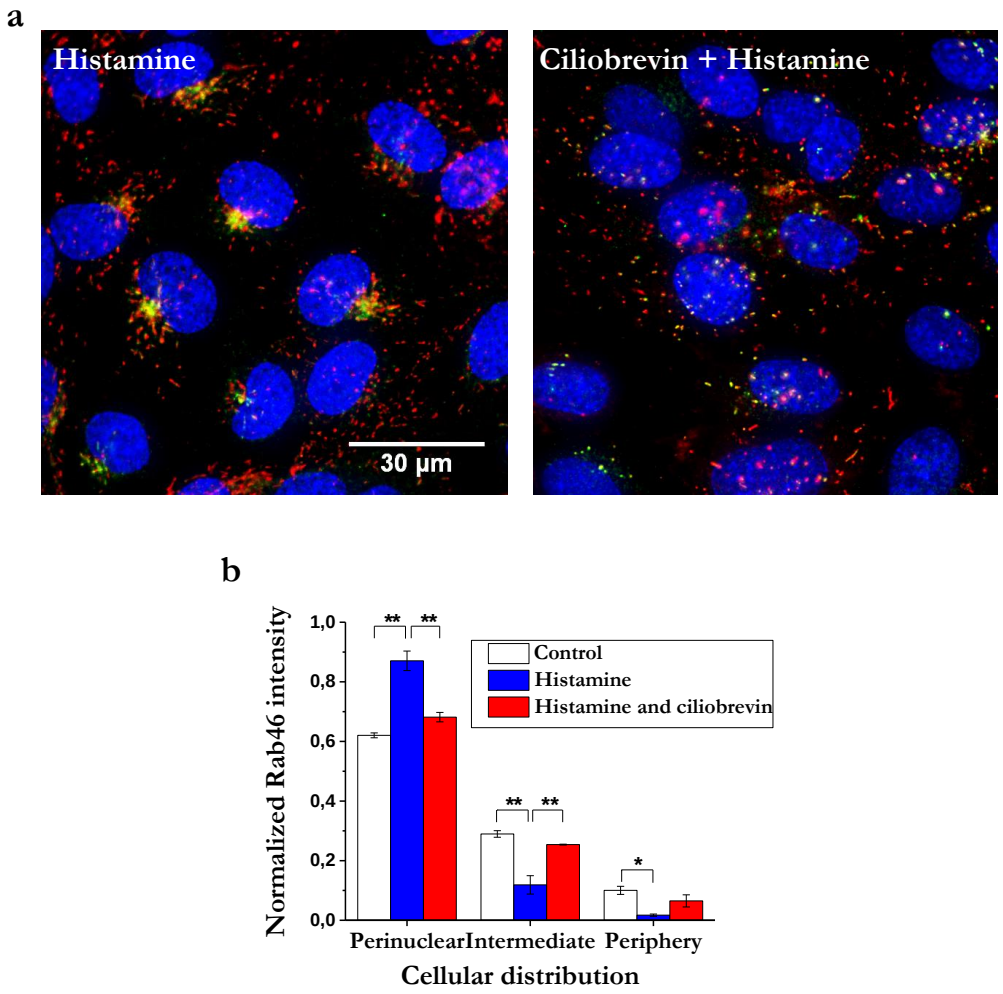

Figure 4.11 Dynein activity is necessary for Rab46-dependent trafficking of WPBs to the MTOC. (a) Histamine treated endothelial cells (left) compared with (right) endothelial cells pre-treated with ciliobrevin D (45 µM) stimulated with 30 µM histamine and then fixed and stained for vWF (red) and Rab46 (green). (b) Mean data showing the cellular distribution of Rab46 upon histamine stimulation in cells pre-treated with ciliobrevin and respective control cells. The plots quantify Rab46 signal intensity in the respective area where the mean (± SEM) was noted as percentage of the total signal intensity. n/N=3/18, *p-value < 0.05 **p-value < 0.01 from 1-way ANOVA.

Chapter 5 Mechanisms underlying Rab46-dependent WPB trafficking

5.1 Introduction

To understand the molecular mechanism underlying Rab46-regulated WPB trafficking, it is essential to identify cellular Rab46 partners which may temporally and spatially control its activity. Although there is a high degree of Rab domain sequence conservation, the functional diversity of all the Rab family members arises from their interaction with a wide variety of effectors. To this extent, Rab-family members acquire particular features that allow them to perform specific cellular functions. By interacting with a wide variety of effectors, they play a key regulatory function in coordinating the consecutive stages of intracellular trafficking.

The characterization of the protein–protein association mechanisms is crucial to understanding how biological processes occur. Srikanth et al., identified Vav1 as a new Rab46 interacting protein in T-cells. Interaction with Vav1 is crucial for recruitment and accumulation of Rab46 vesicles at the immunological synapse. A recent paper from the Vale lab also identifies the dynein protein as a new Rab46 interacting partner in immune cells, presenting Rab46 as a novel dynein adaptor protein. Despite these two studies in immune cells, the mechanisms underlying Rab46 function in endothelial cells is unknown.

The aim of this chapter is to identify putative Rab46-interacting proteins in order to gain insight the molecular machinery which coordinate WPB trafficking. It has already been shown that most of the already known Rab effector proteins preferentially interact with the active GTP-bound form of the Rab GTPase as conformational change expose the binding sites allowing their specific cellular function. In order to identify potential Rab46 effectors, the constitutive active mutant (Q604L) was compared with the inactive (N658I) in proteomic analysis and immunoprecipitation assays, followed by western blots validation of potential candidate proteins.

This chapter establishes two new Rab46-interacting proteins in endothelial cells. The Na^{2+} /K^{+} ATPase subunit 1α (ATP1α) and the Dynein Heavy Chain (DHC) interact with the active form of Rab46 in addition to endogenous Rab46 upon histamine stimulation. Interestingly, and in agreement with (the Vale paper)[173], my data suggest Rab46 interacts directly with the dynein-dynactin complex.

5.2 Identification of Rab46 binding partners

To identify Rab46 interacting partners, pull-down assays with recombinant Rab46 mutants followed by mass spectroscopy were used. Figure 5.1 illustrates a graphical representation of the pull-down workflow for protein identification by mass spectrometry. Briefly, GFP-tagged Rab46 active (Q604L) and inactive (N658I) forms were overexpressed in endothelial cells, expression of a GFP empty vector was used as a negative control. High affinity binding and high specificity of ChromoTek GFP-trap beads allowed purification and specific elution of any protein complex bound to the beads. 20% of the elution fraction from three biological replicates was analysed by western blot (Figure 5.2) to confirm efficient pull-down. Immunoblot with anti-GFP antibody shows a single band at the expected molecular weight (120 kDa) in the total lysates as well as the elution fractions of both Q604L and N658I, indicating that the GFP-Rab46 mutants successfully bound to the GFP-beads. All the interacting proteins which co-purified with the two Rab46 mutants were subsequently identified using mass spectroscopy (LC-MS/MS).

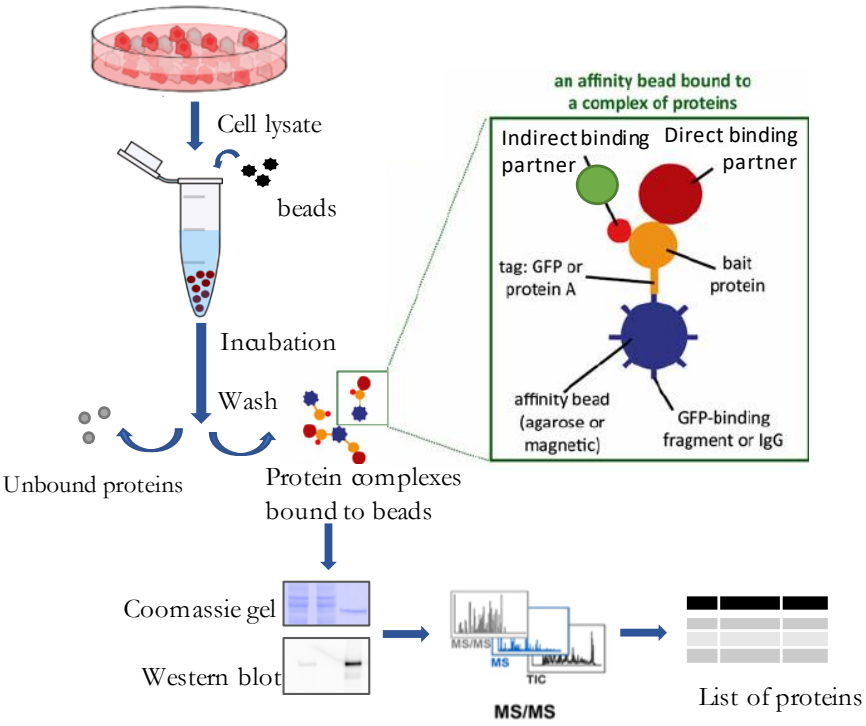

Figure 5.1 Pull-down experiment workflow for endothelial cells proteomics. The flowchart demonstrates the major steps for the purification of tagged proteins along with their interactors. Endothelial cell transfected with GFP-tag protein were lysed and incubated with GFP-trap beads. After incubation the beads were sedimented and a small fraction of the unbound supernatant was taken for subsequent western blot analysis. Following several washing steps the protein complex bound to the beads was eluted with appropriate buffer. 10% of the beads were used for SDS-PAGE/Coomassie staining and western blot analysis. The inset illustrates how the bait protein, tagged with GFP, binds to an affinity bead via direct interaction with a GFP-binding domain. Proteins interacting with the bait protein co-purify on the affinity beads and are subsequently identified using mass spectrometry.

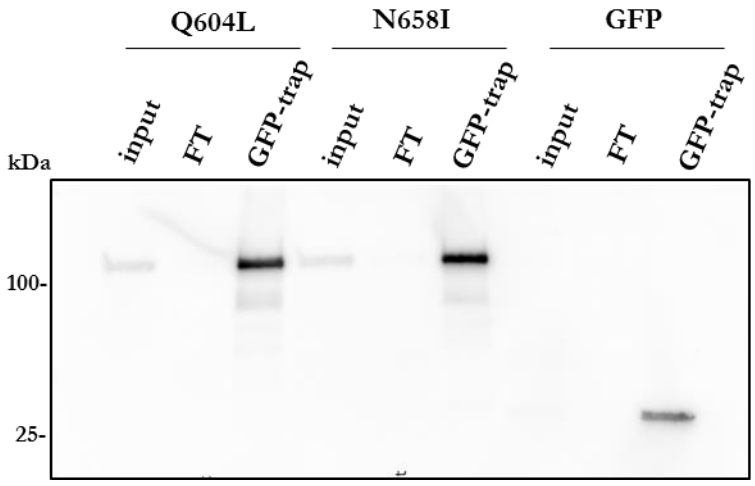

Figure 5.2 Pull-down of Rab46 binding mutants. (a) GFP-tagged active and inactive form of Rab46 (Q604L and N658I respectively) were overexpressed in HUVECs. Cells lysates were incubated with GFP-trap beads (ChromoTek) and pulled down proteins were subjected to SDS-PAGE and western blot. Anti-GFP antibody was used to check successful pull-down. Input represents total lysate, FT represents flow-through after incubation and GFP-trap represents pull-down proteins. n=3.

5.2.1 Proteomic analysis

LC-MS/MS was the method of choice for analysing the components of the final eluted samples from GFP-trap pull-down. The three groups of analysis (QL: active, NI: inactive and GFP: control) generates four different datasets: i) QLvsGFP ii) NIvsGFP (control datasets) iii) QLvsNI and iv) NIvsQL (datasets of interest). These comparisons give a fold change value which is calculated by comparing the peak areas and a p-value for significance between the technical and biological triplicates.

The MS analysis, performed by Gemini Biosciences, identified a large number of peptides from proteins that had been significantly ($p \leq 0.05$) pulled down by the Rab46 mutants. In order to narrow the number of candidate proteins for further investigation, a list of criteria was established. Firstly, a 1.5-fold change cut-off was set and p-value ≤ 0.05 was considered the significant threshold. Figure 5.3 shows the distribution of quantified proteins according to the set criteria. The first sorting, considering fold change values ≥ 1.5 (vertical line), highlights 10% of all the proteins identified in the QL sample by mass spectroscopy and 20% of the one identified in the NI (blue data points). It also shows that proteins with high fold changes do not necessarily have low p-values. Therefore, to further narrow the investigations, an extra selection step was applied to previously sorted proteins based on the significance of p-values. Proteins with fold change ≥ 1.5 and p-value ≤ 0.05 (red data points) result to be 5% of the total proteins identified by mass spectroscopy. In order to prevent missing out any potential trusted candidates, the mean and the median values were also taken into consideration for proteins with fold change ≥ 1.5 but non-significant p-value. Co-purified impurities such as keratin and trypsin were ignored. These criteria were applied to all the datasets.

Next, control datasets were compared to their respective dataset of interest, i.e. QLvsGFP compared to QLvsNI. Venn diagram in Figure 5.4 shows comparisons between all the datasets revealing the percentage of proteins in common between them. Proteins identified in both datasets were highlighted as positive candidate proteins together with the ones uniquely present in the dataset of interest with significant p-value and fold change greater than 1.5. A final list of candidate proteins, sorted by fold change, was compiled (Figure 5.5 and Figure 5.6) and the biological significance in the context of membrane trafficking of the selected proteins was evaluated.

a

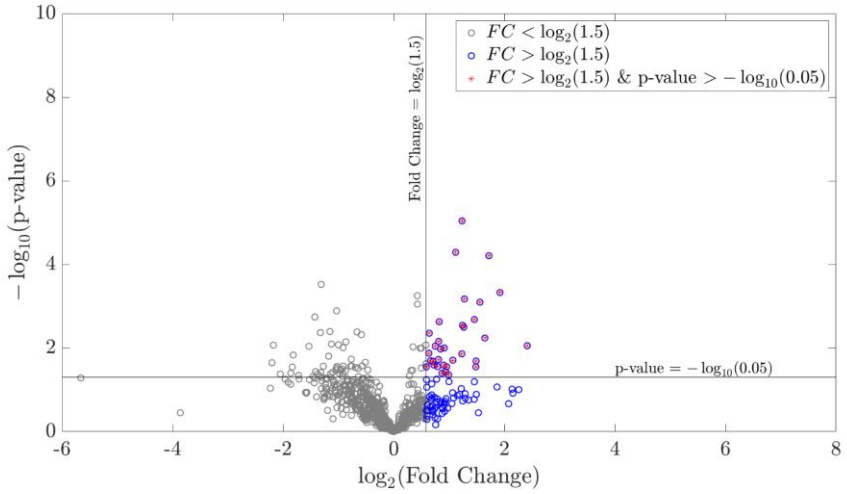

b

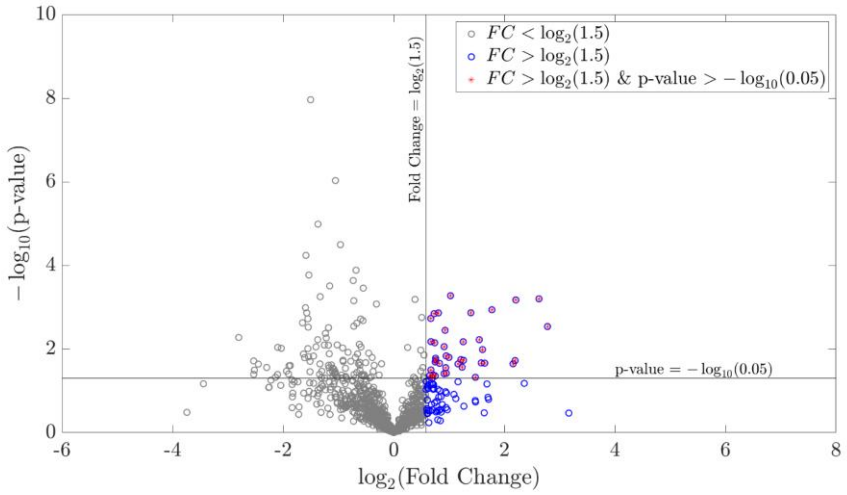

Figure 5.3 Visualization of proteomic data. Scatter plots showing the distribution of proteins that co-precipitated with GFP-tagged Rab46 nucleotide binding mutants or GFP control. Proteins identified from mass spectrometry analysis were plotted according to p-value (-$\log_{10}$ transformed) on the y-axis and fold change ($\log_2$ transformation) on the x-axis. Significance level is indicated with a horizontal straight black line (p-value < 0,05) and fold change threshold with vertical black line (fold change ≥ 1.5). Representative scatter plot from control dataset (a) and dataset of interest (b) where a first sorting filter was applied to highlight proteins with a fold change greater than 1,5 and significant p-values.

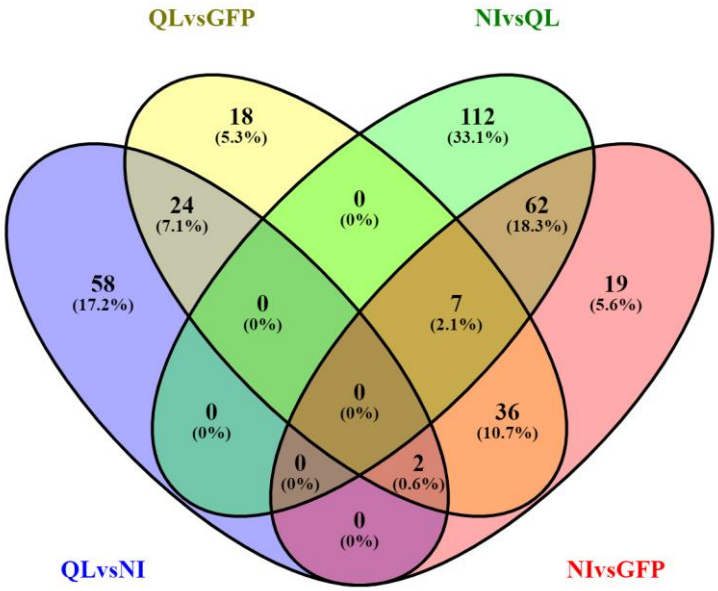

Figure 5.4 Comparison between the datasets illustrate proteins that are uniquely present in one condition and not in others. Venn diagram comparing the accession numbers of proteins identified in four different conditions: QL vs GFP and NI vs GFP (control datasets), QL vs NI and NI vs QL (datasets of interest) illustrating the intersections between the proteomes (Venny, http://bioinfogp.cnb.csic.es/tools/venny).

5.2.2 Candidate protein selection

The proteomic analysis led to a list of candidate proteins for both the active and inactive forms of Rab46 (Figure 5.5a and Figure 5.6a). The PANTHER classification system was used to classify proteins by function in order to identify those functional categories, and respective pathways, which were overrepresented in the two groups. A functional classification was performed using the gene list analysis tool within PANTHER. This tool returns the results in a pie chart, which displays an overview of all ontology terms at the first (or most general) level within the same ontology. When a slice of the pie chart, which represents an ontology term, is clicked, a new pie chart will appear that contains its child ontology term. Analysis of the list of proteins identified for the inactive form of Rab46 (NI) generates the protein function pie chart in Figure 5.5b. 72% of the gene hits were classified as having a nucleic acid binding function which include structural molecular activity and transcription or translation regulation. The other proportion is divided into different protein classes with a very low representation hits which are mainly involved in the apoptosis or autophagy signalling pathway. On the other hand, the gene classification regarding the active form of Rab46 (QL) returns a pie chart (Figure 5.6b) where different protein classes were identified. The most abundant protein classes are the membrane traffic protein class and the hydrolase class. However, to further seek a biological explanation, classification according to the biological process to which a protein contributes was performed. More than 40% of the hits have a role in cellular components organisation and localisation. Interestingly, the second level of classification shows that the most represented function is the establishment of organelle localisation and transport. The most relevant proteins which were often highlighted were vesicle-mediated transport protein (BCAP31, CLTC and COPA), regulatory membrane traffic protein like LAMP1 and MYO9, transporter protein (ATP1α) and (DYNCH1) as proteins involved into establishment of organelles localisation and transport along the microtubules.

To select candidate proteins with possible biological relevance to Rab protein regulation, I performed a literature review and an overview of available resources and tools (i.e. antibody, siRNA) for the proteins highlighted by the panther analysis. Although all highlighted proteins represent interesting candidates, two recent publications[173-187] drove the attention to the Na^{2+} /K^{+} ATPase subunit 1α (ATP1α) and the cytoplasmatic dynein heavy chain (DYNCH1 or DHC). The relevance of the ATP1α arises from its new role in regulating Rab27a localisation and activation in melanocytes proposed by Booth et al[187]. Rab27a is one of the most characterised Rab GTPases associated with WPBs, thereby suggesting a role of the ATP1α in regulating Rab46 and WPBs. Very recently, the identification of Rab46 as a new dynein adaptor protein in immune cells by Wang et al.[173] as well as our previous knowledge about the role of dynein activity in Rab46-depedent WPB trafficking, advocates DHC as a candidate for investigation.

Consequently, ATP1α and DHC were chosen to further characterise Rab46 interactions.

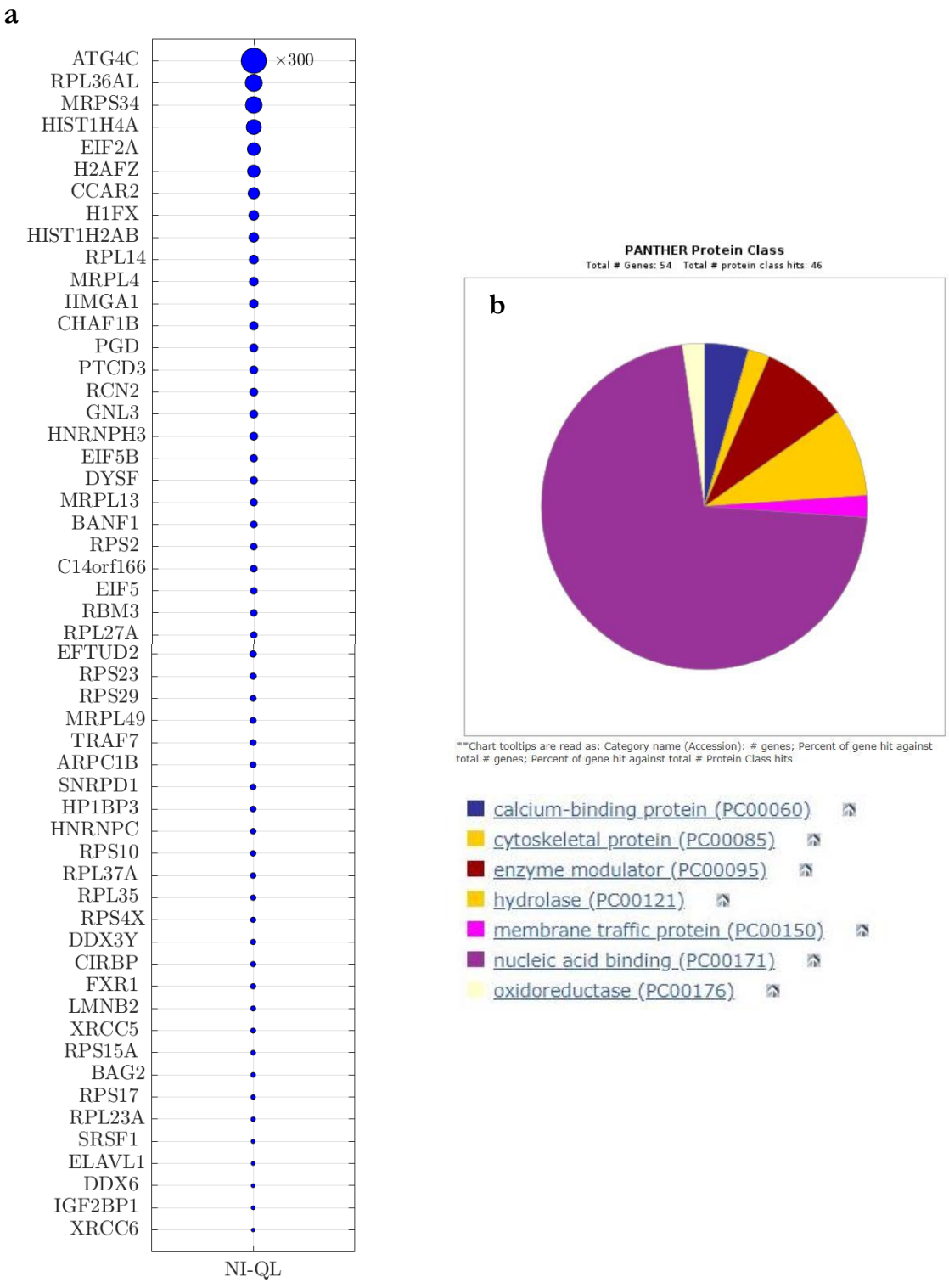

Figure 5.5 Analysis of Rab46 binding mutants interactome. (a) Proteins co-precipitate with GFP-N658I and identified by mass spectrometry analysis, in reference to GFP-Q604L, were sorted by fold change and p-value and then ranked by decreasing fold change. Bubble plots show proteins with Fold change greater than 1,5 and p-value < 0,05. Circled area is proportional to the fold change. (b) Panther Pathway Analysis and classification of the GFP-N658I hits into the most relevant protein classes.

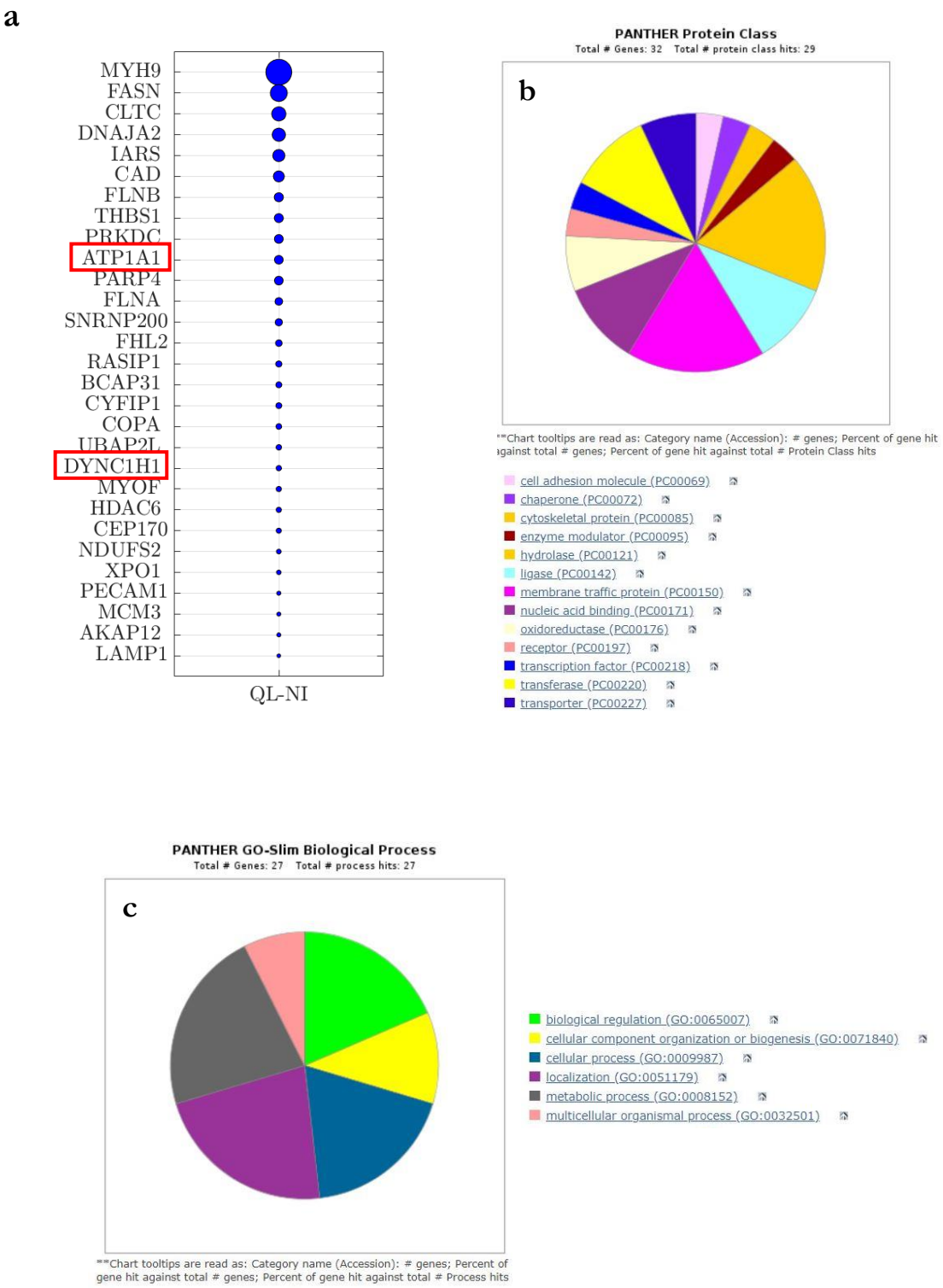

Figure 5.6 Analysis of Rab46 binding mutants interactome. Proteins co-precipitate with GFP-Q604L identified by mass spectrometry analysis in reference to GFP-N658I, were sorted by fold change and p-value and then ranked by decreasing fold change. Bubble plots show proteins with Fold change greater than 1,5 and p-value < 0,05. Circle area is proportional to the fold change. Relevant proteins for this thesis are highlighted (red). (b) Panther Pathway Analysis and classification of the GFP-Q604L hits into the most relevant protein classes. (c) Panther Analysis of the candidate proteins contributions to the highlighted biological process.

5.3 Validation of Rab46 interacting proteins

The GFP-trap pull-down and the mass spectrometry analysis identified a selection of putative Rab46-interacting proteins. In particular, the ATP1α and the DHC proteins were selected due to their potential relevance in terms of organelles trafficking and localisation. In order to validate the presence of ATP1α and DHC in the same complex with the constitutively active Rab46, co-immunoprecipitation (co-IP) experiments were performed. The GFP-Rab46 active and inactive constructs (Q604L and N658I, respectively) were overexpressed in endothelial cells. A GFP immunoprecipitation (IP) was performed and immunoblotting was utilised to detect whether the two selected candidates co-precipitated. Firstly, the interaction between GTP-bound Rab46 (Q604L) and the dynein heavy chain was examined. Immunoblotting using a GFP antibody reveals the presence of a specific band at the expected molecular weight (120 kDa) in the input lysate showing the transfection efficiency of the active (GFP-QL) and inactive (GFP-NI) Rab46 in the total lysate. The GFP antibody used for the IP was able to pull-down both the GFP constructs as indicated by the single band in the IP lanes and immunoblotting for the dynein heavy chain confirms its presence in the same sample with the active form of Rab46 (Figure 5.7). These results validated the mass spectrometry analysis suggesting that both GTP-Rab46 (Q604L) and the dynein heavy chain interact in the same complex.

The result was similar when the expression of ATP1α was validated by IP and immunoblotting. Probing with a GFP antibody shows expression of the Rab46 constructs in the input as well as after IP. Immunoblotting for ATP1α shows single band at the expected molecular weight (110 kDa) in the total lysate and in the IP samples. Notably, the ATP1α preferentially interacts with the active GTP-Rab46 (Figure 5.8). These results propose two new Rab46 interacting proteins; both the dynein protein and the ATP1α preferentially interact with the active form of Rab46 when the GFP-construct is overexpressed in endothelial cells.

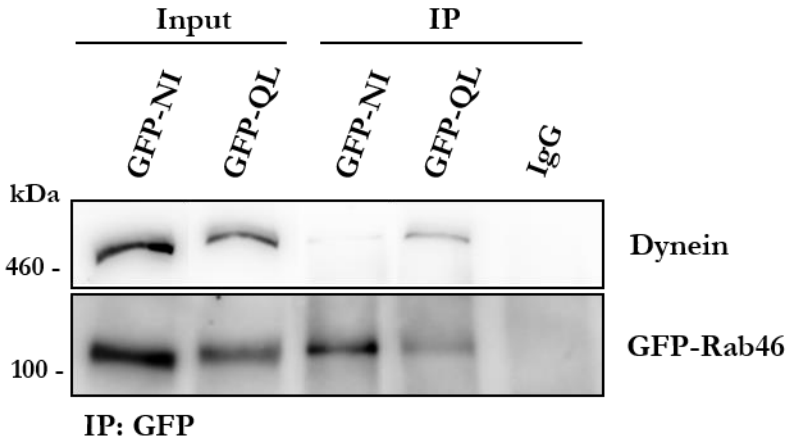

Figure 5.7 Immunoprecipitation of Rab46 nucleotide binding mutants to confirm proteomic analysis. GFP-tagged active and inactive form of Rab46 (Q604L and N658I respectively) were overexpressed in HUVECs and immunoprecipitation performed using an anti-GFP antibody. Input represents lysate before immunoprecipitation and IP denotes samples after GFP immunoprecipitation. Western blot using anti-GFP and anti-dynein heavy chain antibodies shows that the dynein heavy chain co-precipitates with the active form of Rab46 (Q604L). n=3

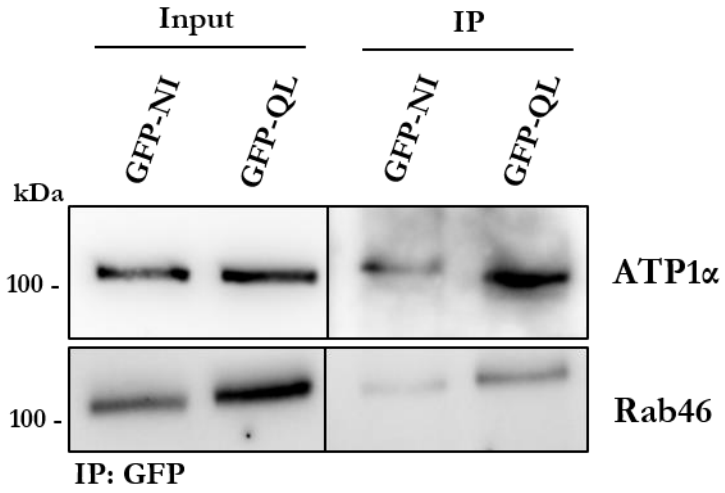

Figure 5.8 Immunoprecipitation of Rab46 nucleotide binding mutants to confirm proteomic analysis. GFP-tagged active and inactive form of Rab46 (Q604L and N658I respectively) were overexpressed in HUVECs and immunoprecipitation performed using an anti-GFP antibody. Input represents lysate before immunoprecipitation and IP denotes samples after GFP immunoprecipitation. Western blot using anti-GFP and anti-ATP1α antibodies shows that the ATP1α co-precipitates with the active form of Rab46 (Q604L). n=2

5.3.1 Validation of endogenous Rab46 protein-protein interaction

High concentrations of proteins can potentially interfere with cellular function in several ways, for example by activating or overloading certain biological pathways, disrupting their regulation, upsetting the balance in protein complexes or by aggregating together[188]. Ultimately, overexpressing any protein will be destructive because it exhausts the resources of the cell to make and transport proteins[189].

It is evident that the concentration of a protein can be a major driving force for any protein interaction; hence, when artificially raising cellular protein concentrations, non-interactors might be forced to associate[190]. In order to avoid side effects of unequal gene dosage causing unbalanced stoichiometry leading to artificial results, it is important to evaluate biologically meaningful interactions under native conditions. This approach should allow spatiotemporal resolution of interactions distinguishing from artefacts caused by overexpression. Highlighting these points, the IP protocol was adapted for the endogenous Rab46 protein. The anti-Rab46 antibody bound to sepharose beads was used to immunoprecipitate endogenous Rab46 from endothelial cell lysate. The ratio between antibody and protein lysate was optimized to avoid saturation and non-specific binding. Figure 5.9 shows successful IP of endogenous Rab46 using 1 µg of antibody and 0.5 mg of total lysate.

The ability to pull-down endogenous Rab46 prompts further more biologically relevant investigations to examine Rab46 protein interactions in endothelial cells under both resting and stimulated conditions.

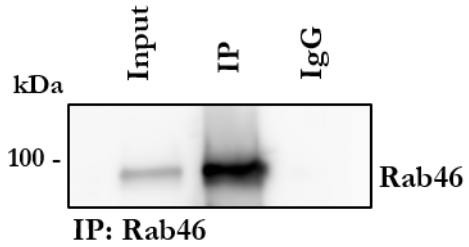

Figure 5.9 Immunoprecipitation of endogenous Rab46. Representative western blot showing successful immunoprecipitation of endogenous Rab46 using sepharose beads conjugated with anti-Rab46 antibody. Input represents HUVECs lysate before the IP and co-precipitated samples after elution are denoted as IP. Anti-rabbit IgG are used as control.

5.3.1.1 Endogenous Rab46 interacts with the ATP1α

Heterologous expression of Rab46 mutants suggests ATP1α interaction with the active form of Rab46. To validate this result for the native protein, endogenous Rab46 IP was repeated and ATP1α co-immunoprecipitation assessed by immunoblotting. I have previously shown (section 3.3.1 and Figure 4.8) that the constitutively active form of Rab46 (Q604L) localises to the perinuclear area which is mimicked by histamine stimulation of endogenous Rab46. Therefore, to mimic GTP-driven Rab46 localisation in native condition, endothelial cells were treated with histamine prior to IP of endogenous Rab46. Cell lysates were incubated with anti-Rab46 antibody or control IgG and pulled down with sepharose beads. Eluted samples were analysed by western blot (Figure 5.10a). Immunoblotting for Rab46 shows a band at 95 kDa confirming positive IP for non-treated and treated cells in contrast with no signal in the negative IgG control. To examine the existence of the ATP1α in the same sample, immunoblotting for the ATP1α was performed. The Na^{2+} /K^{+} ATPase subunit 1α has a predicted molecular weight of 110 kDa, which was confirmed via immunoblotting by the presence of a specific band at the exact molecular weight in the total lysate as well as the IP fractions. Although a faint band is present into the non-treated IP fraction, a stronger band is visible in the histamine-treated sample. To further validate the interaction between Rab46 and the ATP1α, a reverse co-IP was performed using an antibody against the novel target (ATP1α) and immunoblotting for the original "bait" (Rab46). Similarly, the reverse co-IP shows the presence of Rab46 in both the ATP1α IP fractions with a stronger band corresponding to the histamine stimulated IP fraction (Figure 5.10b). The specificity of this interaction is supported by the use of control IgG as negative control showing no interaction between the IgG and the target proteins.

These results suggest that Na^{2+} /K^{+} ATPase subunit 1α is a Rab46-interacting protein and that this interaction is enhanced after histamine stimulation.

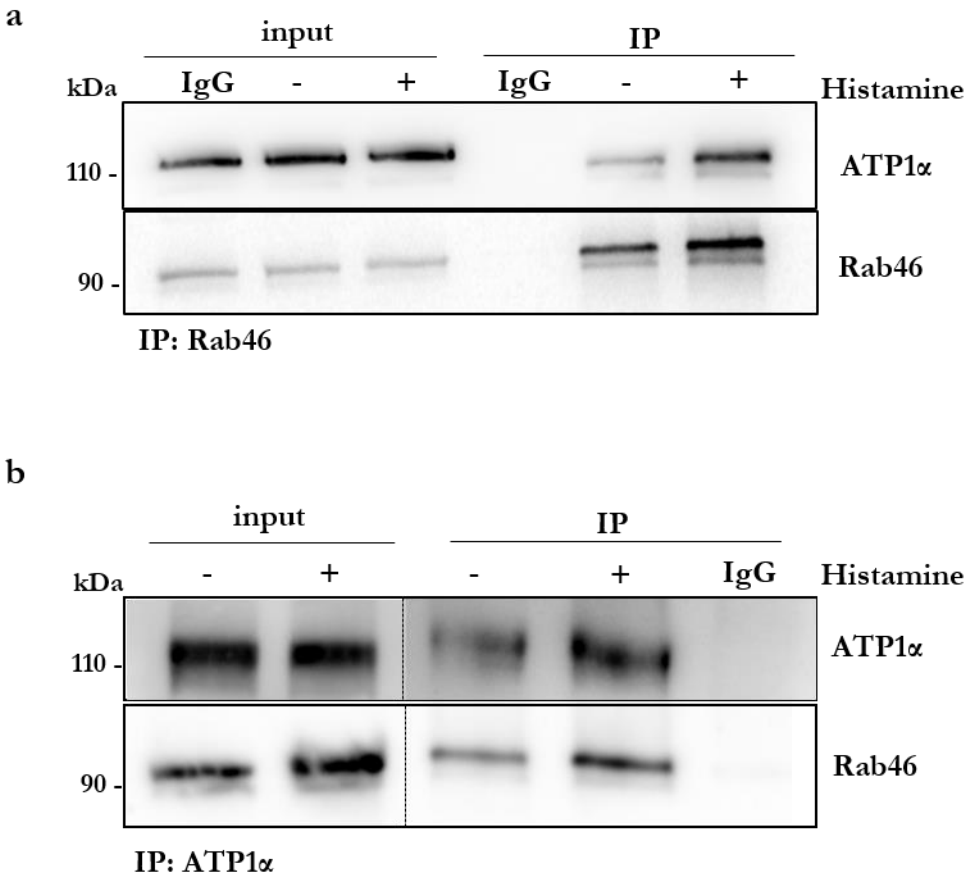

Figure 5.10 Endogenous Rab46 interacts with the Na^+/K^+ ATPase subunit α1. (a) Immunoprecipitation of endogenous Rab46 in HUVECs stimulated with 30 μM histamine or vehicle control was performed using an anti-Rab46 antibody and co-precipitation of ATP1a1 was assessed by immunoblotting. Input represents total lysate before the IP and samples after the IP are denoted as IP. (b) Reverse co-immunoprecipitation of endogenous Rab46 performed using anti-ATP1a1 antibody, co-precipitation was assessed by immunoblotting for Rab46. Input represents total lysate before the IP and samples after the IP are denoted as IP. Anti-rabbit and anti-mouse IgG were respectively used as negative controls. Blots are representative of 3 independent experiments.

5.3.1.2 Endogenous Rab46 interacts with the cytoplasmic dynein

Heterologous expression of Rab46 mutants also suggests DHC interaction with the active form of Rab46. To validate this result and better characterise the nature of the interaction, endogenous Rab46 IP was performed and DHC co-IP assessed by immunoblotting. As described above, to mimic GTP-bound active Rab46, endothelial cells were stimulated with histamine and co-IP was performed. Western blot analysis confirmed similar levels of Rab46 expression in the total lysates and the IP. DHC is a large protein with a predicted molecular mass of 500 kDa, therefore a suitable western blot protocol for large proteins was performed. Immunoblotting for DHC successfully revealed a specific band at the correct molecular weight (500kDa) in the total lysates as well as in the IP corresponding to the non-treated and histamine treated samples (Figure 5.11a). In addition, a reverse co-IP using an anti-DHC antibody to pull-down endogenous dynein and immunoblotting to seek for Rab46 co-IP was performed. Similarly, dynein was pulled down with Rab46 in both the vehicle and histamine treated cells. No cross-reaction was observed in the negative IgG control, suggesting specific interaction between endogenous Rab46 and the DHC in both the tested conditions but with a potential enhanced interaction upon histamine treatment (Figure 5.11b).

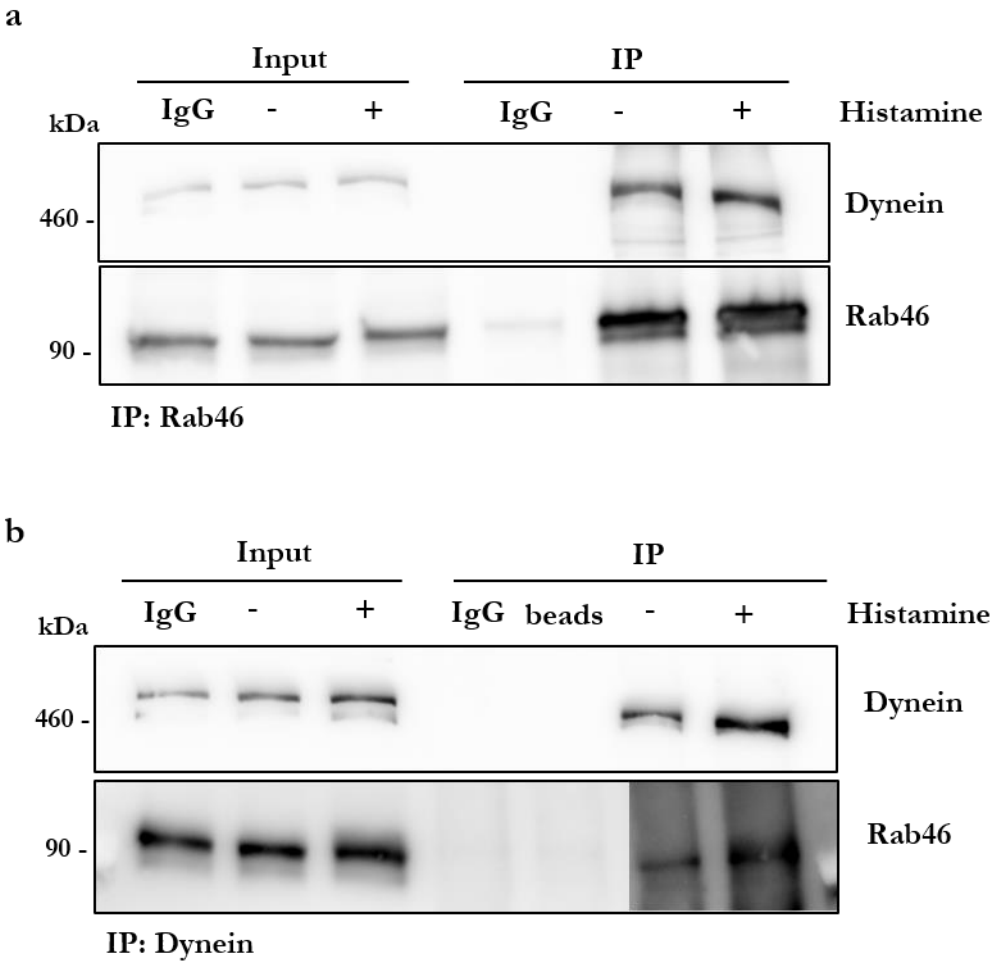

Figure 5.11 Endogenous Rab46 interacts with the dynein motor protein. (a) Immunoprecipitation of endogenous Rab46 in HUVECs stimulated with 30 μM histamine or vehicle control was performed using an anti-Rab46 antibody and co-precipitation of DHC was assessed by immunoblotting for dynein heavy chain. Input represents total lysate before the IP and samples after the IP are denoted as IP. (b) Reverse co-IP of endogenous Rab46 performed using anti-dynein heavy chain antibody, co-precipitation was assessed by immunoblotting for Rab46. Rab46 is shown at an increased exposure and overlaid on the blot. Input represents total lysate before the IP and samples after the IP are denoted as IP. Anti-rabbit IgG or Sepharose beads were used as negative controls. Blots are representative of 3 independent experiments.

5.4 The cytoplasmic dynein-dynactin motor complex interacts with Rab46

Cytoplasmic dynein-1 is a large protein complex that drives long-range retrograde transport along microtubules. Dynein works together with another protein complex called dynactin which is an essential co-factor for all dynein function including dynein motility. To further characterise the interaction between Rab46 and the DHC, I investigated the interaction between Rab46 and the dynactin complex. The largest component of the dynactin complex is $p150^{Glued}$ which binds to dynein and mediates direct association between dynactin and microtubules. Co-immunoprecipitation assays were carried out to ascertain whether Rab46, DHC and p150 co-immunoprecipitate with each other in endothelial cells before and after histamine stimulation. First of all, endogenous Rab46 was pulled-down and immunoblotted for both DHC and $p150^{Glued}$ (Figure 5.12a). Rab46 was equally pulled down before and after histamine stimulation and co-IP of DHC was confirmed by the presence of a single band at 500 kDa in both conditions. Furthermore, probe for p150 revealed a single band at 120 kDa in the total lysate as well as the IP fractions. To confirm this association, the interaction was further investigated by performing the reverse IP. Endothelial cells were lysed and incubated with anti-p150 antibody or anti-DHC antibody. The IP was assessed by immunoblotting for p150, Rab46 and DHC. Probing for these proteins simultaneously revealed a band at the expected molecular weight of endogenous Rab46 (95 kDa) in both the DHC and p150 IP samples (Figure 5.12b-c).

The presence of Rab46, DHC and p150 in the same IP sample suggested the existence of a Rab46-dynein-dynactin motor complex.

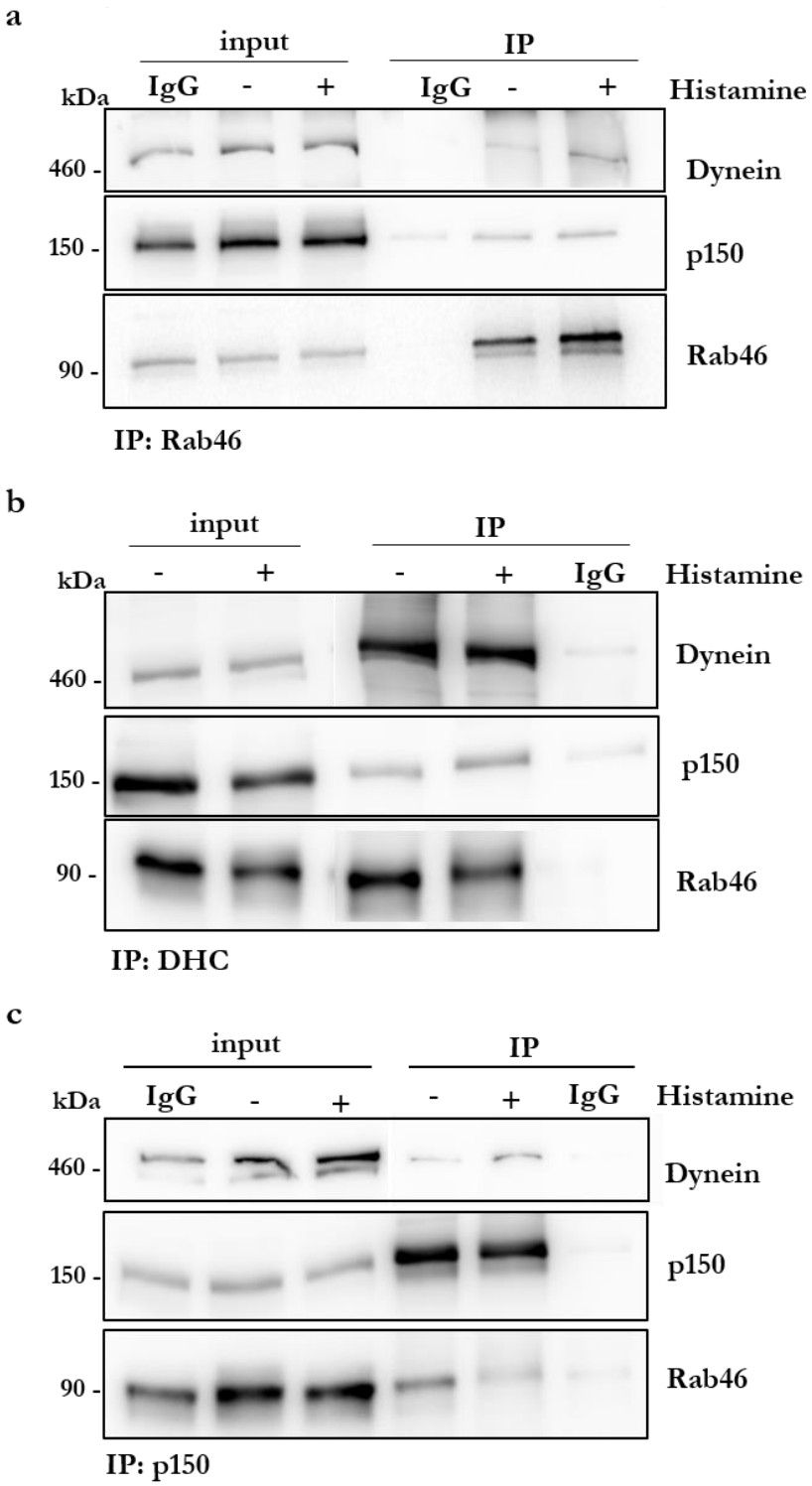

Figure 5.12 Endogenous Rab46 interacts with the dynein-dynactin complex. (a) Immunoprecipitation of endogenous Rab46 in HUVECs stimulated with 30 μM histamine or vehicle control was performed using an anti-Rab46 antibody and co-precipitation of DHC and p150, subunit of dynactin, was assessed by immunoblotting for dynein heavy chain and p150. (b) Reverse co-immunoprecipitation of endogenous Rab46 and p150 subunit was performed using anti-dynein heavy chain antibody, co-precipitation was assessed by immunoblotting for Rab46 and p150. (c) Reverse co-immunoprecipitation of endogenous Rab46 and dynein heavy chain was performed using anti-p150 antibody, co-precipitation was assessed by immunoblotting for Rab46 and DHC. Input represents total lysate before the IP and samples after the IP are denoted as IP. Corresponding IgG were used as negative control. Blots are representative of 3 independent experiments.

5.5 Regulation of dynein-Rab46 interaction by calcium

Rab46 contains two functional Ca^{2+} binding motifs (EF-hands) in the C-terminal[167]. Wang et al[173] recently reported that Ca^{2+} binding to the EF-hands was necessary for the interaction between Rab46 and dynein in T-cells. Therefore, I investigated the role of Ca^{2+} binding to Rab46 in the interaction between dynein and Rab46 in endothelial cells. Ca^{2+} was unable to bind to Rab46 when the EF-hands were mutated ($Rab46^{EFmut}$) regardless of Ca^{2+} concentration[172] (Figure 5.13a). Imaging of $Rab46^{EFmut}$ overexpressed in endothelial cells revealed a strong perinuclear clustering, suggesting anchoring of $Rab46^{EFmut}$ to the MTOC (Figure 5.13b). We have previously shown that Ca^{2+} is necessary for dissociation of Rab46 clustered at the MTOC by histamine stimulation, evoking subsequent dispersal[191]. According to proteomic analysis (5.2.1) and western blot (Figure 5.7), the inactive nucleotide-free Rab46 does not bind to the DHC. Therefore, in order to investigate the effect of Ca^{2+} on Rab46 interaction with dynein, a co-IP was performed. GFP-tagged $Rab46^{EFmut}$, inactive GFP-NI Rab46 construct or a GFP only vector were overexpressed in endothelial cells and an IP performed using anti-GFP antibody. The IP was validated by immunoblotting for GFP and co-IP of dynein assessed by DHC probing (Figure 5.14). Similar levels of expression of all the constructs were observed in the total lysates (input) and successful IP of GFP-tagged Rab46 confirmed by a band at approximately 120 kDa. The use of GFP antibody for the IP rather than GFP-trap and the use of the same antibody for immunoblotting highlighted non-specific bands (asterisks*) corresponding to the IgG heavy (50 kDa) and light chains (25 kDa) but this had no effect on the detection of both Rab46 and DHC. Although the level of $Rab46^{EFmut}$ in the IP fraction is lower than the inactive GFP-NI mutant, immunoblotting for DHC shows a distinct band, at the correct molecular weight, in this fraction as compared to the NI mutant or GFP control. Surprisingly, these results suggest that the interaction between Rab46 and the dynein heavy chain is Ca^{2+}-independent.

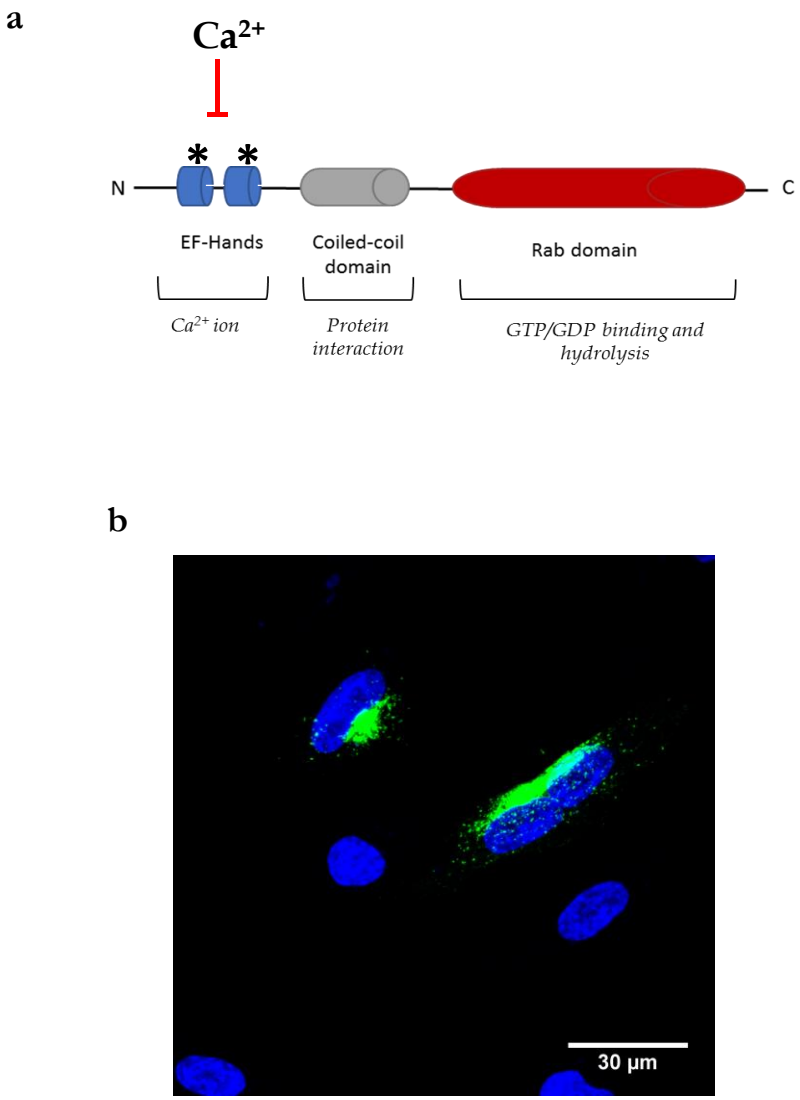

Figure 5.13 Rab46 calcium-binding defective mutant. (a) Schematic representation of Rab46 structure showing mutations in the two EF-hands which abolish calcium binding. (b) Super-resolution imaging of endothelial cells expressing Rab46 EF-hand mutant (green). Deficiency in calcium binding shows Rab46^{EFmut} clustering in the perinuclear area. DAPI (blue) for the nuclei. Scale bar = 30 µm

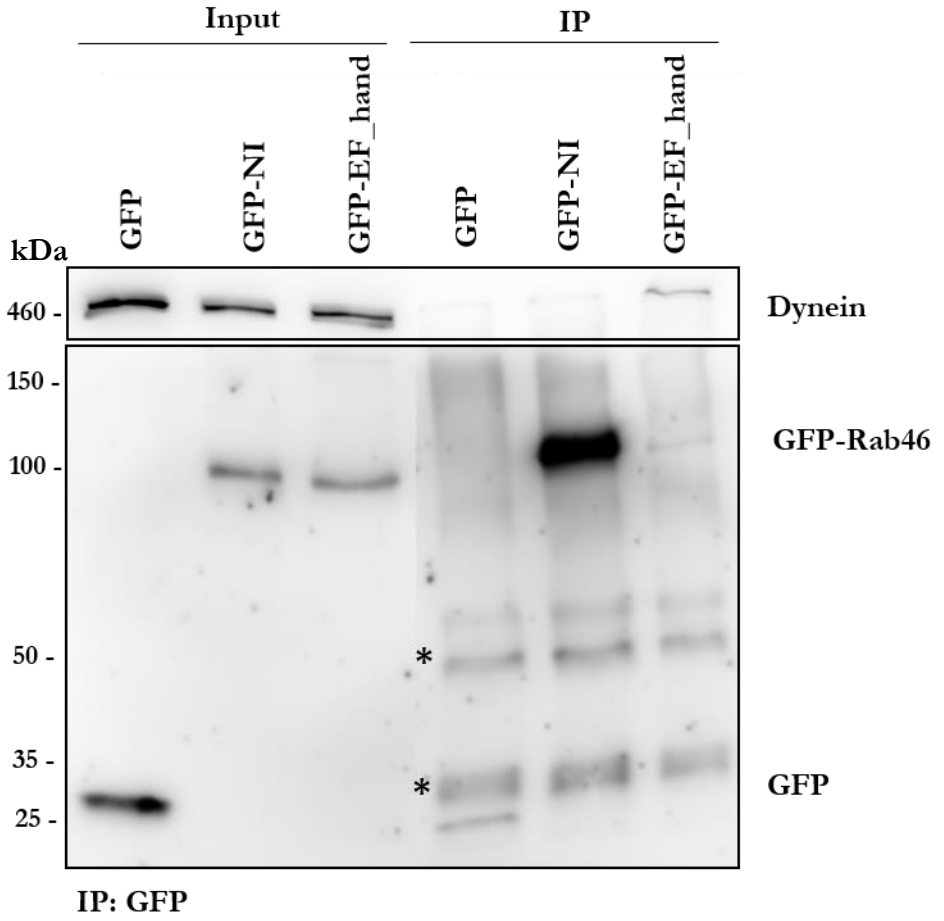

Figure 5.14 Rab46 and dynein interaction is calcium-independent. Immunoprecipitation of Rab46 binding mutants (GFP-NI and GFP-EF hand mutant) in HUVECs was performed using an anti-GFP antibody and co-precipitation of DHC was assessed by immunoblotting for dynein heavy chain. Input represents total lysate before the IP and samples after the IP are denoted as IP. Empty GFP vector was used as negative control. Blots are representative of 2 independent experiments.

5.6 Characterisation of Rab46 and dynein interaction

Cytoplasmic dynein is a minus end-directed motor, composed of two globular heads, each formed from a single dynein heavy chain (DHC) and a base from intermediate (DIC) and light chains (DLC). Dynein binds to microtubules through dimerization of its two heavy chains: the C-terminal of the heavy chain constitute the motor domain with ATP-binding activity (six ATPase subunits) and a stalk domain which link the motor to the microtubules, whereas the N-terminal constitute the tail domain where the association of the DIC and the DLC form a cargo-binding complex[192]. The association of dynein with many membrane cargos or target sites requires the accessory dynactin protein complex, which interact with DIC though the p150 glued subunit.[192] (Figure 5.15a-b).

On one side, the complex dynein structure provides a dynamic interaction with the microtubules through the catalytic heavy chains, on the other side the tail complex is responsible for linking the dynein motor complex to different cargos, directly or through adaptors. Because the tail region links the motor to a cargo, understanding the interactions within this portion is important in determining how dynein is targeted and regulated.

To this end, a commercially available purified protein corresponding to the N-terminal of the dynein heavy chain (Figure 5.15-box) was used to identify whether this sequence directly interacts with Rab46.

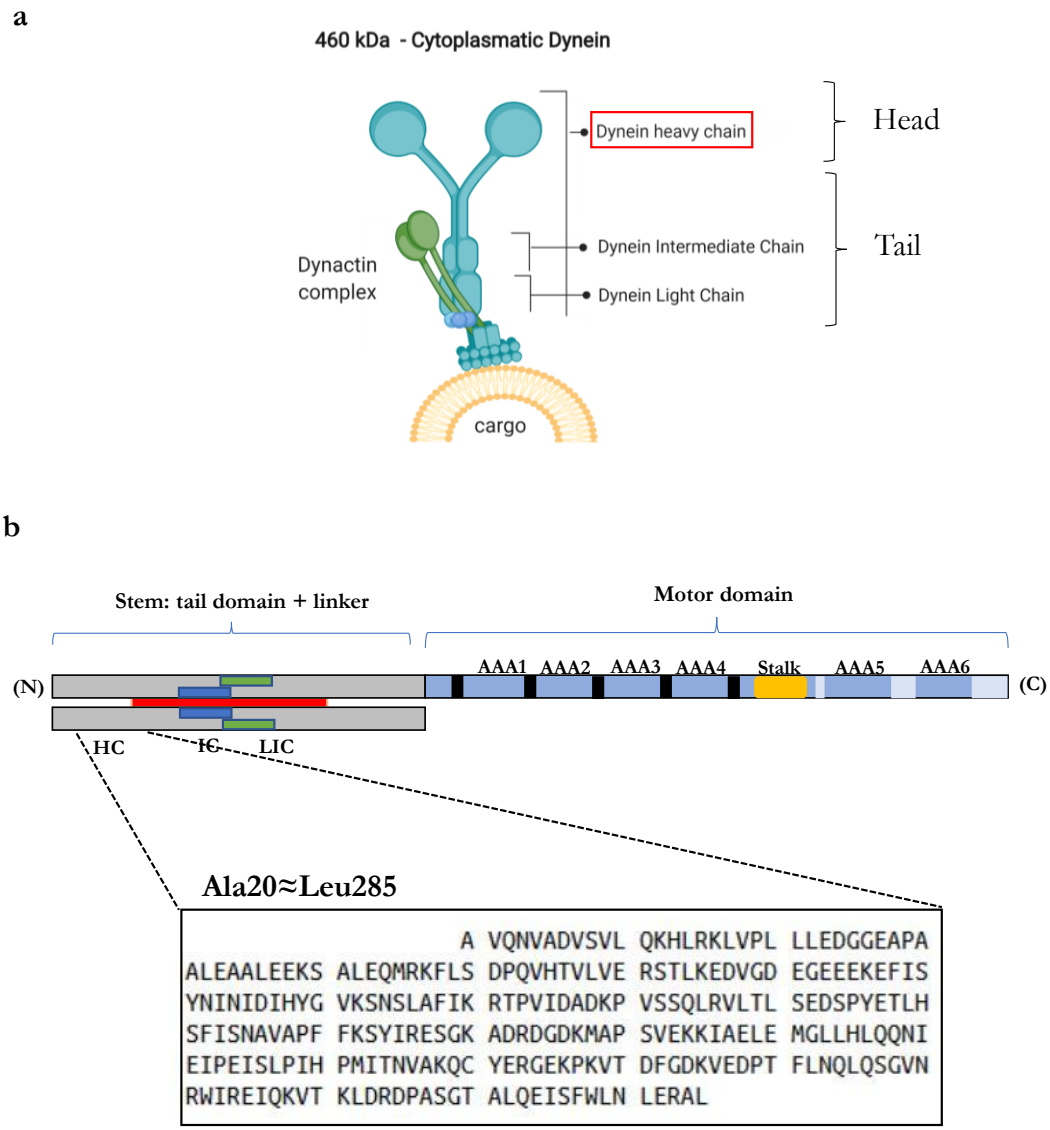

Figure 5.15 Schematic representation of the overall structure of a cytoplasmatic dynein and dynactin complex. (a) Structural organization of a dynein complex: the dynein heavy chain consists of a head region and a tail region which recruits the dynein intermediate chains and light chains. The dynactin complex interacts with dynein and mediates the interaction with cargo membrane. (b) Domain composition of the N-terminal stem region: dynein heavy chain (HC: grey) with interaction site for dimerization in red, dynein intermediate (IC) and light chains (LIC) interaction sites in blue and green respectively. The C-terminal region includes the motor domain with AAA1-6 and a stalk domain. The box below shows the sequence of the purified his-tag DYNC1H1 which is used in the following experiments.

5.6.1 Optimization of His-tag pull-down assay

The recombinant dynein heavy chain protein contains N-terminal His-tags (His-DYNCH1) for purification and identification. Unfortunately, recombinant Rab46 was not available for me to examine if the two proteins had a direct interaction *in vitro*. Therefore, in order to get some insight into this interaction, I ectopically expressed the human WT-Rab46 in monkey Cos-7 cells and designed a pull-down experiment using His-DYNCH1.

A pull-down assay is based on a bait protein captured on a solid support (beads) used to isolate potential binding proteins (prey) from a complex mixture. One of the most common tags used for purification or binding of expressed proteins is a short sequence of six histidine residues which has a unique ability to bind to divalent cations such as nickel, cobalt or copper. A powerful system to bind and immobilize His-tagged proteins is the use of solid support like beads where Ni^{2+} or Co^{2+} ions are immobilized. Here, we hypothesized that His-tagged-DYNCH1, could be used as a bait to identify binding partners (prey) obtained from Cos-7 cell lysate (transfected with human-Rab46), where monkey Rab46 may not be expressed or interact with human Rab46.

The main steps of the pull-down workflow (obtained after a long optimization process) are shown in Figure 5.16. First, human WT-Rab46 was overexpressed in Cos-7 cells and cells were lysed after 24 hours. Cell lysate was pre-cleared with plain Ni^{2+} beads, to reduce non-specific binding and then incubated with purified His-DYNCH1. This incubation permitted the formation of interacting complexes partners. Next, pre-equilibrated magnetic Ni^{2+} beads were mixed with the cell lysate containing the His-DYNCH1 and the WT-Rab46 proteins. After incubation the beads were washed with a gradient of washing buffer containing increasing amounts of imidazole to wash away unbound protein and impurities. Finally, the proteins were eluted with 500 mM imidazole elution buffer and the elution fraction analysed by SDS-Page and western blot.

For validating biologically significant results, negative controls were used. Total lysates (no pull-down) from Cos7 cells were used to indicate if endogenous Rab46 (if expressed in Cos7 cells), was similar to human Rab46 (Rab46 polyclonal antibody recognises 395 amino acid sequence of Rab46), thereby confounding any possible direct interaction. A WT-Rab46 control alone (minus His-DYNCH1) helps identify and eliminate false positives caused by non-specific binding of proteins to the Ni^{2+} beads. A bait control (plus His-DYNCH1, minus WT-Rab46) helps identify and eliminate false positives caused by non-specific binding of Cos-7 proteins to the bait protein. This control also serves as a positive control that verifies successful capture of the His-tag protein to the Ni^{2+} beads.

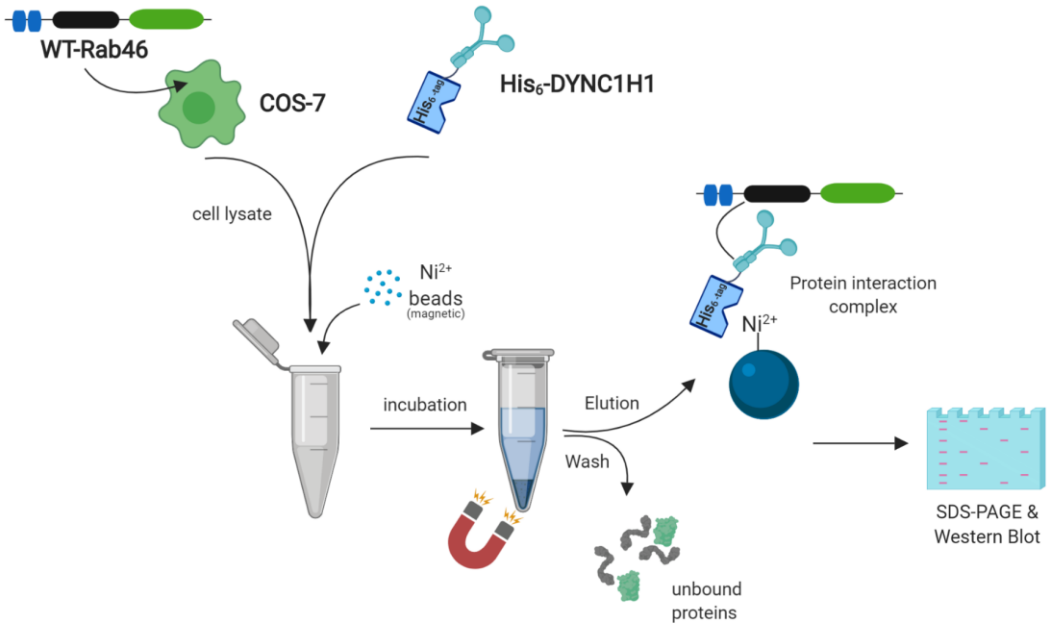

Figure 5.16 Schematic representation of pull-down assay. The flowchart demonstrates the major steps of the purification of histidine tagged proteins along with their interactors. Cos-7 cells transfected with WT-Rab46 construct were lysate after 24hours. Pre-cleared cell lysate was mixed with purified his-tag dynein heavy chain and the mixture added to pre-equilibrated magnetic nickel beads. After 1 hour incubation the beads were washed using a magnetic rack and the protein complex bound to the beads eluted with imidazole buffer and analysed by SDS-PAGE and western blot. Proteins interacting with the bait protein (His-tag DYNC1H1) co-purify on the affinity beads and are subsequently identified by western blot.

5.7 Rab46 directly interacts with dynein

To detect whether the purified DHC and the ectopically expressed Rab46 interact with each other and the complex co-precipitate together, a western blot was performed. Following pull-down, the elution samples were loaded on a gel and immunoblotted for Rab46 and His-tagged DHC. The recombinant portion of the dynein tail domain has a predicted molecular weight of 37 kDa. Its capture and elution from the Ni^{2+} beads was verified using an anti-Histidine antibody. Western blot in Figure 5.17 shows a band at 37kDa in the first elution corresponding to the recombinant dynein in the positive control as well as into the elution fraction where it was mixed with WT-Rab46. Probing for Rab46 revealed a single band at the expected molecular weight (95 kDa) in the total Cos-7 lysate used as input but most importantly in the same elution fraction with the His-tagged dynein. No Rab46 was detected in cells not expressing human Rab46 and no cross-reactivity was observed in the negative control where WT-Rab46 was incubated with the Ni^{2+} beads but in absence of His-DHC.

These results show that the interaction between Rab46 and the dynein heavy chain occurs through the specific tail domain of the dynein heavy chain suggesting a direct interaction between the two proteins.

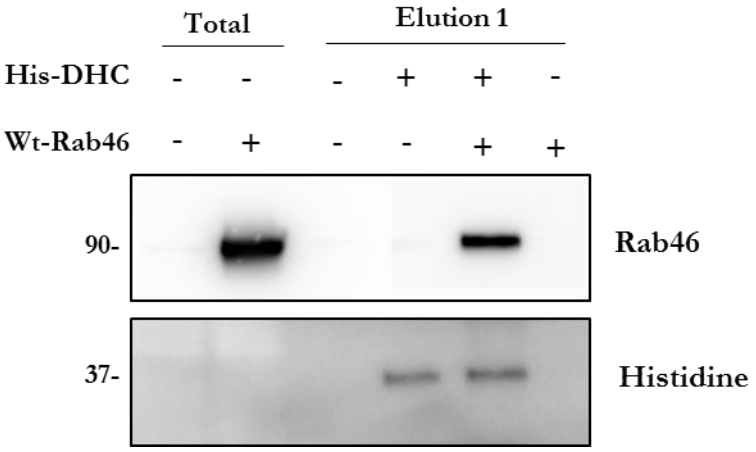

Figure 5.17 Direct interaction of the dynein heavy chain with Rab46. Pull down of human WT-Rab46 overexpressed in Cos7 cells (monkey cells) using purified his-tag dynein heavy chain (His-DHC) bound to Ni^{2+} beads. Non-transfected cells (-) and cells transfected with WT-Rab46 (+) were mixed with (+) or without (-) 10 µg of His-DHC. Magnetic sepharose Ni^{2+} beads were used to pull-down His-tag DHC complexes: the beads were incubated with the mixture of His-DHC + WT-Rab46 (or non-transfected cell as control) or WT-Rab46 only as control to show non-specific binding to the beads. Imidazole buffer (500 mM) was used for elution. 15 µl of the elution fractions were loaded on a gel and co-precipitation of Rab46 with his-DHC assessed by western blot using anti-Rab46 and anti-histidine antibodies. Representative western blot of 3 independent experiments.

5.8 Identification of Rab46-DHC binding sites

Cytoplasmic dynein is a minus end–directed microtubule motor that transports intracellular cargos. The molecular basis by which each cargo is linked to dynein and its cofactor dynactin has started to emerge. A central role for this process is fulfilled by a set of coiled-coil proteins — 'activating adaptors' — which both recruit dynein–dynactin to their cargos and activate dynein motility. Thus far, eight adaptors have been demonstrated to directly bind and activate dynein: BicDL1, BicD2, Hook1, Hook3, Rab11FIP3, Spindly, Ninein, and Ninein-like proteins[193,194]. Recruitment of the dynein–dynactin adaptor complex to specific membrane organelles is often mediated by the interaction between a dynein adaptor and a Rab GTPase, which associates with intracellular membrane compartments through C-terminal prenylation. A common feature of the dynein adaptor proteins is the presence of long coiled-coil domains with conserved residues important for dynein interaction.

Rab46 is an unconventional Rab GTPase that contain a pair of EF-hand, a coiled-coil domain and a Rab GTPase domain (Figure 5.18). The domain architecture, as already suggested by Wang et al., resemble the well-known dynein adaptor Rab11FIP3[116] with two EF-hand followed by coiled-coils domains. Wang et al demonstrated that Rab46 and Rab45 are new dynein adaptor protein in T-cells[173].

This structure similarity raises the question about the presence of conserved residues in Rab11FIP3 sequence which could be shared with Rab46. Comparing the sequence of Rab46 and Rab11FIP3 by a global sequence alignment, 13.6% of identity and 22.9% of similarity was shown (Figure 5.19). Interestingly, the two proteins have high similarity especially within the Ca^{2+} binding motif, in the conserved coiled-coil domain and in a specific Rab-binding domain at the C-terminal called FIP-RBD domain. In particular, two conserved alanine residues responsible for dynein binding in the Rab11FIP3 sequence were highlighted in red as they appear to be in common with Rab46 sequence. The A435 in the coiled-coil domain and the A709 in FIP-RBD domain are also conserved in other dynein adaptors and mutations of these alanine residues to valine abolished dynein interaction. Identification of the A227 at the very beginning of Rab46 coiled-coil domain and the A555 within the Rab domain which perfectly matched the two alanines previously identified in the Rab11FIP3 sequence suggest the possibility that these residues may be important in binding the N-terminal of the dynein heavy chain.

As previously mentioned, a common feature of all the dynein adaptors is the presence of long coiled-coil domain, in particular a short region at the very beginning called CC1 box found in the BICD family, the spindly protein and some candidate dynein activator, is involved in the interaction with dynein. Therefore, comparison between the coiled-coil domain of Rab46 (I226-Q313) and the coiled-coil domains of other dynein adaptors such as BICD2, BICDR2, Spindly and HAP1 was examined (Figure 5.20). Remarkably, a common feature within the CC1 box was observed. Two alanines were also found within the Rab46

coiled-coil domain which are conserved among the already characterized dynein adaptors as they are responsible for the interaction with dynein. However two alanines are present in the Rab46 CC domain, the alignment shows that only the A227 matches with the others.

These preliminary results highlight common features between Rab46 and some dynein adaptors, identifying two putative binding sites. Mutations of the two identified alanines would indicate whether the Rab46 interaction with the dynein heavy chain is disturbed.

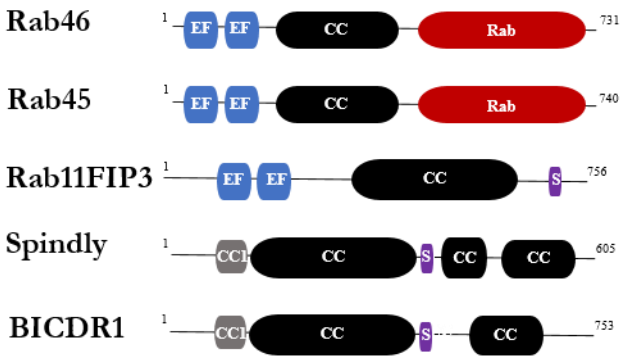

Figure 5.18 Domain organization of structural related Rab GTPases compared to Rab11FIP3, Spindly and BICR1 (dynein activators and adaptors). EF-hand domains (blue): calcium binding sites. Coil-coiled domain (CC: black): protein interactions sites. Rab (red): GTP/GDP binding site. CC1 (grey): coiled-coil segment shared by some dynein binding proteins. Spindly motif (S: purple): conserved features of some dynein activators.

```
CLUSTAL O(1.2.4) multiple sequence alignment

RFIP3 MASAPPASPPGSEPPGPDPEPGGPDGPGAAQLAPGPAELRLGAPVGGPDPQSPGLDEPAP 60
Rab46 ------------------------------------------------------------

RFIP3 GAAADGGARWSAGPAPGLEGGPRDPGPSAPPPRSGPRGQLASPDAPGPGPRSEAPLPELD 120
Rab46 ---------------------------------MAAPDGRV-------------------- 8
                                       :.* *::

RFIP3 PLFSWTEEPEECGPASCPESAPFRLQGSSSSHRARGEVDVFSPFPAPTAGELALEQGPGS 180
Rab46 ------------------VSR----------------------------PQRLGQGSGQ 21
                        *                                 * ** *.

RFIP3 PPQPSDLSQTHPLPSE--------PVGSQEDGPRLRAVFDALDGDGDGFVRIEDFIQFAT 232
Rab46 GPKGSGA-CLHPLDSLEQKETQEQTSGQLVMLRKAQEFFQTCDAEGKGFIARKDMQRLHK 80
       *: *.    *** *          *.     : : .*:: *.:*.**:  :*: :: .

RFIP3 V--YGAEQVKDLTKYLDPSGLGVISFEDFYQGITAIRN--GDPDGQCYGGVASAQDEEPL 288
Rab46 ELPLSLEELEDVFDALDADGNGYLTPQEFTTGFSHFFFSQNNPSQEDAGEQVAQRHEEKV 140
          . *:::*: . ** .* * :: ::*  *:: :    .:*. :  *  .: :.** :

RFIP3 ACPDEFDDFVTYEANEVTDSAYMGSESTYSECETFTDEDTSTLVHPELQPEGDADSAGGS 348
Rab46 --------YLS---RGDEDLGDMGEDEEA----QF------RMLM---------DRLGAQ 170
              :::   .   * . **.:.       *       ::          *  *..

RFIP3 AVPSECLDAMEEPDHGALLLLPGRPHPHGQSVITVIGGEEHFEDYGEGSEAELSPETLCN 408
Rab46 KVL----E--DESDVKQLWLQLKKEEPHLL---------SNFEDFLTRIISQLQEAHEEK 215
       *     :  :* *   * *   : .**           .:***:     ::*.     :

RFIP3 GQLGCSDPAFLTPSPTKRLSSKKVARYLHQSGALTMEA---LEDPS-------PELMEGP 458
Rab46 NELECALK------------RKIAAYDEEIQHLYEEMEQQIKSEKEQFLLKDTERFQAR 262
      .:* *:               :*:* * .:   *  *    ::. .        * ::.

RFIP3 EEDIADKVVFLE--------------RRVLELEKDTAATGEQHSRLRQENLQLVHRANAL 504
Rab46 SQELEQKLLCKEQELEQLTQKQKRLEGQCTALHHDKHETKAENTKLKLTNQELA------ 316
      .::: :*::  *               :   *.:*.  *  ::::*:  * :*.

RFIP3 EEQLKEQELRACEMVLEET----RRQKELLCKMEREKSIEIENLQTRLQQLDEENSELRS 560
Rab46 -R-----ELERTSWELQDAQQQLESLQQEACKLHQEKEMEVYRVTESL------------ 358
       .     **. .   *:::    .  ::  **:.:**.:*: .:   *

RFIP3 CTPCLKANIERLEEEKQKLLDEIESLTLRLSEEQENKRRMGDRLSHER-HQFQRDKEATQ 619
Rab46 ------------QREKAGLLKQLDFLRERNK-----------HLRDERDICFQKNKAAKA 395
                 :.**  **.::: *  * .           :* .**   **::* *.

RFIP3 ELIE-----------DLRKQLEHLQLLKLEA-----EQRRGRSSSMGLQEYHSRARESEL 663
Rab46 NTAASRASWKKRSGSVIGKYVDSRGILRSQSEEEEEVFGIPRRSSLGLSGYPLTEEEPGT 455
      :               : * ::   :*: ::          * **:**. *    .*

RFIP3 ---------EQEVRRLKQDNR-NL-------------------KEQNEELNGQIITL--- 691
Rab46 GEPGPGGPYPRPLRRIISVEEDPLPQLLDGGFEQPLSKCSEEEEVSDQGVQGQIPEAPPL 515
                : :**: . :.  *                   : .:: ::***

RFIP3 ----------------------SIQGAKSLFSTAFSESLAAEISS----VSRDELMEAIQ 725
Rab46 KLTPTSPRGQPVGKEALCKEESSPSAPDRLFKIVFVGNSAVGKTSFLRRFCEDRFSPGMA 575
                           * .. . **. .* .  *.  :*    ...*.:  .:

RFIP3 KQEEINFRLQD--------------------------YI---DRIIVA-IMETNPSILE 754
Rab46 ATVGIDYRVKTLNVDNSQVALQLWDTAGQERYRCITQQFFRKADGVIVMYDLTDKQSFLS 635
          *::*::                            ::   * :**   :  : *:*.

RFIP3 VK---------------------------------------------------------- 756
Rab46 VRRWLSSVEEAVGDRVPVLLLGNKLDNEKEREVPRGLGEQLATENNLIFYECSAYSGHNT 695
      *:

RFIP3 -----------------------------------
Rab46 KESLLHLARFLKEQEDTVREDTIQVGHPAKKKSCCG 731
```

Figure 5.19 Sequence alignment of Rab46 and Rab11FIP3 sequences showing conserved residues involved in dynein binding. Sequence alignment using Clustal Ω shows a conserved region in the first coiled-coil segment of the dynein adaptor Rab11FIP3 (CC1 box) and Rab46 coil-coiled domain. The alignment also shows a second conserved residue in the spindly motif of RFIP3 (708-712) which is shared within the Rab46 sequence. The two alanines (A435 and A709 in RFIP3) important in the interaction with dynein and the conserved alanines in Rab46 sequence (A227 and A555) are marked with red asterisks.

```
CLUSTAL O(1.2.4) multiple sequence alignment

BICD2     ------------------------------------------------------------
spindly   ------------------------------------------------------------EADI 4
BIDR2     MSSPDGPSFPSGPLSGGASPSGDEGFFPFVLERRDSFLGGGPGPEEPEDLALQLQ----- 55
HAP1      ------RFVFQGPFGSRATGRG-TGKAAGIWKTPAAYVGRRPGVSGPERAAFIRELEEAL 53
CC_Rab46  ------------------------------------------------------------

BICD2     --------------EVKRLSHELA----------------ETTREKIQAAEYGLAVLEEK 30
spindly   ITN-----------------------------LRCRLKEAEEERLKAAQYGLQLVESQ 33
BIDR2     ---------------------------------------QKEKDLLLAAELGKMLLERN 75
HAP1      CPNLPPPVKKITQEDVKVMLYLLEELLPPVWESVTYGMVLQRERDLNTAARIGQSLVKQN 113
CC_Rab46  ----------------------------------------------IAAYDEEIQHLY 12
                                                           * . : .

BICD2     HQLKLQFEELEVDYEAIRSEMEQLKEAFGQAHTNHKKVAADGESREESLIQESASKEQYY 90
spindly   NELQNQLDKCRNEMMTMTESYEQEKYTLQREVE-----------LKSRMLESLSCECEA 81
BIDR2     EELRRQLETLSAQH-LEREE------RLQ--QENH----------ELRRGLAAR--GAEW 114
HAP1      SV------------------------LM--EENS----------KLEALLGSAKEEILY 136
CC_Rab46  EEMEQQIKSEKEQFLLKDTE------RFQ--ARSQ----------ELEQKLL-------- 46
                                     :

BICD2     VR--------------------KVLELQTELKQLRNVLTNTQSENERLASVAQELKEINQ 130
spindly   IKQQQKMHLEKLEEQLSRSHGQEVNELKTKIEKLKVELDEARLSEKQLK----------H 131
BIDR2     EA--------------------RAVELEGDVEALRAQLGEQRSEQQDSGR---ERARALS 151
HAP1      LR--------------------HQVNLRDELLQLYSDSDEEDEDEEEEEE---E-KEAEE 172
CC_Rab46  ------------------------------------------------------------

BICD2     NVEIQRGRLRDDIKEYKFREARLLQDY--SELEEENISLQKQVSVLRQNQVEFEGLKHEI 188
spindly   QVDH----QKELLSCKSE-ELRVMSERVQESMSSEMLALQIELT-------EMESMKTTL 179
BIDR2     ELSEQNLRLSQQLAQASQ-----TEQ----ELQRELDALRGQCQ-------AQA------ 189
HAP1      EQEE--EEAEEDLQCAHP-----CDAP--KLISQEALLHQHHCP-------QLEALQEKL 216
CC_Rab46  --------------CKEQ-----ELE----QLTQKQKRLEGQCT-------ALH------ 70
                                       : :     . .

BICD2     KRLEEETEYLNSQLEDAIRLKEISERQLE---EALETLKTEREQKNSLRKELSHYMSIND 245
spindly   KEEVNELQYRQEQLELLIT-------NLM---RQVDRLKEEKEERE---KEAVSYYNALE 226
BIDR2     ----L------------------AGAELR---TRLESLQGENQ------------MLQSR 212
HAP1      RLLEE------------------ENHQLREEASQLDTLEDEEQ------------MLILE 246
CC_Rab46  ----H------------------DKHETK---AENTKLKLTNQ---------------- 88
                                  :          *:  .:
```

Figure 5.20 Multiple motif alignment of some dynein adaptors and Rab46 coil-coiled domain. Sequence alignment using Clustal Ω shows a conserved region (CC1 box) in the first coiled-coil segment of the dynein adaptors BICD2, Spindly, BICDR2, HAP1 and Rab46 coil-coiled domain. Within the conserved region the alanine important in the interaction with dynein and the conserved alanine in Rab46 sequence (A227) are marked in red with red asterisks.

5.9 Summary

In brief, through these last three chapters qualitative and quantitative data have been generated to suggest Rab46 is a novel WPB-associated Rab GTPase which mediates acute histamine, but not thrombin, response in endothelial cells. Histamine stimulates activation of Rab46 thus promoting Rab46 interaction with dynein and retrograde trafficking, along the microtubules, of a sub population of WPBs to the MTOC (Figure 5.21).

Further investigations on the mechanisms regulating Rab46-dependent WPBs trafficking revealed the dynein-dynactin complex as the most promising interacting partner. Direct interaction between the tail domain of the dynein heavy chain and WT-Rab46 and high similarity with already known dynein adaptors suggested Rab46 as new dynein adaptor protein.

All together these data described for the first time a fundamental mechanism by which physiologically diverse agonists coordinate intracellular signals in order to discriminate between cargo-restricted populations of WPBs.

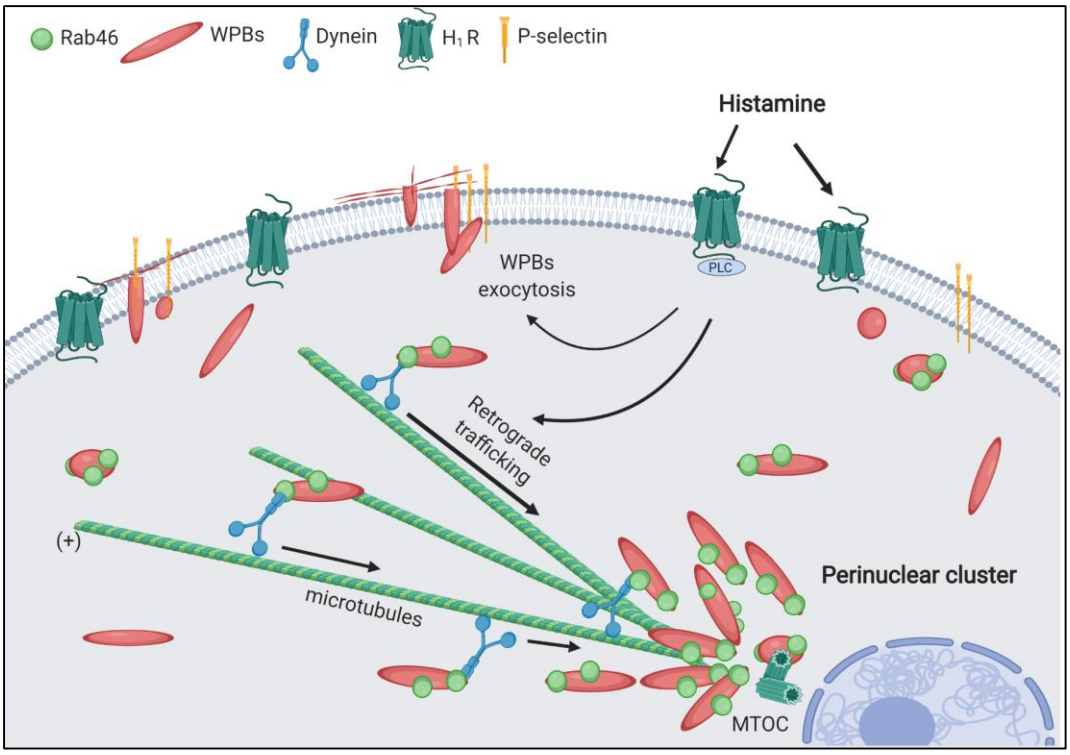

Figure 5.21 Proposed model of Rab46-dependent WPB trafficking. Histamine acts upon its receptor to stimulate the trafficking of WPBs in two opposite directions: WPBs which are negative for Rab46 but contain vWF and P-selectin (data not shown in this thesis) are directed to the cell surface for WPBs exocytosis. Simultaneously, histamine stimulates nucleotide binding of Rab46 thus promoting Rab46 interaction with dynein and trafficking of a sub population of WPBs contain other cargo (e.g. angiopoietin-2) to the microtubule organising centre (MTOC)[191].

Chapter 6 Characterization of Cracr2a knock-out mice

6.1 Introduction

Human CRACR2A gene encodes two validated transcriptional isoforms: a short variant CRACR2A-c and a long variant CRACR2A-a (Rab46). Although the current mouse genome database shows presence of only CRACR2A-c, Srikanth et al validated presence of the long isoform, named Rab46 in this thesis, in murine tissues such as mouse lymphoid organs[167].

A global Cracr2a knockout mice, with global elimination of the gene's function, was available from the KOMP Repository which adopted a definitive null allele design, resulting in deletion of the entire protein-coding sequence of the target gene. Thus, both the short and the long isoforms were deleted in whole body. This line is also a non-conditional knockout; thus, we were not able to generate an endothelial specific Rab46 knock out mice.

Therefore, in order to start the investigation of Rab46 *in vivo*, characterization of this global Cracr2a knockout mice line has been used as just the beginning for further studies which will aim to establish the role of Rab46 in the whole organism.

This chapter presents data that is additional to my thesis where I aim to give a purely phenotypic description of Cracr2a knockout mice. qPCR analysis is used to confirm knockout of both the long and short isoform in the selected organs and the relative effect on expression of structural related Rab proteins. A phenotypic characterization including body weight and organs weight at 12 weeks is presented as preliminary data.

Here, I demonstrate that Cracr2a knockout mice are viable and do no present major phenotypic differences compared to control wild-type mice at the considered time points. Interestingly, a significant difference was observed in liver weight between the two genotypes, therefore a first H&E staining and GTT/ITT tests were performed.

However, all together the preliminary results presented in this extra chapter are still at an early stage to be able to draw significant conclusions about the contribution of Rab46 *in vivo*.

6.2 Validation of Cracr2a $^{-/-}$ mice

The knockout mouse strain Cracr2a $^{tm1.1(KOMP)Vlcg}$ generated from cryo-recovery was obtained from the KOMP repository containing a litter of heterozygous (Het $^{+/-}$) and wild-type (WT $^{+/+}$) mice. After a first round of Het $^{+/-}$ x WT $^{+/+}$ cross to increase the numbers of heterozygous mice, ensuring a stronger breeding colony, a breeding strategy (Het $^{+/-}$ x Het $^{+/-}$) was set in order to generate a homozygous knockout mouse strain (Figure 6.1). The litter was genotyped after 2 weeks by ear notching and qPCR results obtained from the automated

genotyping Transnetyx service. To create an inbred homozygous and WT mice colony, homozygous (Hom $^{-/-}$)and WT mice were selected and crossed as indicated by the breeding scheme (Hom $^{-/-}$ x Hom $^{-/-}$ or WT $^{+/+}$ x WT $^{+/+}$). The offspring is 100% Hom $^{-/-}$ or WT$^{+/+}$ and further genotyping is not required.

The Hom $^{-/-}$ Cracr2a knockout mice did not show any viability or fertility issues, therefore, after establishing a strong colony of both Hom$^{-/-}$ and WT$^{+/+}$ mice to perform the experiments, the heterozygous colony was sacrificed.

Mice with disrupted Cracr2a expression and respective WT$^{+/+}$ control were sacrificed at 12 weeks and gene knockout was validated from different tissues. Quantitative RT-PCR analysis of mRNA abundance in the liver, lung, spleen and heart from Cracr2a $^{-/-}$ and control mice was performed (Figure 6.2). As this transgenic mouse line is designed to delete both the short and the long isoform of Cracr2a (EFCAB2B) gene, three sets of primers were designed to assess the distinct expression of only the short variant (Cracr2a), only the long (Rab46) and both together (Cracra2a + Rab46) in both control and knockout mice. qPCR analysis showed reduced mRNA expression of both the isoforms in all the selected organs, confirming global knockout of Cracr2a gene.

Moreover, Cracr2a knockout was also confirmed at protein level in mouse liver endothelial cells (mLECs). Immunoblotting using anti-Cracr2a antibody, recognizing mouse target, showed a specific band at the expected molecular weight (95 kDa) corresponding to the longer isoform (Rab46) in control mLECs and reduced intensity in knockout mLECs (Figure 6.3). Unfortunately, it was not possible to confirm this result by immunostaining and observe Rab46 localisation in mLECs as the antibody was not optimized for immunofluorescence. These results confirm Rab46 deletion in mLECs as well as confirm that, similar to human endothelial cells, the short isoform (Cracr2a) is not expressed in mLECs.

Genetic compensation in response to gene knockout is a widespread phenomenon, upregulation of related genes following a gene knockout may be a direct consequence of the loss of protein function. Considering the unique structure of Rab46, which is shared by only other two large GTPases namely Rab44 and Rab45, mRNA abundance of these structurally related Rab proteins was measured in WT$^{+/+}$ mice (Figure 6.4). Firstly, mRNA expression relative to the mean of two housekeeping genes was measured from liver, spleen, lung and heart tissues. Rab46 appears to be relatively highly expressed as compared to other Rabs in all the organs analysed, with a great extent in the lung tissues, which is also consistent with previous observation by Srikanth et al (2010). Rab44 demonstrates very low expression compared to Rab46 in all the organs, quite low expression was detected by qPCR analysis. In contrast, qPCR analysis was not able to detect mRNA expression of Rab45 in any of the selected organs (Ct values $\geq$ 34). Therefore, in order to exclude upregulation of Rab44 following Cracr2a knockout, its mRNA abundance was measured in Cracr2a knockout mice and compared to control WT$^{+/+}$ mice (Figure 6.5). Expression of Rab44 mRNA is not

changed in the liver, lung and heart of knockout mice, only a slightly increase is observed in the spleen of Cracr2a knockout mice compared to control.

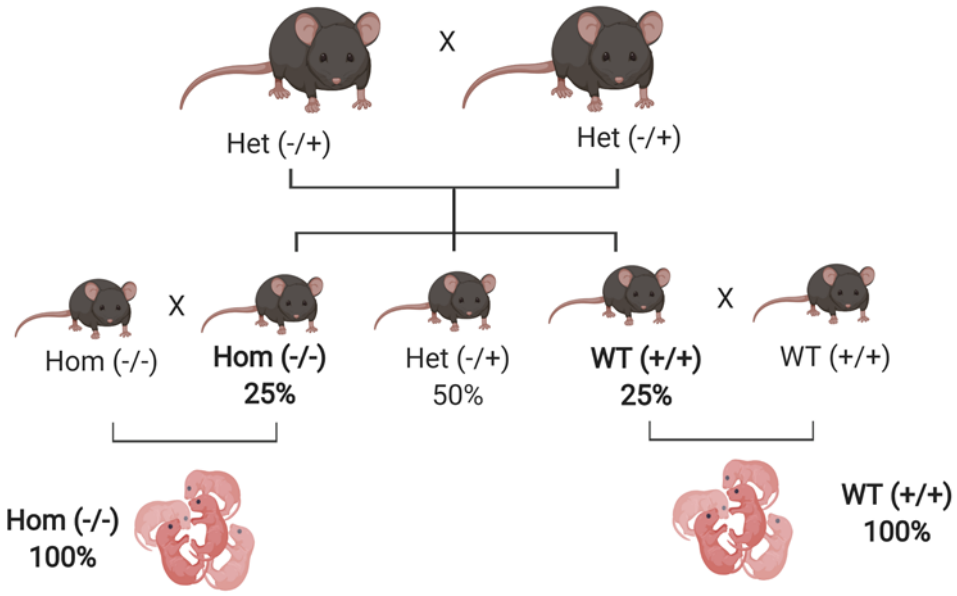

Figure 6.1 Generation of Cracr2a homozygous knockout mice line. Cracr2a heterozygous mice obtained from KOMP Repository were crossed and the litter was genotyped. In order to create an inbred homozygous and WT mice colony, homozygous and WT mice were selected and crossed as indicated by the breeding scheme (Hom $^{-/-}$ x Hom $^{-/-}$ or WT $^{+/+}$ x WT $^{+/+}$). The offspring is 100% homozygous or WT.

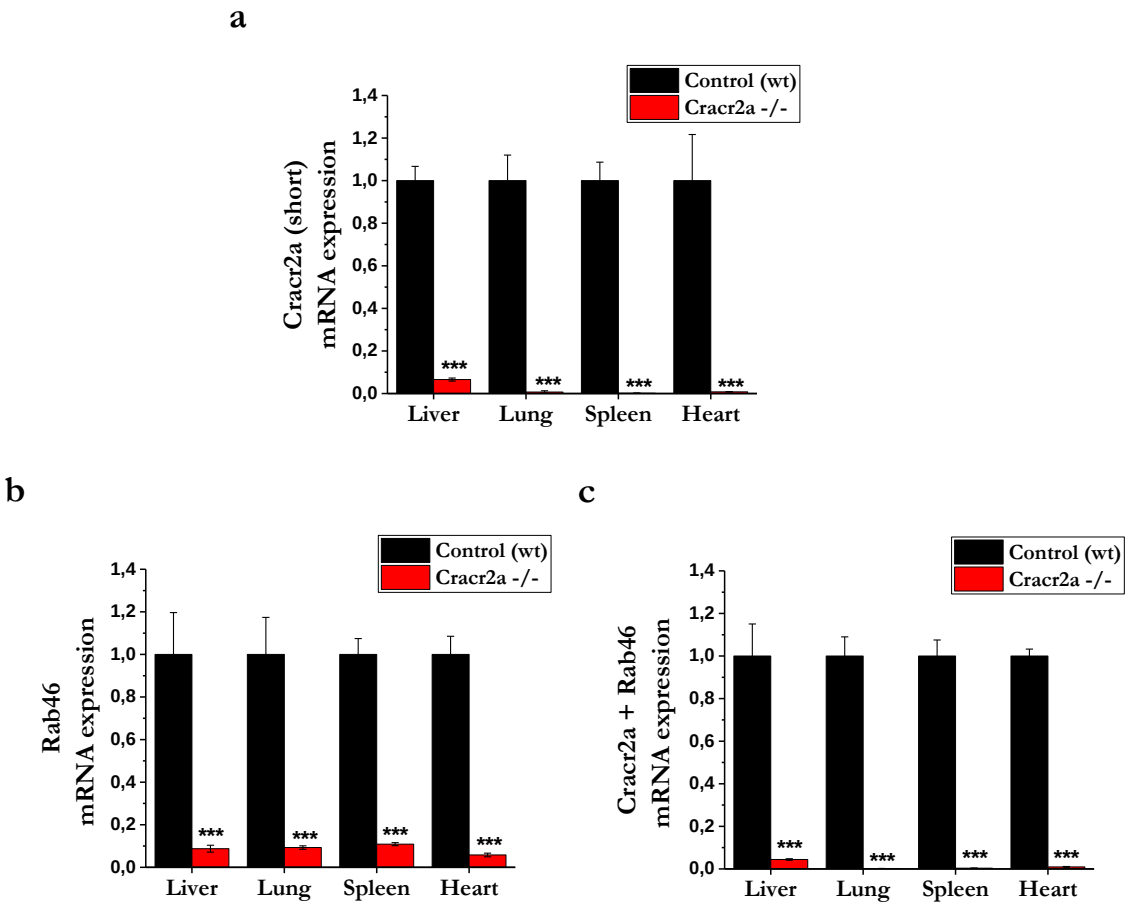

Figure 6.2 Validation of Cracr2a gene knockout in Cracr2a $^{-/-}$ mice. qPCR ΔCt analysis of Cracr2a gene expression relative to HG and normalized to control WT in the liver, lungs, spleen and heart of Cracr2a knockout mice and WT control mice. (a) mRNA expression of Cracr2a short isoform, Rab46 (b:long isoform) and both the 2 isoforms (c). mRNA abundance of both the isoforms is significantly decreased in all the tissues. n=7 *** p<0.001

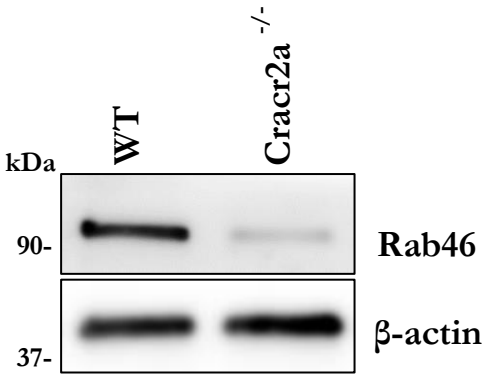

Figure 6.3 Validation of Cracr2a protein knockout in mouse liver endothelial cells (mLECs). Representative immunoblots for anti-Rab46 or anti-beta actin in mLECs from WT control and Cracr2a -/- mice. The anti-EFCAB4B antibody (Invitrogen) shows reactivity for the mouse target recognising a specific band at the expected molecular weight (95 kDa) in control mice and reduction in signal in the knockout mice. N=2.

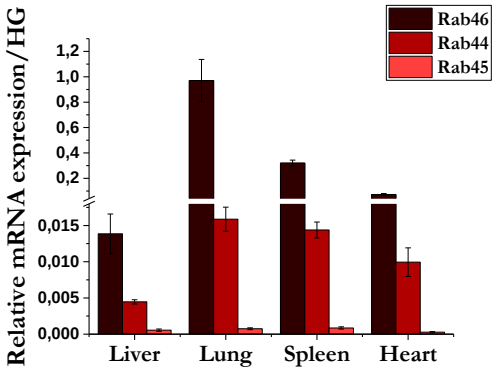

Figure 6.4 Relative expression of Rab46 and the two closest structural related Rab GTPases in control mice. qPCR ΔCt analysis of Rab46, Rab44 and Rab45 gene expression relative to housekeeping genes (HG: GAPDH and β-actin) (x100) in the liver, lungs, spleen and heart of WT control mice. Rab46 mRNA is the most abundant compared to the other two. Rab44 mRNA expression appear to be quite low expressed compared to the housekeeping genes with 10 cycles difference between HG and Rab44. In contrast, Rab45 mRNA was almost not detected with 16 cycles difference compared to HG.

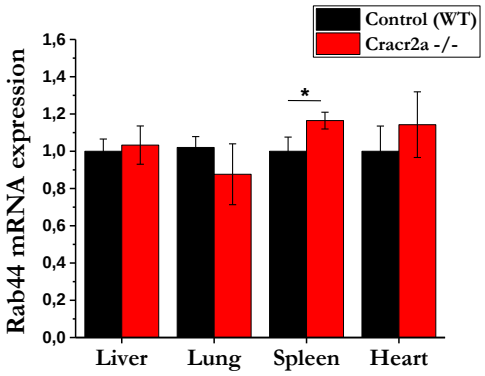

Figure 6.5 Effect of Cracr2a knockout on the expression of Rab44 gene. qPCR ΔCt analysis of Rab44 (top) and Rab45 (bottom) gene expression relative to HG and normalised to control (WT) in the liver, lungs, spleen and heart of Cracr2a knockout mice and WT control mice. mRNA abundance of Rab44 doesn't change in the liver, lungs and heart. Only a slightly increased is observed in the spleen. n=7 * $p<0.05$

6.3 Phenotypic characterization

The preliminary phenotypic characterization of the homozygous Cracr2a knockout mice line includes macroscopic examinations such as viability, body weight and organs weight. Considering the timeframe when the following experiments were performed, much of the phenotyping data is limited to female mice at 12 weeks.

Mice with disrupted Cracr2a are superficially normal with identical physical appearance compared to $WT^{+/+}$ mice. Life span up to 12 weeks is not different between genotypes.

Mice were fed with standard chow diet and body weight assessed at 8 and 12 weeks (Figure 6.6). No difference was seen in body weight at the considered time points between control and knockout mice. At 12 weeks mice were sacrificed and a selection of organs were harvested for future studies. Although the body weight does not change between the genotypes, the main organs were weighted and the organ to body ratio calculated by normalising each organ weight to total body weight of the mouse (Figure 6.7). Interestingly, a significant difference was observed in the livers weight, Crac2a knockout mice have increased liver mass compared to control mice. A small but significant increase in the visceral fat was also observed in mice with deleted Cracr2a.

Considering these preliminary observations, histological exanimation of liver tissues was performed (Figure 6.8). Mice liver tissues, collected from the right lobe of the liver, were fixed, embedded in paraffin and then sliced in order to use Haematoxylin and Eosin (H&E) staining to reveal the main hepatic features. H&E stained liver histology images are characterized by multiple types of tissue structures, including hepatocyte nuclei and cytoplasm, non-parenchymal cells and sinusoidal spaces. The histological analysis of livers from the control $WT^{+/+}$ group indicated a normal liver lobular architecture with central vein and surrounding hepatocytes, sinusoids and nucleus. Cracr2a knockout mice show normal liver morphology, however hepatic mononuclear cell infiltration, congestion of portal vein and blood sinusoids appear to be a common feature. Accumulation of fat droplets was not seen in any of the analysed tissues section. The presence of focal periportal immune cell infiltration, with enlargement of the portal tract may suggest an early inflammatory condition due to Cracr2a deletion.

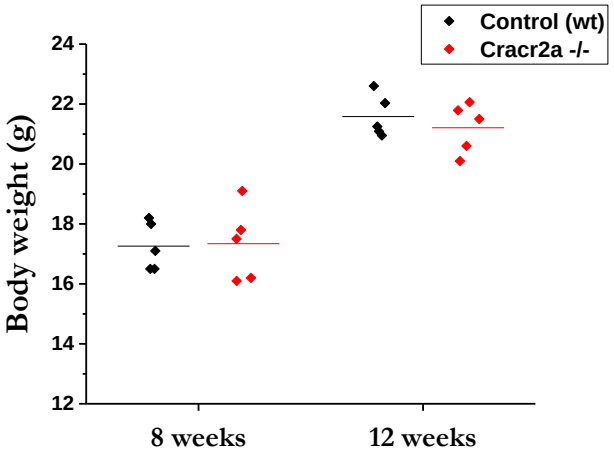

Figure 6.6 Cracr2a $^{-/-}$ mice don't show any difference in body weight. Body weight at the age of 8 and 12 weeks of female control (WT) and female Cracr2a $^{-/-}$ mice. Scatter plot shows body weight (g) of each mice and straight line indicates the mean in each group. No significant difference is observed at these time points between WT (black diamonds) and knockout mice (red diamonds). n=5

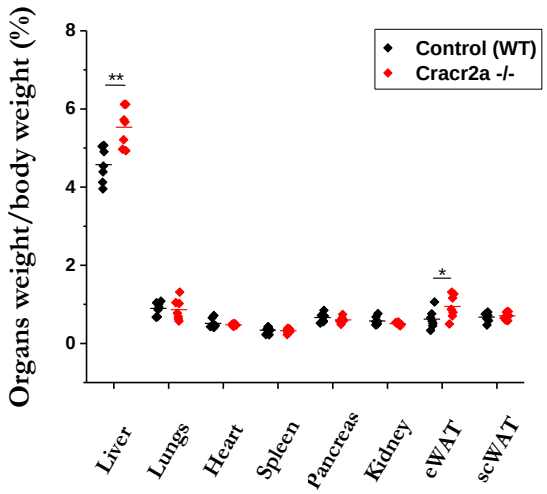

Figure 6.7 Examination of organ-to-body weight ratio of Cracr2a $^{-/-}$ mice compared to control (WT). Male and female mice were sacrificed at the age of 12 weeks and the main organs were harvested and weighted. Scatter plot shows data distribution of each organ from control and Cracr2a $^{-/-}$ mice. Straight line indicates the mean value. Liver weight and eWAT weight is increased in Cracr2a $^{-/-}$ mice compared to control (WT). n=5 **p<0,01 *p<0,05 from Student t-test.

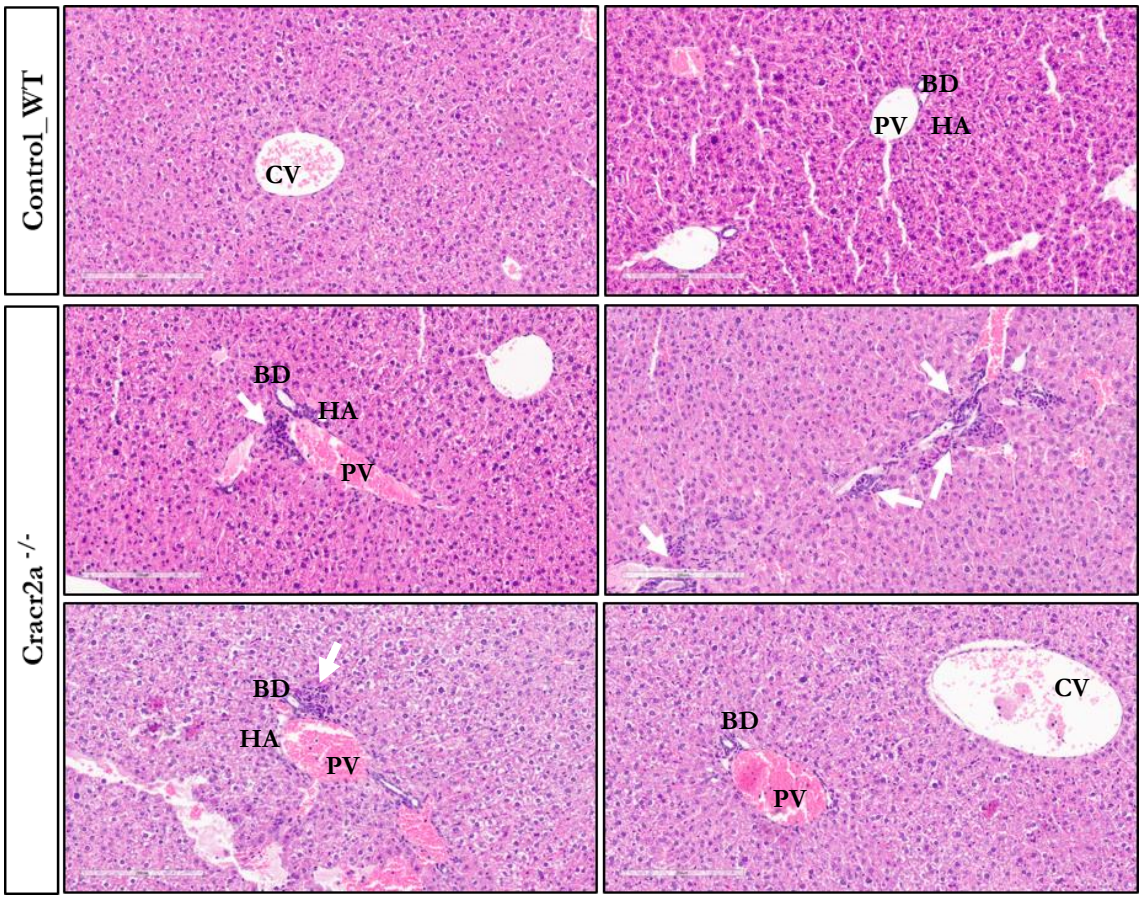

Figure 6.8 Histological examination of liver of Cracr2a $^{-/-}$ mice compared to control (WT). Mice were sacrificed at the age of 12 weeks and the liver was harvested and weighted. Liver tissues were examined by H&E staining. Liver from WT control group revealing normal morphology with central vein (CV) and hepatic cords and normal triad structure with portal vein (PV), bile duct (BD) and the hepatic artery (HA) (top); Liver from Cracr2a $^{-/-}$ mice reveals multiple focal inflammation sites with immune cell infiltration (white arrows) and portal vein and sinusoids congestion. Scale bar= 200 µm.

6.4 Metabolic phenotyping

Considering these preliminary differences observed in Cracr2a knockout mice compared to control WT, a basic metabolic phenotyping assessing glucose homeostasis was performed to determine whether this mouse model exhibits an alteration in glucose metabolism.

Glucose tolerance tests (GTTs) and insulin tolerance tests (ITTs) are first-line experiments to assess glucose and insulin tolerance, respectively, since they are relatively easy to perform and minimally invasive. They consist of measuring blood glucose levels in response to a bolus administration of glucose (GTT) or insulin (ITT). Both GTT and ITT were performed at the age of 8-9 weeks.

Before glucose administration, overnight fasting (16h) was used to provide stable baseline measurements and to obtain consistent excursions in plasma glucose after glucose loading. Baseline (fasting) blood glucose measurements are taken before glucose administration, by intraperitoneal injection, and further measurements are made at regular intervals. Figure 6.9 shows a GTT test where changes in blood glucose levels, following the administration of a bolus of glucose, were measured over 2 hours at 30 minute intervals. The time course of absolute glucose levels shows no significant difference between the two genotypes. Furthermore, no statistically significant difference was observed when fasting glucose levels were compared.

Like GTTs, ITTs monitor glucose concentration over time, but in response to a bolus of insulin instead of glucose. The convention is to conduct ITTs in mice following a short (2-hour) fast. Glucose concentration is monitored every 30 minutes for 90 minutes following a bolus of insulin administered via intraperitoneal injection. Results from ITTs are presented as a time course of glucose levels (Figure 6.10a). No difference in blood glucose level in response to insulin administration was observed. However, fasting glucose levels differ between the groups (Figure 6.10b). The glucose baseline of Cracr2a knockout mice seems to be higher than control WT mice.

These are very preliminary results conducted on only female mice which need to be confirmed in future studies using more powerful tests to interrogate specific mechanisms, such as insulin secretion, sensitivity and glucose effectiveness.

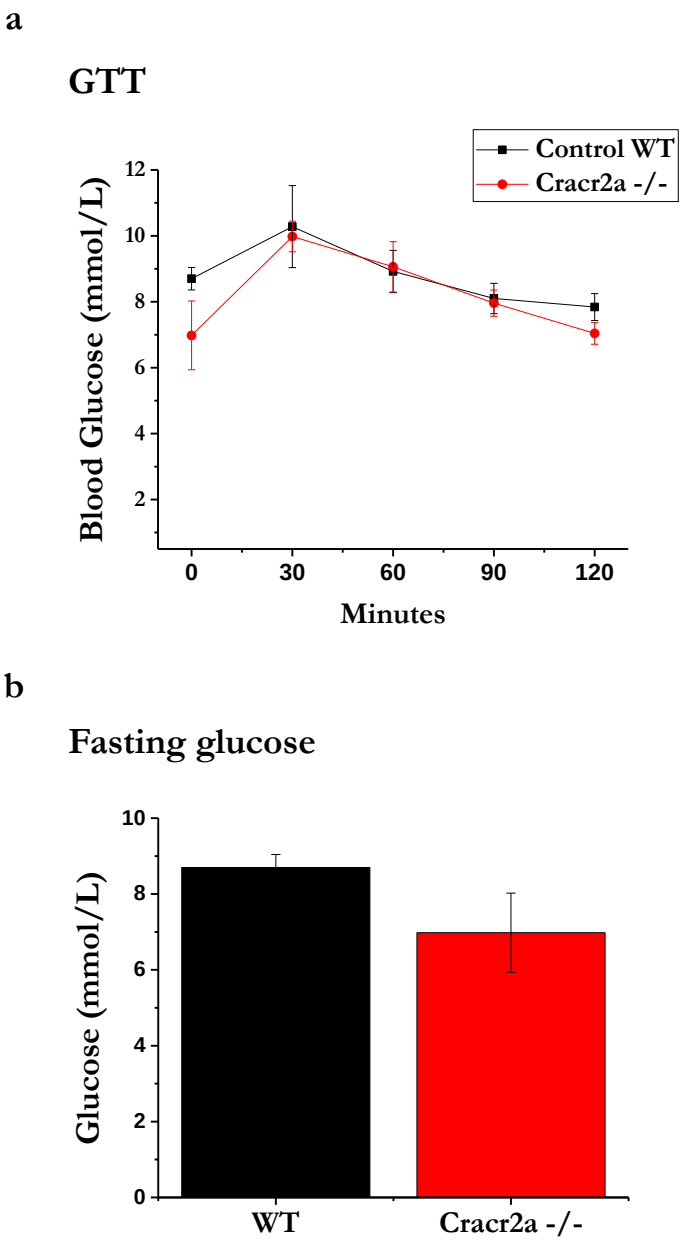

Figure 6.9 Glucose Tolerance Test (GTT). (a) Line plots show the blood glucose concentration in control and Cracr2a -/- mice during glucose tolerance test. Intraperitoneal glucose load (1 mg/g) was given after O.N fasting and the glucose measurement performed every 30 mins. (b) Bar chart shows glucose concentration after 24 hours fasting. N=5

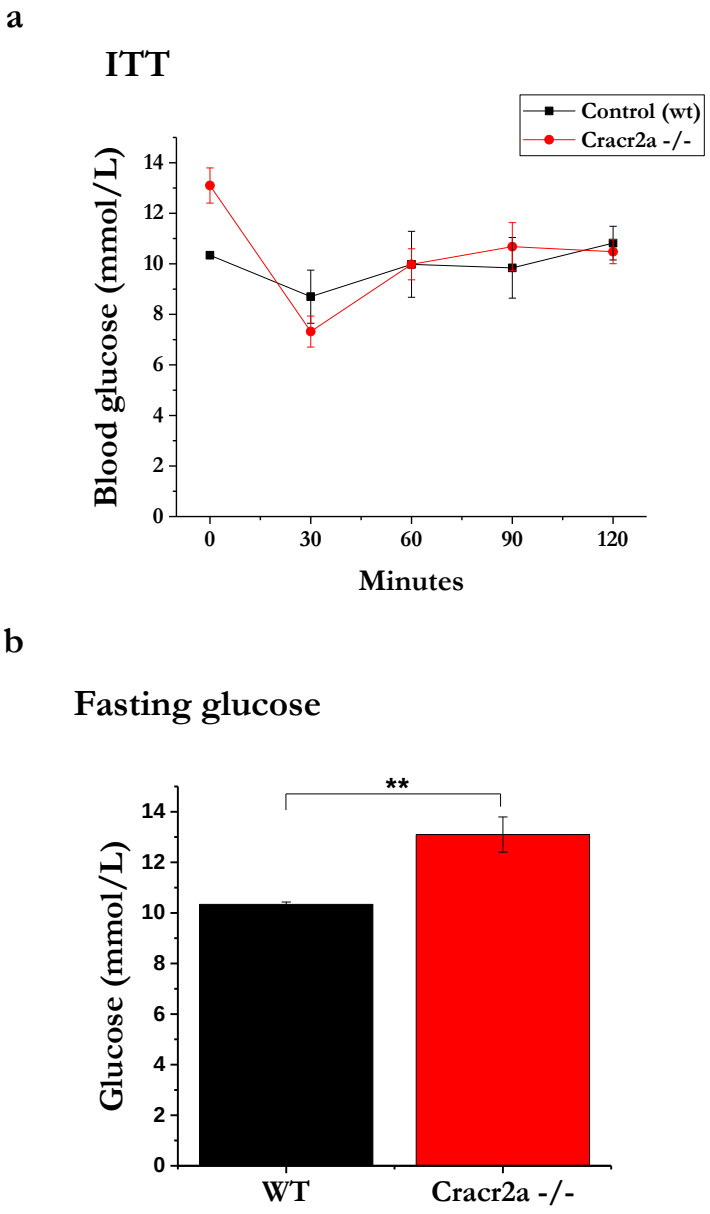

Figure 6.10 Insulin Tolerance Test (ITT). (a) Line plots show the blood glucose concentration in control and Cracr2a -/- mice during insulin tolerance test. Intraperitoneal insulin dose (0,75 IU/kg) was given after 2 hours fasting and the glucose measurement performed every 30 mins. (b) Bar chart shows glucose concentration after 2 hours fasting. N=5 **p<0,01 Student t-test.

6.5 Summary

Briefly, this extra chapter aims to initialize our investigation of Rab46 *in vivo*. The basic phenotyping characterization presented in this chapter do not show any major differences between the genotypes of these young adult mice. Although no difference in body weight was observed at 12 weeks, the liver mass is higher in Cracr2a knockout mice than control WT as well as visceral fat mass. Histological analysis of liver tissues suggests infiltration of immune cells and periportal inflammation in the absence of Cracr2a with no evidence of lipid accumulation.

We found no significant differences in measures of glucose or insulin homeostasis between the genotypes in young adult mice (age 8-9 weeks), although, a significant difference in glucose level after a short-fasting period was noted, with higher glucose level in the knockout mice than $WT^{+/+}$.

Using a global Cracr2a knockout mice currently limits our conclusion regarding the contribution of endothelial Rab46 as well as its attribution to the observed effect as both the short and long isoforms were deleted.

Further work to characterise the nature of the observed differences in liver tissues and visceral fat will be important to decipher the physiological consequences of this phenotype.

Chapter 7 Discussion

Rab46 is a novel Rab GTPase which was first discovered in endothelial cells by Wilson et al (2015)[166]. Rab46 is encoded by the EFCAB4B gene which is shown to go through alternative splicing enabling the expression of a short (CRACR2A) isoform and a long (Rab46) isoform. The extra length of Rab46 is due to the incorporation of a GTPase domain at the C-terminal of CRACR2A which has previously been shown to have functional coil-coiled domain and EF-hand domains[172]. While both isoforms are expressed in human and murine T-cells[167], only the long isoform has been found in endothelial cells. Unlike the majority of small Rab GTPases that are characterised by a single GTPase (Rab) domain, Rab46 represents an unusually large Rab protein with multiple functional domains. Although the expression of Rab46 in endothelial cells has already been validated, the contribution of this unique Rab protein to the function of the endothelium is still unknown.

In this study we unravel the function and preliminary mechanisms of Rab46 in endothelial cells. Here, we show distinct Rab46 localization to a subpopulation of WPBs, specific secretory granules of endothelial cells involved in pro-inflammatory and pro-thrombotic response. The hypothesis that Rab46 could orchestrate WPB trafficking is confirmed by the evidence showing the role of Rab46 in histamine, but not thrombin, evoked WPB trafficking to the perinuclear area. Acute histamine activation of Rab46 induces dynein-dependent trafficking of WPBs carrying non-inflammatory cargo along microtubules towards the MTOC. Further investigations on the mechanisms regulating Rab46-dependent WPB trafficking also revealed the dynein-dynactin motor complex as the most promising interacting partners of Rab46, suggesting Rab46 as new linker by which WPBs are anchored to the dynein motor complex. The formation of WPBs-Rab46-dynein complex may be responsible for retrograde trafficking of specific population of WPBs in response to pro-inflammatory stimulation.

All together these data describe for the first time a fundamental mechanism by which physiologically diverse agonists coordinate intracellular signals in order to discriminate between cargo-restricted populations of WPBs.

7.1 Rab46 localization and function

Preliminary experiments performed in the lab had suggested that exogenous Rab46 localised to WPBs in endothelial cells, however, in order to understand physiological role of Rab46 in endothelial cells, identification of the localization of endogenous Rab46 was paramount to this study. Here, using super-resolution microscopy we show endogenous Rab46 localised to

vWF, a marker for WPBs. Immunofluorescent images of non-stimulated endothelial cells labelled with an antibody against vWF, revealed numerous elongated WPBs throughout the cell with a wide range of sizes. Despite the cigar-like morphology of the majority of WPBs, which appear long and straight, some of them present hinges which reflect vWF tubules flexibility or an oval/rounded shape which in proximity of the plasma membrane may reflect the structural changes occurring upon basal secretion. Short WPBs near the cell nucleus probably represent immature granules formed prior to vWF multimerization[195]. A similar vesicle-like pattern was observed in endothelial cells overexpressing Rab46 which indeed gave the first hint about Rab46 localization with vWF in endothelial cells, as revealed by merged images showing Rab46 and vWF colocalization. Although Rab46 positive vesicles show colocalization with vWF, exogenous Rab46 often shows a perinuclear cluster most likely due to the low intrinsic GTPase activity and high cytosolic GTP concentration which leads to a sustained accumulation of GTP-Rab46 as well as a reduced number of WPBs in these cells. Expression of constitutively active Rab46 (Q604L) shows indeed a strong perinuclear cluster in contrast to the inactive forms (N658I, T559N) which both present a cytosolic phenotype with impaired Rab46 colocalization to WPBs. According to Srikanth et al.[167], the GTPase activity of Rab46 determines its localization. Rab46 localization to the Golgi apparatus in resting T-cell is determined by both the GTPase activity and C-terminal prenylation. Therefore, it will be interesting to further explore whether Rab46 prenylation influences its location to WPBs in endothelial cells. Exploiting the increased resolution given by super-resolution microscopy we could observe and analyse endogenous Rab46 localization. Observing endothelial cells labelled with Rab46 and vWF under resting conditions allowed exploration of the association of Rab46 with WPB. Rab46 vesicles are juxtaposed on the outside of WPBs, facing the cytosolic side of these secretory granules; this is a characteristic necessary for many other Rab proteins, that always decorate the cytosolic face of many distinct membrane compartment, defining their identity[127]. Although WPBs are the main secretory granules of endothelial cells, endothelial cells are also equipped with other vesicles such as tPA granules, lysosomes and different populations of endosomes which have been suggested to be distinct from WPBs. However, my immunofluorescent imaging analysis suggests that Rab46 does not associate with any of these intracellular vesicles (although these data are not exhaustive), thereby suggesting specific targeting to WPBs. In addition, as only approximately 50% of WPBs are labelled with Rab46, it appears therefore to specifically target a subpopulation of WPBs. Differential recruitment of cargo proteins to WPBs, slow recruitment of membrane proteins during WPB maturation, and tissue-specific differences in endothelial cell phenotype lead to a heterogeneous population of WPBs[29].

Spatio-temporal contribution of Rab46 to WPB heterogeneity still need to be elucidated. When Rab46 is recruited to WPBs and how the process is regulated is still an open question which will be investigated in the future. To test the timing of Rab46 recruitment to WPBs, live-cell imaging of endothelial cells expressing a fluorescently tagged pre-pro-vWF will allow

tracking of the maturation of WPBs over time. Hannah et al[33] described this approach to show the maturation-dependent recruitment of Rab27a to WPBs, therefore it may be interesting to investigate whether Rab46 is recruited to immature and/or mature only WPBs. As Rab27a is a marker for mature WPBs, a simpler approach could also be to study the association between Rab27a positive WPBs and Rab46 in fixed cells. Determination of the dynamics of Rab46 recruitment and to establish whether its recruitment to WPBs is content-driven or maturation-dependent will be the next step to assess the role of Rab46 in WPB biogenesis. Here, we show that neither the total number of cells within a normal population of WPBs nor the cellular distribution of WPBs change in Rab46 depleted endothelial cells compared to control cells, thus, excluding a positive role in WPB biogenesis. Moreover, considering that the driving force of WPB biogenesis is vWF synthesis we also ruled out an effect of Rab46 downregulation on vWF mRNA expression. However, Rab46 depleted endothelial cells show increased intracellular vWF at the protein level supported by an increased number of WPBs per cells. The retention of WPBs inside the cells could interfere with WPB trafficking and/or basal vWF secretion, a stimulation independent secretory pathway that is described as the main source of plasma vWF *in vivo*. Lopes and Cutler[58] elegantly describe differences in the three vWF secretory pathways reporting the amount and multimeric state of vWF secreted from the constitutive, basal, and regulated pathways in polarized HUVECs. It was indeed suggested that different retention time inside the cell could drive the differential multimerization pattern observed between the basal and regulated vWF secretion. Therefore, measuring the effect of Rab46 downregulation on vWF basal secretion, by looking at differences in vWF multimers as well as polarity of secretion, will contribute to clarify whether Rab46 contributes to the existence and function of different pool of WPBs. In contrast to Rab27a depleted cells which show increased vWF release and accumulation of WPBs to the perinuclear area[33,69], confirming a role in forward movement of WPBs after maturation, Rab46 depleted cells do not show any difference in cellular distribution of WPBs but increased intracellular vWF. Thus, Rab46 is most likely responsible for WPB trafficking than biogenesis. Moreover, downregulation of Rab46 does not change the expression level of Rab27a or other related Rab GTPases, excluding the possibility of any off-target effect and/or compensation when cells are depleted by specifically targeted Rab46 siRNAs. All together these findings encouraged further investigations into the role of Rab46 in WPB trafficking.

It is known that WPBs are highly dynamic population of secretory granules in endothelial cells. In resting cells, these vesicles are not static but consist of pools with different motilities. Romani de Wit et al. demonstrated that some vesicles barely moved, as if they were tethered; others seem to travel in a stochastic manner and frequently reversed their direction[196]. Intriguingly, on stimulation with several distinct vWF secretagogues, differences in WPB dynamics were observed depending on the type of stimulus. Stimulation of endothelial cells caused regulated trafficking of WPBs toward the plasma membrane to orchestrate

endothelial response to different stimuli. WPBs are released from endothelial cells in response to a large number of secretagogues[56]. Increased levels of cytosolic free Ca^{2+} have been implicated in the mechanism of exocytosis for many of the agonists, such as histamine and thrombin. Endothelial exocytosis occurs within minutes of stimulation and WPB release is an immediate early response of endothelial cells, a rapid response to injury independent of gene transcription[197]. Most Ca^{2+}-raising agonists are mediators of inflammation and/or thrombosis which cause a rapid, immediate (5-15 mins) WPBs fusion with the plasma membrane. cAMP raising agonists, such as epinephrine or vasopressin, function more systemically, with a slow onset of vWF secretion, thereby controlling general vWF levels in the vasculature. Here, considering the presence of the EF-hand domains in Rab46 structure and the possibility to rapidly respond to changes in intracellular Ca^{2+} in order to direct WPB trafficking, we turned our attention on Ca^{2+} raising agonists.

Thrombin triggers an immediate endothelial response during vascular injury: within minutes of exposure to thrombin, endothelial cells release vWF, which mediates platelets rolling along the endothelium[198]. Moreover, endothelial cell activation evoked by thrombin is associated with a profound alteration of cell morphology[199]. Both thrombin and histamine stimulation results in stress fibre formation and loss of endothelial cell barrier function by disassembly of tight and adherens junctions, however thrombin promotes barrier permeabilization to a greater extent than histamine.[63,200] Histamine is an amine involved in transient immune and acute inflammatory responses, evokes leukocyte attraction without the necessity for endothelial cell migration or vasoconstriction[66,201]. Therefore, although histamine and thrombin are both Ca^{2+} raising agonists, they have distinct physiological roles. Despite their prominent role in the initiation of vascular thrombosis and leukocyte adherence, little is known about the molecular machinery driving WPB regulated exocytosis in response to those two main secretagogues. In order to achieve a functionally appropriate response, it is vital that endothelial cells couple physiological stimuli to the release of specific WPB cargo. The selective release of vWF from WPBs is controlled by multiple factors in addition to transcription. Different types of fusion of secretory organelles with the plasma membrane has been proposed as mechanism underlying the selective release or retention of granule contents. Recent studies have proposed some mechanisms underlying the differential release of cargo from WPBs docked at the cell surface[202]. A lingering kiss (small pore formation during weak histamine stimulation), excludes the release of cargo > 40 kDa whilst agonist-dependent recruitment of an actomyosin ring controls the force necessary for expulsion of vWF without affecting release of other cargo. To date there has been no description of differential storage and release of cargo in a contextual responsive process or if a cellular machinery exists to support such regulation. For example, to properly function in the control of thrombosis and the capture of platelets and/or leukocytes in the early stages of inflammation, the WPB constituents must be released on-demand. This prompt release has to be ensured by the molecular machinery which regulate exocytosis of WPBs.

Here we present Rab46 as a new regulator of differential WPB trafficking. Acute histamine (but not thrombin) stimulation evoked Rab46-dependent perinuclear trafficking of a subset of WPBs which accumulated at the MTOC. WPBs are considered rapid emergency responders, therefore to reproduce this on-demand response to either pro-thrombotic or pro-inflammatory stimuli, endothelial cell were treated with histamine or thrombin for only 10 mins, inducing acute release of WPBs. While thrombin stimulation showed large extracellular patches of vWF, a typical feature already described in several studies[196,203], we observed for the first time perinuclear clusters of vWF upon acute histamine stimulation. To date WPB perinuclear redistribution was only observed by stimulation of cAMP pathway[196]. Rondaji and co-workers[204] suggested that endothelial cell stimulation with epinephrine results in retrograde movement of a subset of WPBs to the microtubule organizing centre via PKA-dependent regulation of the dynein– dynactin complex[204]. This suggests that WPBs clustering is mediated by different signalling pathways according to different physiological needs. Histamine and thrombin both induce an increase in intracellular Ca^{2+} but our results showed that WPBs are able to distinguish between these two stimuli. Because the direction and timing of organelle movement needs to be tightly controlled by the cell, a variety of small GTPases have been implicated in WPB trafficking. We therefore speculated that Rab46 might be the mechanism by which WPBs can recognise different stimuli, regulating direction and timing of movement of these granules. Accordingly, downregulation of Rab46 by targeted siRNA reduced WPB clustering towards the MTOC upon histamine stimulation. Although Rab46 is a unique Rab GTPase with extra functional domains, it has the highly conserved Rab domain known to be essential for GTPase activity in other Rab proteins. Therefore we questioned the role of GTP in Rab46-dependent WPB trafficking in endothelial cells by heterologous expression of conserved nucleotide-binding mutants. Our findings showed that GTPase activity of Rab46 is required for histamine-evoked trafficking of WPBs to the MTOC. In agreement with GTP-bound Rab46 being necessary for WPB motility, vWF was colocalised with the constitutively active form of Rab46 at a perinuclear region even in the absence of stimulation. In contrast, histamine fails to induce redistribution of Rab46 or perinuclear clustering of WPBs in cells overexpressing the N658I inactive Rab46 mutant which localizes to the cytosol. These data suggest that Rab46 GTPase domain is functionally active and that GTP binding is necessary for the perinuclear localisation of Rab46 and WPBs as well as for its localization. Whether the Rab domain is necessary and sufficient to target Rab46 to WPBs and initiate the trafficking events could also be confirmed by expressing the individual Rab domain as well as Rab46 with deleted coil-coiled/EF-hand domains.

Microtubules, actin filaments and their associated molecular motors drive bidirectional movement of different intracellular organelles[186]. Evidence from different studies suggests that microtubules provide the tracks for rapid, long-distance transport, whereas actin may be used for local transport or anchorage of cargo to specific locations[205]. The bidirectional movement of WPBs in resting HUVECs and the plasma membrane-directed movement of

WPBs resulting in exocytosis of these organelles, were found previously to require an intact microtubular network[206]. Here, we show that histamine-evoked perinuclear clustering of WPBs also require the integrity of the microtubular network. This microtubular-dependent retrograde trafficking suggested that motor proteins may be involved. While kinesin mediates plus-end (forward) movements, minus-end directed movement toward the MTOC is mediated by the dynein motor protein[207]. Involvement of dynein in the Rab46-dependent retrograde movement of WPBs is supported by our findings showing reduced perinuclear clustering when dynein activity is inhibited by pre-treatment of endothelial cells with ciliobrevin D prior to histamine stimulation. Therefore, we propose a model where histamine stimulation, evokes Rab46 GTPase activity and mediates WPB retrograde movement using the dynein motor, which tracks WPBs back to the MTOC.

7.2 Rab46 mechanisms

In recent years, interactions between microtubule motor proteins and Rab GTPases have been identified and these motor proteins are recognised as Rab effector molecules[107]. Thus, through association with motor complexes, Rab proteins allow directional movement of various vesicular cargos along the microtubule cytoskeleton. The major minus-end-directed microtubule motors in eukaryotic cells are multi-component ATPases termed dyneins[208]. Wang et al proposed Rab46 as a new dynein adaptor in T-cells, necessary for dynein-dependent transport of subsynaptic vesicles to the MTOC. In agreement, my initial findings discussed above suggest a Rab46 and dynein/dynactin interaction in endothelial cells that is enhanced upon histamine stimulation.

To further explore the mechanisms underlying Rab46-dependent WPB trafficking, I performed protein affinity purification followed by mass spectrometry analysis to identify Rab46 interacting proteins. Proteomic analysis and immunoprecipitation assays led to the identification of the dynein heavy chain (DHC) as a new Rab46 interacting protein.

Although I confirmed the interaction of these two proteins in an overexpression system as well as at the endogenous level in endothelial cells, these experiments have some limitations such as the existence of a complex including endogenous endothelial cells proteins interacting with Rab46 or DHC, thus masking direct interaction between these two proteins. Therefore, I sought to explore this interaction using ectopic expression of human Rab46 in Cos-7 (monkey) cells and a recombinant purified portion of the tail domain of DHC. Using a recombinant DHC protein and Rab46 expression in an ectopic (non-human) system will narrow down the possibility of endogenous interacting proteins, leading to a more likely proof of direct interaction. These data suggested a direct interaction between these two proteins. Although we do not know if Cos-7 cells express endogenous Rab46, as they are monkey cells it is likely that its sequence is quite different to human, as if they were very

similar we could expect some detection as our antibody covers half the protein sequence. However, there is a possibility that adaptors that bind to monkey Rab46 could bind to human Rab46 and pull down with dynein, thereby the interaction would occur in a complex and not via a direct interaction. Wang et al suggested that Rab46 directly interacts with the dynein motor protein, however proof of direct interaction between Rab46 and dynein motor protein, in our system, requires further validation using purified proteins. Biochemical and biophysical assays, such as FRET experiments to detect location and distance of the interacting domains or isothermal titration calorimetry assay to have quantitative measurement about properties of protein-protein interaction can be used to further characterize the nature of Rab46 and dynein interaction. Given the similarity with other dynein adaptors, sequence alignment predicted some potential conserved binding sites on Rab46 sequence which may be necessary for the protein -protein interaction. A common feature between some dynein adaptors is the presence of CC1 box at the beginning of their coil-coiled domain where two alanine are responsible for the interaction with dynein[194]. These conserved residues, plus another conserved alanine at the C-terminal, were found in the Rab46 sequence, therefore as suggested in previous studies, mutation of these alanine residues into valine residues should allow us to determine if it causes loss of the dynein interaction. Future ongoing structural studies highlighting Rab46 conformation will also demonstrate the position of these conserved residues, allowing predictions of where they are exposed in space and time thereby elucidating the potential interaction with the dynein motor protein.

The Vale group suggested Rab46 directly recruits dynein in a Ca^{2+}-dependent manner. However, our preliminary results in endothelial cells suggest that Rab46 interaction with dynein is Ca^{2+}-independent. A mutation of Rab46 that is unable to bind to Ca^{2+} ($Rab46^{EFmut}$), as showed by Srikanth et al., does not influence its interaction with the dynein motor protein. Mammalian dyneins do not display processive motility by itself due to the auto-inhibited configuration of its motor domain[209]. Association of dynein with the dynactin complex in the presence of adaptor proteins with coiled-coil domains induces conformational changes which stimulate dynein long-range motility. Wang et al suggested that elevation of the Ca^{2+} concentration significantly increased the processivity of dynein–dynactin–Rab46 complexes on microtubules. Thus, although in endothelial cells Rab46 EF-hand mutant is still able to bind to dynein, it does not exclude that intracellular Ca^{2+} is required on the behalf of dynein-dynactin complex to be able to interact with its adaptors/activators prior any stimulation. Although dynein interaction with Rab46 is enhanced upon histamine stimulation, the interaction appears to exist prior the stimulation suggesting the possibly of ready pool of WPBs anchored to the dynein complex through Rab46 acting as an adaptor. Upon acute histamine stimulation this subset of WPBs is ready to rapidly move backward thus, helping endothelial cell to fine-tune WPB secretion.

The difference in Ca^{2+}-dependency between endothelial and T cells might reflect differences in the physiology and/or the accessory protein expression between the two cell types. Upon T-cell activation, the MTOC and Rab46 traffic to the immunological synapse and this is necessary for signal transmission between the T-cell receptor and the JNK pathway[167]. In addition, whilst endothelial cells only express Rab46, T cells also express the short non-Rab isoform (CRACR2A) that lacks the Rab domain but can interact with Rab46 via the coil-coiled region. Both Rab46 and CRACR2A are necessary for regulating store-operated Ca^{2+} entry (SOCE) in T-cells but we found no function of Rab46 in SOCE in endothelial cells[166].

Studying the role of Ca^{2+} in modulating the interaction or how it may influence Rab46 conformation before and after stimulation will be one of the main points of the next study. Also, more specific approaches to measure dynein motility upon stimulation will help to understand whether and how Rab46 is able to stimulate dynein motility in endothelial cells. Assembly and disassembly dynamic of Rab46 with dynein complex would also allow to find out more about binding properties of these proteins.

In addition to the dynein heavy chain, proteomic analysis identified the Na^+/K^+ ATPase subunit α (ATP1α) as a new Rab46 interacting partner and subsequent immunoprecipitation experiments supported this. Similarly to DHC, ATP1α interaction occurs with endogenous Rab46 either in non-stimulated or histamine stimulated cell. However, histamine stimulation seems to enhance this interaction. Does histamine stimulation stabilize the interaction and/or enable recruitment of other Rab46 effectors? These remain open questions. Additionally, the nature of the interaction (e.g. transient or stable direct interaction) still need to be elucidated. The Na^+/K^+ ATPase functions as an ion pump exchanging three Na^+ across the plasma membrane for two K^+ following hydrolysis of ATP, a crucial function for ion homeostasis. Interestingly, recent studies indicate that the same Na^+/K^+-ATPase also functions in activating signalling cascades independently of its ion-transport role. It is proposed that a separate pool of non-pumping Na^+/ K^+-ATPases mediate this noncanonical function depending on interactions of the Na^+/K^+ ATPase with various proteins including protein and lipid kinases, membrane transporters, channels, and cellular receptors[210]. The Na^+/K^+ ATPase is a heterodimeric transmembrane complex consisting of a 10-transmembrane domain α-subunit and a single transmembrane regulatory β-subunit. Four isoforms of the α-subunit have been identified, with the α1 isoform (ATP1α) being ubiquitously expressed. Recently, for the first time, a study from Booth et al[187] identified a new role for the α1 subunit of Na^+/K^+-ATPase (ATP1α) as a novel Rab27a interacting protein in melanocytes and showed that this interaction is direct with the intracellular loop of ATP1α and independent of nucleotide bound status of the Rab. Several lines of evidence strongly support an essential role for ATP1a1 in the targeting of Rab27a to melanosomes. Rab27a regulates the transport and secretion of lysosome related organelles and secretory granules from a variety of cell types[211]. Particularly, in endothelial cells Rab27a plays a central role in WPB trafficking and secretion. Considering the identification of ATP1α as a putative

interactive Rab46 protein in endothelial cells, it would be extremely interesting to further investigate this relationship in endothelial cells. In contrast to other cell types which present the Na^+/K^+-ATPase at the plasma membrane, endothelial cells present a more intracellular vesicles-like localization (data not shown). Its intracellular localization in relation to Rab46 as well as to WPBs will be the next step in this investigation. Considering that depletion of ATP1α alter Rab27a-dependent distribution of melanocyte causing perinuclear clustering, future studies will aim to depict whether ATP1α is responsible for Rab46 targeting to WPBs as well as regulation its function in WPBs trafficking in response to histamine. Another interesting question is the extent to which Na^+/K^+ ATPase ion pump function might be involved in Rab46 recruitment via regulation of WPBs ion homeostasis. WPBs are lysosome-related organelles therefore characterised by acidic pH. vWF tubulation underpins the elongated shape of WPBs, and that is dependent on an acidic pH. However, to date, little is known about maintain acidic intraluminal pH of WPBs after their budding from the TGN. A relationship exists between the pH within WPBs and their shape: WPBs are predominantly round at pH 7, mostly elongated at pH 6 or pH 5.5, and exhibit an intermediate phenotype at pH 6.5[212]. Therefore, a follow-up study may be about understanding the role of the Na^+/K^+-ATPase in regulating endothelial cells ion homeostasis and Rab46-dependent regulation of WPBs intraluminal pH via ATP1α interaction (i.e. is the ATP1α a pH-sensing protein mediating specific recruitment of Rab46 to WPBs?).

In this study, we attempted to biochemically purify novel Rab-binding proteins from endothelial cell by GFP-trap pull-down using GFP-tagged active and inactive form of Rab46 followed by mass spectrometry analysis. However, the nucleotide free (N658I) mutant, which appeared to be mis-colocalized is quite unstable, as suggested by Srikanth et al. This instability could be the reason why the proteins identified in our N658I pull-down are enriched for degradation pathways and nucleic acid binding activity. Therefore, rather than locking the Rab GTPase in their functional states, we could attempt to identify Rab46 interacting partners either by overexpression of WT-Rab46 or by using endogenous activation of Rab46 via histamine stimulation. Moreover, the use of purified Rab46 protein in the presence of GDP or GTP will also be useful for large-scale screening of potential GEF and GAP proteins. Rab interactors have mostly been defined through *in vitro* pulldown and yeast two-hybrid approaches which are a powerful tool to assess direct binding between a Rab and a specific protein. However, they preclude identification of context specific Rab GEFs, GAPs, or effectors, since the temporal aspects of effector recruitment are lost. Recently, APEX2 proximity labelling of Rab neighbouring proteins, combined with mass spectrometry, has been proposed as a new and efficient tool to rapidly map endogenous Rab regulators/effectors[213]. This latter approach was also recently used by Holthenrich and colleagues to carry out a comprehensive screening of factors associated with WPBs, confirming the presence of Rab46[214].

Nevertheless, our proteomic analysis identified several candidate proteins which still need to be investigated. Thus, it provides a useful first screening tool of Rab46-interacting proteins which could be useful for identification of new mechanisms of action for this novel Rab GTPase in endothelial cells.

7.3 Proposed Rab46-function

Although not part of my submitted data (but shown in our recent JCB paper[191]), I will briefly mention what I consider to be the function of Rab46 mediated trafficking. In addition to the mechanisms underlying Rab46 function we have to consider the function of Rab46-dependent WPB trafficking, for example, why is there a sub-population of WPBs in histamine stimulated cells that is not secreted (i.e. is it a subset of WPBs rescued from exocytosis or is it a polarised response?). We hypothesize that this allows agonist specific secretion of WPB cargo[191](proposed model in Figure 7.1). Previously, P-selectin and the pro-angiogenic tie-2 ligand angiopoietin-2 have been shown to reside in mutually exclusive WPBs, therefore, we questioned whether there is a difference in trafficking of these distinct WPBs in response to different stimuli. In our recent paper, we proved that trafficking of these distinct WPB populations is contextual since perinuclear clustering of P-selectin-negative WPBs is specific to histamine but not thrombin. We demonstrated that histamine promotes Rab46-dependent MTOC localisation of WPBs carrying angiopietin-2 indicating a mechanism to restrict release of angiopoietin-2 and possibly other cargo not necessary for an acute inflammatory response. Thus, whilst histamine stimulates release of P-selectin from WPBs at the cell surface, thereby supporting an inflammatory reaction, histamine limits an excessive vascular injury response by anchoring WPBs containing cargo extraneous to inflammation to the MTOC. We also suggested that mobilisation of intracellular Ca^{2+} binding to the EF-hand of Rab46 is required for dissociation of the perinuclear localised WPBs. In this way, Rab46 integrates transport and Ca^{2+} signals to regulate trafficking of WPBs that is relevant to the physiological signal and thus limits the extensive emergency response evoked by vascular injury.

All together these evidence present Rab46 as a novel and unique key regulator of WPB trafficking which enable specialized secretory responses depending on the applied stimulus. Rab46 could provide a mechanism by which processes such as inflammation might be regulated with a reduced risk of thrombosis. Such a mechanism would have important implications for the understanding of the role of WPBs in health and disease.

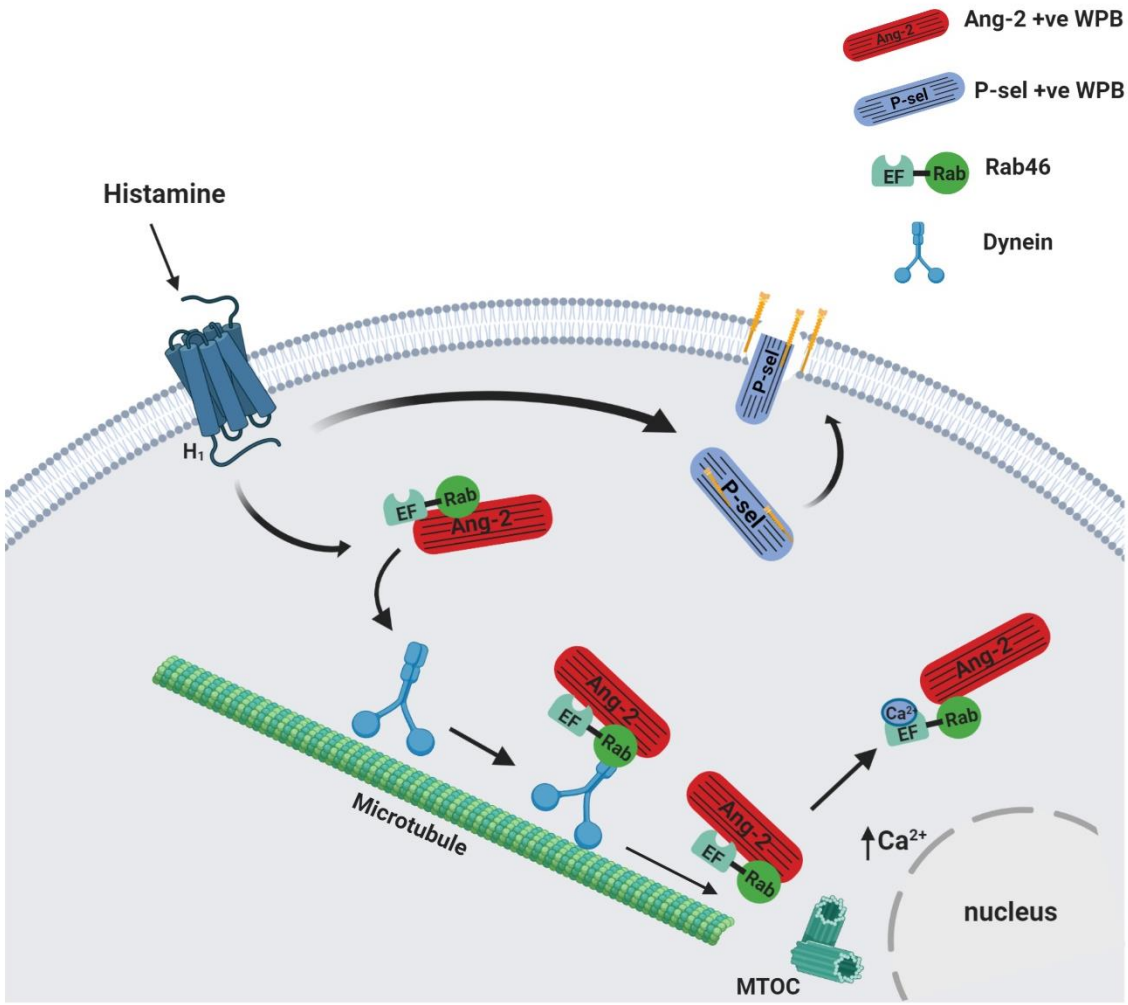

Figure 7.1 Proposed model of Rab46 function. Histamine stimulation of H1 receptor evokes the release of the proinflammatory ligand, P-selectin, while diverting WPBs carrying non-inflammatory cargo away from the plasma membrane to the MTOC. This differential trafficking is dependent on Rab46, a newly identified Ca2+-sensing GTPase, which localizes to a subset of P-selectin–negative WPBs. After acute histamine stimulation GTP-bound Rab46 evokes dynein-dependent retrograde transport of a subset of WPBs along microtubules. Upon continued histamine stimulation, Rab46 senses localized elevations of intracellular calcium and evokes dispersal of MTOC–clustered WPBs.

7.4 Rab46 *in vivo*

This study describes the role of Rab46 in cultured endothelial cells suggesting an important contribution in specialized WPB secretory response depending on the applied stimulus. However, confirmation of these data using an *in vivo* model are still at very early stages. Several difficulties in using a knockout-first strategy to generate a conditional specific knockout which will be eventually used to generate an endothelial specific Rab46 knockout, led us to an alternative commercially available *in vivo* approach. A global Cracr2a knockout was available from the KOMP repository, therefore we started our *in vivo* investigations using this model. We are fully aware of the limitations of this model , which include deletion in the whole body of both the short (CRACR2A) isoform and the long (Rab46) isoform. However, it provided a useful model to initialise our *in vivo* research, settling the foundation for further studies.

Initially, the mouse model was validated by confirming deletion of both isoforms in different tissues as well as from mouse endothelial cells extracted from the liver. Using an anti-CRACR2A antibody which targets both human and mouse sequence we provided preliminary evidence that only the long isoform (Rab46) is expressed in mouse endothelial cells, supporting the *in vitro* results. Thus, Cracr2a knockout was validated at the mRNA level as well as at protein level.

Srikanth et al., described tissue expression of CRACR2A in different human and mice samples, showing higher expression in the lung and immune cells. Our preliminary analysis in murine tissues shows abundance of Rab46 in the lung tissue and it is the most abundant Rab compared to the structurally related Rab44 and Rab45. Rab45 was not detected in any of the analysed tissues, however, Rab44 was detected at low level. Although the level of Rab44 expression is slightly upregulated in the spleen of Cracr2a knockout mice, its mRNA expression did not change in the liver, lung and heart following Cracr2a deletion. Therefore, genetic compensation could be ruled out.

The metabolic profile of the mice included in chapter 4 was investigated with body weight, organ weight and preliminary histology, glucose and insulin tolerance testing. These parameters were recorded in mice aged 8-12 weeks. Although the body weight was similar between the genotypes, an interesting difference in liver weight was observed with increased mass in the knockout female mice analysed. Trying to get some insights about the extent of the increased liver weight, a first H&E staining gave us a general overview of the liver morphology of both the genotypes. Lipid deposition could explain the increased mass; however, no fat accumulation was present. In contrast, Cracr2a knockout liver present multiple focal inflammation sites with immune cell infiltration in the peri-portal tract. Sinusoidal and portal vein congestion also appear to be a frequent feature in liver section analysed. Although characterization of these features with specific identification and quantification of the mononucleated infiltrated cells still need to be clarified, all together

these features may suggest that deletion of Cracr2a leads to an early inflammatory condition in young adult mice. Therefore, it would be extremely interesting to age these mice in order to look how this condition evolves over time. Several studies suggested that genetic variations in Rab46 gene may lead to the pro-inflammatory environment necessary for development of many human diseases characterized by chronic inflammation. In particular, a GWAS study revealed specific associations between a SNP in Rab46 gene (EFCAB4B) and lobular inflammation evident in non-alcoholic fatty liver disease (NAFLD)[176]. Further studies will evaluate whether some common inflammation markers are upregulated in the liver in absence of Cracr2a and specific staining identifying immune cells such as CD68 for macrophage identification, will be performed.

Preliminary glucose measurements show no significant difference between genotypes on either glucose or insulin tolerance testing. However, Cracr2a knockout mice have higher basal glucose level after short time fasting compared to control WT. These data need to be confirmed by increasing the number of mice studied as well as by using male mice. Nevertheless, as mice are active and eat more at night using only 2 hours fasting in the morning before ITT does not give a real fasting glucose measurement. Therefore, many studies suggest a short fasting period of 5-6 hours before the ITT in order to reduce variability in basal blood glucose. To determine the overall physiological tolerance of these mice to glucose and their ability to maintain glucose homeostasis within the normal physiological range, further studies are needed. Whether and how Cracr2a deletion affect glucose metabolism is still an open question.

It is important to recognise the general limitations of the *in vivo* model presented in chapter 6. Firstly, as already mentioned, deletion of Cracr2a gene abolish the expression of both the isoforms which so far have been presented with very different tissue-specific functions. Therefore, determining a cause-effect correlation is much more difficult, i.e. whether an observed effect is attributed to the short or the long variant require an extra level of investigation. Furthermore, the data presented are largely exploratory, and several datasets require further work in order to be completed and confirm some of the preliminary data. Nevertheless, using an endothelial specific Rab46 knockout mouse remain the best option to truly determine the *in vivo* contribution of Rab46 under physiological and pathological conditions.

Chapter 8 Conclusion and Future Directions

8.1 Summary of Key Findings

This thesis presents data examining the role of Rab46 in WPB trafficking in response to acute pro-inflammatory stimulation, adding a new player to the endothelial molecular machinery controlling differential WPB trafficking and exocytosis.

We propose a model where Rab46 is activated following histamine stimulation inducing a subset of WPBs to move backward to the perinuclear area, exploiting dynein motility along the microtubules. Highlighting the molecular mechanism, Rab46 interaction with the dynein complex suggests Rab46 as a new dynein adaptor maybe providing a scaffold to link WPBs (cargo) to its respecting motor protein (dynein) which motility is induced following histamine stimulation.

The key findings of this thesis which support the described model can be summarized by the following main points.

- Endogenous Rab46 localises to WPBs in endothelial cells with Rab46 vesicles juxtaposed to vWF, on the cytosolic face of WPBs.
- WPBs are the primary target of Rab46 in endothelial cells. However, Rab46 localises to a subset of WPBs corresponding to almost half of the full population.
- Acute histamine and thrombin stimulation induce differential WPB trafficking.
- Rab46 regulates histamine, but not thrombin, WPB trafficking to the perinuclear area identified as the MTOC.
- Functional GTPase domain regulates Rab46 localization to WPBs and GTP binding is necessary for the perinuclear localization of WPBs.
- Rab46-dependent retrograde trafficking of WPBs in response to histamine requires intact microtubule network and dynein activity.
- Endogenous Rab46 is able to interact with the dynein-dynactin complex either in non-stimulated or histamine stimulated condition.
- A customised pull-down assay reveals direct interaction between Rab46 and the tail domain of dynein heavy chain.
- Rab46 is suggested as new dynein adaptor used by a subset of WPBs to be rescued from exocytosis upon acute pro-inflammatory stimulation.
- Basic phenotyping characterization of a global Rab46 knockout mouse represents the very beginning of extending our existing *in vitro* model to future *in vivo* studies to detect the physiological role of this novel Rab GTPase.

In conclusion, Rab46 is a new piece of the big puzzle representing WPB contribution to the endothelial tailored secretory response to different stimuli.

8.2 Future work

The work performed in this project provides a basis for future research in several areas. In addition to some specific approaches outlined throughout the discussion section above, a number of broader goals will be important to build on the work produced in this project. More work is needed to answer new emerging questions to fulfil the functions and mechanisms of Rab46 in endothelial cells.

Spatio-temporal resolution

Although in this study we used the AiryScan imaging system which improve the confocal resolution, it is still unable to resolve distances below a certain threshold. Single molecule localization microscopy (SMLM) allows samples to be imaged at resolutions well below the diffraction limit. New SMLM techniques, such as dSTORM or PALM will provide an invaluable tool for the study of biological structure and function at the nanoscale. Therefore, the spatial distribution of Rab46 with WPBs could be further characterize based on their proximity to each other, reaching a 50 nm spatial resolution along all three spatial dimensions.

This study provides several evidence of Rab46-dependent WPB trafficking, however it lacks dynamic observations. Rab46 vesicular dynamic analysis and WPB trafficking using live-cell imaging will be the main goal of the near future to show the common spatio-temporal distribution. So far, the main limitation was the effect of GFP tag on Rab46 localization, therefore we are developing a new labelling approach using the spot-tag/nanobody technique to measure their dynamics and interactions, with better temporal resolution, in biological contexts. The use of alternatives to antibodies in super-resolution microscopy, including nanobodies, affibodies, and affimers has been recently increased to overcome the limitation size of antibodies (these reagents are approximately 10 times smaller than antibodies). Therefore, we are also planning to generate affimers against Rab46 which could represents useful tool for super-resolution microscopy as well as potential specific inhibition function.

vWF secretion

Although we reported that siRNA-mediated downregulation of Rab46 affects the vWF content and WPB number in endothelial cells, we did not investigate vWF secretion in the analysed conditions. We aim to characterize secreted vWF phenotype in response to acute stimulation, determining which secretory pathway may be affected by Rab46. Using the Ibidi pump system set in our lab, functional release of vWF will be analysed by measuring vWF string length under flow. Sting formation reflects vWF haemostatic function as well as it could be indicative of the multimer pattern of vWF and its ability to be stored in WPBs.

Furthermore, the functionality of the released vWF strings will be verified by assessing the recruitment of platelets to the endothelium under physiological flow.

Structural studies

It is known that conformational changes occur during Rab GTPase cycle. Since no structural studies on Rab46 have been performed to date, future studies from our lab aim to investigate the structure, folding and dynamic properties of Rab46. Production of recombinant full-length Rab46 protein and individually recombinant Rab46 domains will provide a useful tool for a number of different studies. First of all, structure and conformational change following activation and inactivation could be investigated by using high-resolution Nuclear Magnetic Resonance (NMR) spectroscopy. Homology modelling will be also used to identify functionally important residues and guide new experiments such as site-directed mutagenesis. Predicted binding-sites between Rab46 and dynein could be analysed to determine whether they are exposed and available for interaction. Availability of purified Rab46 protein will eventually confirm direct interaction with the dynein complex. Moreover, the role of Ca^{2+} could be further analysed by observing conformational change induced by Ca^{2+} binding to the EF-hands of Rab46.

Structural studies will provide an in depth understanding of Rab46 atomic structure, perhaps revealing specific binding pockets that could be modulated by small molecules; thus, providing novel therapeutic targets for cardiovascular disease.

Mechanisms underlying Rab46 function

More work is needed to reveal the exact pathway regulating Rab46 context-dependent trafficking of WPBs. Small GTPase are regulated by many GEFs and GAPs proteins. However, how Rab46 cycle between an ON and OFF state is still unknown. Future studies will aim to identify Rab46 effectors either by using a different proteomic approach, such as the APEX technique, or by characterizing some of the already identified candidates. Immunoprecipitation assays confirms ATP1α interaction with Rab46, however its function still need to be explored. We will initially study its localization in endothelial cells and using siRNA targeting ATP1a we will investigate the effects on Rab46 function as well as differences in Rab46 cellular distribution to WPBs. Recently, it also been show that ATP1α interacts with multiple myosin proteins[215] like Myosin-9, a protein which is also present in our pull-down assay. Therefore, the role of Myosin-9 will also be to be investigated in order to identify mechanisms of Rab46 action. As we have already proved that Rab46-dependent trafficking to the perinuclear area is Ca^{2+} independent, we hypothesise that some phosphorylation events can take place and regulate the histamine response; thus, a phospho-proteomic approach will help us to do a first screening of potential candidates.

Although we are just at the beginning of defining a novel Rab46 pathway in endothelial cells, future studies employing all the different approaches mentioned above will help to put together different pieces of Rab46 puzzle.

Endothelial specific Rab46 knockout mice

In order to be able to draw solid conclusions, global Cracr2a knockout mice need further characterization. Initially, there are a number of datasets which remain incomplete, and therefore the first priority will be to complete these experiments in both female and male mice. In order to address the hypothesis about the presence of early stage inflammation process in the liver of Cracr2a knockout mice, specific staining to identify the presence of immune cells infiltration will be performed. Moreover, qPCR analysis will evaluate whether inflammation markers such as C-reactive protein, IL-6 and TNF are upregulated in Crac2a knockout mice compared to control WT. Aging studies as well as stress conditions to assess their physiological response to different challenges will be performed.

Furthermore, endothelial cells need to be isolated from these mice to confirm that the endogenous Rab46 is functional. qPCR analysis showed that Rab46 is highly expressed in the lung thus, extraction of endothelial cells will be carried out from both liver and lung tissues. So far, the main limitation for confirming Rab46 function in murine cells has been the lack of anti-Rab46 antibody which is able to recognize mouse target for immunofluorescence assays. However, we are planning to start an affimer screening which could be used for future imaging studies.

Although characterization of global Cracr2a knockout mouse will provide useful insights about the Rab46 gene on whole body phenotype, in order to explore the contribution of endothelial Rab46 on the vascular physiology a more targeted approach is needed. The development of endothelial specific Rab46 knockout mice could be a considerable turning point and will facilitate experiments to further understand Rab46 biology in endothelial cells. Using this model, the role of Rab46 in stimulated release of vWF *in vivo* will be assessed by measuring plasma vWF in response to different stimulation as well as by measuring bleeding time. Furthermore, we aim to analyse the ability of vWF to induce platelet aggregation by using intravital microscopy to visualise clot formation.

Following our *in vitro* studies, there are a number of possible avenues for exploration in order to characterise the endothelial specific phenotype further and to elucidate the possible mechanisms underlying Rab46 contribution to the vasculature.

8.3 Conclusions

The broad spectrum of endothelial functions requires the existence of a highly responsive system which is able to rapidly respond to both physiological and pathological changes in the vascular environment. Many scenarios will result in the generation or release of multiple endothelial agonists that even when working through the same pathway, can lead to quite distinct functional consequences. WPBs are the "perfect vascular emergency kit" which is responsible to elicit different functional outcomes following stimulation, in order to maintain vascular homeostasis. Given the importance of endothelial cells to maintain vascular homeostasis, WPB exocytosis need a tight regulatory molecular machinery to precisely modulate their haemostatic and inflammatory function. Unravelling the molecular mechanisms underlying differential release of WPB content is a key challenge which can have important consequences for clinical interventions. Limiting dangerous thrombosis whilst allowing normal inflammatory response (or vice versa) will open new directions to tackle the endothelial dysfunction occurring in different cardiovascular diseases.

Our data present Rab46, a novel and unique GTPase, as a new member of the WPB-associated machinery driving the on-demand endothelial cells response. Rab46 is necessary for dynein-dependent WPB trafficking to the MTOC in response to acute inflammatory stimuli but not to pro-thrombotic stimulation. Therefore, Rab46 could be a key regulator of differential WPB cargo secretion, allowing the separation of haemostatic and inflammatory responses. This extra layer of regulation supports the emerging concept of WPB plasticity, which can tune specialized secretory responses depending on the applied stimulus.

Further work will be needed to explore these findings in a wider variety of settings, from *in vitro* to *in vivo* studies, but the insights presented here provided a solid foundation on which to build future studies. Work towards a greater understanding of the complex signalling processes underlying Rab46 function and WPB tailored secretion could provide novel therapeutic targets for cardiovascular disease.

.

List of References

1. Galley, H. F. & Webster, N. R. Physiology of the endothelium. *British Journal of Anaesthesia* **93**, 105–113 (2004).
2. Fishman, A. P. Endothelium: A Distributed Organ of Diverse Capabilities. *Annals of the New York Academy of Sciences* **401**, 1–8 (1982).
3. Khazaei, M., Moien-Afshari, F. & Laher, I. Vascular endothelial function in health and diseases. *Pathophysiology* **15**, 49–67 (2008).
4. Cines, D. B. *et al.* Endothelial Cells in Physiology and in the Pathophysiology of Vascular Disorders. *Blood* **91**, 3527–3561 (1998).
5. Cooke, J. P. The endothelium: a new target for therapy. *Vasc Med* **5**, 49–53 (2000).
6. Esmon, C. T. Natural Anticoagulants and Their Pathways. in *Antithrombotics* (eds. Uprichard, A. C. G. & Gallagher, K. P.) 447–476 (Springer Berlin Heidelberg, 1999). doi:10.1007/978-3-642-59942-2_16.
7. Esmon, C. T. Cell Mediated Events that Control Blood Coagulation and Vascular Injury. *Annual Review of Cell Biology* **9**, 1–26 (1993).
8. Granger, D. N. & Senchenkova, E. *Leukocyte–Endothelial Cell Adhesion*. (Morgan & Claypool Life Sciences, 2010).
9. Muller, W. A. Mechanisms of Leukocyte Transendothelial Migration. *Annu Rev Pathol* **6**, 323–344 (2011).
10. Rubanyi, G. M. The role of endothelium in cardiovascular homeostasis and diseases. *J. Cardiovasc. Pharmacol.* **22 Suppl 4**, S1-14 (1993).
11. Felmeden, D. C., Blann, A. D., Spencer, C. G. C., Beevers, D. G. & Lip, G. Y. H. A comparison of flow-mediated dilatation and von Willebrand factor as markers of endothelial cell function in health and in hypertension: relationship to cardiovascular risk and effects of treatment: a substudy of the Anglo-Scandinavian Cardiac Outcomes Trial. *Blood Coagul. Fibrinolysis* **14**, 425–431 (2003).

12. Matsushita, K. *et al.* Nitric oxide regulates exocytosis by S-nitrosylation of N-ethylmaleimide-sensitive factor. *Cell* **115**, 139–150 (2003).

13. Dong, Z. M., Brown, A. A. & Wagner, D. D. Prominent role of P-selectin in the development of advanced atherosclerosis in ApoE-deficient mice. *Circulation* **101**, 2290–2295 (2000).

14. Collins, R. G. *et al.* P-Selectin or intercellular adhesion molecule (ICAM)-1 deficiency substantially protects against atherosclerosis in apolipoprotein E-deficient mice. *J. Exp. Med.* **191**, 189–194 (2000).

15. Lahoz, C. & Mostaza, J. M. Atherosclerosis As a Systemic Disease. *Rev Esp Cardiol* **60**, 184–195 (2007).

16. Libby, P., Ridker, P. M. & Hansson, G. K. Progress and challenges in translating the biology of atherosclerosis. *Nature* **473**, 317–325 (2011).

17. Avogaro, A., Albiero, M., Menegazzo, L., de Kreutzenberg, S. & Fadini, G. P. Endothelial Dysfunction in Diabetes. *Diabetes Care* **34**, S285–S290 (2011).

18. Bleakley, C., Hamilton, P. K., Pumb, R., Harbinson, M. & McVeigh, G. E. Endothelial Function in Hypertension: Victim or Culprit? *The Journal of Clinical Hypertension* **17**, 651–654 (2015).

19. Weibel, E. R. & Palade, G. E. NEW CYTOPLASMIC COMPONENTS IN ARTERIAL ENDOTHELIA. *J. Cell Biol.* **23**, 101–112 (1964).

20. Wagner, D. D., Olmsted, J. B. & Marder, V. J. Immunolocalization of von Willebrand protein in Weibel-Palade bodies of human endothelial cells. *J. Cell Biol.* **95**, 355–360 (1982).

21. Aird William C. Phenotypic Heterogeneity of the Endothelium. *Circulation Research* **100**, 158–173 (2007).

22. Gebrane-Younès, J., Drouet, L., Caen, J. P. & Orcel, L. Heterogeneous distribution of Weibel-Palade bodies and von Willebrand factor along the porcine vascular tree. *Am J Pathol* **139**, 1471–1484 (1991).

23. Smith, J. M., Meinkoth, J. H., Hochstatter, T. & Meyers, K. M. Differential distribution of von Willebrand factor in canine vascular endothelium. *Am. J. Vet. Res.* **57**, 750–755 (1996).

24. Ochoa, C. D., Wu, S. & Stevens, T. New Developments in Lung Endothelial Heterogeneity: von Willebrand factor, P-selectin, and the Weibel-Palade Body. *Semin Thromb Hemost* **36**, 301–308 (2010).

25. Jaffe, E. A., Nachman, R. L., Becker, C. G. & Minick, C. R. Culture of Human Endothelial Cells Derived from Umbilical Veins. IDENTIFICATION BY MORPHOLOGIC AND IMMUNOLOGIC CRITERIA. *J Clin Invest* **52**, 2745–2756 (1973).

26. Denis, C. V., André, P., Saffaripour, S. & Wagner, D. D. Defect in regulated secretion of P-selectin affects leukocyte recruitment in von Willebrand factor-deficient mice. *Proc Natl Acad Sci U S A* **98**, 4072–4077 (2001).

27. Haberichter, S. L. *et al.* Re-establishment of VWF-dependent Weibel-Palade bodies in VWD endothelial cells. *Blood* **105**, 145–152 (2005).

28. Wagner, D. D. *et al.* Induction of specific storage organelles by von Willebrand factor propolypeptide. *Cell* **64**, 403–413 (1991).

29. Valentijn, K. M., Sadler, J. E., Valentijn, J. A., Voorberg, J. & Eikenboom, J. Functional architecture of Weibel-Palade bodies. *Blood* **117**, 5033–5043 (2011).

30. Wagner, D. D., Mayadas, T. & Marder, V. J. Initial glycosylation and acidic pH in the Golgi apparatus are required for multimerization of von Willebrand factor. *The Journal of Cell Biology* **102**, 1320–1324 (1986).

31. Haberichter, S. L., Fahs, S. A. & Montgomery, R. R. von Willebrand factor storage and multimerization: 2 independent intracellular processes. *Blood* **96**, 1808–1815 (2000).

32. Hannah, M. J., Williams, R., Kaur, J., Hewlett, L. J. & Cutler, D. F. Biogenesis of Weibel–Palade bodies. *Seminars in Cell & Developmental Biology* **13**, 313–324 (2002).

33. Hannah, M. J. *et al.* Weibel-Palade bodies recruit Rab27 by a content-driven, maturation-dependent mechanism that is independent of cell type. *J. Cell. Sci.* **116**, 3939–3948 (2003).

34. Zenner, H. L., Collinson, L. M., Michaux, G. & Cutler, D. F. High-pressure freezing provides insights into Weibel-Palade body biogenesis. *Journal of Cell Science* **120**, 2117–2125 (2007).

35. Metcalf, D. J., Nightingale, T. D., Zenner, H. L., Lui-Roberts, W. W. & Cutler, D. F. Formation and function of Weibel-Palade bodies. *J. Cell. Sci.* **121**, 19–27 (2008).

36. van Breevoort, D. *et al.* Proteomic Screen Identifies IGFBP7 as a Novel Component of Endothelial Cell-Specific Weibel-Palade Bodies. *J. Proteome Res.* **11**, 2925–2936 (2012).

37. Geng, J.-G. *et al.* Rapid neutrophil adhesion to activated endothelium mediated by GMP-140. *Nature* **343**, 757–760 (1990).

38. Harrison-Lavoie, K. J. *et al.* P-selectin and CD63 use different mechanisms for delivery to Weibel-Palade bodies. *Traffic* **7**, 647–662 (2006).

39. Zannettino, A. C. W. *et al.* Osteoprotegerin (OPG) is localized to the Weibel-Palade bodies of human vascular endothelial cells and is physically associated with von Willebrand factor. *Journal of Cellular Physiology* **204**, 714–723 (2005).

40. Pichiule, P., Chavez, J. C. & LaManna, J. C. Hypoxic regulation of angiopoietin-2 expression in endothelial cells. *J. Biol. Chem.* **279**, 12171–12180 (2004).

41. Fiedler, U. & Augustin, H. G. Angiopoietins: a link between angiogenesis and inflammation. *Trends in Immunology* **27**, 552–558 (2006).

42. Lemieux, C. *et al.* Angiopoietins can directly activate endothelial cells and neutrophils to promote proinflammatory responses. *Blood* **105**, 1523–1530 (2005).

43. Mckinnon, T. A. J., Starke, R. D., Ediriwickrema, K., Randi, A. M. & Laffan, M. Von Willebrand Factor Binds to the Endothelial Growth Factor Angiopoietin-2 Both within Endothelial Cells and Upon Release From Weibel Palade Bodies. *Blood* **118**, 698–698 (2011).

44. Fiedler, U. *et al.* The Tie-2 ligand Angiopoietin-2 is stored in and rapidly released upon stimulation from endothelial cell Weibel-Palade bodies. *Blood* **103**, 4150–4156 (2004).

45. Ozaka, T., Doi, Y., Kayashima, K. & Fujimoto, S. Weibel-Palade bodies as a storage site of calcitonin gene-related peptide and endothelin-1 in blood vessels of the rat carotid body. *The Anatomical Record* **247**, 388–394 (1997).

46. Russell Fraser D., Skepper Jeremy N. & Davenport Anthony P. Human Endothelial Cell Storage Granules. *Circulation Research* **83**, 314–321 (1998).

47. Vischer, U. M. & Wagner, D. D. CD63 is a component of Weibel-Palade bodies of human endothelial cells. *Blood* **82**, 1184–1191 (1993).

48. Doyle, E. L. *et al.* CD63 is an essential cofactor to leukocyte recruitment by endothelial P-selectin. *Blood* **118**, 4265–4273 (2011).

49. Utgaard, J. O., Jahnsen, F. L., Bakka, A., Brandtzaeg, P. & Haraldsen, G. Rapid Secretion of Prestored Interleukin 8 from Weibel-Palade Bodies of Microvascular Endothelial Cells. *J Exp Med* **188**, 1751–1756 (1998).

50. Wolff, B., Burns, A. R., Middleton, J. & Rot, A. Endothelial Cell "Memory" of Inflammatory Stimulation: Human Venular Endothelial Cells Store Interleukin 8 in Weibel-Palade Bodies. *J Exp Med* **188**, 1757–1762 (1998).

51. Øynebråten, I., Bakke, O., Brandtzaeg, P., Johansen, F.-E. & Haraldsen, G. Rapid chemokine secretion from endothelial cells originates from 2 distinct compartments. *Blood* **104**, 314–320 (2004).

52. Wagner Denisa D. New Links Between Inflammation and Thrombosis. *Arteriosclerosis, Thrombosis, and Vascular Biology* **25**, 1321–1324 (2005).

53. Peyvandi, F., Garagiola, I. & Baronciani, L. Role of von Willebrand factor in the haemostasis. *Blood Transfus* **9**, s3–s8 (2011).

54. Wagner, D. D. & Frenette, P. S. The vessel wall and its interactions. *Blood* **111**, 5271–5281 (2008).

55. Frenette, P. S. & Wagner, D. D. Adhesion molecules--Part II: Blood vessels and blood cells. *N. Engl. J. Med.* **335**, 43–45 (1996).

56. Rondaij, M. G., Bierings, R., Kragt, A., van Mourik, J. A. & Voorberg, J. Dynamics and plasticity of Weibel-Palade bodies in endothelial cells. *Arterioscler. Thromb. Vasc. Biol.* **26**, 1002–1007 (2006).

57. Giblin, J. P., Hewlett, L. J. & Hannah, M. J. Basal secretion of von Willebrand factor from human endothelial cells. *Blood* **112**, 957–964 (2008).

58. Silva, M. L. da & Cutler, D. F. von Willebrand factor multimerization and the polarity of secretory pathways in endothelial cells. *Blood* **128**, 277–285 (2016).

59. Schillemans, M., Karampini, E., Kat, M. & Bierings, R. Exocytosis of Weibel–Palade bodies: how to unpack a vascular emergency kit. *Journal of Thrombosis and Haemostasis* **17**, 6–18 (2019).

60. Aird, W. C. Spatial and temporal dynamics of the endothelium. *Journal of Thrombosis and Haemostasis* **3**, 1392–1406 (2005).

61. Fujiwara, K. Platelet endothelial cell adhesion molecule-1 and mechanotransduction in vascular endothelial cells. *J. Intern. Med.* **259**, 373–380 (2006).

62. Birch, K. A., Pober, J. S., Zavoico, G. B., Means, A. R. & Ewenstein, B. M. Calcium/calmodulin transduces thrombin-stimulated secretion: studies in intact and minimally permeabilized human umbilical vein endothelial cells. *J. Cell Biol.* **118**, 1501–1510 (1992).

63. Vischer, U. M., Barth, H. & Wollheim, C. B. Regulated von Willebrand factor secretion is associated with agonist-specific patterns of cytoskeletal remodeling in cultured endothelial cells. *Arterioscler. Thromb. Vasc. Biol.* **20**, 883–891 (2000).

64. Hamilton, K. K. & Sims, P. J. Changes in cytosolic Ca2+ associated with von Willebrand factor release in human endothelial cells exposed to histamine. Study of microcarrier cell monolayers using the fluorescent probe indo-1. *J. Clin. Invest.* **79**, 600–608 (1987).

65. Erent, M. *et al.* Rate, extent and concentration dependence of histamine-evoked Weibel–Palade body exocytosis determined from individual fusion events in human endothelial cells. *J Physiol* **583**, 195–212 (2007).

66. Pober, J. S. & Sessa, W. C. Evolving functions of endothelial cells in inflammation. *Nat. Rev. Immunol.* **7**, 803–815 (2007).

67. Esposito, B. *et al.* NAADP links histamine H1 receptors to secretion of von Willebrand factor in human endothelial cells. *Blood* **117**, 4968–4977 (2011).

68. Lowenstein, C. J., Morrell, C. N. & Yamakuchi, M. Regulation of Weibel–Palade Body Exocytosis. *Trends in Cardiovascular Medicine* **15**, 302–308 (2005).

69. Nightingale, T. D., Pattni, K., Hume, A. N., Seabra, M. C. & Cutler, D. F. Rab27a and MyRIP regulate the amount and multimeric state of VWF released from endothelial cells. *Blood* **113**, 5010–5018 (2009).

70. Rojo Pulido, I. *et al.* Myosin Va acts in concert with Rab27a and MyRIP to regulate acute von-Willebrand factor release from endothelial cells. *Traffic* **12**, 1371–1382 (2011).

71. Conte, I. L. *et al.* Interaction between MyRIP and the actin cytoskeleton regulates Weibel–Palade body trafficking and exocytosis. *J Cell Sci* **129**, 592–603 (2016).

72. Chehab, T. *et al.* A novel Munc13-4/S100A10/annexin A2 complex promotes Weibel-Palade body exocytosis in endothelial cells. *Mol. Biol. Cell* **28**, 1688–1700 (2017).

73. Bierings, R. *et al.* The interplay between the Rab27A effectors Slp4-a and MyRIP controls hormone-evoked Weibel-Palade body exocytosis. *Blood* **120**, 2757–2767 (2012).

74. van Breevoort, D. *et al.* STXBP1 promotes Weibel-Palade body exocytosis through its interaction with the Rab27A effector Slp4-a. *Blood* **123**, 3185–3194 (2014).

75. Knop, M., Aareskjold, E., Bode, G. & Gerke, V. Rab3D and annexin A2 play a role in regulated secretion of vWF, but not tPA, from endothelial cells. *EMBO J.* **23**, 2982–2992 (2004).

76. Nightingale, T. D. *et al.* Actomyosin II contractility expels von Willebrand factor from Weibel–Palade bodies during exocytosis. *J Cell Biol* **194**, 613–629 (2011).

77. Biesemann, A., Gorontzi, A., Barr, F. & Gerke, V. Rab35 Regulates Evoked Exocytosis of Endothelial Weibel-Palade Bodies. *J. Biol. Chem.* (2017) doi:10.1074/jbc.M116.773333.

78. Berntorp, E. Erik von Willebrand. *Thrombosis Research* **120**, S3–S4 (2007).

79. Zimmerman, T. S., Ratnoff, O. D. & Powell, A. E. Immunologic differentiation of classic hemophilia (factor VIII deficiency) and von Willebrand's disease. *J Clin Invest* **50**, 244–254 (1971).

80. Von Willebrand's Disease. *N Engl J Med* **376**, 701–702 (2017).

81. Smith, N. L. *et al.* Novel associations of multiple genetic loci with plasma levels of factor VII, factor VIII, and von Willebrand factor: The CHARGE Consortium. *Circulation* **121**, 1382–1392 (2010).

82. Randi, A. M. Endothelial dysfunction in von Willebrand disease: angiogenesis and angiodysplasia. *Thrombosis Research* **141**, S55–S58 (2016).

83. Seaman, C. D., Yabes, J., Comer, D. M. & Ragni, M. V. Does deficiency of von Willebrand factor protect against cardiovascular disease? Analysis of a national discharge register. *Journal of Thrombosis and Haemostasis* **13**, 1999–2003 (2015).

84. Spiel Alexander O., Gilbert James C. & Jilma Bernd. Von Willebrand Factor in Cardiovascular Disease. *Circulation* **117**, 1449–1459 (2008).

85. McCarthy, L. J. *et al.* Myocardial Infarction njury Is Relatively Common at Presentation of Acute Thrombotic Thrombocytopenic Purpura: The Indiana University Experience. *Therapeutic Apheresis* https://onlinelibrary.wiley.com/doi/abs/10.1046/j.1526-0968.2002.00363.x (2002) doi:10.1046/j.1526-0968.2002.00363.x.

86. Colicelli, J. Human RAS superfamily proteins and related GTPases. *Sci. STKE* **2004**, RE13 (2004).

87. Goud, B., Salminen, A., Walworth, N. C. & Novick, P. J. A GTP-binding protein required for secretion rapidly associates with secretory vesicles and the plasma membrane in yeast. *Cell* **53**, 753–768 (1988).

88. Schmitt, H. D., Wagner, P., Pfaff, E. & Gallwitz, D. The ras-related YPT1 gene product in yeast: a GTP-binding protein that might be involved in microtubule organization. *Cell* **47**, 401–412 (1986).

89. Touchot, N., Chardin, P. & Tavitian, A. Four additional members of the ras gene superfamily isolated by an oligonucleotide strategy: molecular cloning of YPT-related cDNAs from a rat brain library. *Proc. Natl. Acad. Sci. U.S.A.* **84**, 8210–8214 (1987).

90. Stenmark, H. & Olkkonen, V. M. The Rab GTPase family. *Genome Biology* **2**, reviews3007.1 (2001).

91. Bourne, H. R., Sanders, D. A. & McCormick, F. The GTPase superfamily: conserved structure and molecular mechanism. *Nature* **349**, 117–127 (1991).

92. Pereira-Leal, J. B. & Seabra, M. C. Evolution of the rab family of small GTP-binding proteins11Edited by J. Thornton. *Journal of Molecular Biology* **313**, 889–901 (2001).

93. Hutagalung, A. H. & Novick, P. J. Role of Rab GTPases in membrane traffic and cell physiology. *Physiol. Rev.* **91**, 119–149 (2011).

94. Stein, M. *et al.* The Interaction Properties of the Human Rab GTPase Family – A Comparative Analysis Reveals Determinants of Molecular Binding Selectivity. *PLOS ONE* **7**, e34870 (2012).

95. Stenmark, H. Rab GTPases as coordinators of vesicle traffic. *Nat. Rev. Mol. Cell Biol.* **10**, 513–525 (2009).

96. Rensland, H., Lautwein, A., Wittinghofer, A. & Goody, R. S. Is there a rate-limiting step before GTP cleavage by H-ras p21? *Biochemistry* **30**, 11181–11185 (1991).

97. Fukuda, M. TBC proteins: GAPs for mammalian small GTPase Rab? *Bioscience Reports* **31**, 159–168 (2011).

98. Rak, A. *et al.* Crystal structure of the GAP domain of Gyp1p: first insights into interaction with Ypt/Rab proteins. *EMBO J* **19**, 5105–5113 (2000).

99. Bos, J. L., Rehmann, H. & Wittinghofer, A. GEFs and GAPs: Critical Elements in the Control of Small G Proteins. *Cell* **129**, 865–877 (2007).

100. Müller, M. P. & Goody, R. S. Molecular control of Rab activity by GEFs, GAPs and GDI. *Small GTPases* **9**, 5–21 (2017).

101. Rink, J., Ghigo, E., Kalaidzidis, Y. & Zerial, M. Rab Conversion as a Mechanism of Progression from Early to Late Endosomes. *Cell* **122**, 735–749 (2005).

102. Blümer, J. *et al.* RabGEFs are a major determinant for specific Rab membrane targeting. *J Cell Biol* **200**, 287–300 (2013).

103. Aivazian, D., Serrano, R. L. & Pfeffer, S. TIP47 is a key effector for Rab9 localization. *The Journal of Cell Biology* **173**, 917–926 (2006).

104. Seaman, M. N. J., Harbour, M. E., Tattersall, D., Read, E. & Bright, N. Membrane recruitment of the cargo-selective retromer subcomplex is catalysed by the small GTPase Rab7 and inhibited by the Rab-GAP TBC1D5. *J. Cell. Sci.* **122**, 2371–2382 (2009).

105. McLauchlan, H. *et al.* A novel role for Rab5–GDI in ligand sequestration into clathrin-coated pits. *Current Biology* **8**, 34–45 (1998).

106. Semerdjieva, S. *et al.* Coordinated regulation of AP2 uncoating from clathrin-coated vesicles by rab5 and hRME-6. *J Cell Biol* **183**, 499–511 (2008).

107. Horgan, C. P. & McCaffrey, M. W. Rab GTPases and microtubule motors. *Biochem. Soc. Trans.* **39**, 1202–1206 (2011).

108. Wu, X. S. *et al.* Identification of an organelle receptor for myosin-Va. *Nat. Cell Biol.* **4**, 271–278 (2002).

109. Roland, J. T., Kenworthy, A. K., Peranen, J., Caplan, S. & Goldenring, J. R. Myosin Vb interacts with Rab8a on a tubular network containing EHD1 and EHD3. *Mol. Biol. Cell* **18**, 2828–2837 (2007).

110. Hales, C. M., Vaerman, J.-P. & Goldenring, J. R. Rab11 Family Interacting Protein 2 Associates with Myosin Vb and Regulates Plasma Membrane Recycling. *J. Biol. Chem.* **277**, 50415–50421 (2002).

111. Roland, J. T., Lapierre, L. A. & Goldenring, J. R. Alternative Splicing in Class V Myosins Determines Association with Rab10. *J. Biol. Chem.* **284**, 1213–1223 (2009).

112. Echard, A. *et al.* Interaction of a Golgi-associated kinesin-like protein with Rab6. *Science* **279**, 580–585 (1998).

113. Arimura, N. *et al.* Anterograde transport of TrkB in axons is mediated by direct interaction with Slp1 and Rab27. *Dev. Cell* **16**, 675–686 (2009).

114. Wanschers, B. *et al.* Rab6 family proteins interact with the dynein light chain protein DYNLRB1. *Cell Motility* **65**, 183–196 (2008).

115. Jordens, I. *et al.* The Rab7 effector protein RILP controls lysosomal transport by inducing the recruitment of dynein-dynactin motors. *Curr. Biol.* **11**, 1680–1685 (2001).

116. Horgan, C. P., Hanscom, S. R., Jolly, R. S., Futter, C. E. & McCaffrey, M. W. Rab11-FIP3 links the Rab11 GTPase and cytoplasmic dynein to mediate transport to the endosomal-recycling compartment. *J Cell Sci* **123**, 181–191 (2010).

117. Chia, P. Z. C. & Gleeson, P. A. Membrane tethering. *F1000Prime Rep* **6**, (2014).

118. Simonsen, A. *et al.* EEA1 links PI(3)K function to Rab5 regulation of endosome fusion. *Nature* **394**, 494–498 (1998).

119. Coppola, T. *et al.* Pancreatic β-Cell Protein Granuphilin Binds Rab3 and Munc-18 and Controls Exocytosis. *MBoC* **13**, 1906–1915 (2002).

120. Gomi, H., Mizutani, S., Kasai, K., Itohara, S. & Izumi, T. Granuphilin molecularly docks insulin granules to the fusion machinery. *J Cell Biol* **171**, 99–109 (2005).

121. Tsuboi, T. & Fukuda, M. Rab3A and Rab27A cooperatively regulate the docking step of dense-core vesicle exocytosis in PC12 cells. *Journal of Cell Science* **119**, 2196–2203 (2006).

122. Cai, H., Reinisch, K. & Ferro-Novick, S. Coats, Tethers, Rabs, and SNAREs Work Together to Mediate the Intracellular Destination of a Transport Vesicle. *Developmental Cell* **12**, 671–682 (2007).

123. Simonsen, A., Gaullier, J. M., D'Arrigo, A. & Stenmark, H. The Rab5 effector EEA1 interacts directly with syntaxin-6. *J. Biol. Chem.* **274**, 28857–28860 (1999).

124. Nielsen, E. *et al.* Rabenosyn-5, a Novel Rab5 Effector, Is Complexed with Hvps45 and Recruited to Endosomes through a Fyve Finger Domain. *J Cell Biol* **151**, 601–612 (2000).

125. Torii, S., Zhao, S., Yi, Z., Takeuchi, T. & Izumi, T. Granuphilin Modulates the Exocytosis of Secretory Granules through Interaction with Syntaxin 1a. *Mol Cell Biol* **22**, 5518–5526 (2002).

126. Zerial, M. & McBride, H. Rab proteins as membrane organizers. *Nat Rev Mol Cell Biol* **2**, 107–117 (2001).

127. Pfeffer, S. & Aivazian, D. Targeting Rab GTPases to distinct membrane compartments. *Nat. Rev. Mol. Cell Biol.* **5**, 886–896 (2004).

128. Ali, B. R. & Seabra, M. C. Targeting of Rab GTPases to cellular membranes. *Biochem Soc Trans* **33**, 652–656 (2005).

129. Bhuin, T. & Roy, J. K. Rab proteins: the key regulators of intracellular vesicle transport. *Exp. Cell Res.* **328**, 1–19 (2014).

130. Mollard, G. F. von *et al.* rab3 is a small GTP-binding protein exclusively localized to synaptic vesicles. *PNAS* **87**, 1988–1992 (1990).

131. A small rab GTPase is distributed in cytoplasmic vesicles in non polarized cells but colocalizes with the tight junction marker ZO-1 in polarized epithelial cells. *J Cell Biol* **124**, 101–115 (1994).

132. Hume, A. N. *et al.* Rab27a regulates the peripheral distribution of melanosomes in melanocytes. *J. Cell Biol.* **152**, 795–808 (2001).

133. Martin, S. & Parton, R. G. Characterization of Rab18, a Lipid Droplet–Associated Small GTPase. in *Methods in Enzymology* vol. 438 109–129 (Academic Press, 2008).

134. Alto, N. M., Soderling, J. & Scott, J. D. Rab32 is an A-kinase anchoring protein and participates in mitochondrial dynamics. *J Cell Biol* **158**, 659–668 (2002).

135. Iida, H., Noda, M., Kaneko, T., Doiguchi, M. & Mōri, T. Identification of rab12 as a vesicle-associated small GTPase highly expressed in Sertoli cells of rat testis. *Molecular Reproduction and Development* **71**, 178–185 (2005).

136. Pfeffer, S. R. Rab GTPases: master regulators of membrane trafficking. *Curr. Opin. Cell Biol.* **6**, 522–526 (1994).

137. Wilson, D. B. & Wilson, M. P. Identification and subcellular localization of human rab5b, a new member of the ras-related superfamily of GTPases. *J. Clin. Invest.* **89**, 996–1005 (1992).

138. Karniguian, A., Zahraoui, A. & Tavitian, A. Identification of small GTP-binding rab proteins in human platelets: thrombin-induced phosphorylation of rab3B, rab6, and rab8 proteins. *Proc Natl Acad Sci U S A* **90**, 7647–7651 (1993).

139. de Leeuw, H. P. *et al.* Small GTP-binding proteins in human endothelial cells. *Br. J. Haematol.* **103**, 15–19 (1998).

140. Sandri, C. *et al.* The R-Ras/RIN2/Rab5 complex controls endothelial cell adhesion and morphogenesis via active integrin endocytosis and Rac signaling. *Cell Res.* **22**, 1479–1501 (2012).

141. Nayak, R. C., Keshava, S., Esmon, C. T., Pendurthi, U. R. & Rao, L. V. M. Rab GTPases Regulate Endothelial Cell Protein C Receptor-Mediated Endocytosis and Trafficking of Factor VIIa. *PLoS One* **8**, (2013).

142. Jopling Helen M. *et al.* Rab GTPase Regulation of VEGFR2 Trafficking and Signaling in Endothelial Cells. *Arteriosclerosis, Thrombosis, and Vascular Biology* **29**, 1119–1124 (2009).

143. Zografou, S. *et al.* A complete Rab screening reveals novel insights in Weibel-Palade body exocytosis. *J. Cell. Sci.* **125**, 4780–4790 (2012).

144. Pastural, E. *et al.* Griscelli disease maps to chromosome 15q21 and is associated with mutations in the myosin-Va gene. *Nat. Genet.* **16**, 289–292 (1997).

145. Ménasché, G. *et al.* Mutations in RAB27A cause Griscelli syndrome associated with haemophagocytic syndrome. *Nat. Genet.* **25**, 173–176 (2000).

146. Strom, M., Hume, A. N., Tarafder, A. K., Barkagianni, E. & Seabra, M. C. A family of Rab27-binding proteins. Melanophilin links Rab27a and myosin Va function in melanosome transport. *J. Biol. Chem.* **277**, 25423–25430 (2002).

147. Seabra, M. C., Brown, M. S. & Goldstein, J. L. Retinal degeneration in choroideremia: deficiency of rab geranylgeranyl transferase. *Science* **259**, 377–381 (1993).

148. D'Adamo, P. *et al.* Mutations in GDI1 are responsible for X-linked non-specific mental retardation. *Nat. Genet.* **19**, 134–139 (1998).

149. Verhoeven, K. *et al.* Mutations in the small GTP-ase late endosomal protein RAB7 cause Charcot-Marie-Tooth type 2B neuropathy. *Am. J. Hum. Genet.* **72**, 722–727 (2003).

150. Aligianis, I. A. *et al.* Mutations of the catalytic subunit of RAB3GAP cause Warburg Micro syndrome. *Nat. Genet.* **37**, 221–223 (2005).

151. Ginsberg, S. D. *et al.* Upregulation of select rab GTPases in cholinergic basal forebrain neurons in mild cognitive impairment and Alzheimer's disease. *Journal of Chemical Neuroanatomy* **42**, 102–110 (2011).

152. Pal, A., Severin, F., Lommer, B., Shevchenko, A. & Zerial, M. Huntingtin–HAP40 complex is a novel Rab5 effector that regulates early endosome motility and is up-regulated in Huntington's disease. *J Cell Biol* **172**, 605–618 (2006).

153. Dalfó, E. *et al.* Abnormal alpha-synuclein interactions with Rab proteins in alpha-synuclein A30P transgenic mice. *J. Neuropathol. Exp. Neurol.* **63**, 302–313 (2004).

154. Mosesson, Y., Mills, G. B. & Yarden, Y. Derailed endocytosis: an emerging feature of cancer. *Nat. Rev. Cancer* **8**, 835–850 (2008).

155. Tzeng, H.-T. & Wang, Y.-C. Rab-mediated vesicle trafficking in cancer. *Journal of Biomedical Science* **23**, 70 (2016).

156. Wang, S., Hu, C., Wu, F. & He, S. Rab25 GTPase: Functional roles in cancer. *Oncotarget* **8**, 64591–64599 (2017).

157. Hendrix, A. *et al.* Effect of the secretory small GTPase Rab27B on breast cancer growth, invasion, and metastasis. *J. Natl. Cancer Inst.* **102**, 866–880 (2010).

158. Jin, L. *et al.* Down-regulation of Ras-related Protein Rab 5C-dependent Endocytosis and Glycolysis in Cisplatin-resistant Ovarian Cancer Cell Lines. *Mol Cell Proteomics* **13**, 3138–3151 (2014).

159. Prada-Delgado, A. *et al.* Inhibition of Rab5a exchange activity is a key step for Listeria monocytogenes survival. *Traffic* **6**, 252–265 (2005).

160. Sklan, E. H. *et al.* TBC1D20 is a Rab1 GTPase-activating protein that mediates hepatitis C virus replication. *J. Biol. Chem.* **282**, 36354–36361 (2007).

161. Garvey, W. T. *et al.* Evidence for defects in the trafficking and translocation of GLUT4 glucose transporters in skeletal muscle as a cause of human insulin resistance. *J. Clin. Invest.* **101**, 2377–2386 (1998).

162. Imamura, T. *et al.* Insulin-induced GLUT4 translocation involves protein kinase C-lambda-mediated functional coupling between Rab4 and the motor protein kinesin. *Mol. Cell. Biol.* **23**, 4892–4900 (2003).

163. Wu, G. *et al.* Increased myocardial Rab GTPase expression: a consequence and cause of cardiomyopathy. *Circ. Res.* **89**, 1130–1137 (2001).

164. Stein, M.-P., Dong, J. & Wandinger-Ness, A. Rab proteins and endocytic trafficking: potential targets for therapeutic intervention. *Adv. Drug Deliv. Rev.* **55**, 1421–1437 (2003).

165. Prieto-Dominguez, N., Parnell, C. & Teng, Y. Drugging the Small GTPase Pathways in Cancer Treatment: Promises and Challenges. *Cells* **8**, 255 (2019).

166. Wilson, L. A., McKeown, L., Tumova, S., Li, J. & Beech, D. J. Expression of a long variant of CRACR2A that belongs to the Rab GTPase protein family in endothelial cells. *Biochem. Biophys. Res. Commun.* **456**, 398–402 (2015).

167. Srikanth, S. *et al.* A large Rab GTPase encoded by CRACR2A is a component of subsynaptic vesicles that transmit T cell activation signals. *Sci Signal* **9**, ra31 (2016).

168. Yamaguchi, Y. *et al.* Rab44, a novel large Rab GTPase, negatively regulates osteoclast differentiation by modulating intracellular calcium levels followed by NFATc1 activation. *Cell. Mol. Life Sci.* **75**, 33–48 (2018).

169. Shintani, M. *et al.* Characterization of Rab45/RASEF containing EF-hand domain and a coiled-coil motif as a self-associating GTPase. *Biochem. Biophys. Res. Commun.* **357**, 661–667 (2007).

170. Maat, W. *et al.* Epigenetic Regulation Identifies RASEF as a Tumor-Suppressor Gene in Uveal Melanoma. *Invest. Ophthalmol. Vis. Sci.* **49**, 1291–1298 (2008).

171. Nakamura, S. *et al.* Small GTPase RAB45-mediated p38 activation in apoptosis of chronic myeloid leukemia progenitor cells. *Carcinogenesis* **32**, 1758–1772 (2011).

172. Srikanth, S. *et al.* A novel EF-hand protein, CRACR2A, is a cytosolic Ca2+ sensor that stabilizes CRAC channels in T cells. *Nat. Cell Biol.* **12**, 436–446 (2010).

173. Wang, Y. *et al.* CRACR2a is a calcium-activated dynein adaptor protein that regulates endocytic traffic. *J Cell Biol* **218**, 1619–1633 (2019).

174. Murray, R. Z., Kay, J. G., Sangermani, D. G. & Stow, J. L. A Role for the Phagosome in Cytokine Secretion. *Science* **310**, 1492–1495 (2005).

175. Husebye, H. *et al.* The Rab11a GTPase controls Toll-like receptor 4-induced activation of interferon regulatory factor-3 on phagosomes. *Immunity* **33**, 583–596 (2010).

176. Chalasani, N. *et al.* Genome-wide association study identifies variants associated with histologic features of nonalcoholic Fatty liver disease. *Gastroenterology* **139**, 1567–1576, 1576.e1–6 (2010).

177. Lu, X. *et al.* Genome-wide association study in Chinese identifies novel loci for blood pressure and hypertension. *Hum. Mol. Genet.* **24**, 865–874 (2015).

178. Barozzi, C. *et al.* A Combined Targeted and Whole Exome Sequencing Approach Identified Novel Candidate Genes Involved in Heritable Pulmonary Arterial Hypertension. *Sci Rep* **9**, 753 (2019).

179. Mitsunaga, S. *et al.* Exome sequencing identifies novel rheumatoid arthritis-susceptible variants in the *BTNL2*. *Journal of Human Genetics* **58**, 210–215 (2013).

180. Bevilacqua, L. *et al.* A genome-wide association study identifies an association between variants in EFCAB4B gene and periodontal disease in an Italian isolated population. *Journal of Periodontal Research* **53**, 992–998 (2018).

181. Nightingale, T. & Cutler, D. The secretion of von Willebrand factor from endothelial cells; an increasingly complicated story. *J. Thromb. Haemost.* **11 Suppl 1**, 192–201 (2013).

182. Michaux, G. & Cutler, D. F. How to Roll an Endothelial Cigar: The Biogenesis of Weibel-Palade Bodies. *Traffic* **5**, 69–78 (2004).

183. Srikanth, S., Woo, J. S. & Gwack, Y. A large Rab GTPase family in a small GTPase world. *Small GTPases* **8**, 43–48 (2016).

184. Jordens, I. *et al.* The Rab7 effector protein RILP controls lysosomal transport by inducing the recruitment of dynein-dynactin motors. *Curr. Biol.* **11**, 1680–1685 (2001).

185. Pereira-Leal, J. B. & Seabra, M. C. The mammalian Rab family of small GTPases: definition of family and subfamily sequence motifs suggests a mechanism for functional specificity in the Ras superfamily11Edited by M. Yaniv. *Journal of Molecular Biology* **301**, 1077–1087 (2000).

186. Manneville, J.-B. *et al.* Interaction of the actin cytoskeleton with microtubules regulates secretory organelle movement near the plasma membrane in human endothelial cells. *J. Cell. Sci.* **116**, 3927–3938 (2003).

187. Booth, A. E. G., Tarafder, A. K., Hume, A. N., Recchi, C. & Seabra, M. C. A Role for Na+,K+-ATPase α1 in Regulating Rab27a Localisation on Melanosomes. *PLoS One* **9**, (2014).

188. Bolognesi, B. & Lehner, B. Reaching the limit. *eLife* **7**,.

189. Stoebel, D. M., Dean, A. M. & Dykhuizen, D. E. The cost of expression of Escherichia coli lac operon proteins is in the process, not in the products. *Genetics* **178**, 1653–1660 (2008).

190. Xing, S., Wallmeroth, N., Berendzen, K. W. & Grefen, C. Techniques for the Analysis of Protein-Protein Interactions in Vivo. *Plant Physiology* **171**, 727–758 (2016).

191. Miteva, K. T. *et al.* Rab46 integrates Ca2+ and histamine signaling to regulate selective cargo release from Weibel-Palade bodies. *J. Cell Biol.* **218**, 2232–2246 (2019).

192. Vallee, R. B., McKenney, R. J. & Ori-McKenney, K. M. Multiple modes of cytoplasmic dynein regulation. *Nat. Cell Biol.* **14**, 224–230 (2012).

193. Reck-Peterson, S. L., Redwine, W. B., Vale, R. D. & Carter, A. P. The Cytoplasmic Dynein Transport Machinery and its Many Cargoes. *Nat Rev Mol Cell Biol* **19**, 382–398 (2018).

194. Olenick, M. A. & Holzbaur, E. L. F. Dynein activators and adaptors at a glance. *J Cell Sci* **132**, jcs227132 (2019).

195. Ferraro, F. *et al.* Weibel-Palade body size modulates the adhesive activity of its von Willebrand Factor cargo in cultured endothelial cells. *Sci Rep* **6**, 32473 (2016).

196. Romani de Wit Thalia, Rondaij Mariska G., Hordijk Peter L., Voorberg Jan & van Mourik Jan A. Real-Time Imaging of the Dynamics and Secretory Behavior of Weibel-Palade Bodies. *Arteriosclerosis, Thrombosis, and Vascular Biology* **23**, 755–761 (2003).

197. Pober, J. S. & Cotran, R. S. THE ROLE OF ENDOTHELIAL CELLS IN INFLAMMATION. *Transplantation* **50**, 537 (1990).

198. Sporn, L. A., Marder, V. J. & Wagner, D. D. Inducible secretion of large, biologically potent von Willebrand factor multimers. *Cell* **46**, 185–190 (1986).

199. Rabiet Marie-Josèphe *et al.* Thrombin-Induced Increase in Endothelial Permeability Is Associated With Changes in Cell-to-Cell Junction Organization. *Arteriosclerosis, Thrombosis, and Vascular Biology* **16**, 488–496 (1996).

200. Stolwijk, J. A. *et al.* Calcium Signaling is Dispensable for Receptor-Regulation of Endothelial Barrier Function. *J. Biol. Chem.* jbc.M116.756114 (2016) doi:10.1074/jbc.M116.756114.

201. Sun, W. Y. *et al.* Rapid histamine-induced neutrophil recruitment is sphingosine kinase-1 dependent. *Am. J. Pathol.* **180**, 1740–1750 (2012).

202. Kiskin, N. I., Babich, V., Knipe, L., Hannah, M. J. & Carter, T. Differential Cargo Mobilisation within Weibel-Palade Bodies after Transient Fusion with the Plasma Membrane. *PLoS One* **9**, (2014).

203. Vischer, U. M. & Wagner, D. D. von Willebrand factor proteolytic processing and multimerization precede the formation of Weibel-Palade bodies. *Blood* **83**, 3536–3544 (1994).

204. Rondaij, M. G. *et al.* Dynein-dynactin complex mediates protein kinase A-dependent clustering of Weibel-Palade bodies in endothelial cells. *Arterioscler. Thromb. Vasc. Biol.* **26**, 49–55 (2006).

205. Langford, G. M. Actin- and microtubule-dependent organelle motors: interrelationships between the two motility systems. *Current Opinion in Cell Biology* **7**, 82–88 (1995).

206. Sinha, S. & Wagner, D. D. Intact microtubules are necessary for complete processing, storage and regulated secretion of von Willebrand factor by endothelial cells. *Eur. J. Cell Biol.* **43**, 377–383 (1987).

207. Gennerich, A. & Vale, R. D. Walking the walk: how kinesin and dynein coordinate their steps. *Curr Opin Cell Biol* **21**, 59–67 (2009).

208. Karki, S. & Holzbaur, E. L. Cytoplasmic dynein and dynactin in cell division and intracellular transport. *Curr. Opin. Cell Biol.* **11**, 45–53 (1999).

209. Zhang, K. *et al.* Cryo-EM Reveals How Human Cytoplasmic Dynein Is Auto-inhibited and Activated. *Cell* **169**, 1303-1314.e18 (2017).

210. Liang, M. *et al.* Identification of a pool of non-pumping Na/K-ATPase. *J. Biol. Chem.* **282**, 10585–10593 (2007).

211. Fukuda, M. Versatile role of Rab27 in membrane trafficking: focus on the Rab27 effector families. *J. Biochem.* **137**, 9–16 (2005).

212. Michaux, G. *et al.* The Physiological Function of von Willebrand's Factor Depends on Its Tubular Storage in Endothelial Weibel-Palade Bodies. *Developmental Cell* **10**, 223–232 (2006).

213. Del Olmo, T. *et al.* APEX2-mediated RAB proximity labeling identifies a role for RAB21 in clathrin-independent cargo sorting. *EMBO Rep.* **20**, (2019).

214. Holthenrich, A., Drexler, H. C. A., Chehab, T., Naß, J. & Gerke, V. Proximity proteomics of endothelial Weibel-Palade bodies identifies novel regulator of von-Willebrand factor secretion. *Blood* blood.2019000786 (2019) doi:10.1182/blood.2019000786.

215. Dash, B., Dib-Hajj, S. D. & Waxman, S. G. Multiple myosin motors interact with sodium/potassium-ATPase alpha 1 subunits. *Mol Brain* **11**, (2018).

Appendix

Macro code "WPBs and Rab46 cellular distribution"

The code is to be saved as a .txt file and loaded in ImageJ as macro

```
//for 16bit Z-stack images
//Channel 1 -> DAPI nucleus staining
//Channel 2 -> Green Rab46 staining
//Channel 3 -> Red vWF staining
//2018-05-25
//created by L.Pedicini

macro "distanceMapRed&Green [y]"
 {
//variables definition
imageTitle = getTitle();
imageDir = getDirectory("image");
dotIndex = indexOf(imageTitle, ".");
imageTitleNoExt = substring(imageTitle, 0, dotIndex);

// input z-stack image
run("Z Project...", "projection=[Max Intensity]");          //max.intensity projection
run("Duplicate...", "duplicate");
saveAs("Tiff", imageDir + "\\results\\Max_" + imageTitleNoExt + "-1.tiff" );
close();
selectWindow("MAX_" + imageTitle);
run("Split Channels");
selectWindow("C2-MAX_" + imageTitle);
waitForUser( "Pause","Measure Background C2");       // background subtraction  according to the noise level for each channel
selectWindow("C3-MAX_" + imageTitle);
waitForUser( "Pause","Measure Background C3");

selectWindow("C1-MAX_" + imageTitle);                                    //DAPI channel
run("Auto Threshold", "method=Default white");
setOption("BlackBackground", true);
run("Make Binary");
run("Fill Holes");
```

```
run("Despeckle");
run("Close-");
run("Fill Holes");
run("Median...");   // the user sets the radius between 2 and 5  according to the image
run("Fill Holes");
run("Despeckle");
run("Watershed");                                    // divides overlapping nuclei
waitForUser( "Pause","Quality check");          // QC for the watershed step
run("Invert");
run("Distance Map");

//Analyse Red channel
selectWindow("C3-MAX_" + imageTitle);
run("Red");
run("Duplicate...", " ");
selectWindow("C3-MAX_" + imageTitle);
run("Auto Threshold", "method=MaxEntropy white");

//to measure particles distance from the nucleus
run("Set Measurements...", "area mean min integrated redirect=C1-MAX_" + imageTitle + " decimal=3");

selectWindow("C3-MAX_" + imageTitle);
run("Analyze Particles...", "size=0.03-Infinity display exclude slice");
saveAs("Results", imageDir + "\\results\\distance_Red" + imageTitleNoExt + ".csv" );
waitForUser( "Pause","Close results window");

//to measure particles intensities from the raw image
selectWindow("C3-MAX_" + imageTitle);
run("Set Measurements...", "area mean min integrated redirect=C3-MAX_" + imageTitleNoExt + "-1.dv
decimal=3");
selectWindow("C3-MAX_" + imageTitle);
run("Analyze Particles...", "size=0.03-Infinity display exclude slice");
saveAs("Results", imageDir + "\\results\\intensity_Red" + imageTitleNoExt + ".csv" );
selectWindow("C3-MAX_" + imageTitleNoExt + "-1.dv");
run("RGB Color");
saveAs("Tiff", imageDir + "\\results\\Red_" + imageTitleNoExt + "-1.tiff" );
close();
waitForUser( "Pause","Close results window to analyse the next channel");

// Analyse Green channel
selectWindow("C2-MAX_" + imageTitle);
run("Green");
```

```
run("Duplicate...", " ");
selectWindow("C2-MAX_" + imageTitle);
run("Auto Threshold", "method=MaxEntropy white")
run("Set Measurements...", "area mean min integrated redirect=C1-MAX_" + imageTitle + " decimal=3");
selectWindow("C2-MAX_" + imageTitle);
run("Analyze Particles...", "size=0.03-Infinity display exclude slice");
saveAs("Results", imageDir + "\\results\\distance_Green" + imageTitleNoExt + ".csv" );
waitForUser( "Pause","Close results window");
selectWindow("C2-MAX_" + imageTitle);
run("Set Measurements...", "area mean min integrated redirect=C2-MAX_" + imageTitleNoExt + "-1.dv decimal=3");
selectWindow("C2-MAX_" + imageTitle);
run("Analyze Particles...", "size=0.03-Infinity display exclude slice");
saveAs("Results", imageDir + "\\results\\intensity_Green" + imageTitleNoExt + ".csv" );
selectWindow("C2-MAX_" + imageTitleNoExt + "-1.dv");
run("RGB Color");
saveAs("Tiff", imageDir + "\\results\\green_" + imageTitleNoExt + "-1.tiff" );
close();
selectWindow("C1-MAX_" + imageTitle);
saveAs("Tiff", imageDir + "\\results\\distMap_" + imageTitleNoExt + ".tiff" );
close();
selectWindow("C3-MAX_" + imageTitle);
close();
selectWindow("C2-MAX_" + imageTitle);
close();
selectWindow(imageTitle);
close();
}
```

Raw Proteomic data

Dataset QLvsNI

Group	p-value	Mean 1	Mean 2	Median 1	Median 2	Fold change QL to NI
Myosin-9 OS=Homo sapiens GN=MYH9 PE=1 SV=4	0.00881	1035107.3	5513859.2	575288.5	4575465.2	5.3268
Fatty acid synthase OS=Homo sapiens GN=FASN PE=1 SV=3	0.00047	216432.4	818854.6	124286.8	1011299.6	3.7834
Clathrin heavy chain OS=Homo sapiens GN=CLTC PE=1 SV=1	0.00006	141206.3	465390.0	123329.0	533316.4	3.2958
DnaJ homolog subfamily A member 2 OS=Homo sapiens GN=DNAJA2 PE=1 SV=1	0.00577	3867.4	12115.4	2188.6	11760.4	3.1327
Isoleucine--tRNA ligase, cytoplasmic OS=Homo sapiens GN=IARS PE=1 SV=2	0.00080	27719.0	81643.9	30623.5	99219.3	2.9454
CAD protein OS=Homo sapiens GN=CAD PE=1 SV=1	0.00208	129910.2	356813.2	71983.4	423091.0	2.7466
Filamin-B OS=Homo sapiens GN=FLNB PE=1 SV=2	0.00067	206444.6	500749.7	110338.3	483883.1	2.4256
Thrombospondin-1 OS=Homo sapiens GN=THBS1 PE=1 SV=2	0.00318	811406.8	1952072.7	705225.0	1903450.4	2.4058
DNA-dependent protein kinase catalytic subunit OS=Homo sapiens GN=PRKDC PE=1 SV=3	0.00286	128885.6	305170.4	120622.0	234149.1	2.3678
Sodium/potassium-transporting ATPase subunit alpha-1 OS=Homo sapiens GN=ATP1A1 PE=1 SV=1	0.00001	115250.0	271029.4	118095.9	308547.2	2.3517

Poly [ADP-ribose] polymerase 4 OS=Homo sapiens GN=PARP4 PE=1 SV=3	0.01376	20209.3	47435.7	16712.9	60639.9	2.3472
Filamin-A OS=Homo sapiens GN=FLNA PE=1 SV=4	0.00005	208314.7	452316.5	165847.8	418776.2	2.1713
U5 small nuclear ribonucleoprotein 200 kDa helicase OS=Homo sapiens GN=SNRNP200 PE=1 SV=2	0.01954	31203.9	65489.9	30556.7	79343.4	2.0988
Four and a half LIM domains protein 2 OS=Homo sapiens GN=FHL2 PE=1 SV=1	0.04377	12210.5	24285.2	11542.4	25873.9	1.9889
Ras-interacting protein 1 OS=Homo sapiens GN=RASIP1 PE=1 SV=1	0.03748	6624.0	12688.1	5939.1	13229.4	1.9155
B-cell receptor-associated protein 31 OS=Homo sapiens GN=BCAP31 PE=1 SV=3	0.00997	35504.3	66868.7	40157.2	73321.4	1.8834
Cytoplasmic FMR1-interacting protein 1 OS=Homo sapiens GN=CYFIP1 PE=1 SV=1	0.02565	23321.8	43590.7	19695.4	53383.2	1.8691
Coatomer subunit alpha OS=Homo sapiens GN=COPA PE=1 SV=2	0.04028	357178.5	652580.2	463160.0	858988.1	1.8270
Ubiquitin-associated protein 2-like OS=Homo sapiens GN=UBAP2L PE=1 SV=2	0.01053	11178.9	20084.7	10086.8	22670.7	1.7967
Cytoplasmic dynein 1 heavy chain 1 OS=Homo sapiens GN=DYNC1H1 PE=1 SV=5	0.00235	152549.1	269519.9	158459.0	285311.4	1.7668
Myoferlin OS=Homo sapiens GN=MYOF PE=1 SV=1	0.00694	77092.3	135350.1	69350.1	137563.2	1.7557
Histone deacetylase 6 OS=Homo sapiens GN=HDAC6 PE=1 SV=2	0.01879	514561.4	900963.4	507403.6	927612.6	1.7509

Centrosomal protein of 170 kDa OS=Homo sapiens GN=CEP170 PE=1 SV=1	0.02782	33489.5	58025.5	25507.2	62699.4	1.7326
NADH dehydrogenase [ubiquinone] iron-sulfur protein 2, mitochondrial OS=Homo sapiens GN=NDUFS2 PE=1 SV=2	0.02549	52743.7	87182.1	51238.7	106379.8	1.6529
Exportin-1 OS=Homo sapiens GN=XPO1 PE=1 SV=1	0.02067	44029.5	71910.5	48160.6	84822.8	1.6332
Platelet endothelial cell adhesion molecule OS=Homo sapiens GN=PECAM1 PE=1 SV=1	0.02011	68714.8	108840.2	70640.9	90373.9	1.5839
DNA replication licensing factor MCM3 OS=Homo sapiens GN=MCM3 PE=1 SV=3	0.00442	240685.4	375702.3	242406.5	422236.3	1.5610
A-kinase anchor protein 12 OS=Homo sapiens GN=AKAP12 PE=1 SV=4	0.01332	54114.4	83997.6	55086.6	76489.4	1.5522
Lysosome-associated membrane glycoprotein 1 OS=Homo sapiens GN=LAMP1 PE=1 SV=3	0.02832	130786.5	196839.7	144108.4	158986.6	1.5050

Dataset NIvsQL

Group	p-value	Mean 1	Mean 2	Median 1	Median 2	Fold change NI to QL
REVERSED Cysteine protease ATG4C OS=Homo sapiens GN=ATG4C PE=1 SV=1	2.48E-09	2799745	1427.21	2583028	1069.504	1961.6918
60S ribosomal protein L36a-like OS=Homo sapiens GN=RPL36AL PE=1 SV=3	0.02244	63319.2	13739.39	86435.62	7039.723	4.6086
28S ribosomal protein S34, mitochondrial OS=Homo sapiens GN=MRPS34 PE=1 SV=2	0.00855	22936.05	5068.914	22375.1	4346.953	4.5248
Histone H4 OS=Homo sapiens GN=HIST1H4A PE=1 SV=2	0.04192	3065066	739103.3	1376825	688341.1	4.1470
Eukaryotic translation initiation factor 2A OS=Homo sapiens GN=EIF2A PE=1 SV=3	0.04001	23282.97	6399.625	16046.33	3089.723	3.6382
Histone H2A.Z OS=Homo sapiens GN=H2AFZ PE=1 SV=2	0.02852	37479.6	10501.31	22353.84	7300.094	3.5690
Cell cycle and apoptosis regulator protein 2 OS=Homo sapiens GN=CCAR2 PE=1 SV=2	0.04517	113335.3	34378.73	58145.15	31023.55	3.2967
Histone H1x OS=Homo sapiens GN=H1FX PE=1 SV=1	0.00078	60091.94	20383.62	64876.2	15422.7	2.9481
Histone H2A type 1-B/E OS=Homo sapiens GN=HIST1H2AB PE=1 SV=2	0.00913	27022.46	9327.686	26548.36	7099.551	2.8970

60S ribosomal protein L14 OS=Homo sapiens GN=RPL14 PE=1 SV=4	0.04765	1989137	724276	1030298	724012.5	2.7464
39S ribosomal protein L4, mitochondrial OS=Homo sapiens GN=MRPL4 PE=1 SV=1	0.00181	125273.7	46566.86	105088.1	25986.04	2.6902
High mobility group protein HMG-I/HMG-Y OS=Homo sapiens GN=HMGA1 PE=1 SV=3	0.03662	341458.5	128162.5	205386.1	92175.96	2.6643
Chromatin assembly factor 1 subunit B OS=Homo sapiens GN=CHAF1B PE=1 SV=1	0.04176	59176.73	22804.27	37934.78	22385.57	2.5950
6-phosphogluconate dehydrogenase, decarboxylating OS=Homo sapiens GN=PGD PE=1 SV=3	0.04717	14309.56	5658.703	11946.41	5038.89	2.5288
Pentatricopeptide repeat domain-containing protein 3, mitochondrial OS=Homo sapiens GN=PTCD3 PE=1 SV=3	0.00961	117757.8	46914.84	113532	27429.95	2.5100
Reticulocalbin-2 OS=Homo sapiens GN=RCN2 PE=1 SV=1	0.00428	11298.25	4502.685	9663.809	4621.307	2.5092
Guanine nucleotide-binding protein-like 3 OS=Homo sapiens GN=GNL3 PE=1 SV=2	0.03839	6224.475	2492.092	4316.785	2461.33	2.4977
Heterogeneous nuclear ribonucleoprotein H3 OS=Homo sapiens GN=HNRNPH3 PE=1 SV=2	0.0003	105425.4	42419.25	95504.12	36362.73	2.4853
Eukaryotic translation initiation factor 5B OS=Homo sapiens GN=EIF5B PE=1 SV=1	0.02726	116763	48264.25	140411.1	33589.68	2.4192
Dysferlin OS=Homo sapiens GN=DYSF PE=1 SV=1	0.0288	35783.85	14870.17	31405.94	12535.55	2.4064

39S ribosomal protein L13, mitochondrial OS=Homo sapiens GN=MRPL13 PE=1 SV=1	0.01969	32576.53	13919.8	26348.04	12372.25	2.3403
Barrier-to-autointegration factor OS=Homo sapiens GN=BANF1 PE=1 SV=1	0.01571	46991.62	20774.48	42992.07	10631.95	2.2620
40S ribosomal protein S2 OS=Homo sapiens GN=RPS2 PE=1 SV=2	0.01903	736981.4	326378.6	630084	297595.9	2.2581
UPF0568 protein C14orf166 OS=Homo sapiens GN=C14orf166 PE=1 SV=1	0.01973	56915.5	25205.92	45051.32	13781.63	2.2580
Eukaryotic translation initiation factor 5 OS=Homo sapiens GN=EIF5 PE=1 SV=2	0.00404	44765.32	20116.99	54607.7	15450.4	2.2252
RNA-binding protein 3 OS=Homo sapiens GN=RBM3 PE=1 SV=1	0.041	71588.6	32478.85	48938.48	35359.28	2.2042
60S ribosomal protein L27a OS=Homo sapiens GN=RPL27A PE=1 SV=2	0.04999	1372758	624404.3	741042.5	680821.5	2.1985
116 kDa U5 small nuclear ribonucleoprotein component OS=Homo sapiens GN=EFTUD2 PE=1 SV=1	0.00801	187007.1	85664.56	151487.1	88676.4	2.1830
40S ribosomal protein S23 OS=Homo sapiens GN=RPS23 PE=1 SV=3	0.03797	758102.5	353186.8	494973.3	354610.4	2.1465
40S ribosomal protein S29 OS=Homo sapiens GN=RPS29 PE=1 SV=2	0.03014	190156.5	92523.5	130475.7	85971.65	2.0552
39S ribosomal protein L49, mitochondrial OS=Homo sapiens GN=MRPL49 PE=1 SV=1	0.03336	9200.989	4485.909	9419.155	3818.794	2.0511
E3 ubiquitin-protein ligase TRAF7 OS=Homo sapiens GN=TRAF7 PE=1 SV=1	0.00129	33950.45	16559.36	40693.99	16436.71	2.0502

Actin-related protein 2/3 complex subunit 1B OS=Homo sapiens GN=ARPC1B PE=1 SV=3	0.02762	41194.77	20213.75	43880.83	15099.43	2.0380
Small nuclear ribonucleoprotein Sm D1 OS=Homo sapiens GN=SNRPD1 PE=1 SV=1	0.00838	68559.19	34258.77	64549.44	32673	2.0012
Heterochromatin protein 1-binding protein 3 OS=Homo sapiens GN=HP1BP3 PE=1 SV=1	0.00132	164228.6	82107.14	173595.1	91383.04	2.0002
Heterogeneous nuclear ribonucleoproteins C1/C2 OS=Homo sapiens GN=HNRNPC PE=1 SV=4	0.04064	950382.9	481267.5	768478.9	347116.3	1.9748
40S ribosomal protein S10 OS=Homo sapiens GN=RPS10 PE=1 SV=1	0.03373	611180.2	313402.7	442633.4	273488.4	1.9501
60S ribosomal protein L37a OS=Homo sapiens GN=RPL37A PE=1 SV=2	0.02311	50412.84	25852.79	45357.01	25287.26	1.9500
60S ribosomal protein L35 OS=Homo sapiens GN=RPL35 PE=1 SV=2	0.03188	389909.2	204366.5	284909.8	192471.2	1.9079
40S ribosomal protein S4, X isoform OS=Homo sapiens GN=RPS4X PE=1 SV=2	0.04722	1374195	721981.4	928460.7	696791.8	1.9034
ATP-dependent RNA helicase DDX3Y OS=Homo sapiens GN=DDX3Y PE=1 SV=2	0.03941	8818.671	4651.626	12403.36	5173.79	1.8958
Cold-inducible RNA-binding protein OS=Homo sapiens GN=CIRBP PE=1 SV=1	0.0098	73339.32	38819.45	66361.54	32655.27	1.8892
Fragile X mental retardation syndrome-related protein 1 OS=Homo sapiens GN=FXR1 PE=1 SV=3	0.0271	37125.28	19694.29	28951.86	22111.91	1.8851

Lamin B2, isoform CRA_a OS=Homo sapiens GN=LMNB2 PE=1 SV=1	0.03562	79292.85	43302.97	69675.84	41272.13	1.8311
X-ray repair cross-complementing protein 5 OS=Homo sapiens GN=XRCC5 PE=1 SV=3	0.0071	312700	171423.1	277648.1	196869.2	1.8241
40S ribosomal protein S15a OS=Homo sapiens GN=RPS15A PE=1 SV=2	0.0486	1165641	661162.4	735952	608180.9	1.7630
40S ribosomal protein S17 OS=Homo sapiens GN=RPS17 PE=1 SV=2	0.01845	157704.9	92589.97	141413.9	103144.3	1.7033
60S ribosomal protein L23a OS=Homo sapiens GN=RPL23A PE=1 SV=1	0.02703	430780.5	253980.8	468251.6	237435.6	1.6961
Serine/arginine-rich splicing factor 1 OS=Homo sapiens GN=SRSF1 PE=1 SV=2	0.0292	320849.9	198343.3	295228.7	203274	1.6176
ELAV-like protein 1 OS=Homo sapiens GN=ELAVL1 PE=1 SV=2	0.00412	231362.2	145768.9	227976.8	160993.9	1.5872
Probable ATP-dependent RNA helicase DDX6 OS=Homo sapiens GN=DDX6 PE=1 SV=2	0.03051	77260.89	49460.11	78265.49	38767.9	1.5621
Insulin-like growth factor 2 mRNA-binding protein 1 OS=Homo sapiens GN=IGF2BP1 PE=1 SV=2	0.04789	127066	81581.48	150685.9	57828.43	1.5575
X-ray repair cross-complementing protein 6 OS=Homo sapiens GN=XRCC6 PE=1 SV=2	0.0048	444537.7	296231	440989.2	273008.3	1.5006

Dataset QLvsGFP

Group	p-value	Mean 1	Mean 2	Median 1	Median 2	Fold Change
EF-hand calcium-binding domain-containing protein 4B OS=Homo sapiens GN=CRACR2A PE=1 SV=1	4.94E-09	36450750	20971.34	37078683	18588.3	1738.122
EF-hand calcium-binding domain-containing protein 4B (Fragment) OS=Homo sapiens GN=CRACR2A PE=1 SV=1	2.90E-03	345998	50363.58	449403.1	19274.1	6.870
Protein transport protein Sec61 subunit beta OS=Homo sapiens GN=SEC61B PE=1 SV=2	6.30E-04	19890.25	3222.497	15964.12	625.1	6.172
10 kDa heat shock protein, mitochondrial OS=Homo sapiens GN=HSPE1 PE=1 SV=2	6.70E-04	32498.65	7034.95	27734.58	6472.2	4.620
26S proteasome non-ATPase regulatory subunit 4 OS=Homo sapiens GN=PSMD4 PE=1 SV=1	2.25E-02	214412.6	48074.81	121648.3	34000.2	4.460
EGF-containing fibulin-like extracellular matrix protein 1 OS=Homo sapiens GN=EFEMP1 PE=1 SV=2	1.15E-03	182355.5	53274.78	243018.9	45014.4	3.423
Collagen alpha-1(VIII) chain OS=Homo sapiens GN=COL8A1 PE=1 SV=2	2.17E-02	572816.9	183165.4	577558.2	137847.1	3.127
Archain 1, isoform CRA_a OS=Homo sapiens GN=ARCN1 PE=1 SV=1	1.03E-02	93421.45	30699.43	58342.39	27473.4	3.043
DnaJ homolog subfamily A member 2 OS=Homo sapiens GN=DNAJA2 PE=1 SV=1	5.99E-03	11112.97	3805.443	10794.24	3918.5	2.920

Matrix Gla protein OS=Homo sapiens GN=MGP PE=1 SV=2	4.74E-02	17182.56	6173.229	13544.39	6935.6	2.783
CAD protein OS=Homo sapiens GN=CAD PE=1 SV=1	1.36E-03	327299.3	124544.2	388047	134778.6	2.628
40S ribosomal protein S27-like OS=Homo sapiens GN=RPS27L PE=1 SV=3	1.86E-02	42622.33	17783.79	51894.95	13053.4	2.397
7-dehydrocholesterol reductase OS=Homo sapiens GN=DHCR7 PE=1 SV=1	6.70E-03	60634.23	25382.85	71693.96	21752.3	2.389
cAMP-dependent protein kinase catalytic subunit alpha OS=Homo sapiens GN=PRKACA PE=1 SV=2	2.72E-02	25684.71	10910.91	31918.64	11351.5	2.354
Protein CYR61 OS=Homo sapiens GN=CYR61 PE=1 SV=1	1.79E-02	660083.7	284612.8	704581	290462.5	2.319
Macrophage migration inhibitory factor OS=Homo sapiens GN=MIF PE=1 SV=4	2.27E-02	1621261	724478	1639035	310534.4	2.238
Serpin B6 OS=Homo sapiens GN=SERPINB6 PE=1 SV=1	5.30E-04	82668.79	40596.84	80625.01	36824.3	2.036
Protein phosphatase 1F OS=Homo sapiens GN=PPM1F PE=1 SV=3	1.59E-02	47905.3	23986.53	53801.93	20756.3	1.997
Microsomal glutathione S-transferase 1 (Fragment) OS=Homo sapiens GN=MGST1 PE=1 SV=1	3.81E-02	39368.42	20365.37	34207.89	18162.0	1.933
Ig heavy chain V-III region TUR OS=Homo sapiens PE=1 SV=1	1.46E-02	144280.7	74764.13	132748.7	73668.2	1.930
Lysozyme OS=Homo sapiens GN=LYZ PE=1 SV=1	2.79E-02	98693.55	51442.75	74275.49	59511.8	1.919
Cystatin-B OS=Homo sapiens GN=CSTB PE=1 SV=2	3.57E-03	218847.7	115006.5	225369.5	89760.0	1.903
Interferon-induced protein 44 OS=Homo sapiens GN=IFI44 PE=2 SV=2	8.79E-03	46109.92	24522.43	55519.34	28510.2	1.880

GTPase IMAP family member 8 OS=Homo sapiens GN=GIMAP8 PE=2 SV=2	3.89E-02	31104.11	16558.12	37067.99	8164.7	1.878
Hemoglobin subunit alpha OS=Homo sapiens GN=HBA1 PE=1 SV=2	2.20E-02	188512.5	106268.1	208176	89898.3	1.774
Profilin OS=Homo sapiens GN=PFN2 PE=1 SV=1	1.37E-03	212607.2	121524.5	214836	103203.7	1.750
40S ribosomal protein S3 OS=Homo sapiens GN=RPS3 PE=1 SV=2	1.84E-02	2432289	1438922	3130268	1447215.6	1.690
ATP synthase subunit gamma, mitochondrial OS=Homo sapiens GN=ATP5C1 PE=1 SV=1	1.66E-02	535509.9	317196.4	651726.5	315997.7	1.688
RNA 3'-terminal phosphate cyclase OS=Homo sapiens GN=RTCA PE=1 SV=1	4.39E-02	46675.19	27766.7	54539.64	28114.0	1.681
Thrombospondin-1 OS=Homo sapiens GN=THBS1 PE=1 SV=2	2.04E-02	1790628	1065906	1745867	1035020.6	1.680
Elongation factor Tu, mitochondrial OS=Homo sapiens GN=TUFM PE=1 SV=2	7.10E-03	992966.5	593937.2	1178492	626400.7	1.672
Zyxin OS=Homo sapiens GN=ZYX PE=1 SV=1	1.43E-03	172548	104052.2	176332.2	107541.7	1.658
Synaptic vesicle membrane protein VAT-1 homolog OS=Homo sapiens GN=VAT1 PE=1 SV=2	4.12E-02	39302.98	24041.95	36693.46	24593.9	1.635
26S proteasome non-ATPase regulatory subunit 3 OS=Homo sapiens GN=PSMD3 PE=1 SV=2	4.89E-02	304469.2	187294.8	374661.3	173747.7	1.626
Heat shock cognate 71 kDa protein OS=Homo sapiens GN=HSPA8 PE=1 SV=1	6.66E-03	3590261	2253553	3878215	2204240.4	1.593
NADH dehydrogenase [ubiquinone] iron-sulfur protein 2, mitochondrial	3.17E-02	79970.4	50205.66	97567.17	50639.6	1.593

OS=Homo sapiens GN=NDUFS2 PE=1 SV=2						
Cytoplasmic dynein 1 heavy chain 1 OS=Homo sapiens GN=DYNC1H1 PE=1 SV=5	1.86E-03	247223.3	155451.4	261668.8	162179.6	1.590
Cold shock domain-containing protein E1 OS=Homo sapiens GN=CSDE1 PE=1 SV=2	4.30E-02	81258.32	51715.82	86396.19	51307.3	1.571

Dataset NIvsGFP

Group	p-value	Mean 1	Mean 2	Median 1	Median 2	Fold Change
EF-hand calcium-binding domain-containing protein 4B OS=Homo sapiens GN=CRACR2A PE=1 SV=1	1.3E-07	20454767	23236.38	17334192	20597.41	880.2906
REVERSED Cysteine protease ATG4C OS=Homo sapiens GN=ATG4C PE=1 SV=1	2.5E-09	2845596	3609.32	2625261	1431.963	788.4022
10 kDa heat shock protein, mitochondrial OS=Homo sapiens GN=HSPE1 PE=1 SV=2	1.7E-03	65464.76	7795.113	76596.29	7170.227	8.3982
Pentatricopeptide repeat domain-containing protein 3, mitochondrial OS=Homo sapiens GN=PTCD3 PE=1 SV=3	3.3E-05	119685.8	14827.76	115388.4	9809.47	8.0717
26S proteasome non-ATPase regulatory subunit 4 OS=Homo sapiens GN=PSMD4 PE=1 SV=1	9.9E-03	377925.4	53270.25	316204.9	37675.26	7.0945
EF-hand calcium-binding domain-containing protein 4B (Fragment) OS=Homo sapiens GN=CRACR2A PE=1 SV=1	4.8E-02	307065.8	55806.07	134967.8	21357.35	5.5024
Protein transport protein Sec61 subunit beta OS=Homo sapiens GN=SEC61B PE=1 SV=2	2.7E-03	16398.95	3570.78	22179.45	692.5911	4.5925
Uncharacterized protein OS=Homo sapiens PE=3 SV=1	2.1E-02	38942.02	10599.56	34602.7	7412.545	3.6739
40S ribosomal protein S29 OS=Homo sapiens GN=RPS29 PE=1 SV=2	3.0E-03	193269.6	58696.53	132611.6	44693.39	3.2927

Barrier-to-autointegration factor OS=Homo sapiens GN=BANF1 PE=1 SV=1	2.3E-03	47760.76	15025.61	43694.5	6358.187	3.1786
Cell cycle and apoptosis regulator protein 2 OS=Homo sapiens GN=CCAR2 PE=1 SV=2	4.6E-02	115193	36761.41	59095.82	37049.64	3.1335
Microsomal glutathione S-transferase 1 (Fragment) OS=Homo sapiens GN=MGST1 PE=1 SV=1	8.8E-04	64191.29	22566.39	45099.72	20125.06	2.8446
40S ribosomal protein S15a OS=Homo sapiens GN=RPS15A PE=1 SV=2	1.1E-02	1184722	427233.5	747999.6	241526.5	2.7730
Collagen alpha-1(VIII) chain OS=Homo sapiens GN=COL8A1 PE=1 SV=2	1.3E-02	545217.7	202953.1	621056.7	152722	2.6864
cAMP-dependent protein kinase catalytic subunit alpha OS=Homo sapiens GN=PRKACA PE=1 SV=2	7.5E-03	31968.81	12089.61	35710.95	12578.45	2.6443
EGF-containing fibulin-like extracellular matrix protein 1 OS=Homo sapiens GN=EFEMP1 PE=1 SV=2	2.5E-03	151901.6	59030.37	187637.8	49879.86	2.5733
26S proteasome non-ATPase regulatory subunit 7 OS=Homo sapiens GN=PSMD7 PE=1 SV=2	4.1E-02	23827.24	9581.498	21116.57	6572.9	2.4868
Dysferlin OS=Homo sapiens GN=DYSF PE=1 SV=1	3.1E-02	36369.31	14692.05	31923.82	11923.67	2.4754
Matrix Gla protein OS=Homo sapiens GN=MGP PE=1 SV=2	2.0E-03	16615.62	6840.249	17978.88	7685.293	2.4291
7-dehydrocholesterol reductase OS=Homo sapiens GN=DHCR7 PE=1 SV=1	2.2E-03	66981.46	28124.87	50270.29	24103.46	2.3816

Heat shock cognate 71 kDa protein OS=Homo sapiens GN=HSPA8 PE=1 SV=1	1.3E-04	5897532	2497019	5873136	2442097	2.3618
Cystatin-B OS=Homo sapiens GN=CSTB PE=1 SV=2	4.2E-03	300876	127434.7	273835.9	99440.97	2.3610
39S ribosomal protein L13, mitochondrial OS=Homo sapiens GN=MRPL13 PE=1 SV=1	1.6E-02	33110.14	14191	26777.15	14201.42	2.3332
UPF0568 protein C14orf166 OS=Homo sapiens GN=C14orf166 PE=1 SV=1	1.7E-03	57847.17	25458.1	45793.56	28088	2.2723
40S ribosomal protein S2 OS=Homo sapiens GN=RPS2 PE=1 SV=2	1.8E-02	749045	331891.9	640398.5	216536.1	2.2569
Splicing factor U2AF 35 kDa subunit OS=Homo sapiens GN=U2AF1 PE=1 SV=3	1.1E-02	31111.79	13830.3	25437.73	16935.51	2.2495
PDZ and LIM domain protein 7 OS=Homo sapiens GN=PDLIM7 PE=1 SV=1	4.8E-02	14167.55	6300.214	13334.81	4198.381	2.2487
Squamous cell carcinoma antigen recognized by T-cells 3 OS=Homo sapiens GN=SART3 PE=1 SV=1	3.1E-02	23509.36	10801.62	21677.03	6801.831	2.1765
Macrophage migration inhibitory factor OS=Homo sapiens GN=MIF PE=1 SV=4	2.9E-02	1724566	802775.4	1464931	344099.1	2.1483
Heterogeneous nuclear ribonucleoprotein Q OS=Homo sapiens GN=SYNCRIP PE=1 SV=2	1.2E-02	97238.07	45432.22	88811.36	45825.51	2.1403
60S ribosomal protein L37a OS=Homo sapiens GN=RPL37A PE=1 SV=2	9.1E-03	51238.09	24214.62	46098.08	24298.57	2.1160

60S ribosomal protein L23 OS=Homo sapiens GN=RPL23 PE=1 SV=1	2.8E-02	991906	483057.4	805014.3	320824.5	2.0534
Zinc finger CCHC domain-containing protein 3 OS=Homo sapiens GN=ZCCHC3 PE=1 SV=1	3.0E-03	23996.41	11701.98	26539.26	11964.54	2.0506
Hemoglobin subunit alpha OS=Homo sapiens GN=HBA1 PE=1 SV=2	3.2E-03	234757.7	117750.8	238410.3	99615.16	1.9937
Aminoacyl tRNA synthase complex-interacting multifunctional protein 2 OS=Homo sapiens GN=AIMP2 PE=1 SV=2	3.3E-03	6893.202	3620.845	7165.761	3787.688	1.9038
Small nuclear ribonucleoprotein Sm D2 OS=Homo sapiens GN=SNRPD2 PE=1 SV=1	1.4E-02	87741.98	46623.22	82329.6	49300.69	1.8819
Proteasome subunit beta type-3 (Fragment) OS=Homo sapiens GN=PSMB3 PE=1 SV=1	2.5E-02	54499.87	29126.43	64283.94	27707.71	1.8711
Histone H1x OS=Homo sapiens GN=H1FX PE=1 SV=1	1.3E-02	61075.49	32908.24	65932.8	31769.07	1.8559
Profilin OS=Homo sapiens GN=PFN2 PE=1 SV=1	2.3E-03	247966.8	134655.9	232054.9	114340.3	1.8415
26S protease regulatory subunit 7 OS=Homo sapiens GN=PSMC2 PE=1 SV=3	1.5E-02	15833.5	8960.797	16046.32	14798.65	1.7670
RNA 3'-terminal phosphate cyclase OS=Homo sapiens GN=RTCA PE=1 SV=1	2.4E-03	54203.86	30766.63	55102.11	31152.75	1.7618
39S ribosomal protein L38, mitochondrial OS=Homo sapiens GN=MRPL38 PE=1 SV=2	3.6E-02	40190.84	23052.77	35062.34	22915.12	1.7434
Insulin-like growth factor 2 mRNA-binding protein 2 OS=Homo	3.8E-02	97048.27	57049.7	98342.93	56150.84	1.7011

sapiens GN=IGF2BP2 PE=1 SV=1						
Thioredoxin OS=Homo sapiens GN=TXN PE=1 SV=3	5.0E-02	388171.7	234174.7	353873.6	126218	1.6576
ATPase family AAA domain-containing protein 3A (Fragment) OS=Homo sapiens GN=ATAD3A PE=1 SV=1	7.5E-03	145729.6	88540.21	113788	89409.44	1.6459
Heterochromatin protein 1-binding protein 3 OS=Homo sapiens GN=HP1BP3 PE=1 SV=1	8.6E-04	166917.2	102555.1	176436.9	96264	1.6276
Serpin B6 OS=Homo sapiens GN=SERPINB6 PE=1 SV=1	2.4E-02	72536.86	44983.39	70233.3	40797.9	1.6125
Calponin OS=Homo sapiens GN=CNN2 PE=1 SV=1	2.5E-02	94616.84	59586.53	100767	64470.54	1.5879
ATP synthase subunit gamma, mitochondrial OS=Homo sapiens GN=ATP5C1 PE=1 SV=1	1.5E-08	548805.7	351467.4	527193.7	350152.9	1.5615
L-lactate dehydrogenase A chain OS=Homo sapiens GN=LDHA PE=1 SV=2	2.4E-02	2632868	1691518	2920045	1686296	1.5565
Elongation factor Tu, mitochondrial OS=Homo sapiens GN=TUFM PE=1 SV=2	5.1E-03	1022326	658105.1	1069408	694106.4	1.5534
Synaptic vesicle membrane protein VAT-1 homolog OS=Homo sapiens GN=VAT1 PE=1 SV=2	4.8E-02	41156.26	26639.58	40696.02	27252.24	1.5449
Interferon-induced protein 44 OS=Homo sapiens GN=IFI44 PE=2 SV=2	4.0E-02	41770.22	27171.54	42393.65	31585.08	1.5373
Annexin A1 OS=Homo sapiens GN=ANXA1 PE=1 SV=2	4.1E-02	707839.1	461166.4	787897.6	442902	1.5349
Heterogeneous nuclear ribonucleoprotein U-like protein 1	1.8E-02	39993.74	26099.08	41517.7	19985.23	1.5324

OS=Homo sapiens GN=HNRNPUL1 PE=1 SV=2						